ANALYTICAL STUDY OF THE SPECTRAL-ANALYSIS-OF-SURFACE-WAVES METHOD AT COMPLEX GEOTECHNICAL SITES

A Thesis
Presented to
The Faculty of the Graduate School
University of Missouri-Columbia

In Partial Fulfillment
Of the Requirements for the Degree

Master of Science

By
JEFFREY D. BERTEL

Dr. Brent Rosenblad, Thesis Supervisor

DECEMBER 2006

The undersigned, appointed by the Dean of the Graduate School, have examined the thesis entitled

ANALYTICAL STUDY OF THE SPECTRAL-ANALYSIS-OF-SURFACE-WAVES METHOD AT COMPLEX GEOTECHNICAL SITES

Presented by Jeffrey D. Bertel

A candidate for the degree of Masters of Science in Civil & Environmental Engineering and hereby certify that in their opinion it is worthy of acceptance.

_____

Brent L. Rosenblad, PhD
Department of Civil and Environmental Engineering

_____

J. Erik Loehr, PhD, PE
Department of Civil and Environmental Engineering

_____

Michael B. Underwood, PhD
Department of Geological Sciences

Acknowledgements

I would like to thank Dr. Brent Rosenblad, my thesis advisor, for his guidance, demand for quality and patience while completing this research. I would also like to thank Dr. Mike Underwood and Dr. Erik Loehr for serving on this committee and for providing guidance, in and out of the classroom. I would also like to thank fellow graduate student Andy Boeckmann for all of his help and friendship. Thanks also to my wife Julie Bertel for everything you have done.

Table of Contents

Acknowledgments ii

Table of Contents iii

List of Figures vii

List of Tables xxvii

Abstract xxix

Chapter 1 Introduction 1

1.1 Background 1

1.2 Problem Statement 2

1.3 Project Objectives and Scope 3

1.4 Thesis Organization 4

Chapter 2 Surface Wave Propagation & Measurement 5

2.1 Introduction 5

2.2 Surface Wave Propagation in a Uniform Halfspace 5

2.3 Surface Wave Propagation in a Layered Halfspace 10

2.4 Modal versus Effective Phase Velocity 12

2.5 Spectral-Analysis-of-Surface-Waves-Method 14

2.5.1 SASW Overview 14

2.5.2 Data Collection 15

2.5.2.1 Sources Used in SASW Testing 18

2.5.2.2 Receivers Used in SASW Testing 19

2.5.2.3 Data Acquisition System 20

2.5.3 Data Processing 23

2.5.4 Data Analysis 28
2.5.4.1 Averaging Procedures 28
2.5.4.2 Forward Modeling 30
2.5.4.3 Inversion Analysis 35
2.6 Past Theoretical Studies of Surface Wave Propagation 35
2.6.1 Gucunski and Woods Study 35
2.6.2 Tokimatsu Study 39
2.6.3 Foti Study 41
2.7 Summary 46
Chapter 3 Methodology 47
3.1 Introduction 47
3.2 Synthetic Time Records 47
3.3 Development of Simulated Experimental Dispersion Curves 51
3.4 Theoretical Effective Velocity Dispersion Curve 54
3.5 Modal Dispersion Curve 56
3.6 Soil Profile Model 59
3.6.1 Creation of Reference Profile 59
3.6.2 Baseline Profiles 63
3.7 Summary 68
Chapter 4 Results 71
4.1 Introduction 71
4.2 Reference Profile 72
4.3 Soft-over-Stiff 75

4.3.1 Profile 1a 75
4.3.2 Profile 1b 78
4.3.3 Profile 1c 81
4.3.4 Profile 2a 84
4.3.5 Profile 2b 87
4.3.6 Profile 2c 90
4.3.7 Profile 2d 93
4.4 Stiff-over-Soft 96
4.4.1 Profile 3a 96
4.4.2 Profile 3b 99
4.4.3 Profile 3c 102
4.4.4 Profile 4a 105
4.4.5 Profile 4b 108
4.4.6 Profile 4c 111
4.5 Profiles with an Embedded Stiff Layer 114
4.5.1 Profile 5a 114
4.5.2 Profile 5b 117
4.5.3 Profile 5c 120
4.5.4 Profile 6a 123
4.5.5 Profile 6b 126
4.5.6 Profile 6c 129
4.6 Profiles with an Embedded Soft Layer 132
4.6.1 Profile 7a 132

4.6.2 Profile 7b 135
4.6.3 Profile 7c 138
Chapter 5 Discussion and Anaylsis 141
5.1 Introduction 141
5.2 Reference Profile 141
5.3 Soft-over-Stiff 144
5.4 Stiff-over-Soft 150
5.5 Profiles with an Embedded Stiff Layer 154
5.6 Profiles with an Embedded Soft Layer 157
5.7 Further Analysis of Soft-over-Stiff 161
5.8 Effect of Poisson's Ration on Dispersion Curves at Soft-over-Stiff Sites 168
5.9 Practical Implications of Conventional SASW Interpretation at Soft-over-Stiff Sites 170
5.10 Summary 172
Chapter 6 Conclusions and Recommendations 174
6.1 Conclusions 174
6.2 Recommendations 177
Appendix A 179
References 192

List of Figures

Figure **Page**

2-1: Normalized vertical and horizontal particle motions for a Raleigh-type surface wave (*from* Richart et al., 1970). 6

2-2: Wave generated from a symmetric circular footing on a homogenous elastic half-space (*from* Richart, Hall and Woods, 1970). 7

2-3: Ratio of Rayleigh wave velocity to shear wave velocity as a function of Poisson's Ratio (*from* Bedford and Crumheller, 1994). 8

2-4: Relationship between Poisson's ratio and V_P, V_R and V_S waves (*from* Richart, Hall and Woods, 1970). 9

2-5: Dispersion curve for a homogeneous halfspace with a shear wave velocity equal to 500 fps and ν=0.25. 10

2-6: Three layer non-homogeneous profile. 11

2-7: Dispersion curve for three layer profile shown in Figure 2-6. 12

2-8: Typical SASW testing arrangement showing forward and reverse impacts. 16

2-9: Receiver arrangement showing common mid-point array for SASW testing (Hollrah, 2005). 17

2-10: (Left) Transient hammer impact source, (Top Right) Random Bulldozer source, (Bottom Right) Continuous-type Vibroseis source. 18

2-11: Time records at 200 feet (Top) and 400 feet (Bottom) from a vertically oriented disk load. 21

2-12: Wrapped phase spectrum for receiver spacing of 200 feet. 23

2-13: Illustration of the phase difference between two time signals (*from* Joh, 1996). 24

2-14: Comparison of a Wrapped Phase Spectrum and an Unwrapped Phase Spectrum (*from* Joh, 1996). 26
2-15: Dispersion curve for 200 feet receiver spacing and phase plot shown in Figure 2-12. 27
2-16: Composite dispersion curve for six receiver spacing. 27
2-17: Example global experimental dispersion curve generated from the individual dispersion curves shown in Figure 2-16. 29
2-18: Example array experimental dispersion curve generated from the individual dispersion curves shown in Figure 2-16. 30
2-19: Demonstration of phase velocity calculation for determining the theoretical dispersion curve (from Joh, 1996) 33
2-20: Global and array theoretical dispersion curves for the data shown in Figure 2-16 34
2-21: Stiffness profiles analyzed by Gucunski and Woods, 1992. 36
2-22: Case 1, modal and simulated dispersion curves (*from* Gucunski and Woods, 1992) 37
2-23: Modal and simulated dispersion curves for Case 2 and 3 shown in Figure 2-21 (*from* Gucunski and Woods, 1992). 37
2-24: Case 4 modal and simulated dispersion curves (*from* Gucunski and Woods, 1992) 38
2-25: Modal and simulated dispersion curves for Case 1 (*from* Tokimatsu et al., 1992) 40

2-26: Modal and simulated dispersion curves for Cases 2 (left) and Case 3 (right) (*from* Tokimatsu et al., 1992). 41
2-27: Rayleigh modes and effective dispersion curve for Profile A (*from* Foti, 2000). 42
2-28: Comparison of dispersion curves for SASW simulation, effective phase velocity and Rayleigh wave fundamental mode for Profile A (*from* Foti, 2000). .. 43
2-29: Rayleigh modes and effective dispersion curve determined from Profile B (from Foti, 2000). 44
2-30: SASW simulation dispersion curve and effective phase velocity dispersion curve determined from Profile B (from Foti, 2000). 44
2-31: Rayleigh modes and effective dispersion curve determined from Profile C (from Foti, 2000). 45
2-32: SASW simulation dispersion curve and effective phase velocity dispersion curve determined from Profile C (from Foti, 2000). 45
3-1: Sample soil profile with an 800 ft/sec halfspace. 49
3-2: Synthetic time records created for a 200 ft spacing with the receivers spaced at 200 ft (top) and 400 ft (bottom) from the source using FitSASW (Joh, 2003). 50
3-3: Time record file upload screen for WinSASW 2.3.1 with simulated time records. 51
3-4: Unwrapped phase plots and masking for receiver spacings of 6, 12, 25, 50, 100 and 200 ft. 52
3-5: Composite dispersion curve for receiver spacing of 6, 12, 25, 50, 100 and 200 feet. 53

3-6: Composite, array and global experimental dispersion curves generated from the profile shown in Figure 3-1. 54
3-7: Array theoretical and experimental dispersion curves determined from the V_S profiles shown in Figure 3-1. 55
3-8: Global theoretical and experimental dispersion curves determined from the V_S profile shown in Figure 3-1. 56
3-9: Modal dispersion curve replicated from Gucinski and Woods (1992) Case 2 58
3-10: Modal dispersion curve from Gucinski and Woods (1992) Case 2. 59
3-11: Reference V_S profile calculated using Hardin's equation. 62
3-12: 10-layer reference V_S profile used to construct 7 baseline V_S profiles. 62
3-13: Profiles 1a, 1b and 1c plotted with the reference profile. 63
3-14: Profiles 2a, 2b, 2c and 2d plotted with the reference profile. 64
3-15: Profiles 3a, 3b and 3d plotted with the reference profile. 65
3-16: Profiles 4a, 4b and 4c plotted with the reference profile. 65
3-17: Profiles 5a, 5b and 5c plotted with the reference profile. 66
3-18: Profiles 6a, 6b and 6c plotted with the reference profile. 67
3-19: Profiles 7a, 7b and 7c plotted with the reference profile. 68
3-20: Flowchart showing the progression of calculations and data generation. .. 69
4-1: Reference profile shown with layering used for simulations. 72
4-2: Simulated experimental dispersion curves (individual and global average) versus global theoretical dispersion curve, plotted versus frequency for the reference profile. 73

4-3: Experimental individual dispersion curves and the array theoretical dispersion curves plotted versus frequency for the reference profile. 73
4-4: Simulated experimental dispersion curves (individual and global average) versus global theoretical dispersion curve, plotted versus wavelength for the reference profile. 74
4-5: Experimental individual dispersion curves and the array theoretical dispersion curves plotted versus wavelength for the reference profile. 74
4-6: Profile 1a shown with the reference profile. 75
4-7: Simulated experimental dispersion curves (individual and global average) versus global theoretical dispersion curve, plotted versus wavelength for Profile 1a. 76
4-8: Experimental individual dispersion curves and the array theoretical dispersion curves plotted versus frequency for the baseline Profile 1a. 76
4-9: Simulated experimental dispersion curves (individual and global average) versus global theoretical dispersion curve, plotted versus wavelength for Profile 1a. 77
4-10: Experimental individual dispersion curves and the array theoretical dispersion curves plotted versus wavelength for the baseline Profile 1a. 77
4-11: Profile 1b shown with the reference profile. 78
4-12: Simulated experimental dispersion curves (individual and global average) versus global theoretical dispersion curve, plotted versus wavelength for Profile 1b. 79

4-13: Individual experimental dispersion curves and array theoretical dispersion curves plotted versus frequency for Profile 1b. 79
4-14: Simulated experimental dispersion curves (individual and global average) versus global theoretical dispersion curve, plotted versus wavelength for Profile 1b. 80
4-15: Individual experimental and array theoretical dispersion curves plotted versus wavelength for Profile 1b. 80
4-16: Profile 1c shown with the reference profile. 81
4-17: Simulated experimental dispersion curves (individual and global average) versus global theoretical dispersion curve, plotted versus wavelength for Profile 1c. 82
4-18: Individual experimental and array theoretical dispersion curves plotted versus frequency for Profile 1c. 82
4-19: Simulated experimental dispersion curves (individual and global average) versus global theoretical dispersion curve, plotted versus wavelength for Profile 1c. 83
4-20: Individual experimental and array theoretical dispersion curves plotted versus wavelength for Profile 1c. 83
4-21: Profile 2a shown with the reference profile. 84
4-22: Simulated experimental dispersion curves (individual and global average) versus global theoretical dispersion curve, plotted versus wavelength for Profile 2a. 85

4-23: Individual experimental and array theoretical dispersion curves plotted versus frequency for Profile 2a. 85
4-24: Simulated experimental dispersion curves (individual and global average) versus global theoretical dispersion curve, plotted versus wavelength for Profile 2a. 86
4-25: Individual experimental and array theoretical dispersion curves plotted versus wavelength for Profile 2a. 86
4-26: Profile 2b shown with the reference profile. 87
4-27: Simulated experimental dispersion curves (individual and global average) versus global theoretical dispersion curve, plotted versus wavelength for Profile 2b. 88
4-28: Individual experimental and array theoretical dispersion curves plotted versus frequency for Profile 2b. 88
4-29: Simulated experimental dispersion curves (individual and global average) versus global theoretical dispersion curve, plotted versus wavelength for Profile 2b. 89
4-30: Individual experimental and array theoretical dispersion curves plotted versus wavelength for Profile 2b. 89
4-31: Profile 2c shown with the reference profile. 90
4-32: Simulated experimental dispersion curves (individual and global average) versus global theoretical dispersion curve, plotted versus wavelength for Profile 2c. 91

4-33: Individual experimental and array theoretical dispersion curves plotted versus frequency for Profile 2c. 91
4-34: Simulated experimental dispersion curves (individual and global average) versus global theoretical dispersion curve, plotted versus wavelength for Profile 2c. 92
4-35: Individual experimental and array theoretical dispersion curves plotted versus wavelength for Profile 2c. 92
4-36: Profile 2d shown with the reference profile. 93
4-37: Simulated experimental dispersion curves (individual and global average) versus global theoretical dispersion curve, plotted versus wavelength for Profile 2d. 94
4-38: Individual experimental and array theoretical dispersion curves plotted versus frequency for Profile 2d. 94
4-39: Simulated experimental dispersion curves (individual and global average) versus global theoretical dispersion curve, plotted versus wavelength for Profile 2d. 95
4-40: Individual experimental and array theoretical dispersion curves plotted versus wavelength for Profile 2d. 95
4-41: Profile 3a shown with the reference profile. 96
4-42: Simulated experimental dispersion curves (individual and global average) versus global theoretical dispersion curve, plotted versus wavelength for Profile 3a. 97

4-43: Individual experimental and array theoretical dispersion curves plotted versus frequency for Profile 3a. 97
4-44: Simulated experimental dispersion curves (individual and global average) versus global theoretical dispersion curve, plotted versus wavelength for Profile 3a. 98
4-45: Individual experimental and array theoretical dispersion curves plotted versus wavelength for Profile 3a. 98
4-46: Profile 3b shown with the reference profile. 99
4-47: Simulated experimental dispersion curves (individual and global average) versus global theoretical dispersion curve, plotted versus wavelength for Profile 3b. 100
4-48: Individual experimental and array theoretical dispersion curves plotted versus frequency for Profile 3b. 100
4-49: Simulated experimental dispersion curves (individual and global average) versus global theoretical dispersion curve, plotted versus wavelength for Profile 3b. 101
4-50: Individual experimental and array theoretical dispersion curves plotted versus wavelength for Profile 3b. 101
4-51: Profile 3c shown with the reference profile. 102
4-52: Simulated experimental dispersion curves (individual and global average) versus global theoretical dispersion curve, plotted versus wavelength for Profile 3c. 103

4-53: Individual experimental and array theoretical dispersion curves plotted versus frequency for Profile 3c. 103
4-54: Simulated experimental dispersion curves (individual and global average) versus global theoretical dispersion curve, plotted versus wavelength for Profile 3c. 104
4-55: Individual experimental and array theoretical dispersion curves plotted versus wavelength for Profile 3c. 104
4-56: Profile 4a shown with the reference profile. 105
4-57: Simulated experimental dispersion curves (individual and global average) versus global theoretical dispersion curve, plotted versus wavelength for Profile 4a. 106
4-58: Individual experimental and array theoretical dispersion curves plotted versus frequency for Profile 4a. 106
4-59: Simulated experimental dispersion curves (individual and global average) versus global theoretical dispersion curve, plotted versus wavelength for Profile 4a. 107
4-60: Individual experimental and array theoretical dispersion curves plotted versus wavelength for Profile 4a. 107
4-61: Profile 4b shown with the reference profile. 108
4-62: Simulated experimental dispersion curves (individual and global average) versus global theoretical dispersion curve, plotted versus wavelength for Profile 4b. 109

4-63: Individual experimental and array theoretical dispersion curves plotted versus frequency for Profile 4b. 109
4-64: Simulated experimental dispersion curves (individual and global average) versus global theoretical dispersion curve, plotted versus wavelength for Profile 4b. 110
4-65: Individual experimental and array theoretical dispersion curves plotted versus wavelength for Profile 4b. 110
4-66: Profile 4c shown with the reference profile. 111
4-67: Simulated experimental dispersion curves (individual and global average) versus global theoretical dispersion curve, plotted versus wavelength for Profile 4c. 112
4-68: Individual experimental and array theoretical dispersion curves plotted versus frequency for Profile 4c. 112
4-69: Simulated experimental dispersion curves (individual and global average) versus global theoretical dispersion curve, plotted versus wavelength for Profile 4c. 113
4-70: Individual experimental and array theoretical dispersion curves plotted versus wavelength for Profile 4c. 113
4-71: Profile 5a shown with the reference profile. 114
4-72: Simulated experimental dispersion curves (individual and global average) versus global theoretical dispersion curve, plotted versus wavelength for Profile 5a. 115

4-73: Individual experimental and array theoretical dispersion curves plotted versus frequency for Profile 5a. 115
4-74: Simulated experimental dispersion curves (individual and global average) versus global theoretical dispersion curve, plotted versus wavelength for Profile 5a. 116
4-75: Individual experimental and array theoretical dispersion curves plotted versus wavelength for Profile 5a. 116
4-76: Profile 5b shown with the reference profile. 117
4-77: Simulated experimental dispersion curves (individual and global average) versus global theoretical dispersion curve, plotted versus wavelength for Profile 5b. 118
4-78: Individual experimental and array theoretical dispersion curves plotted versus frequency for Profile 5b. 118
4-79: Simulated experimental dispersion curves (individual and global average) versus global theoretical dispersion curve, plotted versus wavelength for Profile 5b. 119
4-80: Individual experimental and array theoretical dispersion curves plotted versus wavelength for Profile 5b. 119
4-81: Profile 5c shown with the reference profile. 120
4-82: Simulated experimental dispersion curves (individual and global average) versus global theoretical dispersion curve, plotted versus wavelength for Profile 5c. 121

4-83: Individual experimental and array theoretical dispersion curves plotted versus frequency for Profile 5c. 121
4-84: Simulated experimental dispersion curves (individual and global average) versus global theoretical dispersion curve, plotted versus wavelength for Profile 5c. 122
4-85: Individual experimental and array theoretical dispersion curves plotted versus wavelength for Profile 5c. 122
4-86: Profile 6a shown with the reference profile. 123
4-87: Simulated experimental dispersion curves (individual and global average) versus global theoretical dispersion curve, plotted versus wavelength for Profile 6a. 124
4-88: Individual experimental and array theoretical dispersion curves plotted versus frequency for Profile 6a. 124
4-89: Simulated experimental dispersion curves (individual and global average) versus global theoretical dispersion curve, plotted versus wavelength for Profile 6a. 125
4-90: Individual experimental and array theoretical dispersion curves plotted versus wavelength for Profile 6a. 125
4-91: Profile 6b shown with the reference profile. 126
4-92: Simulated experimental dispersion curves (individual and global average) versus global theoretical dispersion curve, plotted versus wavelength for Profile 6b. 127

4-93: Individual experimental and array theoretical dispersion curves plotted versus frequency for Profile 6b. 127
4-94: Simulated experimental dispersion curves (individual and global average) versus global theoretical dispersion curve, plotted versus wavelength for Profile 6b. 128
4-95: Individual experimental and array theoretical dispersion curves plotted versus wavelength for Profile 6b. 128
4-96: Profile 6c shown with the reference profile. 129
4-97: Simulated experimental dispersion curves (individual and global average) versus global theoretical dispersion curve, plotted versus wavelength for Profile 6c. 130
4-98: Individual experimental and array theoretical dispersion curves plotted versus frequency for Profile 6c. 130
4-99: Simulated experimental dispersion curves (individual and global average) versus global theoretical dispersion curve, plotted versus wavelength for Profile 6c. 131
4-100: Individual experimental and array theoretical dispersion curves plotted versus wavelength for Profile 6c. 131
4-101: Profile 7a shown with the reference profile. 132
4-102: Simulated experimental dispersion curves (individual and global average) versus global theoretical dispersion curve, plotted versus wavelength for Profile 7a. 133

4-103: Individual experimental and array theoretical dispersion curves plotted versus frequency for Profile 7a. 133
4-104: Simulated experimental dispersion curves (individual and global average) versus global theoretical dispersion curve, plotted versus wavelength for Profile 7a. 134
4-105: Individual experimental and array theoretical dispersion curves plotted versus wavelength for Profile 7a. 134
4-106: Profile 7b shown with the reference profile. 135
4-107: Simulated experimental dispersion curves (individual and global average) versus global theoretical dispersion curve, plotted versus wavelength for Profile 7b. 136
4-108: Individual experimental and array theoretical dispersion curves plotted versus frequency for Profile 7b. 136
4-109: Simulated experimental dispersion curves (individual and global average) versus global theoretical dispersion curve, plotted versus wavelength for Profile 7b. 137
4-110: Individual experimental and array theoretical dispersion curves plotted versus wavelength for Profile 7b. 137
4-111: Profile 7c shown with the reference profile. 138
4-112: Simulated experimental dispersion curves (individual and global average) versus global theoretical dispersion curve, plotted versus wavelength for Profile 7c. 139

4-113: Individual experimental and array theoretical dispersion curves plotted versus frequency for Profile 7c. 139
4-114: Simulated experimental dispersion curves (individual and global average) versus global theoretical dispersion curve, plotted versus wavelength for Profile 7c. 140
4-115: Individual experimental and array theoretical dispersion curves plotted versus wavelength for Profile 7c. 140
5-1: Modal dispersion curve shown with the global experimental and theoretical dispersion curves for the reference profile. 142
5-2: Experimental and theoretical dispersion curves from the array analysis generated for the reference profile. 144
5-3: Global experimental and theoretical dispersion curves for Profile 1a. 145
5-4: Global experimental and theoretical dispersion curve for Profile 2c. 146
5-5: Array experimental and theoretical dispersion curves for Profile 1a. 147
5-6: Array experimental and theoretical dispersion curves for Profile 1c. 148
5-7: Array experimental and theoretical dispersion curves for Profile 2c. 148
5-8: Modal dispersion curves and global theoretical dispersion curves for Profile 1c. 149
5-9: Global theoretical and experimental dispersion curve for Profile 3a. 151
5-10: Global theoretical and experimental dispersion curve for Profile 3c. 151
5-11: Array experimental and theoretical dispersion curves for Profile 3b. 152
5-12: Array experimental and theoretical dispersion curves for Profile 4c. 153

5-13: Modal dispersion curve with the global theoretical dispersion curve for Profile 3a. 154
5-14: Global experimental and theoretical dispersion curve for Profile 6c. 155
5-15: Array experimental and theoretical dispersion curve for Profile 6c. 156
5-16: Global experimental and theoretical dispersion curves for Profile 7a. 158
5-17: Global experimental and theoretical dispersion curves for Profile 7c. 158
5-18: Modal and array theoretical dispersion curve for Profile 7c. 159
5-19: Array experimental and theoretical dispersion curves for Profile 7a. 160
5-20: Array experimental and theoretical dispersion curves for Profile 7c. 161
5-21: Global theoretical and fundamental mode dispersion curves for Profiles 1a, 1b and 1c. 162
5-22: Theoretical global dispersion curves with a halfspace of 1500 ft/sec at a depth of 10, 30, 50 and 80 ft. 163
5-23: Conventional phase unwrapping of the 100 ft spacing for Profile 2d. 165
5-24: Conventional phase unwrapping of the 200 ft spacing for Profile 2d. 165
5-25: Effective velocity and modal dispersion curves for Profile 2d. 166
5-26: Masking procedure to account for the fundamental mode for Profile 2d, 100 ft spacing. 166
5-27: Masking to account for jump to higher mode for Profile 2d, 200 ft spacing 167
5-28: Individual experimental and array theoretical dispersion curves created through amended masking procedures for Profile 2d. 167

5-29: Individual experimental and array theoretical dispersion curves for Profile 2c with poisson's ratio equal to 0.35. 168
5-30: Individual experimental and array theoretical dispersion curve for Profile 2c with poisson's ration equal to 0.45. 169
5-31a: Simulated dispersion curve from Profile 2d with 100 ft spacing data removed. 171
5-31b: Match achieved from inversion analysis between fundamental mode theoretical dispersion curve and average simulated dispersion curve from Profile 2d. 171
5-32: Comparison between predicted V_S profile from fundamental mode inversion analysis and actual V_S profile for profile 2d 172
A-1: Masked phase plots for receiver spacing of 6, 12, 25, 50, 100 and 200 ft for the Reference Profile. 180
A-2: Masked phase plots for receiver spacing of 6, 12, 25, 50, 100 and 200 ft for the Baseline Profile 1a. 180
A-3: Masked phase plots for receiver spacing of 6, 12, 25, 50, 100 and 200 ft for the Baseline Profile 1b. 181
A-4: Masked phase plots for receiver spacing of 6, 12, 25, 50, 100 and 200 ft for the Baseline Profile 1c. 181
A-5: Masked phase plots for receiver spacing of 6, 12, 25, 50, 100 and 200 ft for the Baseline Profile 1a. 182
A-6: Masked phase plots for receiver spacing of 6, 12, 25, 50, 100 and 200 ft for the Baseline Profile 2b. 182

A-7: Masked phase plots for receiver spacing of 6, 12, 25, 50, 100 and 200 ft for the Baseline Profile 2c. 183
A-8: Masked phase plots for receiver spacing of 6, 12, 25, 50, 100 and 200 ft for the Baseline Profile 2d. 183
A-9: Masked phase plots for receiver spacing of 6, 12, 25, 50, 100 and 200 ft for the Baseline Profile 3a. 184
A-10: Masked phase plots for receiver spacing of 6, 12, 25, 50, 100 and 200 ft for the Baseline Profile 3b. 184
A-11: Masked phase plots for receiver spacing of 6, 12, 25, 50, 100 and 200 ft for the Baseline Profile 3c. 185
A-12: Masked phase plots for receiver spacing of 6, 12, 25, 50, 100 and 200 ft for the Baseline Profile 4a. 185
A-13: Masked phase plots for receiver spacing of 6, 12, 25, 50, 100 and 200 ft for the Baseline Profile 4b. 186
A-14: Masked phase plots for receiver spacing of 6, 12, 25, 50, 100 and 200 ft for the Baseline Profile 4c. 186
A-15: Masked phase plots for receiver spacing of 6, 12, 25, 50, 100 and 200 ft for the Baseline Profile 5a. 187
A-16: Masked phase plots for receiver spacing of 6, 12, 25, 50, 100 and 200 ft for the Baseline Profile 5b. 187
A-17: Masked phase plots for receiver spacing of 6, 12, 25, 50, 100 and 200 ft for the Baseline Profile 5c. 188

A-18: Masked phase plots for receiver spacing of 6, 12, 25, 50, 100 and 200 ft for the Baseline Profile 6a. 188
A-19: Masked phase plots for receiver spacing of 6, 12, 25, 50, 100 and 200 ft for the Baseline Profile 6b. 189
A-20: Masked phase plots for receiver spacing of 6, 12, 25, 50, 100 and 200 ft for the Baseline Profile 6c. 189
A-21: Masked phase plots for receiver spacing of 6, 12, 25, 50, 100 and 200 ft for the Baseline Profile 7a. 190
A-22: Masked phase plots for receiver spacing of 6, 12, 25, 50, 100 and 200 ft for the Baseline Profile 7b. 190
A-23: Masked phase plots for receiver spacing of 6, 12, 25, 50, 100 and 200 ft for the Baseline Profile 7c. 191

List of Tables

Table **Page**

2-1: Soil layer models (*from* Tokimatsu et al., 1992). 39

2-2: Profiles A, B and C soil layer characteristics (*from* Foti, 2000). 42

3-1: Typical values of V_S for soil and rock profiles 61

4-1: Individual layer characteristics of the layered reference profile. 72

4-2: Individual layer characteristics for Profile 1a. 75

4-3: Individual layer characteristics for Profile 1b. 78

4-4: Individual layer characteristics for Profile 1c. 81

4-5: Individual layer characteristics for Profile 2a. 84

4-6: Individual layer characteristics for Profile 2b. 87

4-7: Individual layer characteristics for Profile 2c. 90

4-8: Individual layer characteristics for Profile 2d. 93

4-9: Individual layer characteristics for Profile 3a. 96

4-10: Individual layer characteristics for Profile 3b. 99

4-11: Individual layer characteristics for Profile 3c. 102

4-12: Individual layer characteristics for Profile 4a. 105

4-13: Individual layer characteristics for Profile 4b. 108

4-14: Individual layer characteristics for Profile 4c. 111

4-15: Individual layer characteristics for Profile 5a. 113

4-16: Individual layer characteristics for Profile 5b. 117

4-17: Individual layer characteristics for Profile 5c. 120

4-18: Individual layer characteristics for Profile 6a. 123

4-19: Individual layer characteristics for Profile 6b. 126

4-20: Individual layer characteristics for Profile 6c. 129

4-21: Individual layer characteristics for Profile 7a. 132

4-22: Individual layer characteristics for Profile 7b. 135

4-23: Individual layer characteristics for Profile 7c. 138

Analytical Study of the Spectral-Analysis-of-Surface-Waves (SASW) Method at Complex Geotechnical Sites

Jeff Bertel

Dr. Brent Rosenblad, Thesis Supervisor

Abstract

The Spectral-Analysis-of-Surface-Waves (SASW) method is an accepted means of measuring shear wave velocity (V_S) profiles that has been used successfully for a variety of engineering applications. However, experience in the field has shown that in some settings, SASW measurements have produced results that were inconsistent with the results from other methods of measurement. In this study the effectiveness of the SASW surface wave methodology at complex geotechnical sites was investigated to identify site conditions where the SASW approach may produce erroneous results. This was accomplished by performing analytical simulations of surface wave measurements for a variety of realistic geotechnical conditions involving large and abrupt changes in V_S. The simulated surface wave measurements were processed using both the traditional SASW methodology (termed a global analysis), and a more rigorous approach (termed an array analysis) to generate experimental dispersion curves for the site. The effectiveness of these approaches was evaluated by comparing the experimental results to the true dispersion curve for the site.

It was found that the traditional global analysis approach yielded dispersion curves that underestimated surface wave velocities at long wavelengths for nearly all of the profiles tested. The array approach worked well

for both simple, gradually increasing V_S profiles as well as for many of the more complex profiles with large V_S contrasts. However, for some of the profiles tested, both the global and array analysis produce an experimental dispersion curve that is not consistent with the theoretical dispersion curve for the site. Most notably, this problem was observed for the case of soft-over-stiff profiles, a common profile encountered in the field. The V_S profiles determined under these conditions are greatly in error from the true V_S profiles for the site. These results have implications for site-specific earthquake site response analysis as well as the determination of site classification for code-based earthquake design.

Chapter 1.0 Introduction

1.1 Background

Since the 1960's geophysical methods have been applied to the characterization of near-surface materials for use in geotechnical applications. Traditional methods of near-surface material classification include boring and sampling, cone penetration testing (CPT), and standard penetration testing (SPT). Early work with geophysical methods for applications pertinent to geotechnical engineering primarily focused on the measurement of stress wave velocities. These stress-wave based methods can be used for subsurface profiling and characterization of geotechnical material properties. The measurement of shear wave velocity (V_S) profiles has particular application in the area of soil dynamics and earthquake engineering where V_S profiles can provide soil stiffness information for use in earthquake site response analysis and evaluation of soil liquefaction potential (Andrus and Stokoe, 1999). Other common applications for surface wave measurements include waste material characterization, pavement subgrade evaluation, and ground improvement quality control (Stokoe et al., 2004).

Measurement of shear wave velocity profiles can be accomplished through either intrusive or non-intrusive means. Intrusive methods require either boreholes or a cone penetrometer and involve measuring the propagation time of compression (P) and shear wave (S) between two or more points. Common intrusive methods include the crosshole method (ASTM, 1991), downhole method (Redpath et al., 1982; Redpath and Lee, 1986; EPRI, 1993), seismic

cone penetrometer (Robertson and Campanella, 1985), and suspension logger (Nigbor and Imai, 1994). Non-intrusive measurements are performed with all of the instrumentation located on the ground surface. Common non-intrusive methods applied in geotechnical engineering applications include seismic refraction and surface wave methods. Widely used surface wave methods include the Spectral-Analysis-of-Surface Waves (SASW) method (Heisey et al., 1982; Nazarian and Stokoe, 1984; Stokoe et al., 1994) and the Multi-Channel-Analysis-of-Surface Waves (MASW) method (Park et al., 1999). The cost associated with intrusive methods is typically greater than that involved with non-intrusive methods. Due to their cost efficiency, surface wave methods have found wide application in geotechnical engineering in recent years.

1.2 Problem Statement

In the last 20 to 30 years, the SASW method has been successfully applied to a variety of geotechnical problems (Stokoe et al., 1994). In general, the results from SASW measurements have compared well with traditional borehole methods. However, in some instances, SASW results have produced V_S profiles that were inconsistent with other measurements (Brown et al., 2002). Past studies have shown that at sites with complicated layering of soil and rock, large contrasts in V_S may confine stress waves in some layers and cause multiple reflections and refractions which result in different propagation velocities at the same frequency (Stokoe et al., 1994). The result is that the surface wave velocity measured by the SASW method is often not a single mode but is instead

an effective velocity resulting from the superposition of multiple modes. It is hypothesized that under some conditions, the conventional 2-receiver phase unwrapping procedure used in SASW data processing will produce an experimental effective velocity dispersion curve that is inconsistent with the theoretical effective velocity dispersion curve for the site. This inconsistency could result in an erroneous V_S profile and possible misclassification of geotechnical sites for earthquake engineering applications.

1.3 Project Objectives and Scope

The primary objectives of this research are to investigate the effectiveness of the SASW surface wave methodology at complex geotechnical sites and identify conditions where the SASW approach may produce erroneous results. This was accomplished by performing analytical simulations of surface wave measurements for a variety of realistic geotechnical conditions involving large and abrupt changes in V_S. The synthetic time records generated for the study were interpreted and processed using the SASW methodology to create a simulated experimental dispersion curve. The simulated SASW results were compared to the true dispersion curves for each of the sites.

The scope of this project was limited to investigating four general shear wave velocity profile types: 1) gradually increasing V_S (reference profile) 2) high V_S soil over lower V_S soil (stiff-over-soft) 3) embedded high V_S layer in soil with lower V_S (soft-stiff-soft), and 4) embedded low V_S layer in soil with higher V_S (stiff-soft-stiff). The four general profiles were created by introducing higher

velocity layers into the reference profile. Each of the four general profiles was varied by changing velocity contrasts, layer thicknesses, and layer depths. Overall, simulated SASW results were generated for 23 different stiffness profiles in this study.

1.4 Thesis Organization

This thesis is organized into 6 chapters. Chapter 2 reviews the principles of surface wave propagation, surface wave measurements and provides a literature review of past studies regarding surface wave measurements at complex soil profiles. Chapter 3 presents the methodology used to generate the synthetic time records and theoretical surface wave dispersion curves. The analysis and interpretation of the simulated data are also discussed in Chapter 3. Chapter 4 is a presentation of the results of the analysis for each of the simulated profiles analyzed in this study. Chapter 5 presents analyses and discussion of the simulated results and the practical implications of the findings. Lastly, Chapter 6 contains conclusions regarding the content of this research and recommendations for future research.

Chapter 2 Surface Wave Propagation & Measurement

2.1 Introduction

In this chapter, surface wave propagation in both a uniform and layered halfspace will be discussed. The differences between modal and effective phase velocity dispersion curves will be presented. In addition, the data collection, data processing and data analysis methods using the SASW approach are described. Lastly, the chapter presents a review of relevant research regarding the measurement of surface waves at complex geotechnical sites.

2.2 Surface Wave Propagation in a Uniform Halfspace

Energy excited at the surface of an elastic half-space will produce both body wave propagation into the half-space as well as surface wave propagation along the solid/air interface. Body waves propagate as compression or primary waves (P) and shear or secondary waves (S). The surface wave, called a Rayleigh wave, results from the interaction of P and S waves with the stress-free interface. Although P and S waves form the Rayleigh wave, the attributes of the Rayleigh wave are distinctly different than those of its parent waves.

Rayleigh wave motion decreases exponentially with depth. At a single frequency, most of the particle motions occur at depths less than one wavelength below the surface. The particle motion of the Rayleigh surface wave is a retrograde elliptical motion at the surface, containing both vertical and horizontal

motions. Figure 2-1 demonstrates the normalized wave amplitudes of the vertical and horizontal particle motions with respect to Poisson's ratio.

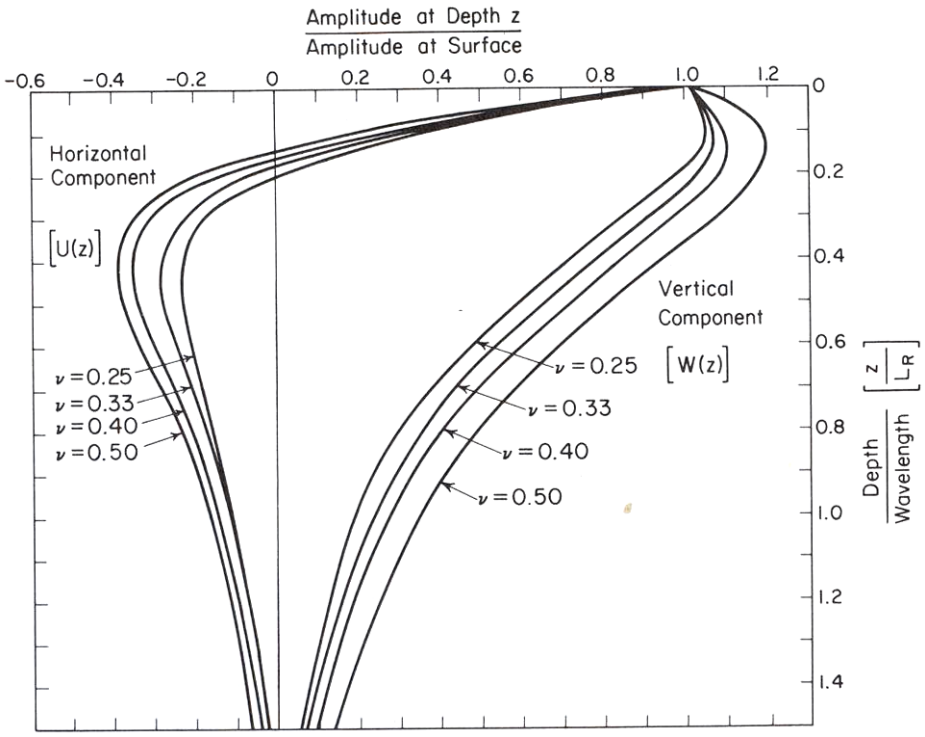

Figure 2-1 **Normalized vertical and horizontal particle motions for a Raleigh-type surface wave (*from* Richart et al., 1970).**

In a soil medium with a Poisson's ration of 0.25, 67% of the energy resulting from an impact is converted to Rayleigh surface waves. The energy converted to shear waves and compression waves is 26% and 7%, respectively (Miller and Pursey, 1955).

Rayleigh waves propagate in a cylindrical wavefront from a circular source while body waves propagate with a hemispherical wavefront, as shown in Figure 2.2.

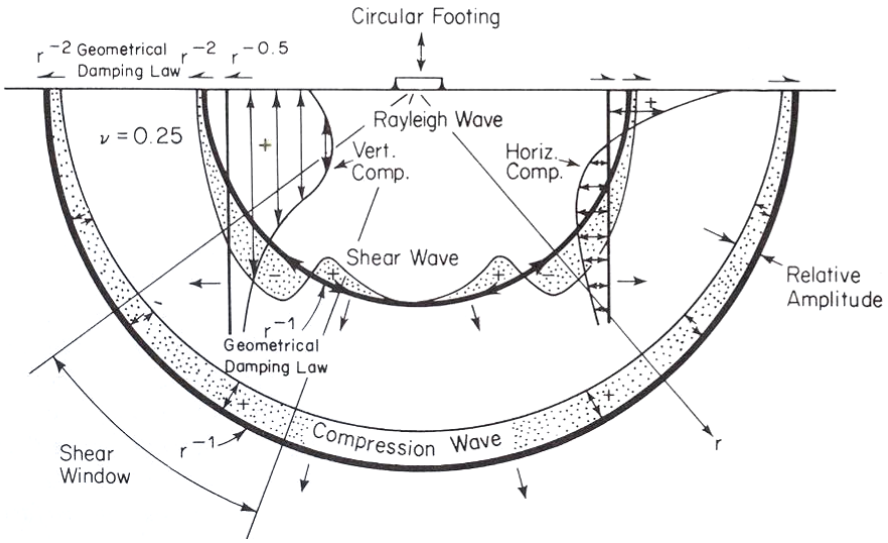

Figure 2-2 Wave generated from a symmetric circular footing on a homogenous elastic half-space (*from* Richart, Hall and Woods, 1970).

In a uniform halfspace, surface wave amplitudes decrease in proportion to$1/\sqrt{r}$, where r is the radius from the energy source. Body waves decrease in proportion to $1/r^2$ due to geometric spreading at the surface. Since the majority of energy resulting from an impact is converted to surface wave motion and surface waves have lower geometric damping, surface wave motions are generally the dominate motion measured at the surface away from the source.

The relationship between V_S and Rayleigh wave velocity (V_R) in a uniform halfspace is solely a function of Poisson's ratio (Achenbach, 1973). The approximate relationship is:

$$V_R = \frac{0.86 + 1.14\nu}{1 + \nu} V_S \qquad (2.1)$$

where ν is Poisson's ratio of the material. The ratio of V_R to V_S as a function of Poisson's ratio is shown in Figure 2-3. The ratio can range from approximately 0.88 to 0.96 for Poisson's ratios of 0 to 0.5, respectively.

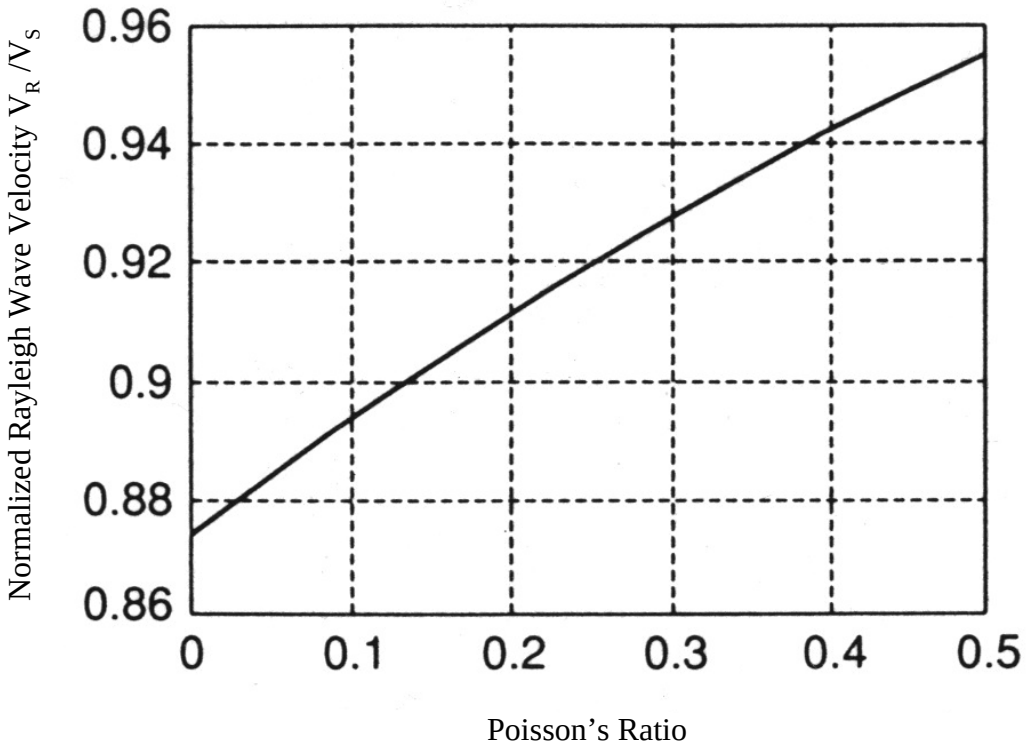

Figure 2-3 **Ratio of Rayleigh wave velocity to shear wave velocity as a function of Poisson's Ratio (*from* Bedford and Drumheller, 1994).**

The relationship between surface wave velocity and compression wave velocity (V_P) can be described by using an elastic relationship for body waves:

$$\frac{V_P}{V_S} = \sqrt{\frac{2(1+\nu)}{1-2\nu}} \tag{2.2}$$

and substituting equation 2.1 into equation 2.2.

$$\frac{V_R}{V_P} = \left(\frac{1+\nu}{0.86+1.14\nu}\right) * \sqrt{\frac{1-2\nu}{2(1+\nu)}} \tag{2.3}$$

Figure 2-4 shows the relationship between V_P, V_S and V_R as a function of Poisson's ratio for a continuous semi-infinite elastic medium with constant values of material density and small-strain stiffness.

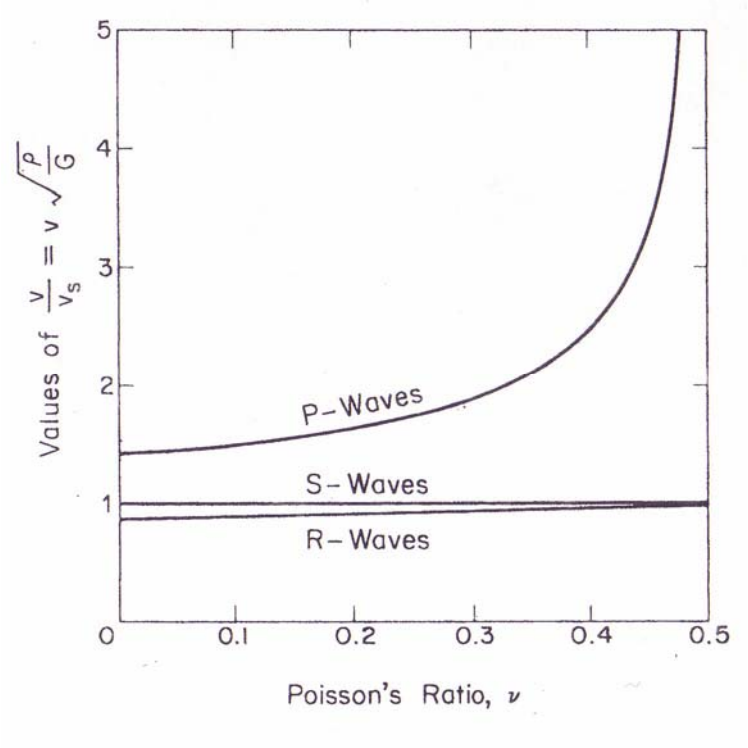

Figure 2-4 Relationship between Poisson's ratio and V_P, V_R and V_S waves (*from* Richart, Hall and Woods, 1970).

For a uniform, elastic halfspace, surface wave velocities are non-dispersive, meaning that V_R is independent of frequency. A dispersion curve is a plot of surface wave velocity versus frequency or wavelength. A dispersion curve for a uniform halfspace with a V_S equal to 500 fps is shown in Figure 2-5.

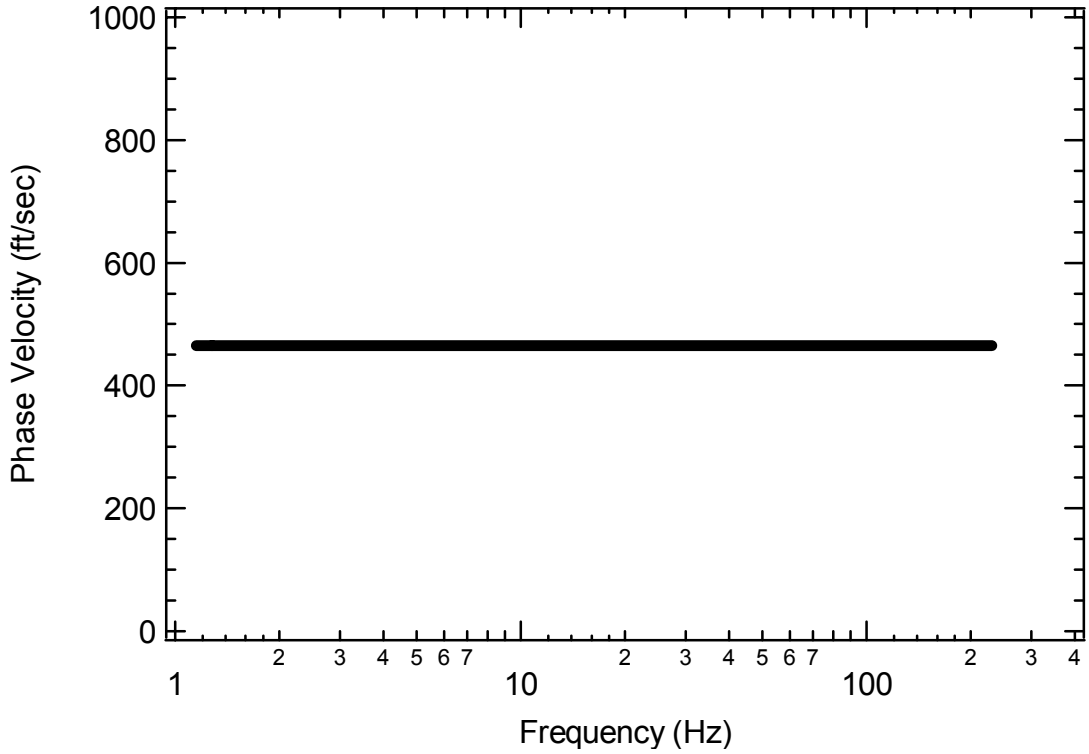

Figure 2-5 **Dispersion curve for a homogeneous halfspace with a shear wave velocity equal to 500 fps and ν =0.25.**

2.3 Surface Wave Propagation in a Layered Halfspace

A layered halfspace consists of strata with changing elastic properties with depth. Surface waves propagating in a layered halfspace are dispersive, meaning waves with different frequencies will travel at different velocities. Figure 2-6 shows a layered profile with V_S of 300 and 400 fps and thicknesses of 10 feet overlying a halfspace with V_S equal to 500 fps. Figure 2-7 is the corresponding surface wave phase velocity dispersion curve showing the V_R versus frequency for the layered profile shown in Figure 2-6. The velocity transitions from approximately 280 fps at high frequencies (20 to 150 Hz) to 450 fps at low

frequencies (< 2 Hz). Lower frequencies penetrate deeper (as shown in Figure 2.1) and hence sample the deeper high velocity portions of the profile.

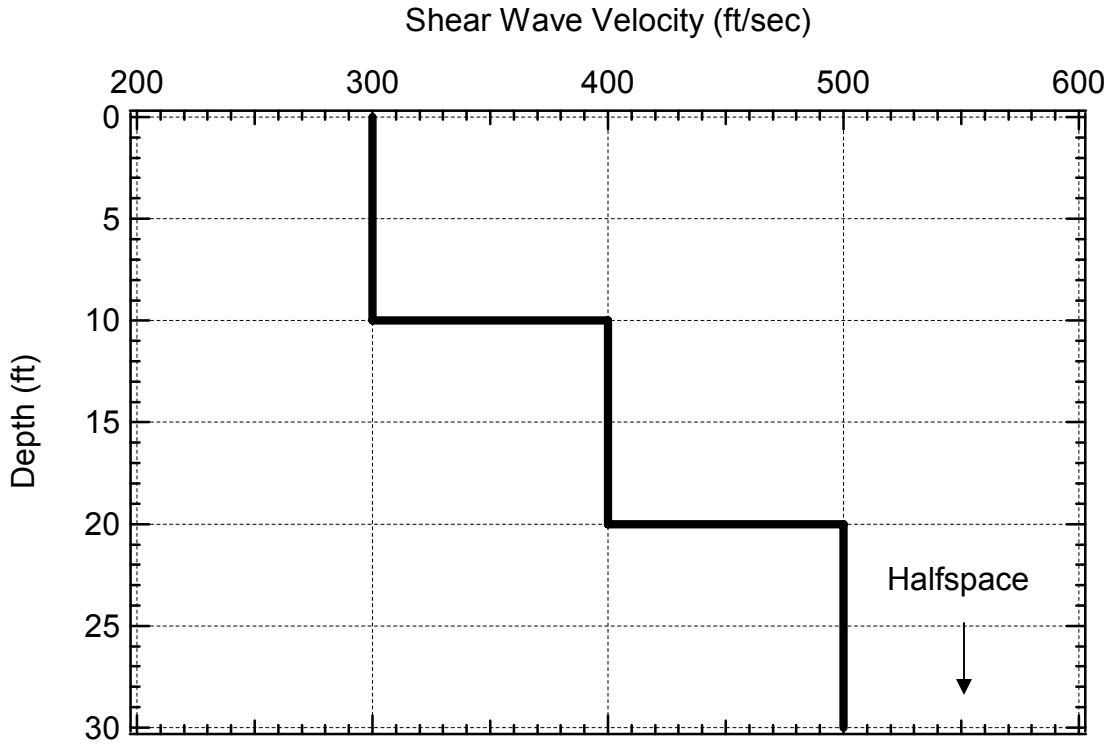

Figure 2-6 Three-layer, non-homogeneous profile.

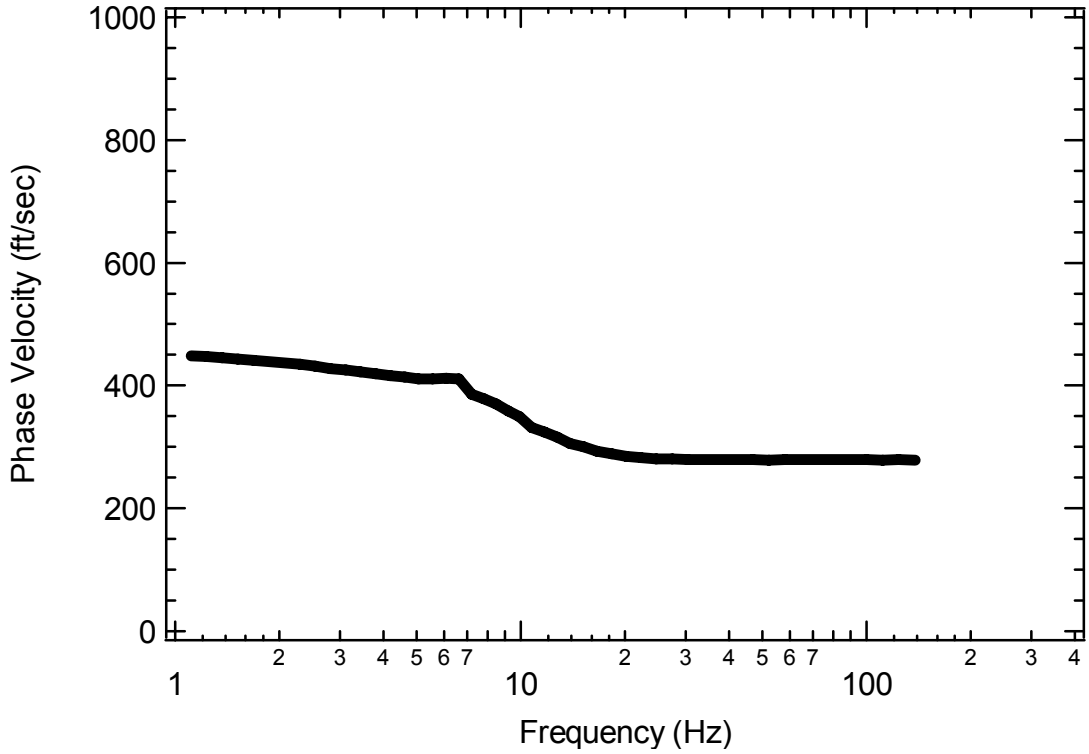

Figure 2-7 Dispersion curve for three layer profile shown in Figure 2-6.

In a layered halfspace with large velocity contrasts multiple modes of propagation may be generated due to stress waves being confined in some layers and multiple reflections and refractions of stress waves, which result in different propagation velocities at the same frequency or wavelength (Stokoe et al., 1994). Higher Rayleigh wave modes arise from the interaction of reflected P and S waves from layer interfaces.

2.4 Modal versus Effective Phase Velocity

Surface wave dispersion can be presented in different ways. A modal dispersion curve presents the phase velocity of the fundamental and higher modes versus frequency or wavelength. An effective dispersion curve is the phase velocity determined from the superposition of modes plotted versus

frequency or wavelength. The effective phase velocity is a local quantity that will depend on position relative to the source (Stokoe et al., 2004). In a layered halfspace with gradual V_S changes, the V_R will tend to follow the fundamental mode. When the V_S contrast between layers in a halfspace become sufficiently large a superposition of modes will result and the effective dispersion curve will deviate from the fundamental mode.

There are two general approaches to the measurement of surface wave velocities. The first approach involves sampling extensively in space and using wavefield transformation procedures to isolate individual modes (Park et al., 1999). A common method used for this type of measurement is the Multi-channel-Analysis-of-Surface-Waves (MASW) method. The second approach involves performing measurements at fewer spatial locations and determining an effective phase velocity that includes the contributions of multiple modes and body waves. A common method that uses this procedure is the Spectral-Analysis-of-Surface- Waves (SASW) method. The first approach typically uses a theoretical dispersion curve that is the fundamental mode, whereas the second approach requires calculation of an effective phase velocity that includes contribution from body and surface wave modes. The SASW approach is the focus of this study and is described in the following section.

2.5 Spectral-Analysis-of-Surface-Waves (SASW) Method

2.5.1 SASW Overview

The SASW method was initiated in the late 1970's at the University of Texas at Austin (Nazarian and Stokoe, 1984). The method built on an existing method called the steady-state Rayleigh wave method (Richart et al., 1970). Initially it was intended to be used as a tool for characterization of pavement systems, but subsequently its application has grown and now includes earthquake site response, pavement stiffness characterization, liquefaction resistance evaluation, waste characterization in landfills, and offshore applications (Stokoe et al., 2004).

The basic approach of the SASW method is to measure an experimental dispersion curve and determine a V_S profile that produces a theoretical dispersion curve matching the experimental curve. The approach can be divided into three general steps: 1) data collection 2) data processing and 3) data analysis. In the data collection step, field measurements are performed to determine the phase difference as a function of frequency between two receivers located on the ground surface. Because it is not practical to collect all data from a single source and single receiver set-up, multiple receiver spacings and sources are used in this step. In the data processing step the phase differences measured between receivers are transformed to an experimental dispersion curve which relates the phase velocity to frequency (or wavelength).

In the data analysis step, a theoretical dispersion curve is calculated from an assumed V_S profile and an iterative forward modeling or inversion procedure is used to find the V_S profile that provides the best match between the theoretical and experimental dispersion curves. The details of each of these analysis steps are provided in the following sections along with example data.

2.5.2 Data Collection

The objective of field measurements using the SASW method is to measure the phase difference between two receivers over a wide range of frequencies. A typical measurement configuration is shown in Figure 2-8. The testing arrangement includes a source, two receivers, and a data acquisition system. The receivers are typically arranged about a common midpoint with the source to near-receiver distance equal to the distance between the two receivers. Maintaining a sufficient distance between the source and first receiver allows the surface wave to be established and minimizes near-field effects (Sanchez-Salinero, 1987).

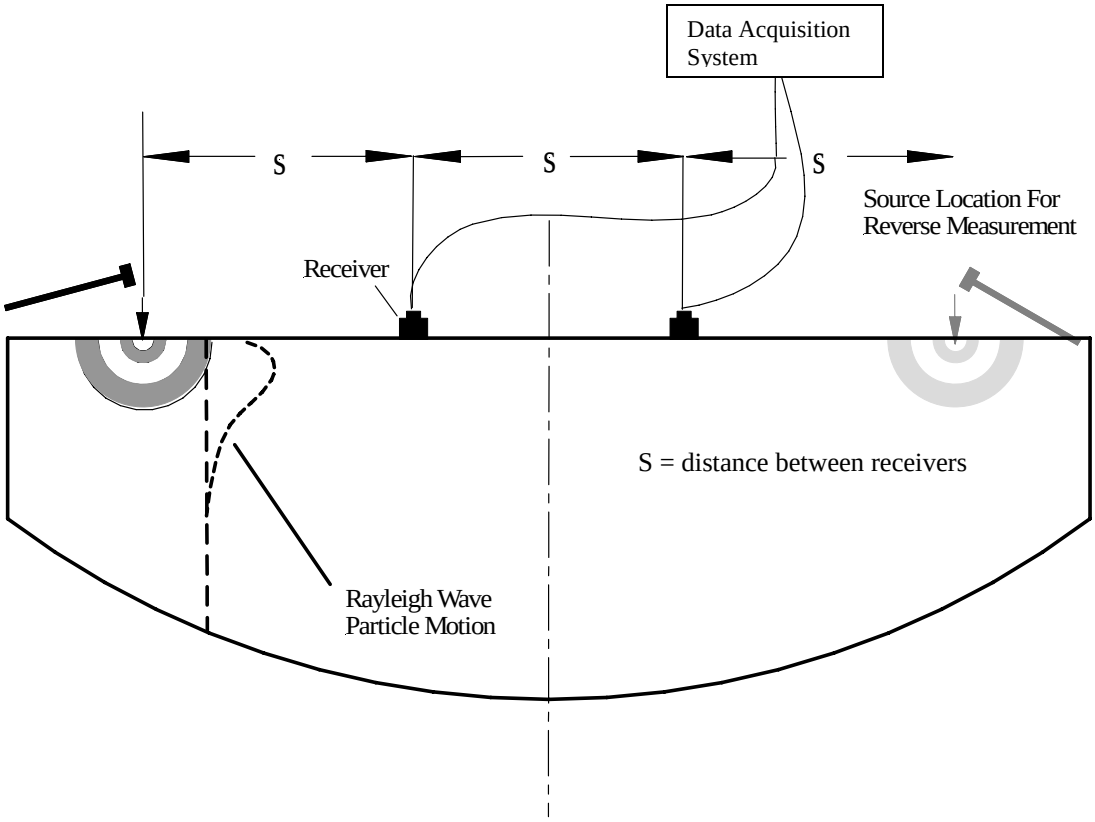

Figure 2-8 Typical SASW testing arrangement showing forward and reverse impacts.

The measurement is initiated with closely-spaced receivers and a high-frequency source. Because it is not possible to generate and measure a broad range of frequencies from a single source, multiple sources and receiver spacings are used. Increasing the receiver spacing and exciting lower-frequency energy allows for measurement to greater depths. Measurements at each receiver spacing are repeated with the source in the reverse location, as shown in Figure 2-9, to minimize the effects of dipping layers, reduce effects of lateral inhomogeneity between the source and the first receiver, and compensate for any potential phase differences in the measurement equipment (Joh, 1996).

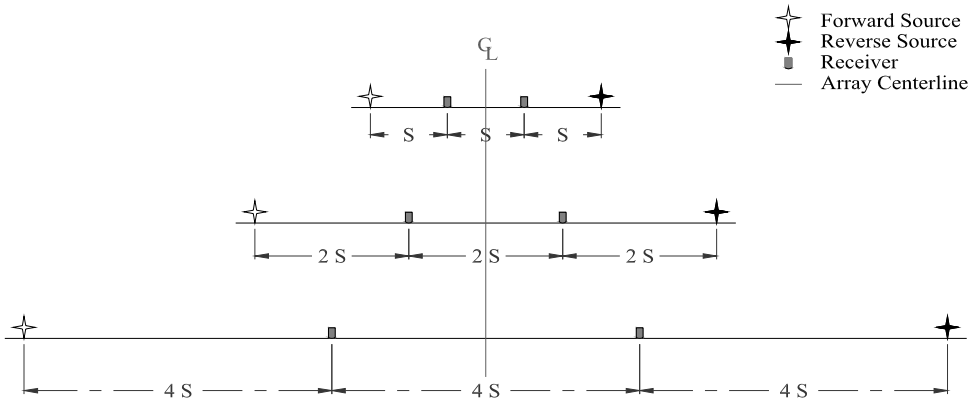

Figure 2-9 **Receiver arrangement showing common mid-point array for SASW testing, where S is equal to the distance between receivers (Hollrah, 2005).**

Selection of receiver spacing, frequency span, and appropriate source and receivers should be based on the expected V_S profile at the site and the desired profiling depth. The appropriate receiver spacing is chosen so that data are obtained over the wavelength range of interest. Typically, V_S profiles can be obtained to depths of approximately one-half of the maximum wavelength measured. The wavelength (λ) is related to the phase velocity (V_{ph}) and the frequency (f) by:

$$V_{PH} = f \cdot \lambda \qquad (2.4)$$

The minimum receiver spacing should be one to three times the minimum wavelength expected to be measured. The largest receiver spacing should be approximately one-half the longest wavelength expected to be generated. V_S profiles can be resolved to a depth of about one-half of the maximum wavelength, therefore, the maximum receiver spacing is approximately equal to the profiling depth of interest. The measurements are typically initiated at the

shortest receiver spacing and additional measurements are performed by doubling the receiver spacing up to the maximum wavelength, as shown in Figure 2-9. Matching sources with the desired frequency content is an important aspect of surface wave testing. Typical sources used in SASW testing are discussed in the following section.

2.5.2.1 Sources Used in SASW Testing

An appropriate source for SASW measurements is able to generate energy over a band of frequencies which covers the frequency span used in the measurements. Typical sources can be subdivided into three categories: transient, steady state, and random wave sources. The physical size of a source is highly variable and can range from a small hand-held hammer to a large Vibroseis truck. Figure 2-10 shows a variety of potential sources that can be used for SASW measurements.

Figure 2-10 Transient hammer impact source (left), random noise bulldozer source (top right), continuous steady state vibroseis source (bottom right).

Transient sources such as impact hammers and drop weights are most commonly used for shallow (<100 ft) profiling. In general, more massive impact sources will generate lower frequency (longer wavelength) energy at a given site. A continuous steady-state source, such as a Vibroseis, generates energy at a single frequency and has the capability to sweep through a suite of frequencies. Vibroseis sources are used for deep surface wave profiling (>250 ft) applications. SASW performed with a steady-state source is typically operated in a swept-sine mode and produces high signal-to-noise ratios due to the concentration of energy at individual frequencies (Joh, 1996). Random wave sources, such as a bulldozers or other heavy machinery, can be effective for profiling to intermediate depths (100 to 250 ft).

2.5.2.2 Receivers Used in SASW Testing

The ground motions produced by SASW sources are very small and require sensitive receivers. Typically, vertically-oriented geophones are used in SASW measurements to measure vertical particle velocity at the ground surface. Geophones are sensitive instruments that generate their output from a coil moving through a magnetic field. The induced voltage is proportional to the ground velocity at frequencies above the natural frequency of the geophone. At typical soil sites, measurements are performed in the frequency range of less than 5 to hundreds of Hertz (Hz). Therefore, geophones with natural frequencies of 4.5 Hz and lower are typically used for geotechnical applications.

An accelerometer can be used for SASW measurements when the frequency range of interest is very high, such as with measurements on rock. Two types of accelerometers that are typically used are charge-mode accelerometers and voltage-mode accelerometers. Charge-mode accelerometers contain only the sensing element and are used in conjunction with a signal conditioner to produce high impedance voltage output. Voltage-mode accelerometers have built-in microelectronic signal conditioning which converts high-impedance charge signal to a low-impedance voltage signal.

2.5.2.3 Data Acquisition System

Time records are digitized and recorded using a dynamic signal analyzer or a computer-based data acquisition interface. The data acquisition system is used to optimize the measurement by setting the frequency span to provide the best resolution available over the range of frequencies of interest. It is also used to average multiple impacts at the same receiver spacing to improve the signal-to-noise ratio. An example of simulated time records from two locations 200 ft and 400 ft from a vertically oriented disk load are shown in Figure 2-11.

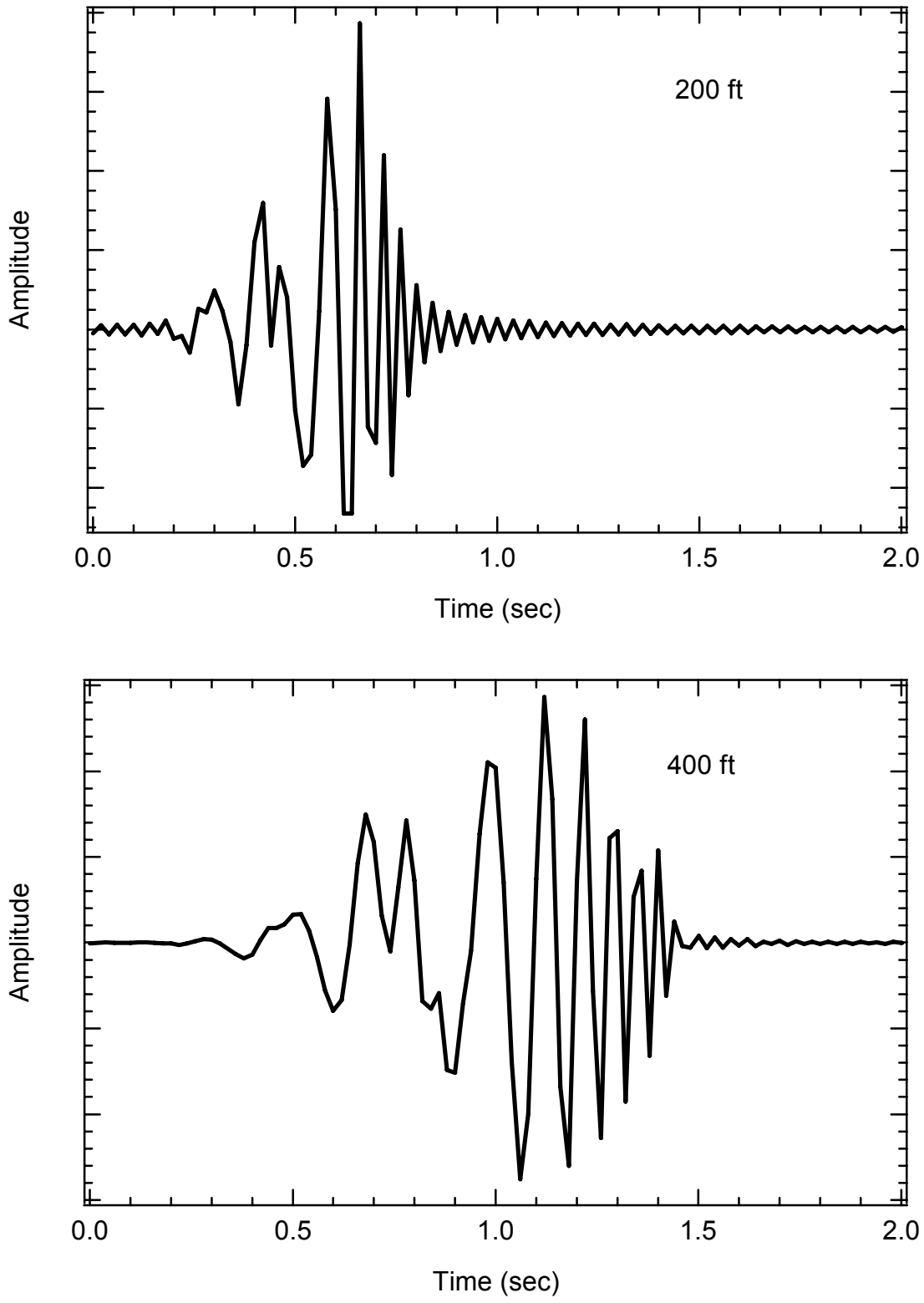

Figure 2-11 **Time records at 200 ft (Top) and 400 ft (Bottom) from a vertically oriented disk load.**

The phase difference between the two receiver locations is determined by using a Fast Fourier Transform (FFT) procedure to transform the time domain records into the frequency domain. After transformation into the frequency domain the wave components at a certain frequency are expressed as complex numbers and can be described by the following equations:

$$z_1 = A_1(\cos\phi_1 + i\sin\phi_1) \tag{2.5}$$

$$z_2 = A_2(\cos\phi_2 + i\sin\phi_2) \tag{2.6}$$

The phase difference between the two wave components, Φ_2-Φ_1, can be determined from either of the following two complex number operations:

$$\frac{z_2}{z_1} = \frac{A_2}{A_1}(\cos(\phi_2 - \phi_1) + i\sin(\phi_2 - \phi_1)) \tag{2.7}$$

$$z_2 z_1^* = A_1 A_2(\cos(\phi_2 - \phi_1) + i\sin(\phi_2 - \phi_1)) \tag{2.8}$$

Equation 2.7 corresponds to the frequency response spectrum and equation 2.8 corresponds to the cross power spectrum (Joh, 1996). Figure 2-12 shows the cross power spectrum calculated from the time records shown in Figure 2-11. This phase plot shows the relative lead or lag in phase (+ or – 180 degrees) between the two receivers as a function of frequency. Calculation of the experimental dispersion curve from the phase plot is presented in the following section.

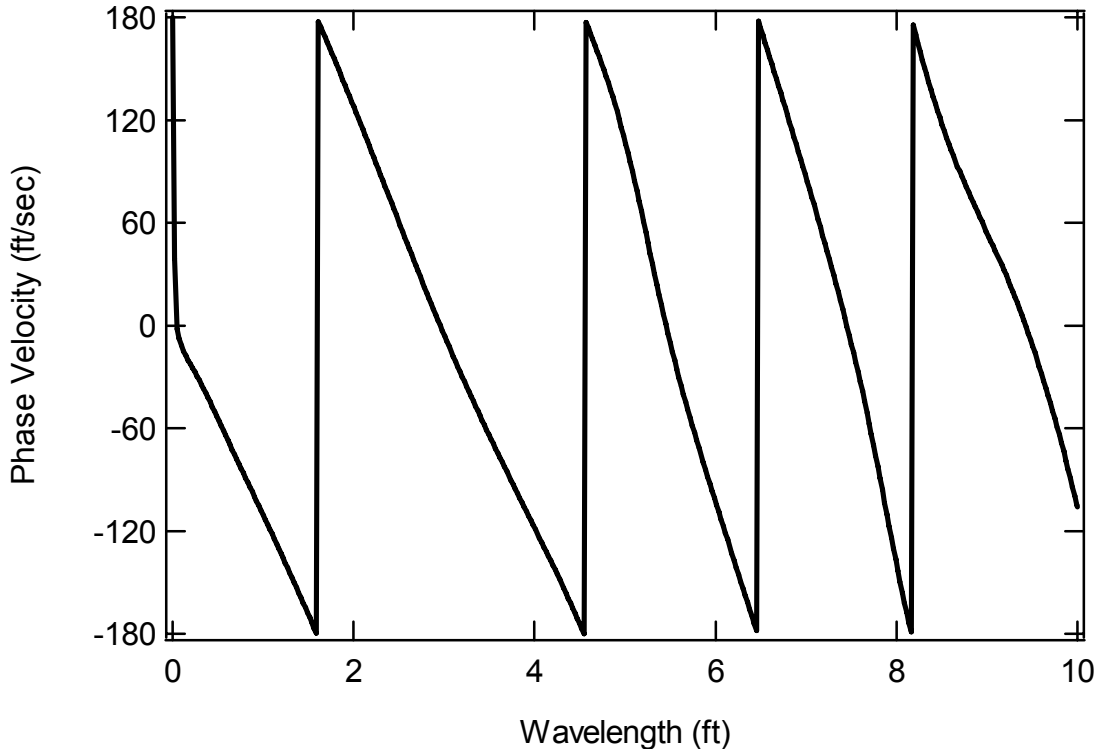

Figure 2-12 Wrapped phase spectrum for receiver spacing of 200 ft.

2.5.3 Data Processing

Data processing involves interpreting the phase spectra generated in the field and constructing an experimental dispersion curve. The travel time of a wave at a given frequency is evaluated using the phase difference between the receiver pair. Figure 2-13 illustrates the phase difference between two time signals for a wave traveling with a frequency of f_o (Joh, 1996). The phase difference between each receiver is calculated using the following expressions.

$$y_1 = \sin(2\pi f_o t) \tag{2.9}$$

$$y_2 = \sin(2\pi f_o (t - t_1)) \tag{2.10}$$

$$= \sin(2\pi f_o t - 2\pi f_o t_1) \tag{2.11}$$

$$= \sin(2\pi f_o t - \phi) \qquad (2.12)$$

Where y_1 is the wave motion at location A, y_2 is the wave motion at location B, t is the time it takes for a wave to travel from the source to location A and t_1 is the time it takes for the wave to travel from location A to location B. Φ is the phase difference between location A and B for a frequency of f_o (Joh, 1996).

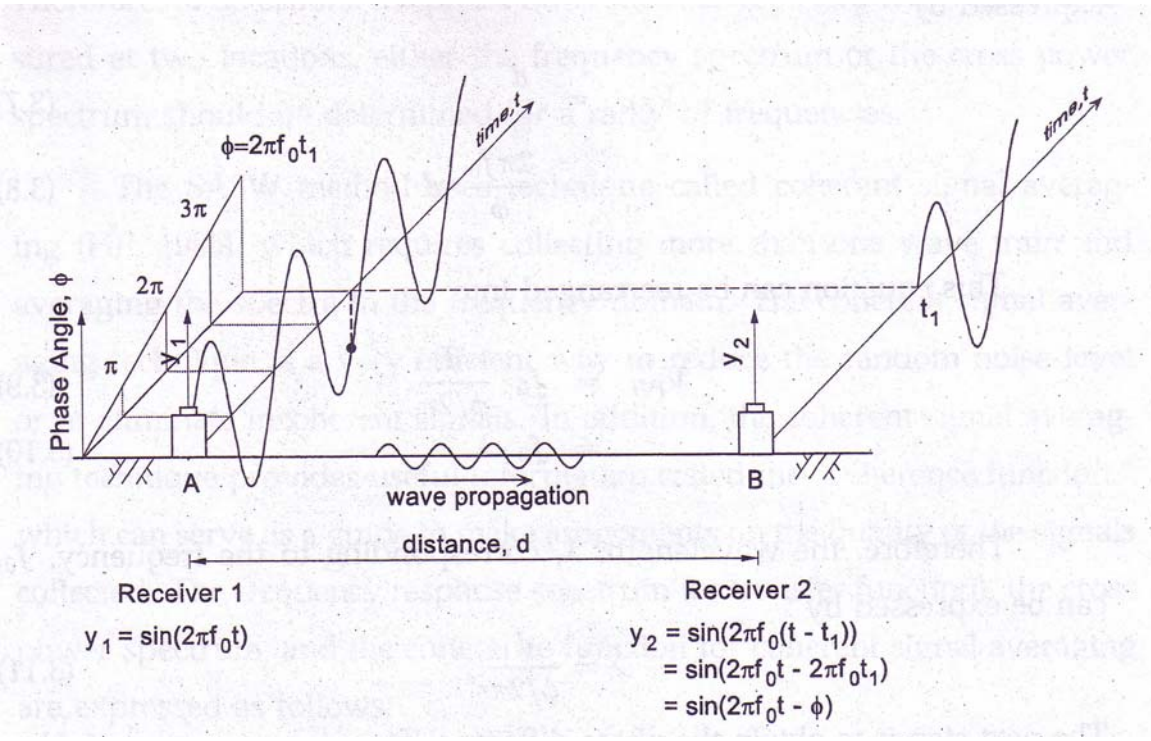

Figure 2-13 Illustration of the phase difference between two time signals (*from* Joh, 1996).

The phase difference between the two locations for the wave traveling with a frequency f_o can be related to the travel time by the following equation.

$$\phi = 2\pi f_o t_1 \qquad (2.13)$$

The phase velocity corresponding to the frequency f_o can then be calculated using the distance (d) between location A and B and the following equation:

$$V_{PH} = \frac{d}{t_1} \qquad (2.14)$$

Substituting equation 2.13 into 2.14 yields:

$$V_{PH} = d * \frac{2\pi f}{\phi} \qquad (2.15)$$

The phase angle shown in equation 2.15 is the cumulative phase between the two receiver locations. To obtain this value the phase plot calculated in the field must be unwrapped. This process involves identifying the number of cycles or "jumps" in the unwrapped phase spectra. An example of an unwrapped phase spectra determined from a wrapped phase spectrum is shown in Figure 2-14. The unwrapping procedure also involves masking out of data that should not be included in the calculation of the dispersion curve. This includes near-field data (wavelengths longer than twice the source-to-receiver spacing) and data with low signal-to-noise ratios. The shaded portion in Figure 2-14 shows the data that are typically masked out due to near-field effects.

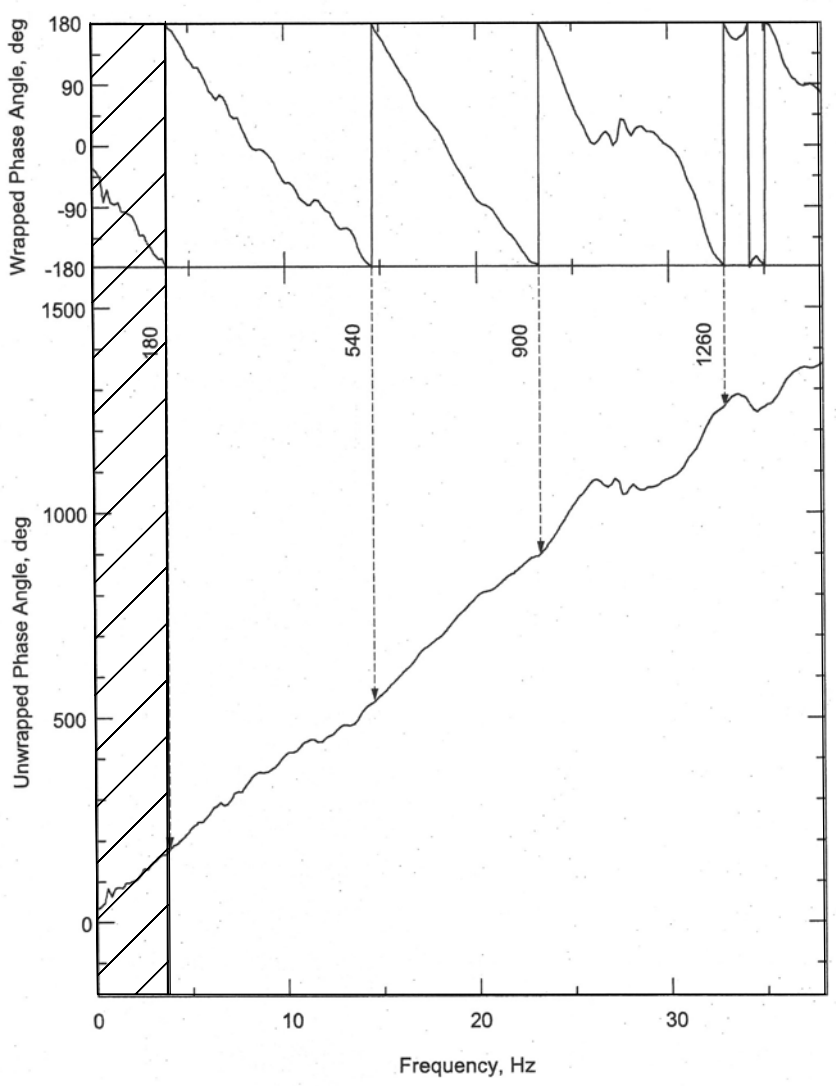

Figure 2-14 Comparison of a wrapped phase spectrum and an unwrapped phase spectrum (*from* Joh, 1996).

Individual dispersion curves are calculated for each receiver pair using the unwrapped phase plot, receiver spacing and Equation 2.15. Figure 2-15 shows the individual dispersion curve calculated from the phase plot shown in Figure 2-12. The individual dispersion curves from several receiver spacings are combined to form the composite dispersion curve for the site. Figure 2-16 shows the composite experimental dispersion curve created from six receiver spacings.

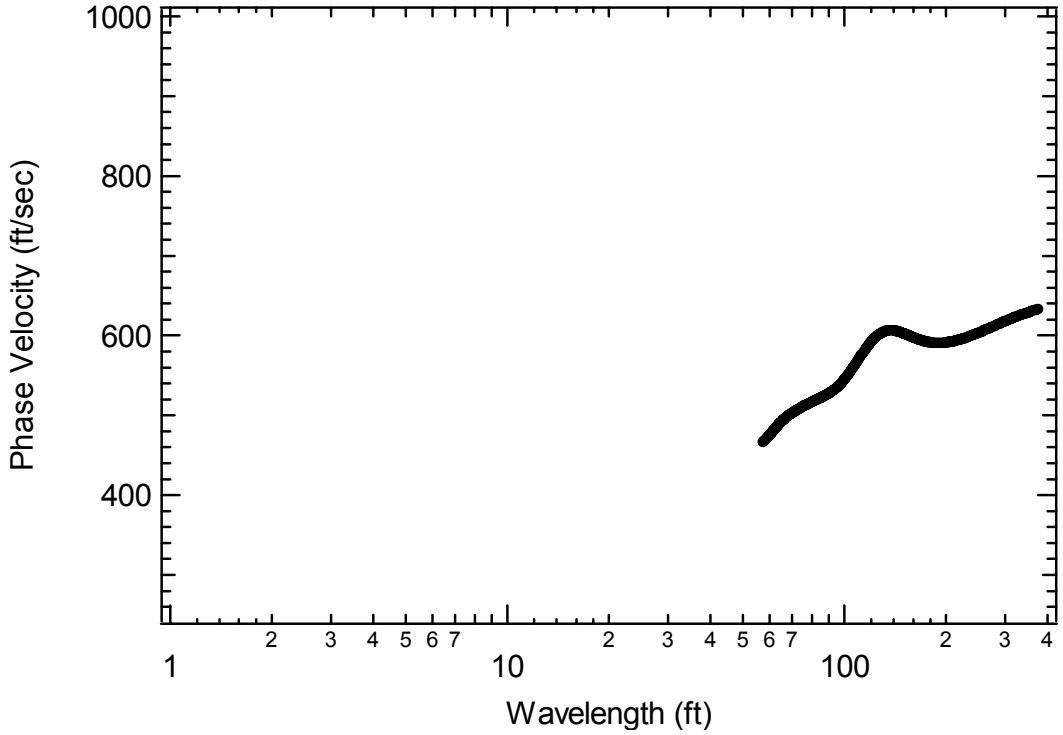

Figure 2-15 **Dispersion curve for 200 ft receiver spacing generated from the phase plot shown in Figure 2-12.**

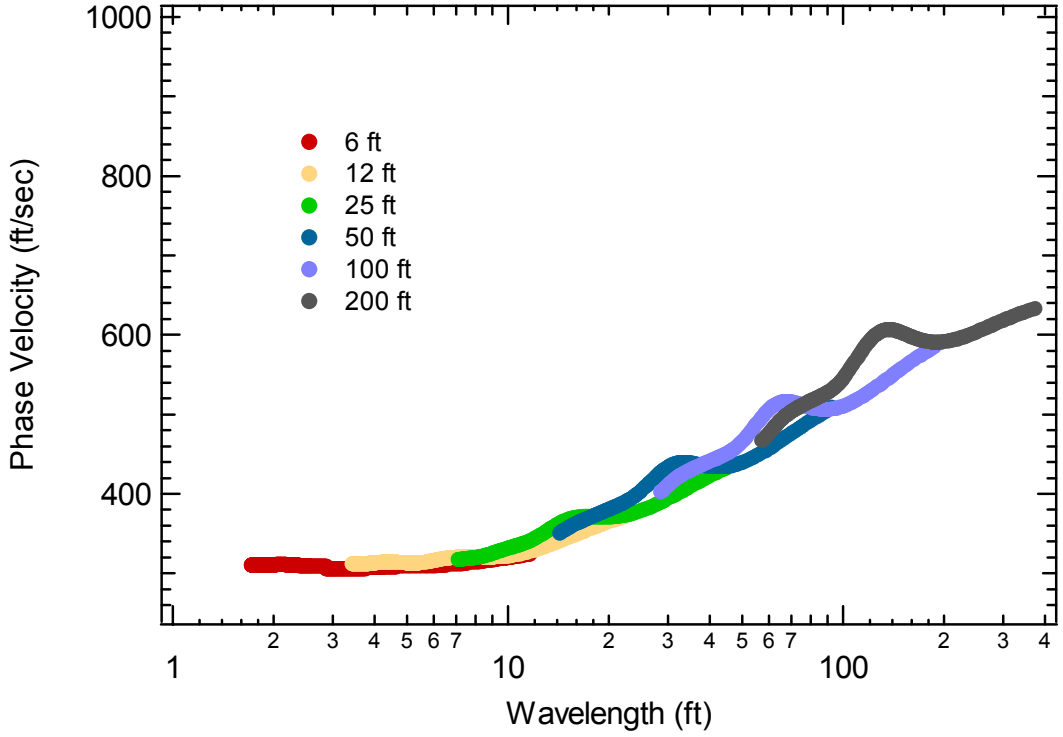

Figure 2-16 **Composite dispersion curve for six receiver spacings.**

2.5.4 Data Analysis

The final step in SASW measurements is the data analysis procedure. This procedure involves generating an average experimental dispersion curve for the site and performing a forward modeling or inversion analysis to fit a theoretical dispersion curve to the experimentally determined dispersion curve. There are two different approaches to SASW data analysis. The conventional SASW approach, which will be termed a *global analysis*, involves generating a single average experimental dispersion curve from the composite dispersion curve for the site and finding the V_S profile that provides the best fit between a global theoretical dispersion curve and the average experimental dispersion curve. The second approach, which will be termed an *array analysis,* involves generating individual average experimental dispersion for each of the receiver spacings and determining a single V_S profile that provides the best fit to all of the individual dispersion curves. The steps involved in these two approaches are discussed below.

2.5.4.1 Averaging Procedures

The first step in the analysis procedure is to create an average dispersion curve from the composite dispersion curve for the site. The conventional method for averaging the experimental dispersion curve is to create a single average dispersion curve for the site consisting of approximately 30 to 50 frequency points. Averaging effectively creates an experimental dispersion curve that represents the general trend of the data. Several averaging procedures have been proposed. Examples of averaging procedures are those presented by Rix

(1987) and Nazarian and Desai (1993). Another procedure, presented by Joh (1996) and used in this study, uses a moving average to extract basic trends in the data. The single average dispersion curve created from the composite dispersion curve is called the global experimental dispersion curve. An example of a global experimental dispersion curve is plotted with the composite dispersion curve in Figure 2-17.

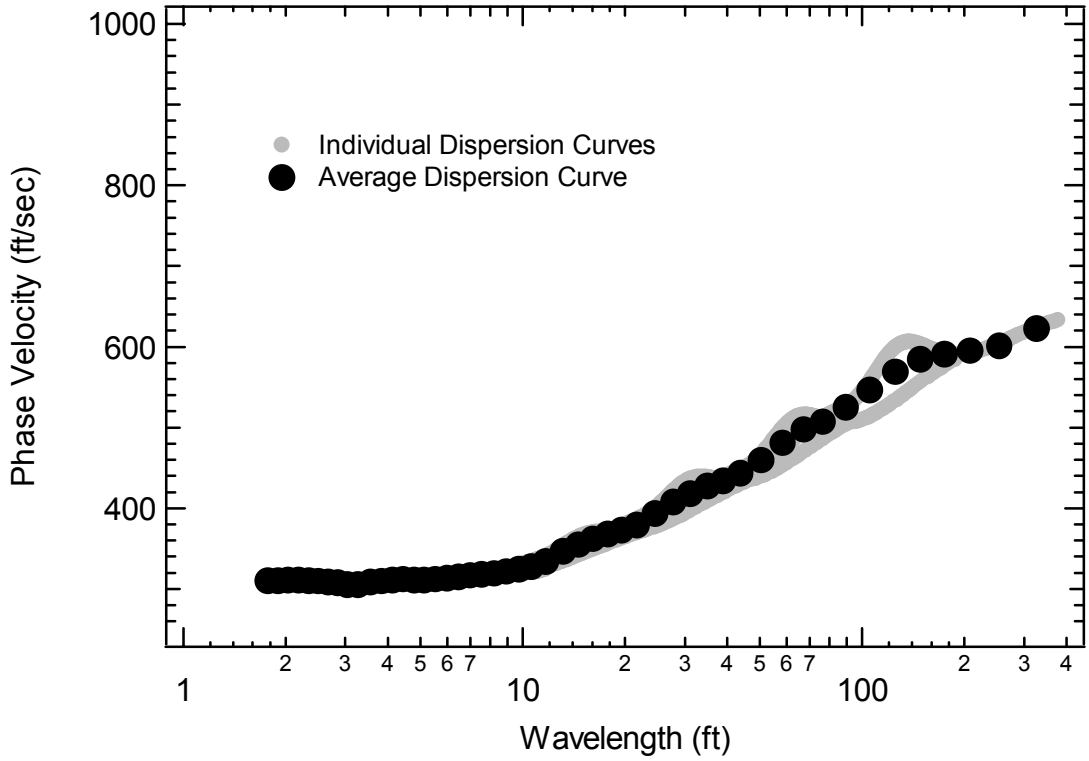

Figure 2-17 Example global experimental dispersion curve generated from the individual dispersion curves shown in Figure 2-16.

At complex sites, the composite dispersion curve may not follow a single trend and it may not be possible to accurately depict the dispersion data with a single average dispersion curve. In these cases, average dispersion curves are created for each of the individual dispersion curves from each receiver pair. Like the global dispersion curve, the averaging algorithm is based on a moving

average for each individual dispersion curve. The experimental data are again reduced to 30 to 50 frequency points. The difference between the experimental array dispersion curve and the experimental global dispersion curve is that the array dispersion curve includes the average dispersion curve for each receiver spacing. An example of an array dispersion curve generated from the same composite dispersion curve is shown in Figure 2-18.

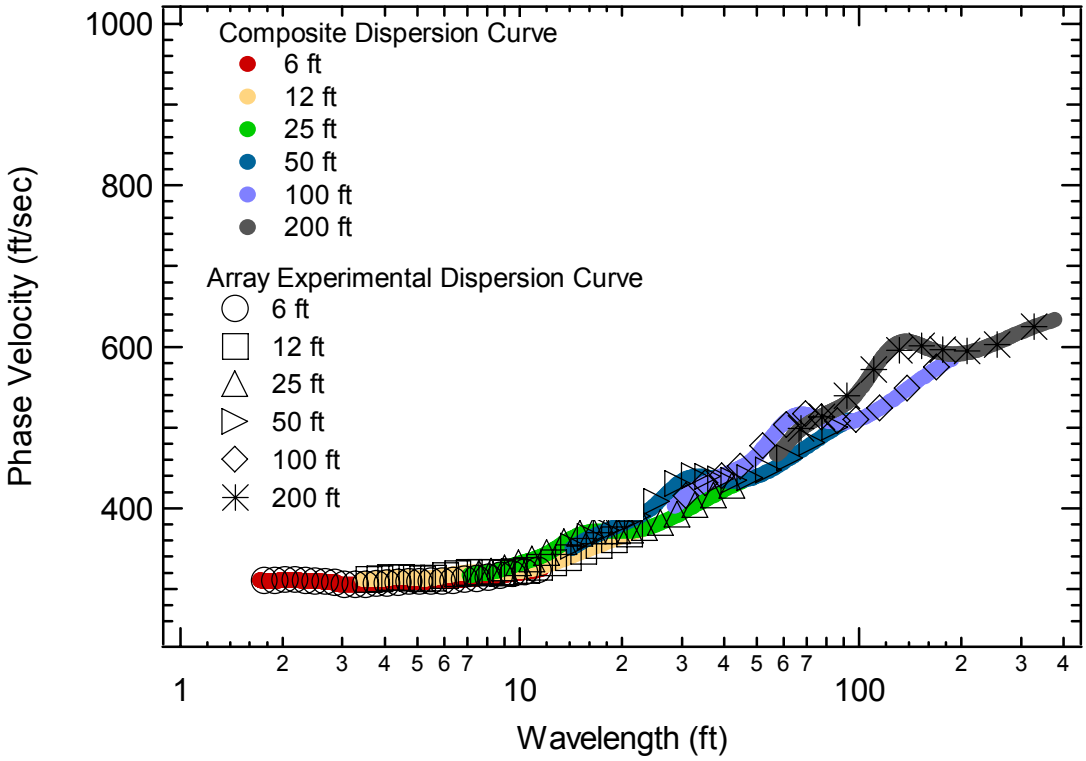

Figure 2-18 **Example array experimental dispersion curve generated from the individual dispersion curves shown in Figure 2-16.**

2.5.4.2 Forward Modeling Procedures

Forward modeling is a procedure in which the elastic properties and layering of a soil profile are assumed and a theoretical dispersion curve is calculated. The assumed soil profile must contain data specific to each soil layer

within the profile. Layer properties that must be specified include V_S, layer thickness, Poisson's ratio (ν) and mass density (ρ). Typically, parameters other than V_S are assumed and held constant while the V_S is iteratively adjusted until a reasonable fit is achieved between the theoretical and experimental dispersion curves.

The theoretical dispersion curve is calculated based on the solution of surface displacements due to a transient disk load applied at the surface of a layered soil system. The programs used in this study utilize a dynamic stiffness matrix approach that relates applied forces to displacements at the interfaces between layers (Kausel and Roesset, 1981, Kausel and Peek, 1982). Vertical displacements from the dynamic stiffness matrix method in the spatial domain can be expressed by the following equation.

$$w(r) = -\frac{i\pi qR}{2}\sum_{l=1}^{2N}\frac{(\phi_z^{1l} J_1(k_l R)H_o^{(2)}(k_l r)}{k_l} \qquad (2.16)$$

Where q is the amplitude of the vertically distributed disk load of radius R, r is the location where the vertical displacement is calculated, $\phi^{il}{}_z$ is the vertical displacement of the l^{th} mode at the surface, k_l is the lth eigenvalue, J_1 is the first-kind Bessel function of the first order, and $H^{(2)}{}_o$ is second-kind Hankel function of the first order (Joh, 1996). Figure 2.19 shows the vertical displacements calculated at a frequency of 10 Hz for an idealized system. The theoretical dispersion curve is calculated from the phase difference determined between two points on the surface. In the global approach, the two points are assumed to be at 2λ and 4λ from the source for all frequencies (where λ is wavelength). In this

way, a single far-field theoretical global dispersion curve is calculated for the site. For the array analysis, the actual receiver locations are used to calculate theoretical dispersion curves for each of the receiver pair locations. In both cases, the resulting dispersion curve does not represent a single mode of propagation, but instead includes the superposition of surface wave modes and body wave contributions.

In the global approach, a V_S profile is determined that provides the best fit between the global average dispersion curve and the global (2λ-4λ) theoretical dispersion curve. This approach works reasonably well for simple sites where the dispersion curve follows a general trend. The array analysis involves determining a single V_S profile that minimizes the mismatch between the individual experimental dispersion curves and the individual theoretical dispersion curves calculated at the same receiver locations. The array approach is more realistic because it duplicates the experimental set-up in the theoretical solution. Figure 2-20 (Joh, 1996) compares the global (2λ-4λ) theoretical dispersion curve to the array dispersion curve for a simple geotechnical site.

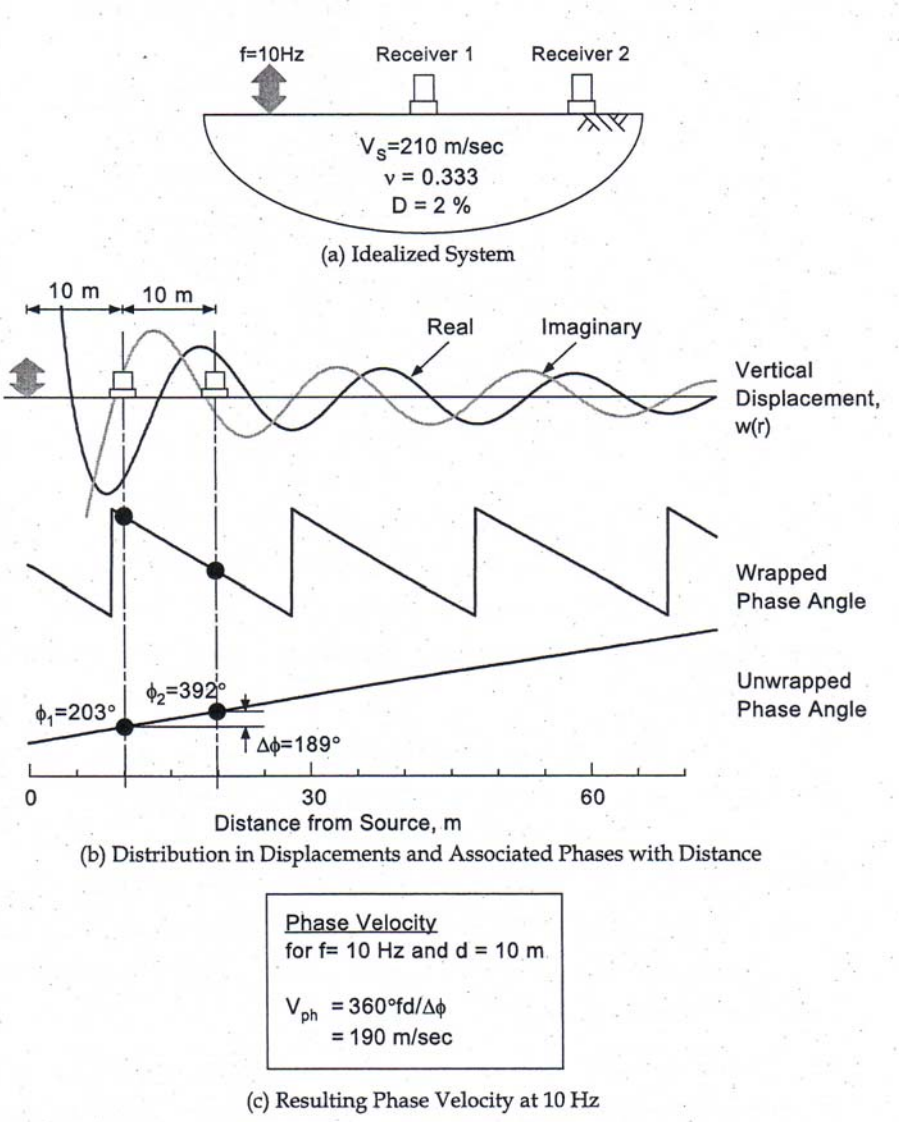

Figure 2-19 Demonstration of phase velocity calculation for determining the theoretical dispersion curve (from Joh, 1996).

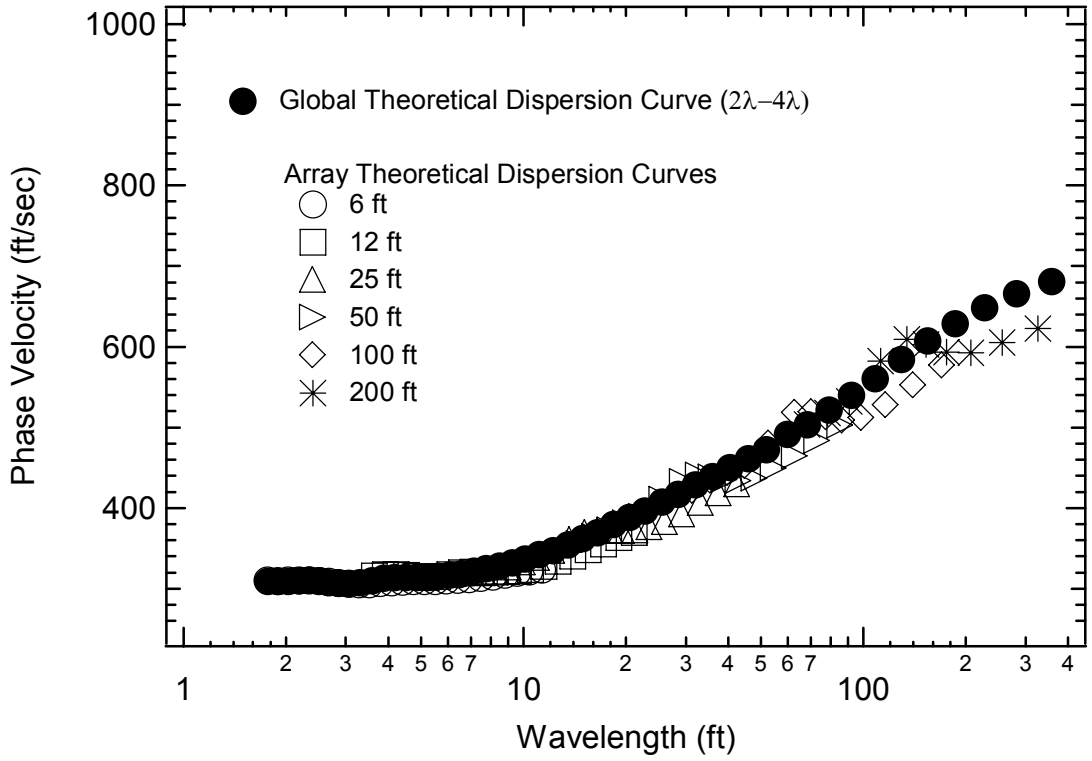

Figure 2-20 Comparison of global and array theoretical dispersion curves for the data shown in Figure 2-16.

2.5.4.3 Inversion Analysis

An inversion analysis is an automated procedure where a starting model is assumed and the soil profile is adjusted by an optimization technique to converge to a final solution. For SASW measurements applicable inversion analysis approaches include those presented by Rix and Leipski (1991), Tarantola (1987), Tokimatsu (1992) and Yuan and Nazarian (1992). Joh (1996) presents a maximum likelihood approach that includes automated inversion using the array analysis procedure described above. Inversion analyses were not performed as a part of this study.

2.6 Past Theoretical Studies of Surface Wave Propagation

There have been several notable studies of surface wave propagation at complex geotechnical sites that are relevant to this investigation. A review of these studies is presented in this section along with the salient findings.

2.6.1 Gucunski and Woods Study

Gucunski and Woods (1992) examined surface wave propagation in several simple layered systems. The authors compared a simulated SASW dispersion curve to the modal dispersion curves for the profile. The simulated dispersion curve was an effective phase velocity dispersion curve calculated from the surface displacement phase difference at 2λ and 4λ from a disk source. The surface displacements were calculated using the dynamic stiffness matrix approach (Kausel and Roesset, 1981, Kausel, 1981, Kausel and Peek, 1982, Wolf and Obernhuber, 1982 and Wolf, 1985). Four cases of soil stratification were examined by Gucunski and Woods (1992). These four cases are shown in Figure 2-21. Case 1 represents a soil profile in which the shear wave velocity gradually increases with depth. Cases 2 and 3 represents soil systems with a soft layer trapped between two layers with higher shear wave velocities. Case 4 represents a soil profile with a stiff layer trapped between two softer layers.

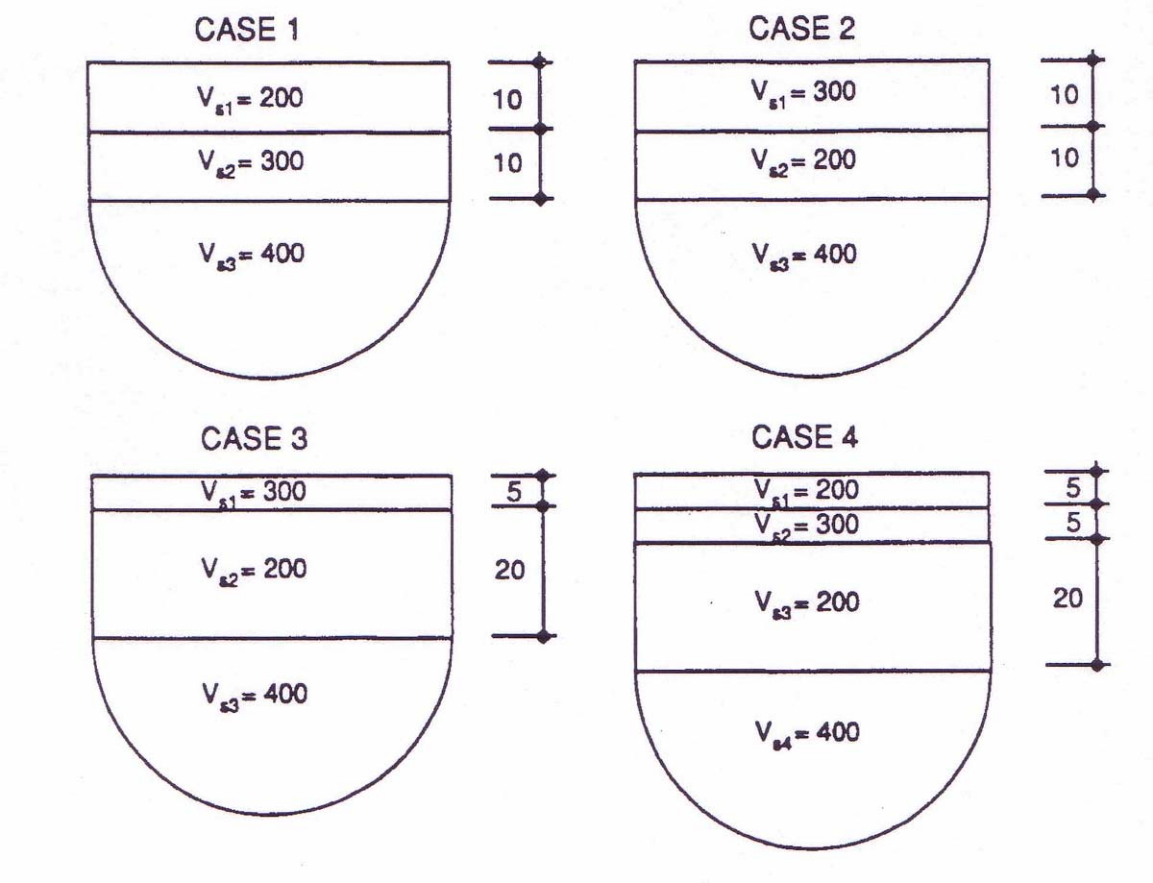

Figure 2-21 Stiffness profiles analyzed by Gucunski and Woods, 1992.

For Case 1, their results showed that the 'simulated' dispersion curve closely followed the fundamental Rayleigh mode and that there was minimal influence from higher modes. Figure 2-22 shows the individual dispersion curves for the fundamental and higher modes and the simulated dispersion curve.

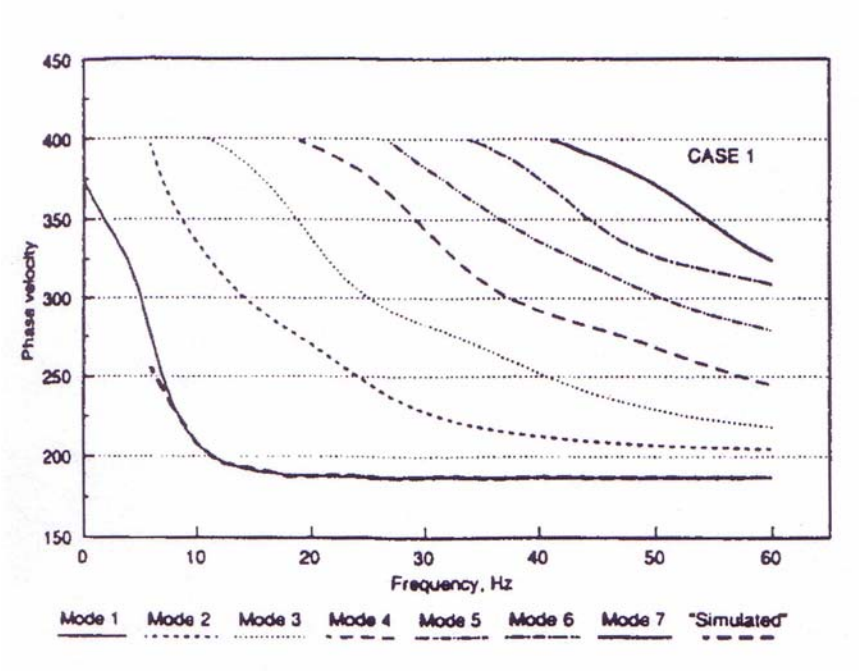

Figure 2-22 Case 1, modal and simulated dispersion curves (*from* Gucunski and Woods, 1992).

The dispersion curves for Cases 2 and 3 are shown in Figure 2-23. In these cases, the effective dispersion curve deviated from the fundamental mode and did not follow any single mode at higher frequencies. The simulated dispersion curve approached the Rayleigh wave velocity of the surface layer at high frequencies.

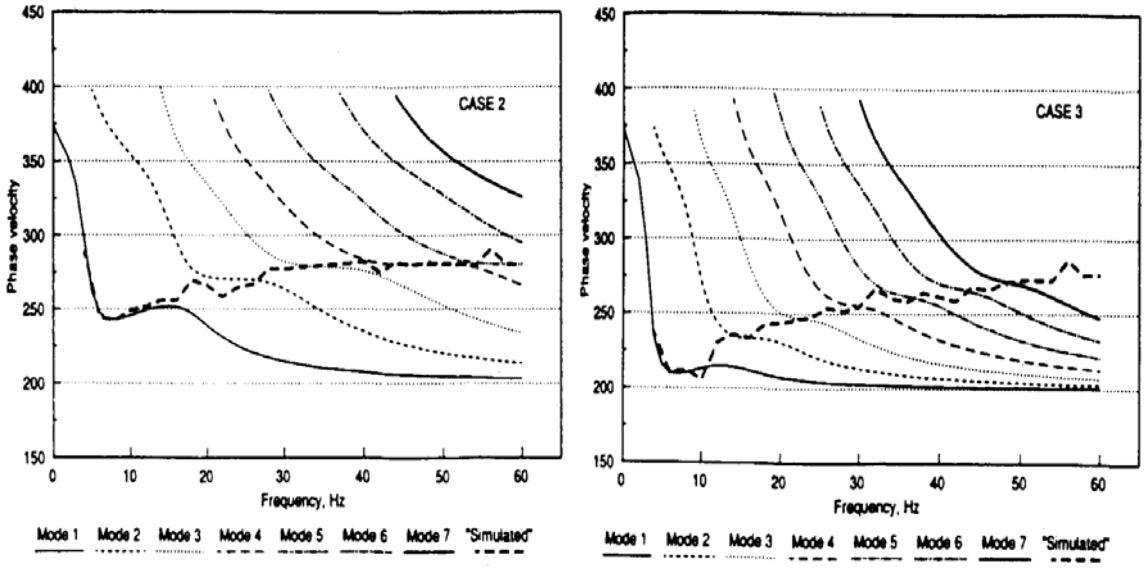

Figure 2-23 Modal and simulated dispersion curves for Case 2 and 3 shown in Figure 2-21 (*from* Gucunski and Woods, 1992).

For Case 4, the simulated curve closely followed the fundamental mode dispersion curve over most of the frequency range but followed the second mode over a frequency range of approximately 10 to 20 Hz, as shown in Figure 2-24.

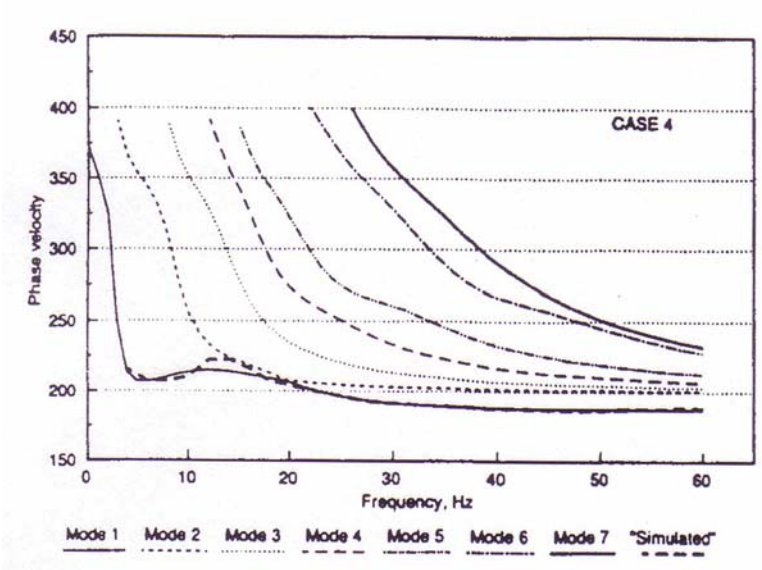

Figure 2-24 Case 4 modal and simulated dispersion curves (*from* Gucunski and Woods, 1992).

Gucunski and Woods (1992) concluded that when the shear wave velocity profile increases gradually with depth, the wave field generated by a vertical circular surface loading is dominated by the fundamental Rayleigh mode. In soils with irregular stratification, higher modes can play a significant role in wave propagation. A superposition of two or more modes of Rayleigh and body waves can significantly influence the simulated dispersion curve. Also, they found that the simulated dispersion curve for an irregular soil profile behaves similarly to the profile with increasing shear wave velocity with depth until the wavelength of the Rayleigh wave is less than approximately the thickness of the top portion of the system.

2.6.2 Tokimatsu Study

Tokimatsu et al. (1992) computed dispersion curves of multiple mode Rayleigh waves for three, four-layer models. The three models are listed in Table 2-1. In Case 1 the stiffness increases with depth and Cases 2 and 3 have stiffness inversions. Particle motions were simulated assuming harmonic vertical point loading and based on the transfer matrix method proposed by Thomson (1950) and Haskell (1953). The simulations assumed that the two sensors were located at 2λ and 2.5λ from the source.

Table 2-1 Soil layer models (*from* Tokimatsu et al., 1992).

Layer number	Thickness, H (m)	Density, ρ (Mg/m^3)	V_P (m/s)	V_S (m/s)		
				Case 1	Case 2	Case 3
1	2	1.8	300	80	180	80
2	4	1.8	1000	120	120	180
3	8	1.8	1400	180	180	120
4	-	1.8	1400	360	360	360

For the case with increasing stiffness with depth (Case 1), Tokimatsu found that the fundamental mode dominates throughout the frequency range of interest. In this case, inversion using only a fundamental mode theoretical dispersion curve would work well. The resulting dispersion curves for the fundamental, higher modes and simulated curve for Case 1 are shown in Figure 2-25.

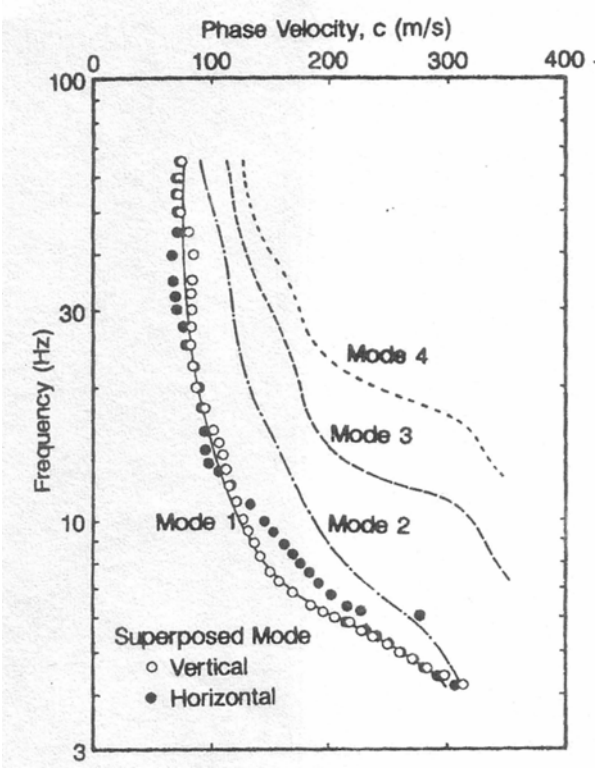

Figure 2-25 Modal and simulated dispersion curves for Case 1 (*from* Tokimatsu et al., 1992).

For soil profiles with V_S varying irregularly with depth, Tokimatsu found that a higher mode or multiple modes dominate in some frequency ranges. The dispersion curves for Case 2 and Case 3 are shown in Figure 2-26. Tokimatsu concluded that inversion using the fundamental mode only cannot work well when the shear wave velocity varies irregularly with depth.

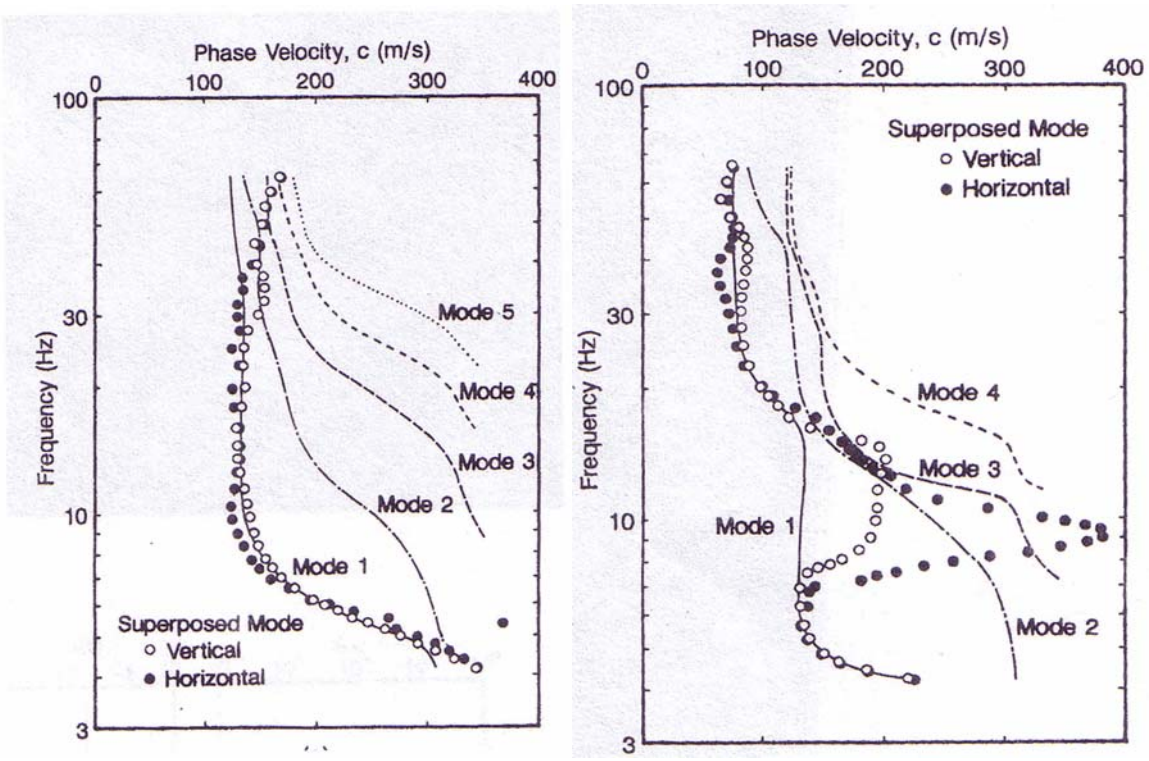

Figure 2-26 Modal and simulated dispersion curves for Case 2 (left) and Case 3 (right) (*from* Tokimatsu et al., 1992).

2.6.3 Foti Study

Foti (2000) examined various stiffness profiles including: (1) a normally dispersive profile, (2) soft layer trapped between stiffer layers and (3) a stiff layer over softer soil. His study differed from the previously cited studies in that he simulated SASW measurements by calculating synthetic seismograms using computer programs written by R.B. Herrmann at Saint Louis University. The computer program computes synthetic seismograms using modal superposition of surface waves and doesn't account for body wave contributions. The synthetic data were analyzed using the SASW phase unwrapping approach as well as multi-channel approaches. The characteristics of the stiffness profiles that were

analyzed are described in Table 2-2. The mass density of soil was 1800 kg/m^3 for all layers.

Table 2-2 Profiles A, B and C soil layer characteristics (*from* Foti, 2000).

Profile A			Profile B			Profile C		
Thickness (m)	V_P (m/s)	V_S (m/s)	Thickness (m)	V_P (m/s)	V_S (m/s)	Thickness (m)	V_P (m/s)	V_S (m/s)
5	600	350	5	700	400	3	800	450
10	700	400	3	500	300	5	600	350
-	800	450	-	800	450	10	700	400
						-	800	450

Results from simulations of Profile A demonstrated that for profiles with stiffness increasing with depth the fundamental mode was dominant over the entire frequency range. The effective phase velocity closely followed the fundamental mode, as shown in Figure 2-27. A dispersion curve determined through the SASW simulation more closely followed the fundamental mode as compared to the effective phase velocity, as is shown in Figure 2-28. Foti defines the effective phase velocity as the measurement of the superposed mode with the receivers located 2λ and 4λ from the source.

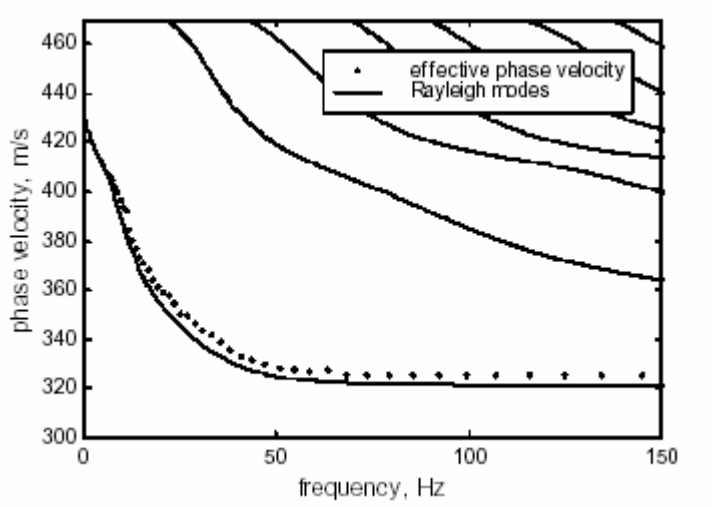

Figure 2-27 Rayleigh modes and effective dispersion curve for Profile A (*from* Foti, 2000).

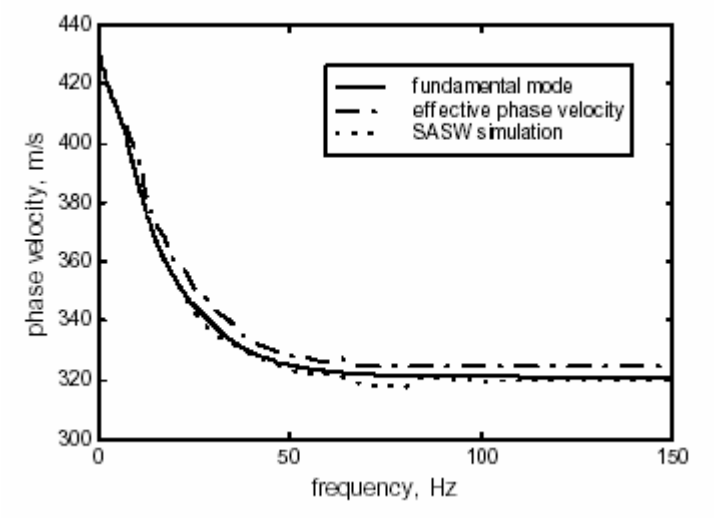

Figure 2-28 Comparison of dispersion curves for SASW simulation, effective phase velocity and Rayleigh wave fundamental mode for Profile A (*from* Foti, 2000).

The irregular soil Profile B, which consisted of a soft layer trapped between two stiffer layers, produced an effective dispersion curve that transitioned from the fundamental mode to higher modes as the frequency increased, as is shown in Figure 2-29. The fundamental mode was dominant over frequencies less than approximately 25 Hz. Foti (2000) observed that averaging of points between different SASW receiver configurations does not ensure a stable estimate of the effective phase velocity. He also found that the simulated SASW dispersion curve for this case provided an underestimation of the effective phase velocity. Figure 2-30 shows the SASW simulation dispersion curve plotted with the effective phase velocity dispersion curve for Profile B.

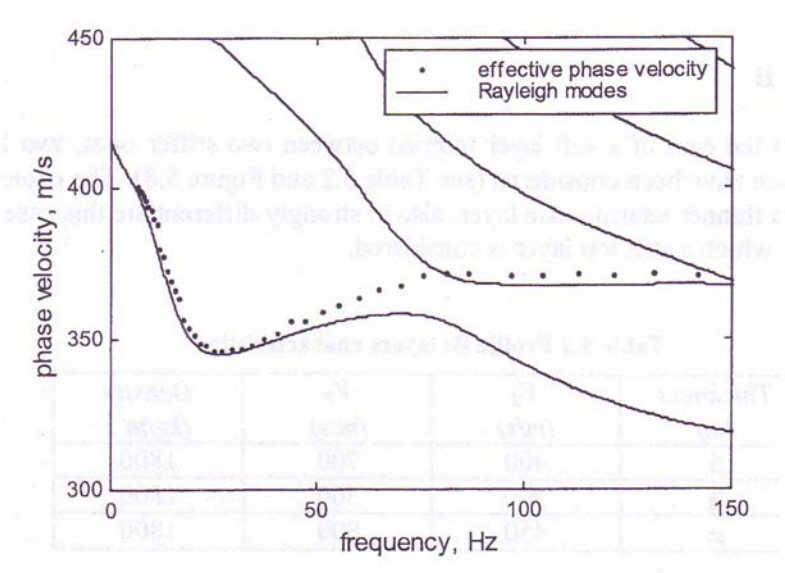

Figure 2-29 Rayleigh modes and effective dispersion curve determined from Profile B (from Foti, 2000).

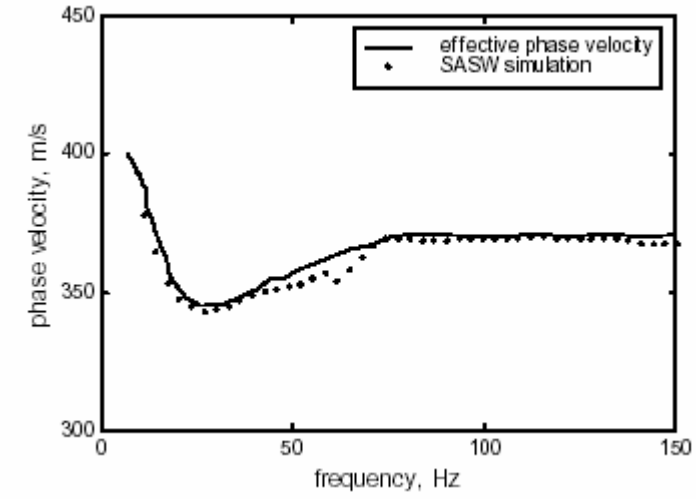

Figure 2-30 SASW simulation dispersion curve and effective phase velocity dispersion curve determined from Profile B (from Foti, 2000).

Profile C consists of a stiff top layer over a softer soil. The results from simulations of this profile demonstrated that several modes have a strong influence on the effective and simulated phase velocity measurements. The transition from the fundamental mode to higher modes was gradual, as shown in

Figure 2-31. Foti concluded that this profile would lead to a stable global estimate from the averaging process and that the simulated SASW dispersion curve would closely match the effective phase velocity, as shown in Figure 2-32.

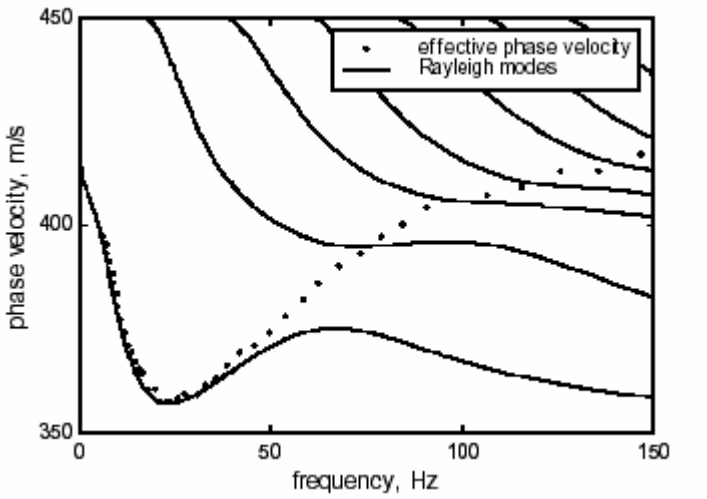

Figure 2-31 Rayleigh modes and effective dispersion curve determined from Profile C (from Foti, 2000).

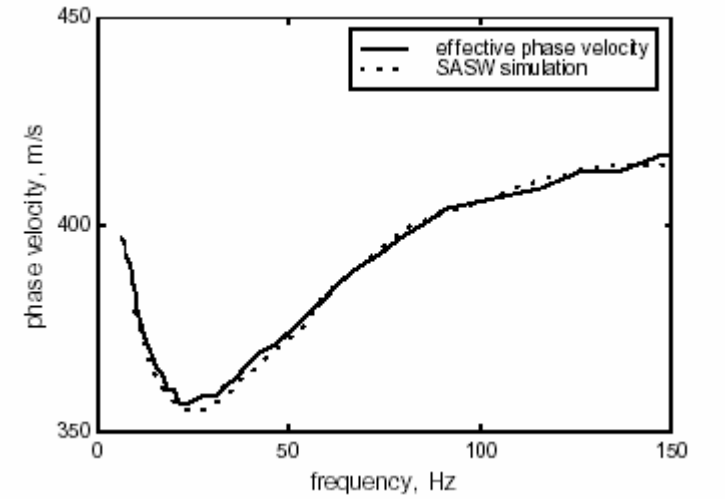

Figure 2-29 SASW simulation dispersion curve and effective phase velocity dispersion curve determined from Profile C (from Foti, 2000).

The results from these studies demonstrate the effect higher modes can have on surface wave propagation when measurements are performed on irregular profiles. All of these studies examined sites with relatively small

changes in velocity with depth (typically 50% or less). Many natural field conditions consist of profiles with far greater changes in V_S between layers. The aim of the study presented here is to examine the SASW technique over a wider range of V_S profile conditions. The methodology that was used to perform this study is presented in Chapter 3.

2.7 Summary

In Chapter 2, the fundamentals of surface wave propagation in a uniform and layered halfspace were presented. Two common ways of analyzing surface wave measurements are to use a modal or effective phase velocity dispersion curve. Differences between these dispersion curves were discussed. The SASW method was also described, especially the methods of data collection, data processing and data analysis.

Chapter 3 Methodology

3.1 Introduction

The objectives of this research are to investigate the effectiveness of the SASW surface wave methodology at complex geotechnical sites and identify conditions where the SASW approach may produce erroneous results. As previously described in Chapter 2, the SASW methodology involves the generation of an effective phase velocity dispersion curve from the "unwrapping" of the phase difference plot determined between a pair of sensors. To simulate SASW measurements for this study, analytical programs were used to generate synthetic time records for a variety of complex geotechnical sites. The synthetic time records were used to create experimental dispersion curves that simulate the dispersion curves that would be created from phase unwrapping of field measurements.

For each simulated site, theoretical dispersion curves (both global and array) as well as modal dispersion curves (in some cases) were calculated to compare to the simulated experimental curves. In this chapter, the methods used to create the synthetic time records, effective phase velocity dispersion curves and modal dispersion curves are presented. In addition, the geotechnical profiles that were analyzed in this study are presented.

3.2 Synthetic Time Records

Synthetic time records were created using the program FitSASW developed at the University of Texas-Austin and later updated at Chung-Ang

University in AngSeong, Korea in 2003 (Joh, 2003). The program creates time records based on a one dimensional (1-D) profile with individual layer parameters consisting of: layer thickness, compression wave velocity (V_P), V_S, Poisson's ratio (ν), mass density (ρ), and damping ratio (D). Other program input parameters include the number of receivers, receiver locations and the frequency range of interest. The dynamic stiffness matrix approach, as described in Section 2.5.4.2, is used to calculate the synthetic time records. The program uses the assumed 1-D profile to calculate surface displacements that involve contributions from surface wave modes as well as body wave modes. For this study time records were created for receiver pairs spaced at 6 ft, 12 ft, 25 ft, 50 ft, 100 ft and 200 ft. These receiver spacings are typical of those used to profile to depths of 100 to 200 ft. An example of the time records generated for two receivers located 200 and 400 ft from the source (200-ft spacing) for the profile shown in Figure 3-1 is shown in Figure 3-2.

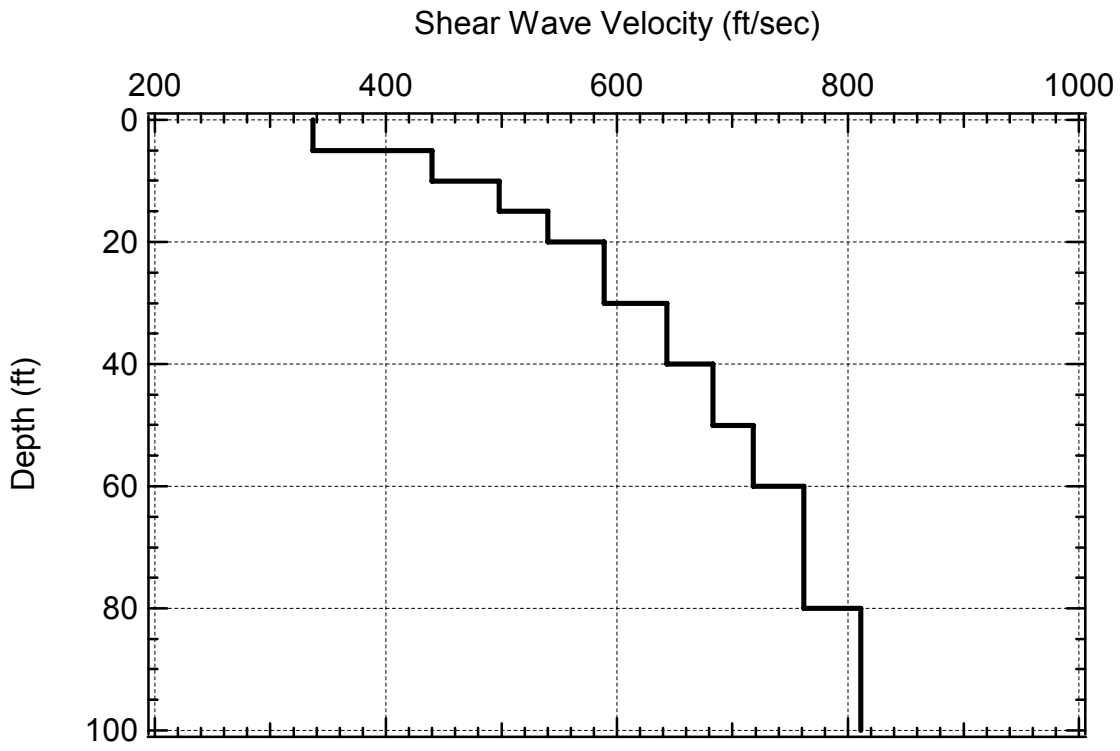

Figure 3-1 Sample soil profile with an 800 ft/sec halfspace.

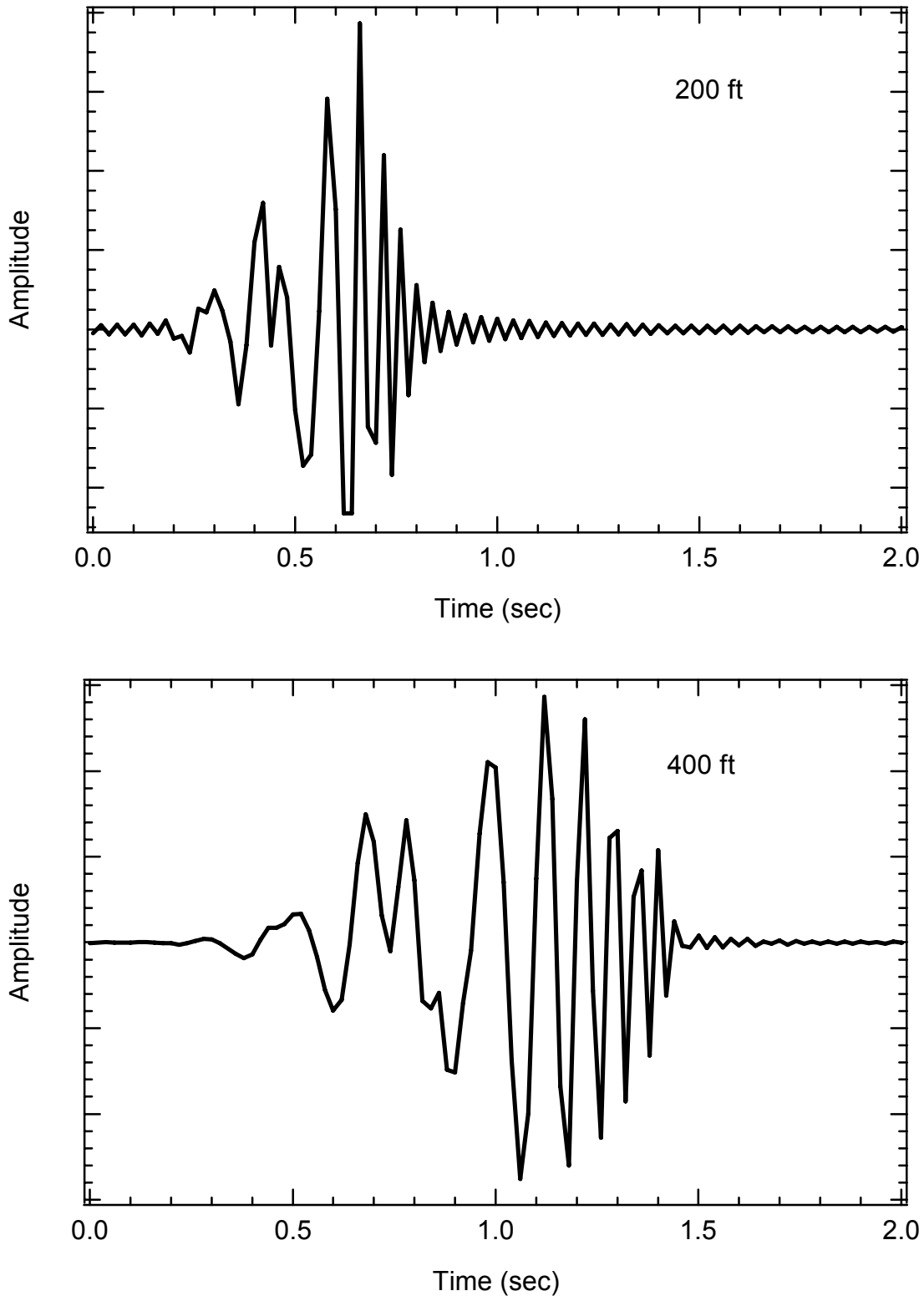

Figure 3-2 **Synthetic time records created using FitSASW (Joh, 2003) for a 200-ft spacing with the receivers spaced at 200 ft (top) and 400 ft (bottom) from the source.**

3.3 Development of Simulated Experimental Dispersion Curves

A simulated experimental dispersion curve was created for each site using the procedures discussed in Section 2.5.3 and 2.5.4. The program WinSASW 2.3.1 (Joh, 1996) was used for these purposes. Time records for each receiver pair were loaded into WinSASW 2.3.1. Figure 3-3 shows a screen shot of the uploaded simulated time records in WinSASW 2.3.1. The receiver locations were specified and the unwrapped phase was calculated from the simulated time records.

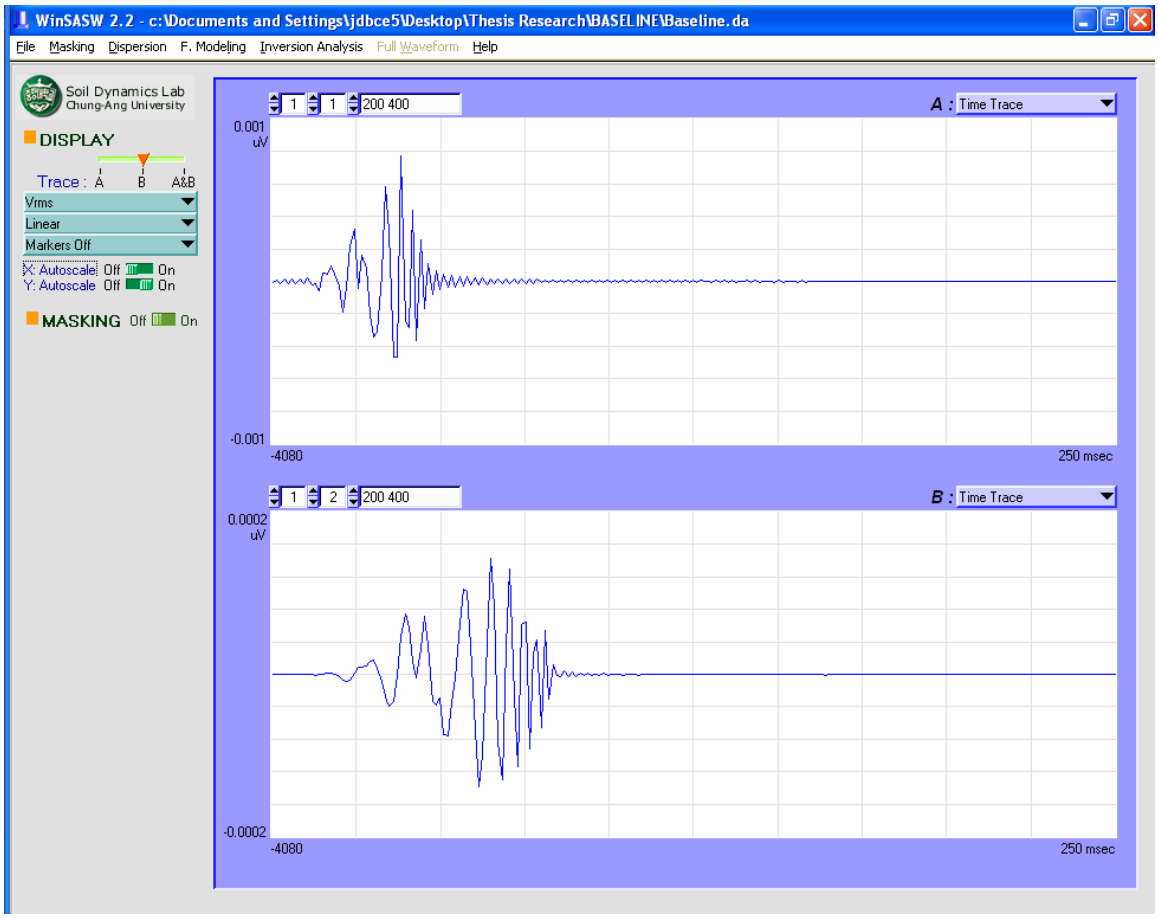

Figure 3-3 **Time record file upload screen for WinSASW 2.3.1 with simulated time records.**

Figure 3-4 presents the wrapped phase plots calculated from the simulated time records for six receiver pair locations. Phase unwrapping was then accomplished by masking out near-field data, and all data beyond the third or fourth cycles of the frequency response spectrum. This was done to mimic typical field conditions where data is not of good quality past approximately 3-4 cycles from the source. 360° jumps in phase were manually identified and the cumulative phase was calculated. The phase unwrapping procedures used in this research are consistent with those described in Section 2.5.3 and illustrated in Figure 2-14.

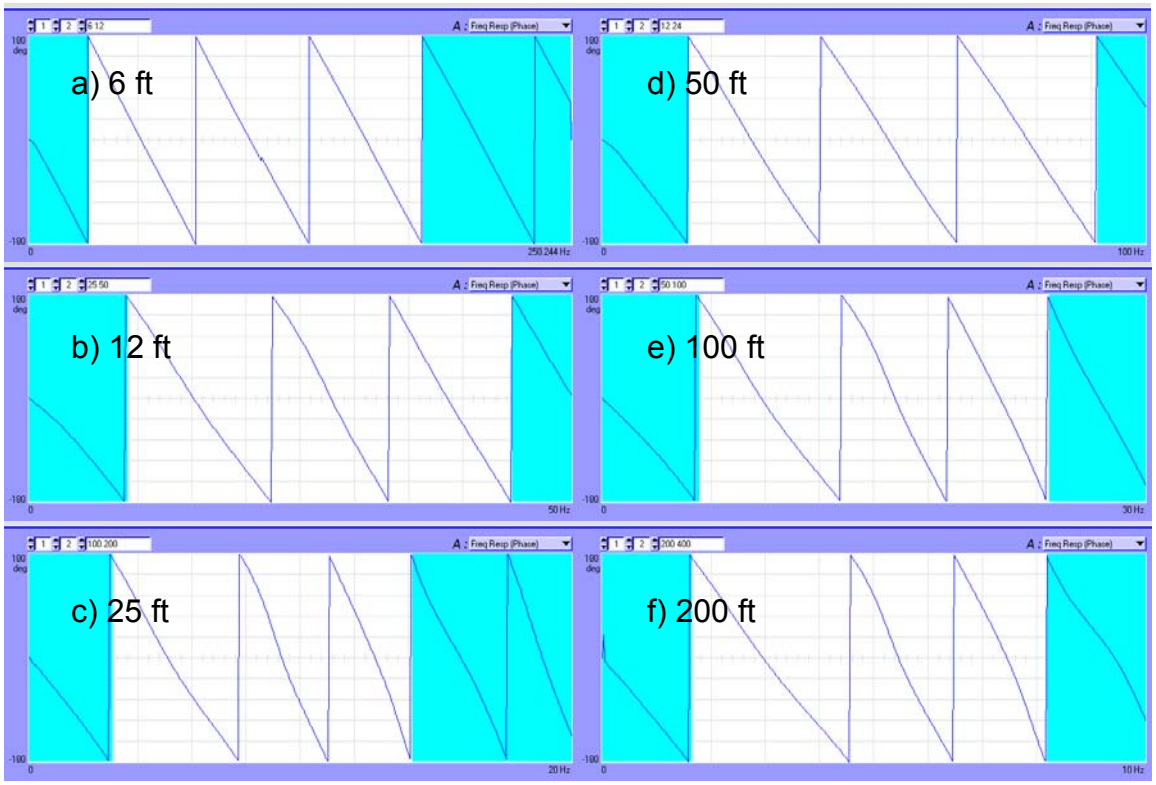

Figure 3-4 **Wrapped phase plots and masking for receiver spacings of 6, 12, 25, 50, 100 and 200 ft.**

The program was then used to calculate the simulated composite or experimental dispersion curve from the unwrapped phase plots. Both global and array experimental dispersion curve were calculated. The averaging schemes used to create the global and array experimental dispersion curves were discussed in Section 2.5.4. An example of a composite dispersion curve generated from the phase plots shown in Figure 3-4 is presented in Figure 3-5. Figure 3-6 is a plot of the array and global experimental dispersion curves plotted with the composite dispersion curve.

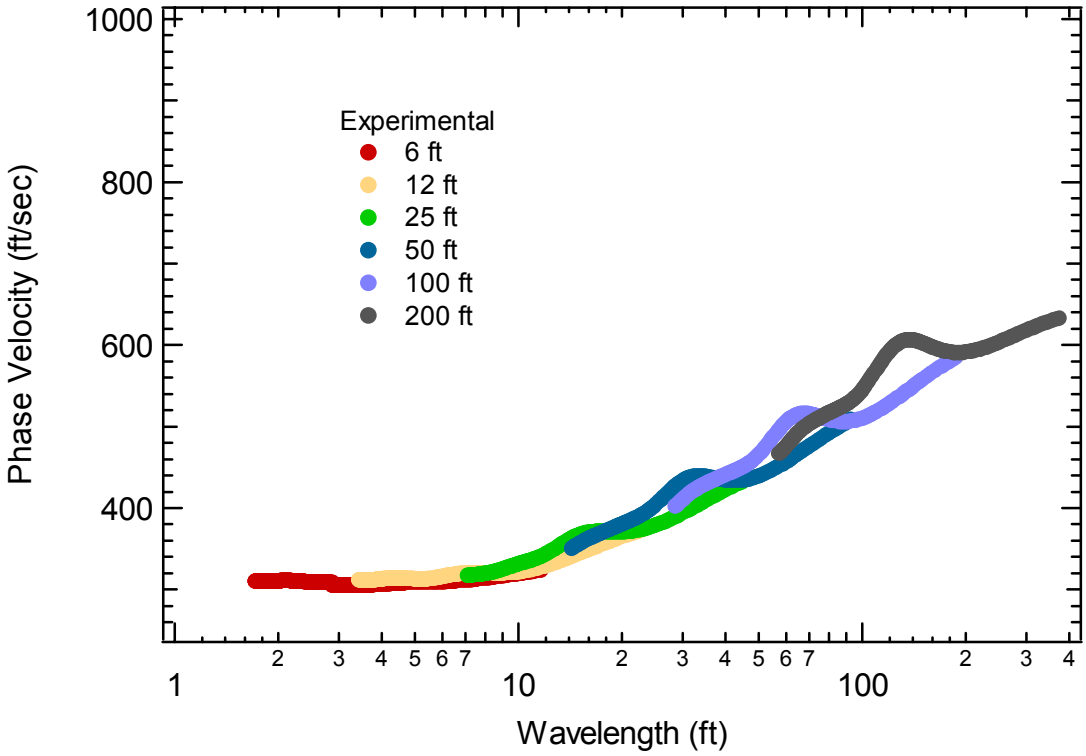

Figure 3-5 **Composite dispersion curve for receiver spacing of 6, 12, 25, 50, 100 and 200 ft.**

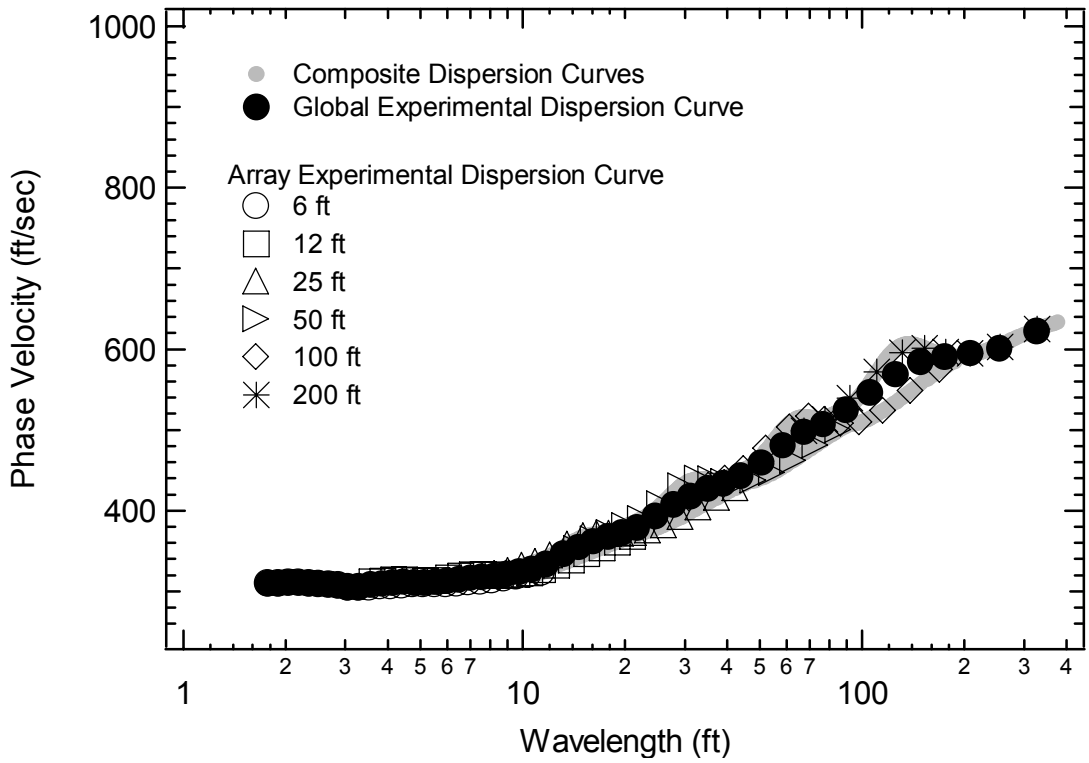

Figure 3-6 **Composite, array and global experimental dispersion curves generated from the profile shown in Figure 3-1.**

3.4 Theoretical Effective Velocity Dispersion Curve

The theoretical effective phase velocity dispersion curves were calculated using the program WinSASW 2.3.1. An earlier version of the program (WinSASW 1.2.3) was also used for some of the profiles. The spatial distribution of vertical displacements was calculated using the dynamic stiffness approach. The effective phase velocity was determined from the phase difference (determined in the spatial domain) at two points. The procedure for determining the theoretical effective phase velocities is illustrated in Figure 2-19. Both global and array theoretical dispersion curves were calculated for each site. The global dispersion curve was determined assuming that the receivers were located at distances of 2λ and 4λ from the source, thereby creating a single dispersion curve for the site.

The array dispersion curve was calculated using the actual receiver locations thereby creating individual theoretical dispersion curves for each receiver pair.

An example of an array theoretical dispersion curve plotted with the array experimental dispersion curve is shown in Figure 3-7. A global theoretical dispersion curve is plotted with a global experimental dispersion curve in Figure 3-8. The experimental dispersion curves are the same ones shown in Figure 3-6.

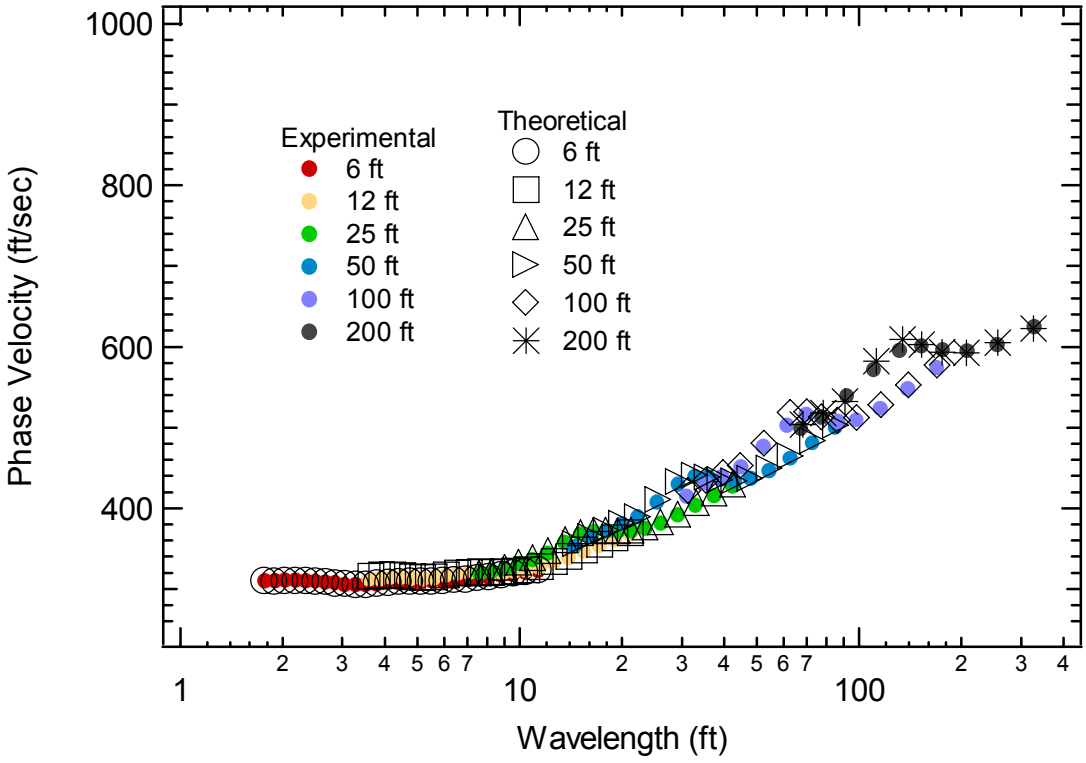

Figure 3-7 **Array theoretical and experimental dispersion curves determined from the V_S profiles shown in Figure 3-1.**

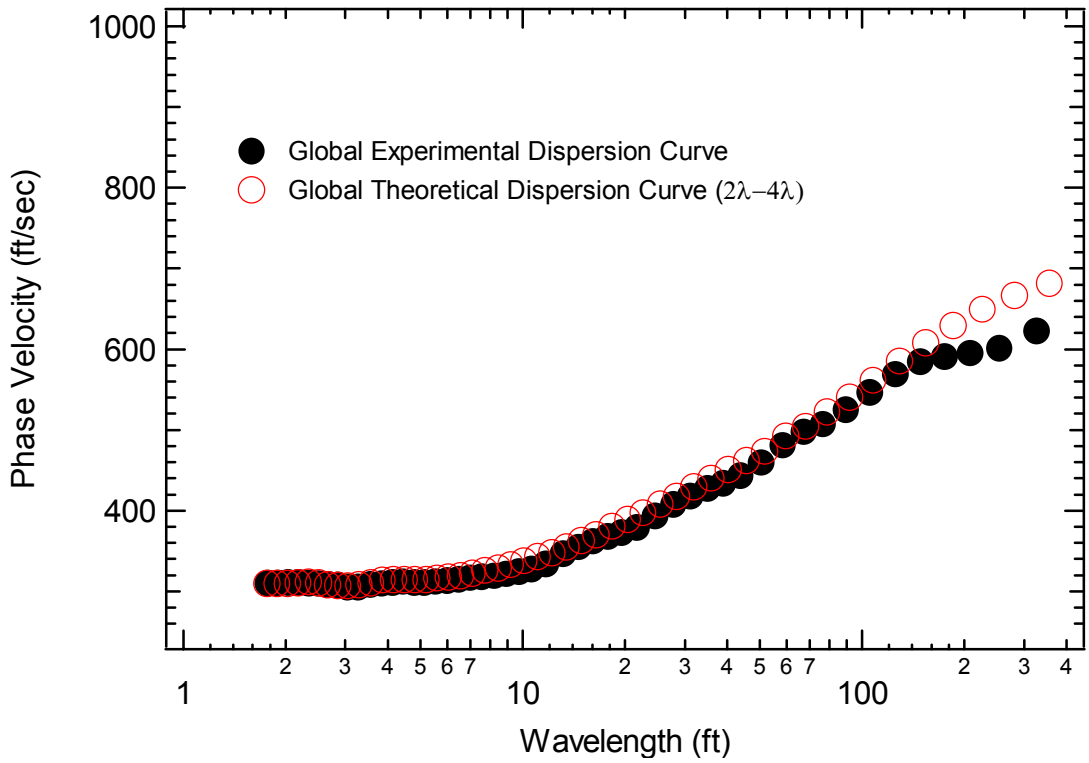

Figure 3-8 **Global theoretical and experimental dispersion curves determined from the V_S profile shown in Figure 3-1.**

3.5 Modal Dispersion Curves

To provide additional insight into the surface wave propagation behavior, modal dispersion curves were calculated. The modal dispersion curves were calculated using a program called Underwater Surface WAVE (USWAVE) developed at the University of Texas at Austin (Lee, 1996). As the name implies the program was developed to analyze layered soil deposits overlain by water, but can also be used to perform terrestrial calculations of surface wave propagation.

The modal dispersion curves were calculated using a numerical method known as the "bisection method" (Hamming, 1973) to find the roots of the

characteristic equation. The characteristic equation was formulated using the dynamic stiffness matrix method and can be found by expressing:

$$[K]\{U\} = 0 \tag{3.1}$$

where [K] is the global stiffness matrix of the system and {U} is the vector for displacements at the layer interfaces of the system. Details of this calculation can be found in Lee, 1996. To obtain a non-trivial solution for displacements the determinant of the stiffness matrix should be zero:

$$\left|K\right| = 0 \tag{3.2}$$

The roots of the characteristic equation are the normal modes of surface wave propagation (Lee, 1996).

To obtain the roots, a range of phase velocities is assumed. The velocity range is divided into intervals and is used to obtain discrete trial velocities which are used in equation 3.2. The trial velocities are assumed to range from zero to a value near the maximum shear wave velocity of the soil system (Lee, 1996). The velocity interval is then identified by changes in the sign of the determinant. The velocity interval is bisected repeatedly to obtain a velocity which, when used in equation 3.2, results in a value nearly equal to zero. When the difference between the repeated trial velocities bounding the interval is below a prescribed limit the repeated bisection stops (Lee, 1996). The entire range of phase velocities is searched for roots so that all of the normal modes are found. Model input parameters for this program include layer thickness, V_P, V_S, Poisson's ratio (ν) and density (ρ).

In order to verify the calculations in USWAVE, modal dispersion curves were calculated for Case 2 used in the Gucinski and Woods (1992) study. The calculated modal dispersion curves from USWAVE are shown in Figure 3-9. The dispersion curves created by Gucinski and Woods are shown in Figure 3-10. The model dispersion curves are utilized in Chapter 5 to assist in understanding the results of the SASW simulations.

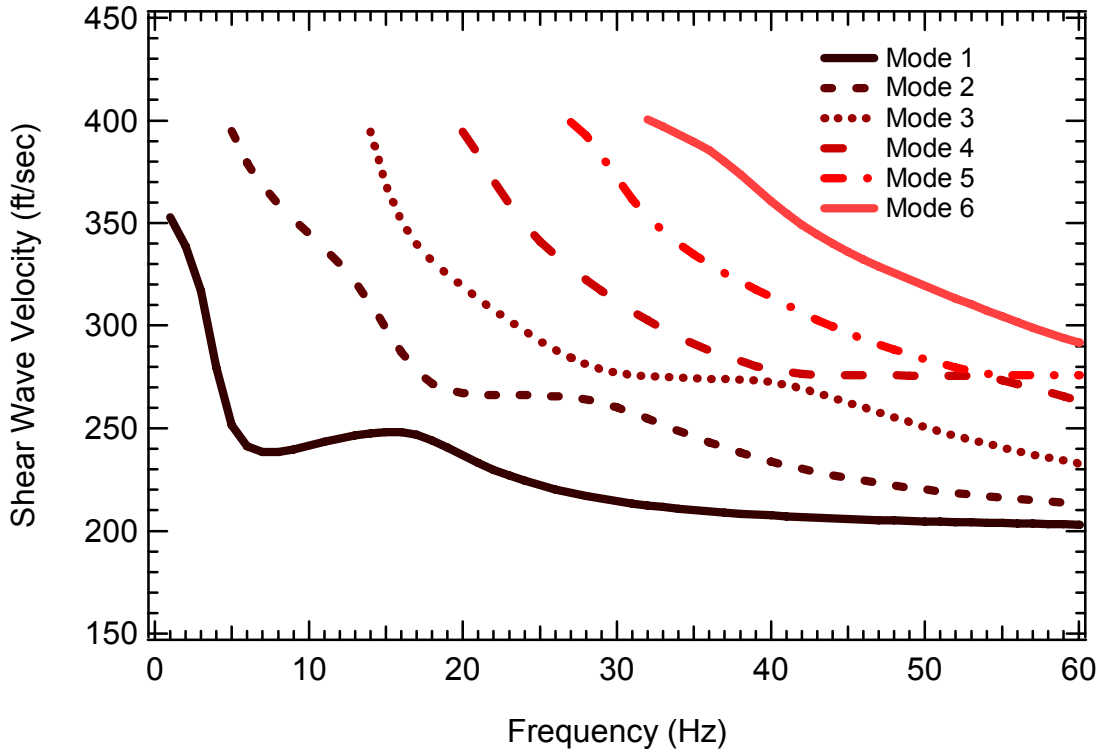

Figure 3-9 Modal dispersion curve replicated from Gucinski and Woods (1992) Case 2.

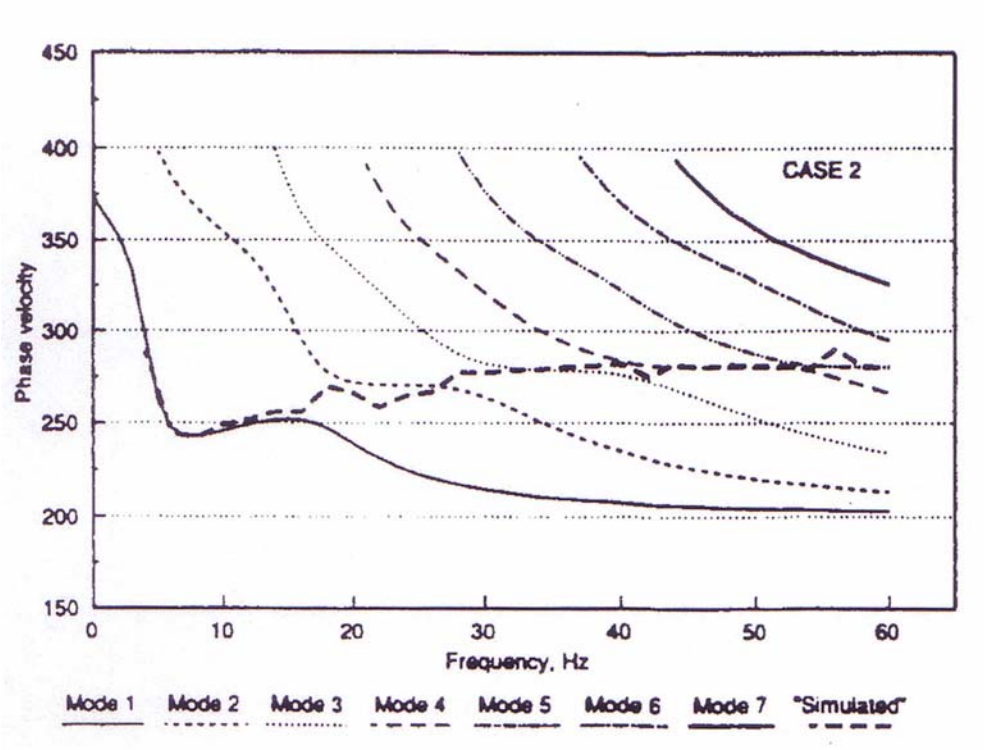

Figure 3-10 Modal dispersion curve from Gucinski and Woods (1992) Case 2.

3.6 Soil Profile Models

3.6.1 Creation of Reference Profile

V_S profile models were created to emulate common geotechnical profiles encountered in the field. The soil models that were developed included: (1) profiles with gradually increasing V_S with depth, (2) a soft layer over a stiff layer, (3) a stiff layer trapped between two softer layers, (4) a stiff layer over a softer layer and (5) a soft layer trapped between two stiffer layers. Profiles with continuously increasing V_S with depth are characteristic of normally consolidated soil sites and are often encountered in the field. The soft-over-stiff condition is encountered in a variety of cases, including a sand or soft clay layer overlying a highly overconsolidated clay, or soil overlying bedrock. V_S profiles with a stiff

layer trapped between two softer layers can be encountered when a cemented sand layer is present, for example. A stiff layer over a softer layer is commonly encountered where a dessicated crust exists over softer soil. All of the profiles analyzed in this study were created by modifying a normally consolidated reference soil model as described below. A total of 7 baseline profiles were created to represent these various profiles. These profiles are designated as Profile 1 through 7. Additional variations were created from these baseline profiles by altering the shear wave velocity of one layer of the profiles resulting in a total of 23 V_S profiles that were analyzed.

The reference profile with increasing V_S with depth was created using the relationships shown in Equations 3.3 and 3.4.

$$V_S = \sqrt{\frac{G_{MAX}}{\rho}} \tag{3.3}$$

Equation 3.3 is used to calculate V_S based on the small-strain shear modulus (G_{MAX}) and mass density of the material (ρ). G_{MAX} was calculated using the empirical relationship (Hardin, 1978):

$$G_{MAX} = 625F(e)(OCR)^k Pa^{(1-n)}(\sigma'_m)^n \tag{3.4}$$

where OCR is equal to the overconsolidation ratio and is defined as:

$$OCR = \frac{P'_{MAX}}{\sigma'_v} \tag{3.5}$$

where P'_{MAX} is the maximum past vertical effective stress and σ'_v is equal to the vertical effective stress. k is a constant related to soil plasticity, P_a is atmospheric pressure and n is a constant equal to 0.5. F(e) is a void ratio (e) function defined as:

$$F(e) = \frac{1}{0.3 + 0.7e^2} \tag{3.6}$$

where e is the void ratio of the soil. The term σ'_m in equation 3.4 is the mean effective stress which is defined as:

$$\sigma'_m = \frac{(\sigma'_v + 2K_o\sigma'_v)}{3} \tag{3.7}$$

where K_o is equal to the coefficient of earth pressure at rest. In this study, the reference V_S profile was calculated assuming: γ = 120 pcf, e = 0.75, K_o = 0.5, and k = 1.

The reference profile calculated using Hardin's equation is shown in Fig 3-11. The profile was subdivided into 10 layers as shown in Figure 3-12. The 7 baseline profiles created to represent various V_S conditions were constructed from the reference profile by inserting stiffer layers in the profile. Typical values of V_S for different soil and rock conditions obtained from the International Building Code (IBC, 2003) and calculated using Hardin's equation are presented in Table 3-1. Additional profiles were developed from the 7 baseline profiles by varying the magnitude of contrast provided by the stiffer layers that were inserted in the profile. These additional profiles are designated with a,b,c and d appended to the name of the reference profile.

Table 3-1 Typical values of V_S for soil and rock profiles.

	Typical Range of V_S (ft/sec)	
Material Type	**IBC (2003)**	**Harden (1978)**
Soft Soil	< 600	< 500
Stiff Soil	600 - 1200	500 - 1000
Very dense soil and soft rock	1200 - 2500	1000 - 2250
Rock	2500 - 5000	
Hard Rock	> 5000	

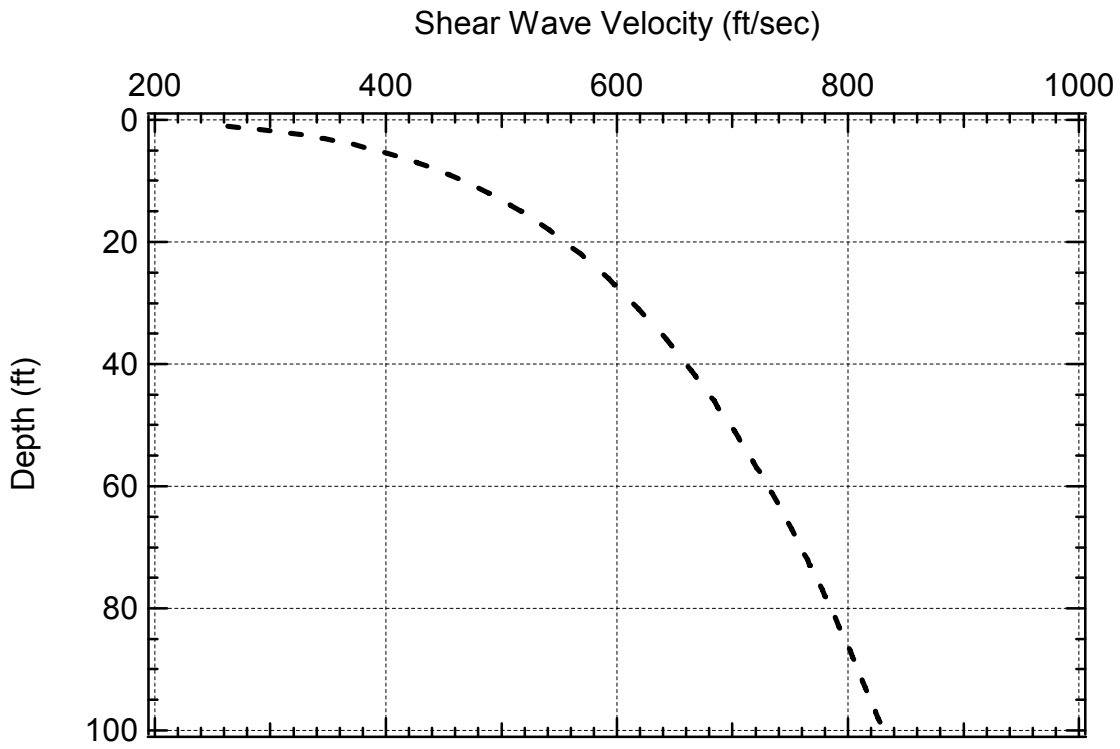

Figure 3-11 Reference V_S profile calculated using Hardin's equation.

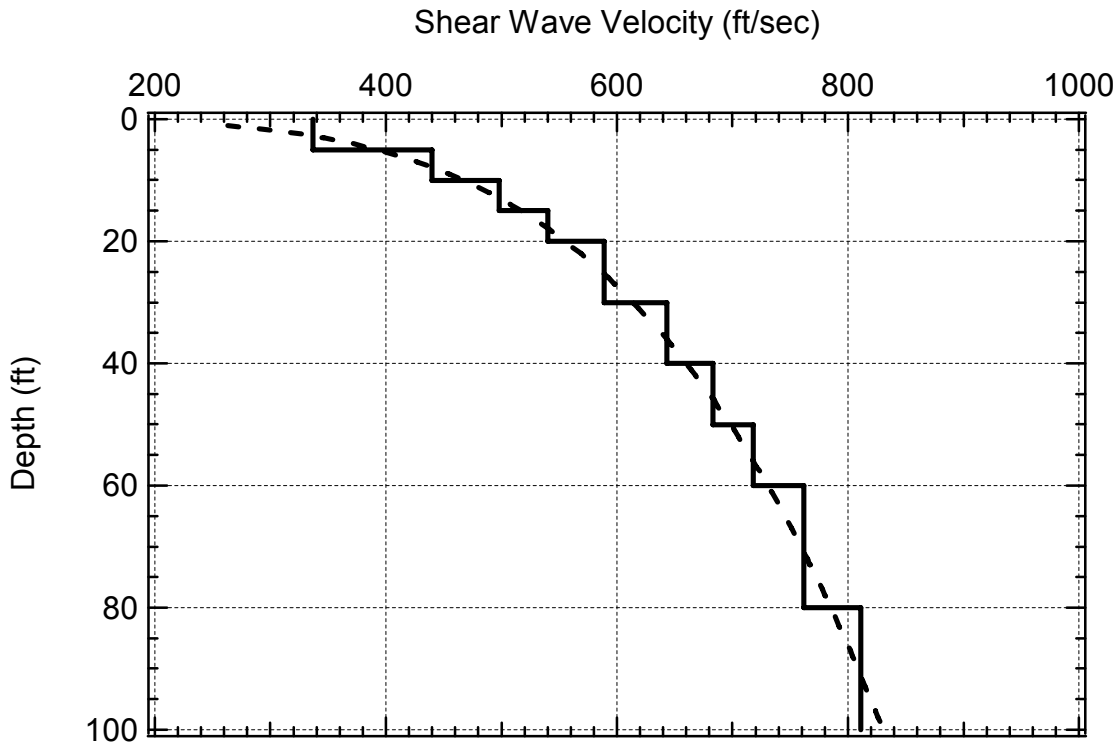

Figure 3-12 10-layer reference V_S profile used to construct 7 baseline V_S profiles.

3.6.2 Baseline Profiles

Profiles 1 and 2 are soft-over-stiff profiles. They consist of the reference profile underlain by a stiff halfspace. The depth to the stiff layer in Profile 1 is 10 ft and the depth to the stiff layer in Profile 2 is 30 ft. Profile 1 was simulated with three different halfspace stiffness values. The shear wave velocities of the three stiffness halfspaces are 800, 1200 and 1500 ft/sec, and are designated as Profile 1 a, b and c, respectively. Profile 2 was simulated with four halfspace stiffness values of 800, 1000, 1500, 2000 ft/sec and are designated as Profile 2 a, b, c and d, respectively. Profiles 1a, 1b, and 1c are presented in Figure 3-13 and Profiles 2a, 2b, 2c and 2d are shown in Figure 3-14.

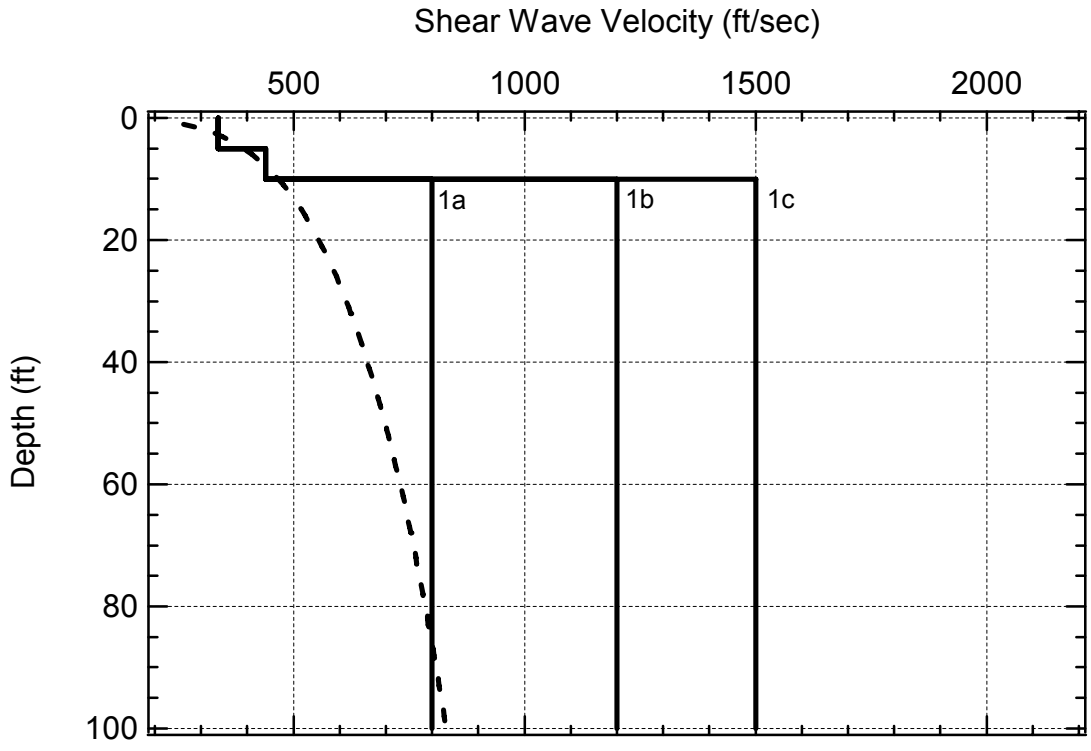

Figure 3-13 Profiles 1a, 1b and 1c plotted with the reference profile.

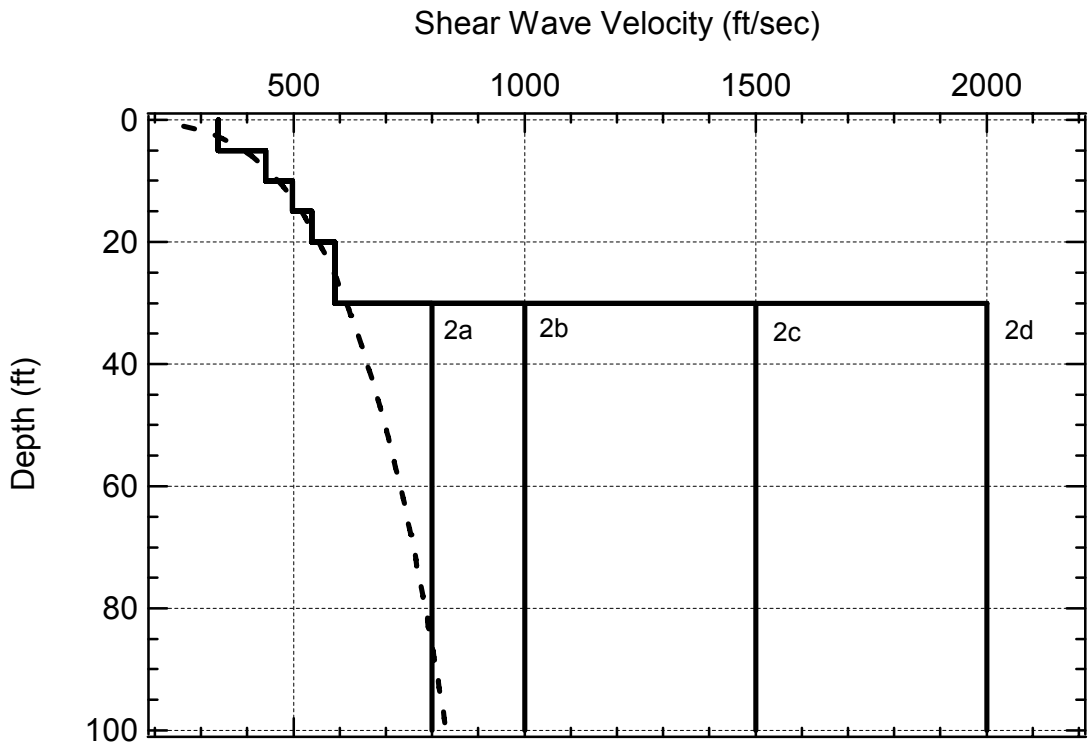

Figure 3-14 Profiles 2a, 2b, 2c and 2d plotted with the reference profile.

Profiles 3 and 4 are stiff-over-soft profiles. They consist of the reference profile overlain by a stiff surface layer. The thickness of the stiff layer in Profile 3 is 5 ft and the thickness of the stiff layer in Profile 4 is 20 ft. Profiles 3 and 4 were simulated with three different stiffness values of the surface layer. The shear wave velocities of the three different stiff layers are 1000, 1500 and 2000 ft/sec for both Profile 3 and Profile 4 and designated with a, b and c respectively. Profiles 3a, 3b, and 3c are shown in Figure 3-15 and Profiles 4a, 4b and 4c are shown in Figure 3-16.

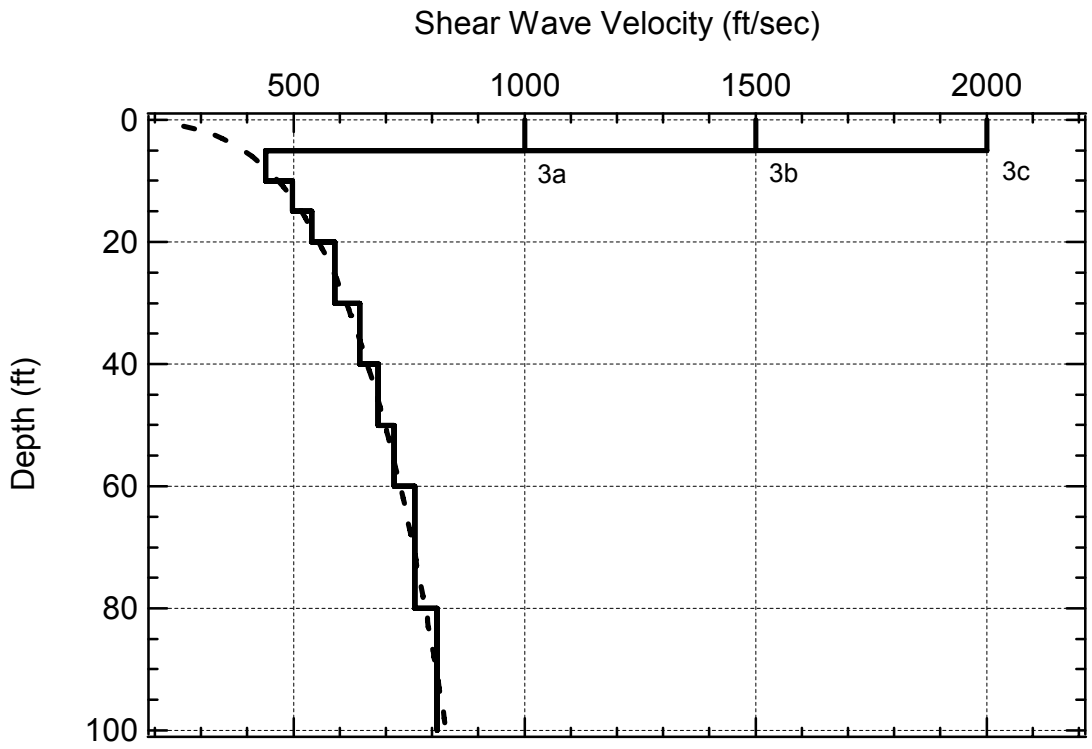

Figure 3-15 Profiles 3a, 3b and 3d plotted with the reference profile.

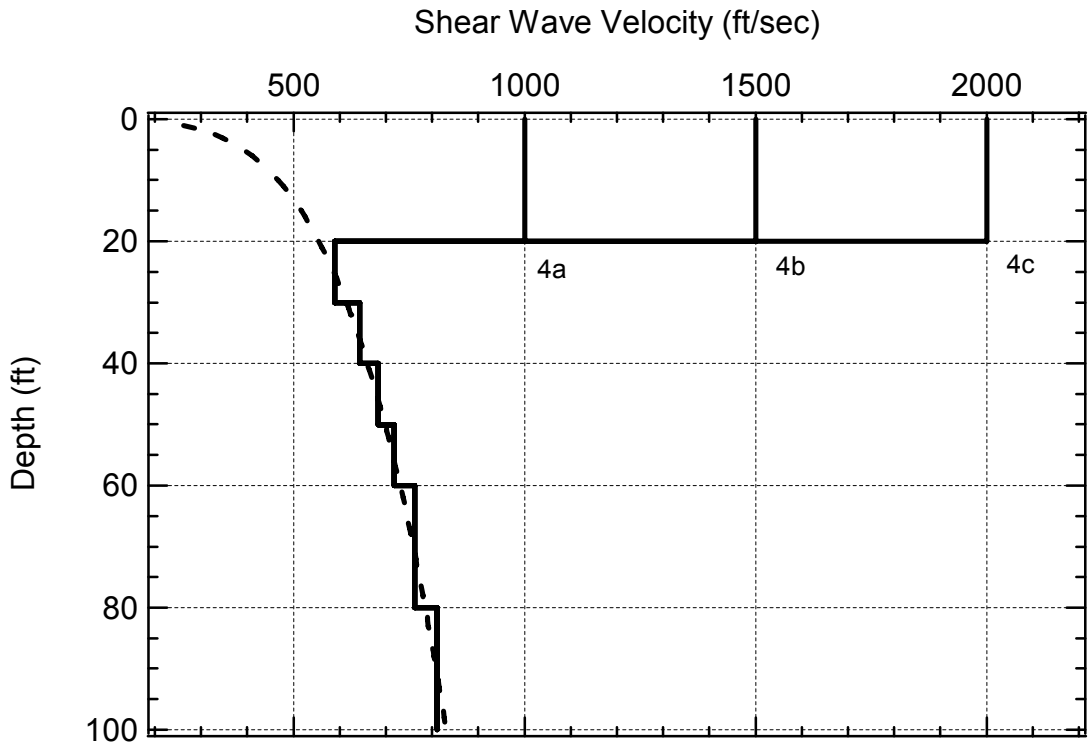

Figure 3-16 Profiles 4a, 4b and 4c plotted with the reference profile.

Profiles 5 and 6 are profiles with an embedded stiff layer. Both profiles consist of the reference profile with a stiff layer embedded at a depth of 20 ft. The thickness of the stiff layer in Profile 5 and 6 is 10 and 20 ft respectively. Profiles 5 and 6 were simulated with the velocity of the stiff layer at three different values. The shear wave velocities of the stiff layers are 1000, 1500 and 2000 ft/sec, and these differences are indicated by designating Profile 5 and 6 with a, b and c, respectively. Profiles 5a, 5b and 5c are shown with the reference profile in Figure 3-17 and Profiles 6a, 6b and 6c are plotted with the reference profile in Figure 3-18.

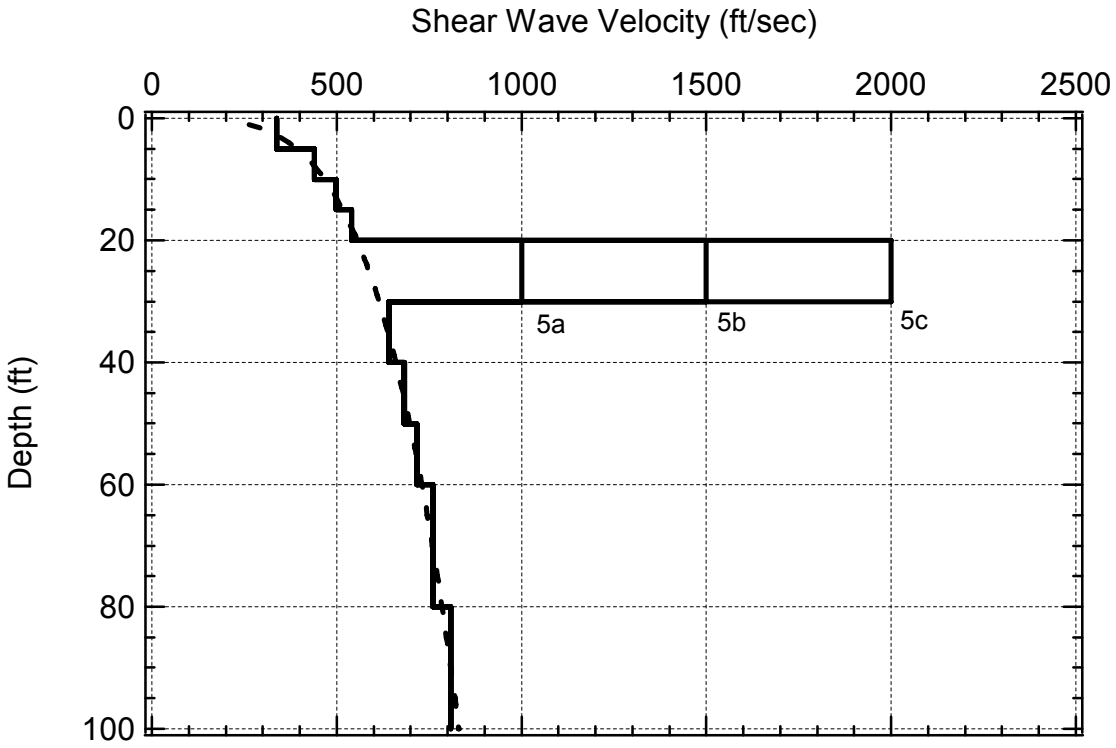

Figure 3-17 Profiles 5a, 5b and 5c plotted with the reference profile.

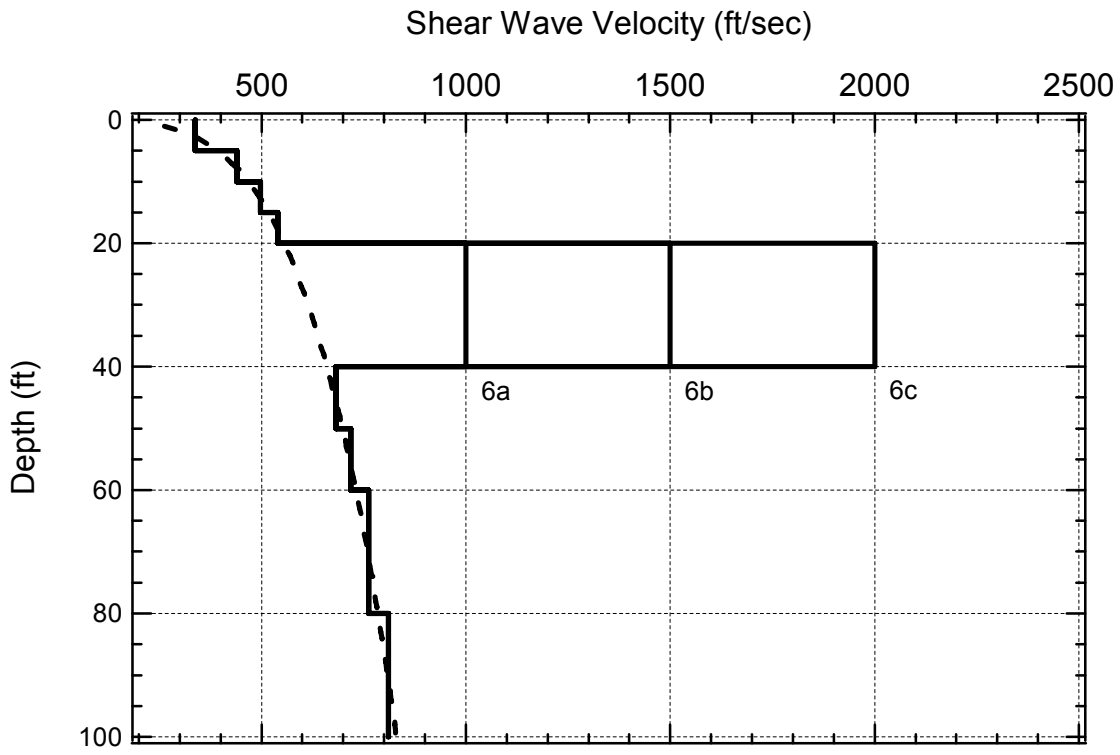

Figure 3-18 Profiles 6a, 6b and 6c plotted with the reference profile.

Profile 7 is a stiff-over-soft-over-stiff profile. It consists of the reference profile with a 20-ft thick stiff layer at the surface and a stiff halfspace at a depth of 50 ft. Three different shear wave velocities of the stiff layer for Profile 7 were simulated. The shear wave velocities of the stiff layers were 1000, 1500 and 2000 ft/sec, for Profiles 7a, 7b and 7c respectively. Profiles 7a, 7b and 7c are plotted with the reference profile in Figure 3-19.

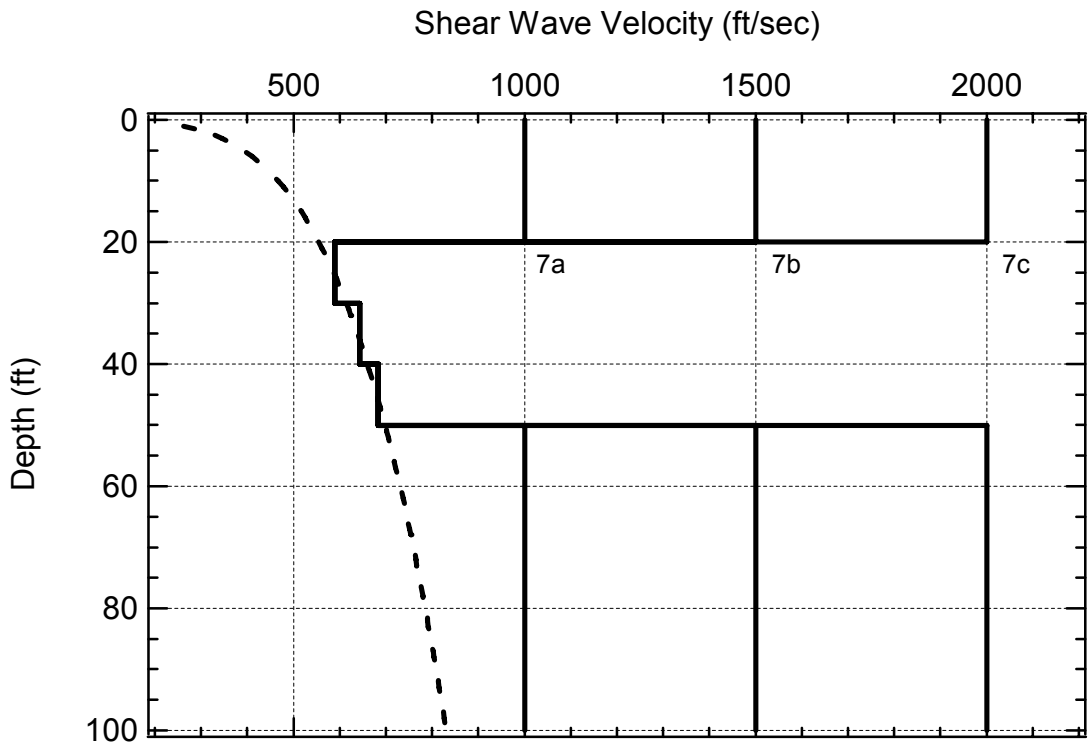

Figure 3-19 Profiles 7a, 7b and 7c plotted with the reference profile.

3.7 Summary

The data analysis procedures used to develop simulated experimental and theoretical dispersion curves were presented in this chapter. The first step in the data analysis was the creation of synthetic time records using FitSASW for receiver spacing of 6, 12, 25, 50, 100 and 200 feet. A simulated experimental dispersion curve was then created for each receiver spacing from the phase unwrapping procedures previously described in Section 3.3. The individual dispersion curves were combined to form a composite dispersion curve for that profile. Average global and array experimental dispersion curves were then created from the simulated effective velocity experimental dispersion curve as described in Section 2.5.4.

Theoretical effective velocity dispersion curves were generated for each site as described in Section 2.5.4. The global dispersion curve was determined at distances of 2λ and 4 λ from the source to create a single theoretical curve for the site. In addition, theoretical array dispersion curves were calculated for each pair of receivers used to develop the simulated experimental dispersion curve. Figure 3-20 is a flow chart summarizing the calculations and data generation involved in conducting this research.

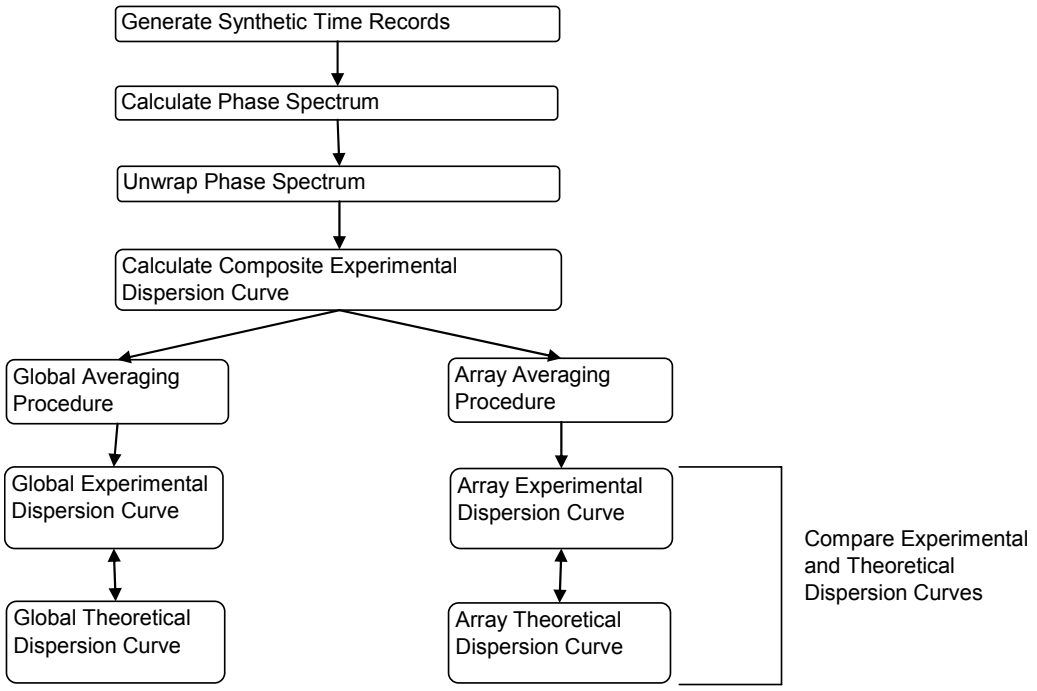

Figure 3-20 Flowchart showing the progression of calculations and data generation.

A total of 23 shear wave velocity profiles were created which represent various geotechnical conditions. The profiles were developed from a reference shear wave velocity profile with gradually increasing V_S with depth. Comparisons between the simulated experimental dispersion curves and the theoretical dispersion curves for each of the profiles were made to evaluate the

effectiveness of the global and array SASW approaches. The comparisons are presented in Chapter 4 and discussed in Chapter 5.

Chapter 4 Results

4.1 Introduction

Time records were simulated for 7 baseline profiles. The 7 profiles were created from variations of the reference profile that has a gradually increasing shear wave velocity with depth. Four soil layering schemes with distinct velocity changes were created, including: (1) soft-over-stiff, (2) stiff-over-soft, (3) embedded stiff layer and (4) embedded soft layer. For each baseline profile additional simulations were performed by modifying the stiffness of one or more of the layers. These additional profiles are identified with a, b, c and d. Phase plots were unwrapped as described in Chapter 3, and experimental and theoretical dispersion curves were calculated. The experimental dispersion curves calculated were the composite and individual experimental dispersion curves and the array and global average dispersion curves. Global and array theoretical dispersion curves were calculated, as described in Chapter 3, and compared to the experimental dispersion curves.

In this chapter the results from the simulations are presented for the soil profiles described in Chapter 3. Four plots are shown for each profile comparing the simulated experimental results to the theoretical results. The plots consist of the global analysis presented in both the wavelength and frequency domains and the array analysis, also presented in both the wavelength and frequency domains.

4.2 Reference Profile

The reference profile is presented in Figure 4-1. The simulated dispersion curves for the reference profile are shown in Figures 4.2, 4.3, 4.4 and 4.5. Table 4.1 lists the individual layer characteristics of the reference profile.

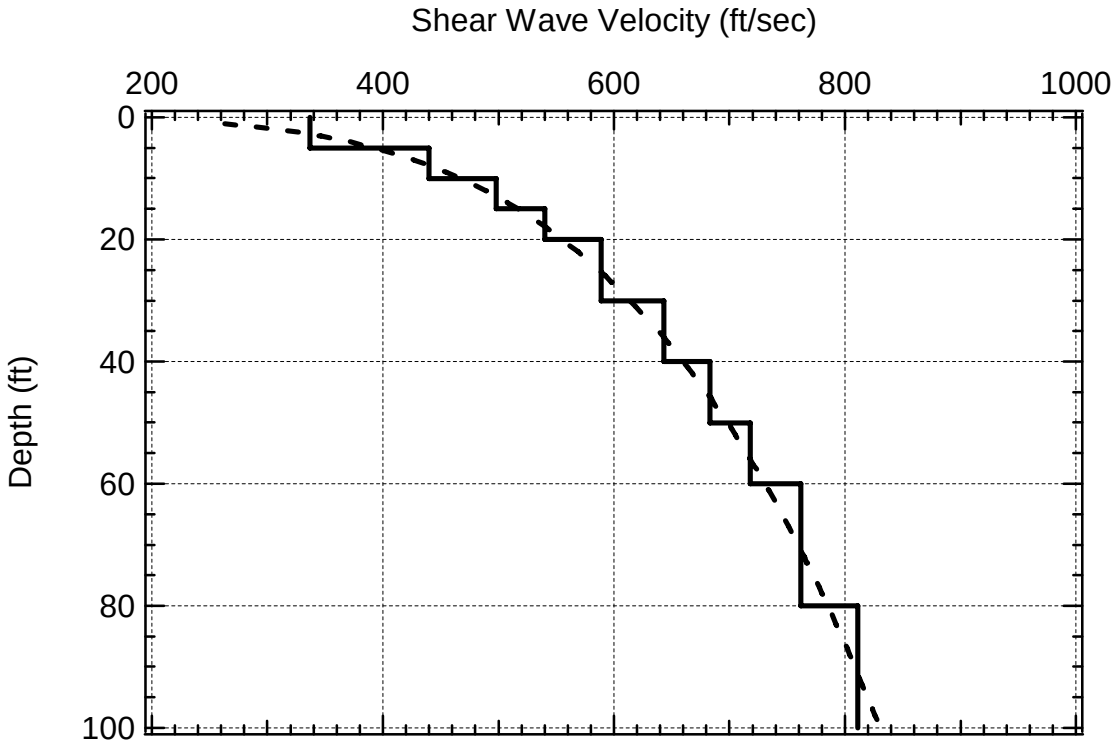

Figure 4-1 Reference profile shown with layering used for simulations.

Table 4-1 Individual layer characteristics of the layered reference profile.

Layer	Thickness (ft)	V_S (ft/sec)	ν	Unit Weight (pcf)
1	5	337	0.25	120
2	5	440	0.25	120
3	5	498	0.25	120
4	5	540	0.25	120
5	10	589	0.25	120
6	10	643	0.25	120
7	10	683	0.25	120
8	10	718	0.25	120
9	20	762	0.25	120
10	Halfspace	811	0.25	120

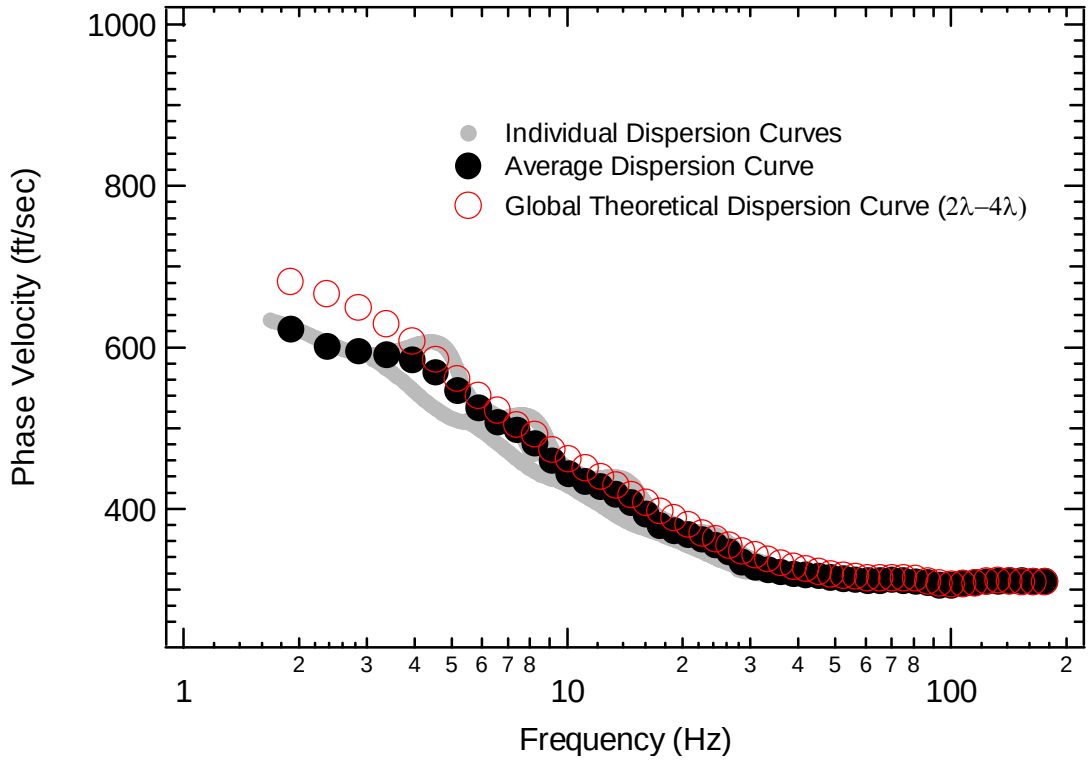

Figure 4-2 **Simulated experimental dispersion curves (individual and global average) versus global theoretical dispersion curve, plotted versus frequency for the reference profile.**

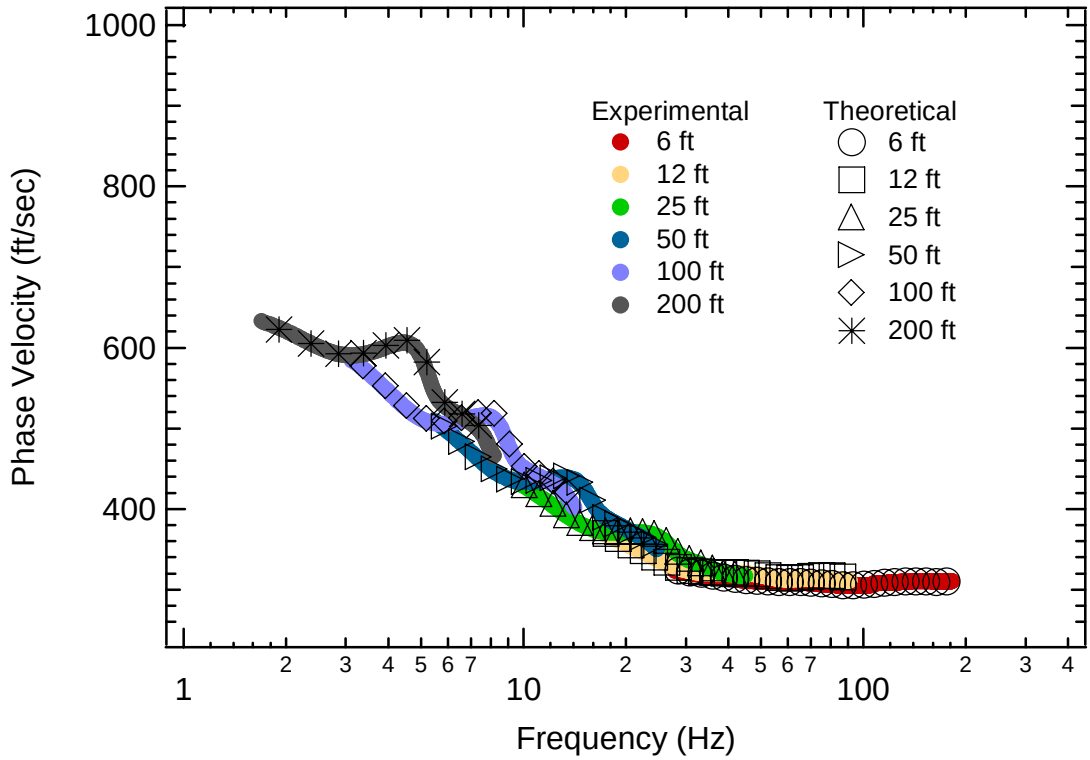

Figure 4-3 **Experimental individual dispersion curves and the array theoretical dispersion curves plotted versus frequency for the reference profile.**

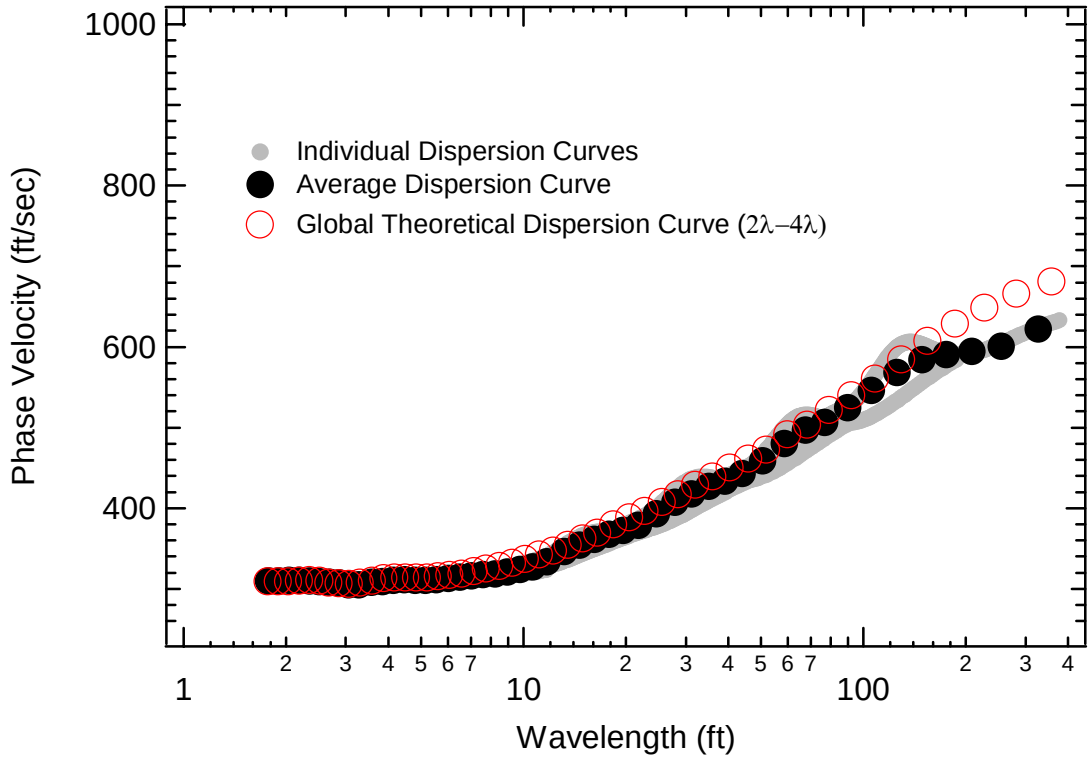

Figure 4-4 **Simulated experimental dispersion curves (individual and global average) versus global theoretical dispersion curve, plotted versus wavelength for the reference profile.**

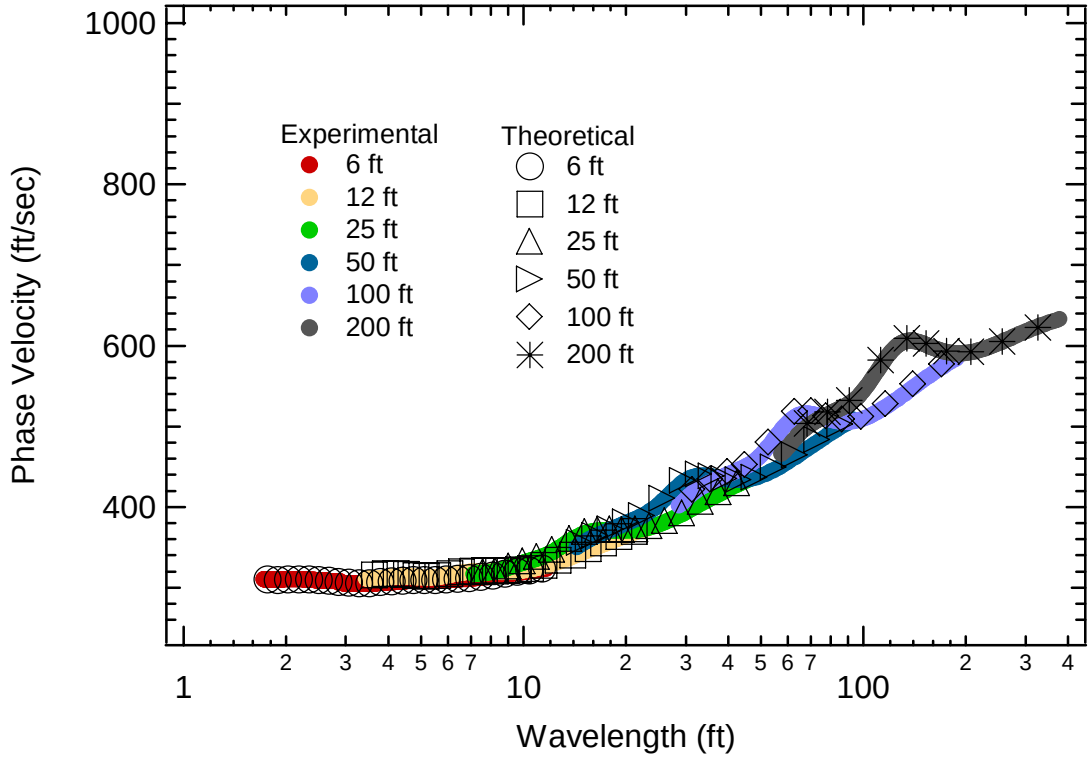

Figure 4-5 **Experimental individual dispersion curves and the array theoretical dispersion curves plotted versus wavelength for the reference profile.**

4.3 Soft-over-Stiff Profiles

4.3.1 Profile 1a

Profile 1a is presented in Figure 4-6. Table 4-2 shows the individual layer characteristics for Profile 1a. Figures 4-6, 4-7, 4-8 and 4-9 show the simulated experimental and theoretical dispersion curves developed for this profile.

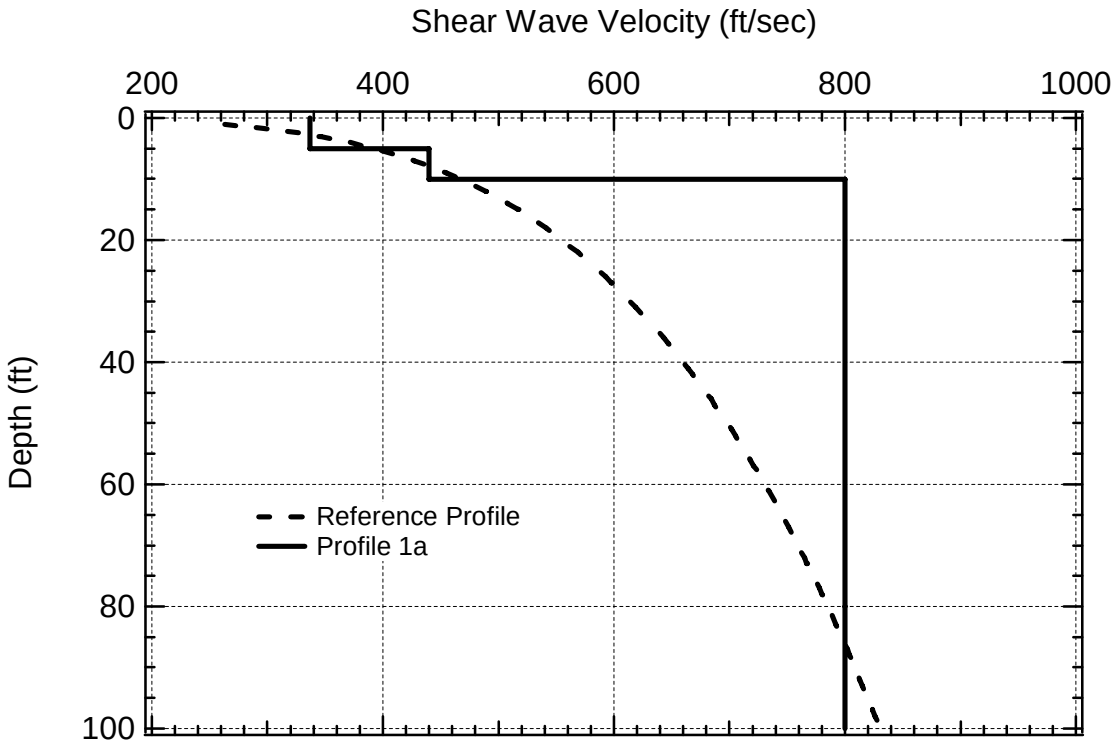

Figure 4-6 Profile 1a shown with the reference profile.

Table 4-2 Individual layer characteristics for Profile 1a.

Layer	Thickness (ft)	V_S (ft/sec)	ν	Unit Weight (pcf)
1	5	337	0.25	120
2	5	440	0.25	120
3	Halfspace	800	0.25	120

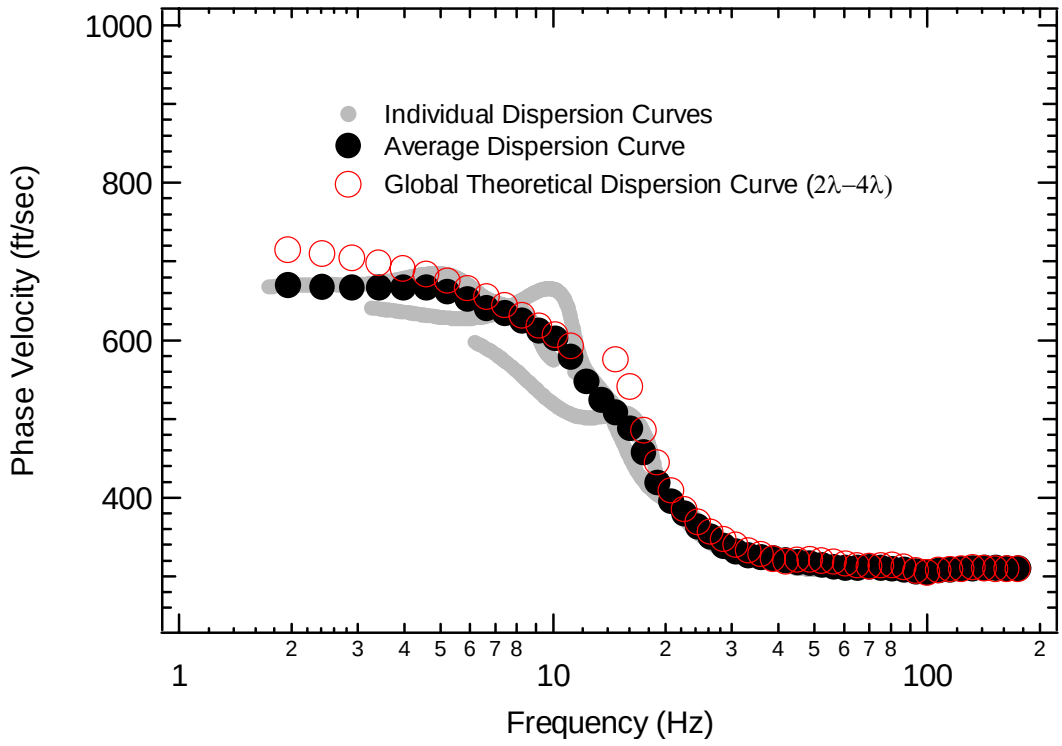

Figure 4-7 **Simulated experimental dispersion curves (individual and global average) versus global theoretical dispersion curve, plotted versus frequency for Profile 1a.**

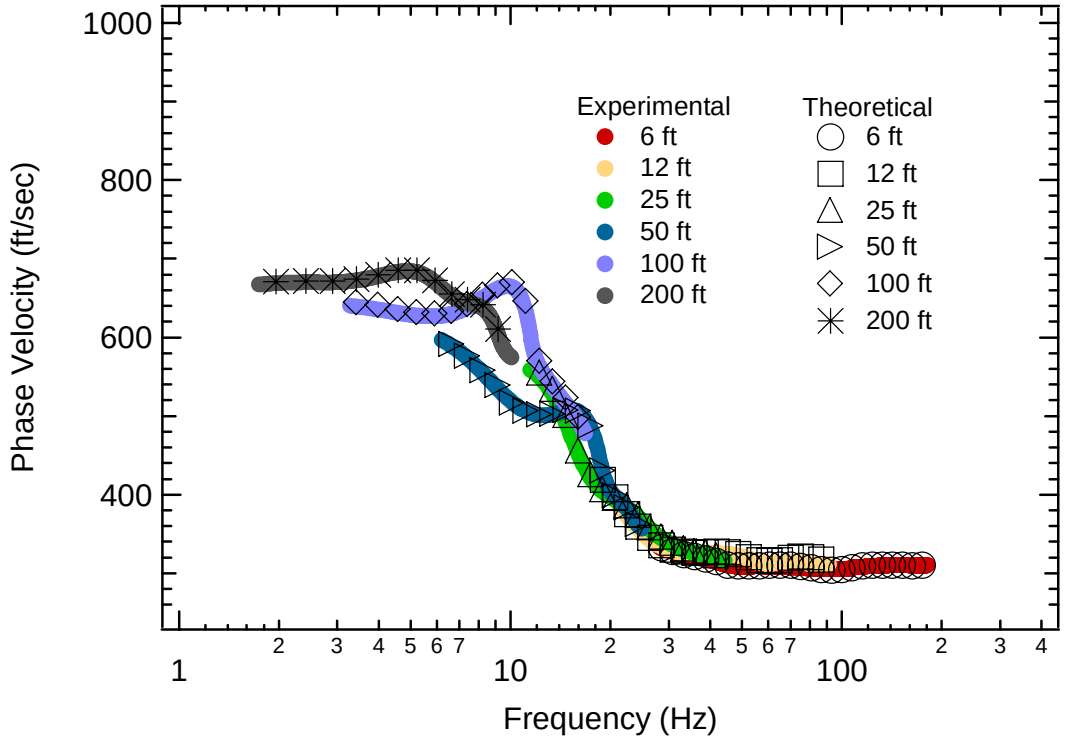

Figure 4-8 **Experimental individual dispersion curves and the array theoretical dispersion curves plotted versus frequency for Profile 1a.**

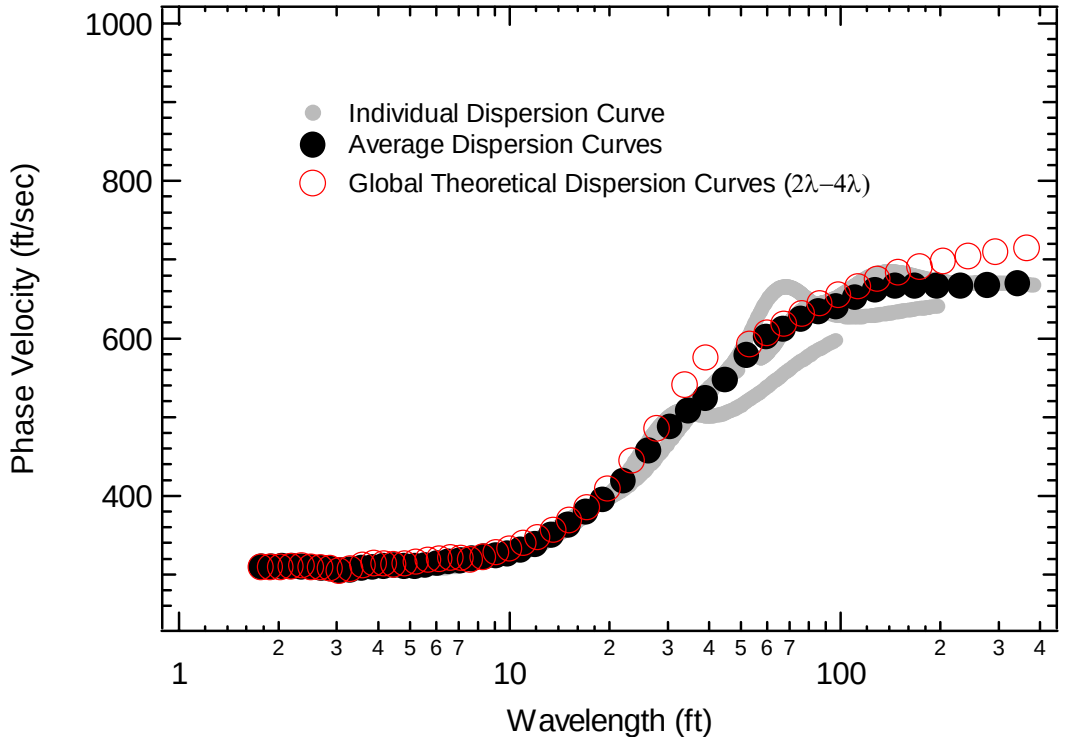

Figure 4-9 **Simulated experimental dispersion curves (individual and global average) versus global theoretical dispersion curve, plotted versus wavelength for Profile 1a.**

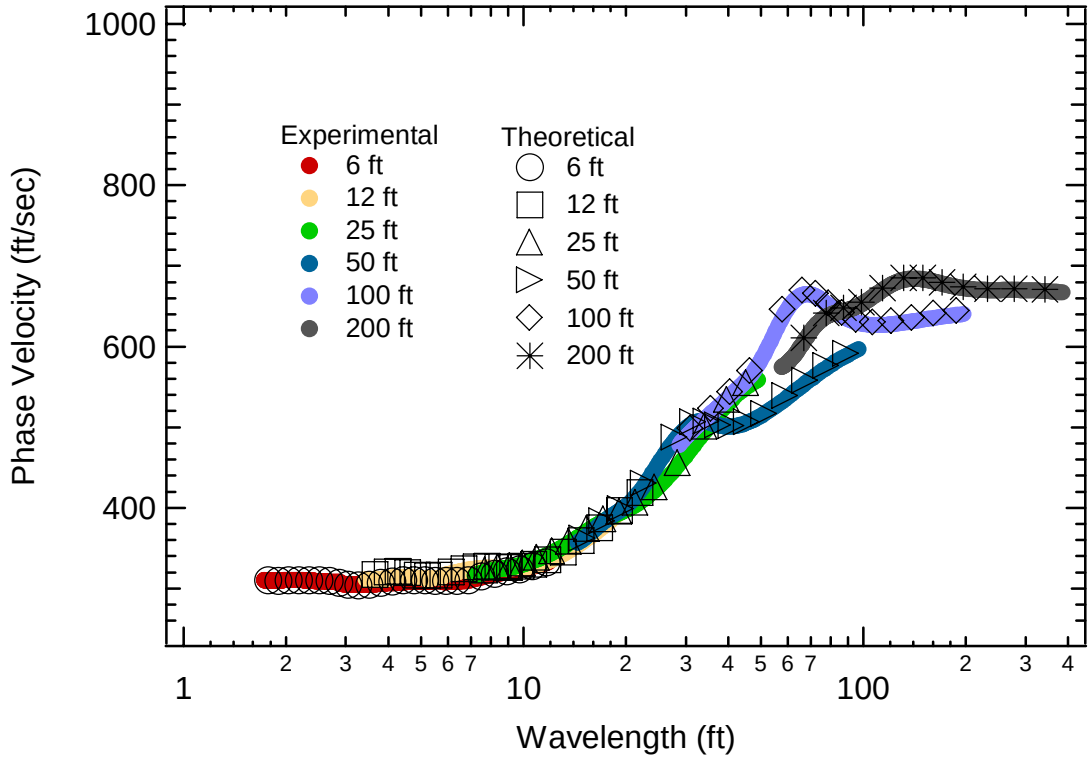

Figure 4-10 **Experimental individual dispersion curves and the array theoretical dispersion curves plotted versus wavelength for Profile 1a.**

4.3.2 Profile 1b

Profile 1b is presented in Figure 4-11. Table 4-3 shows the individual layer characteristics for Profile 1b. Figures 4-12, 4-13, 4-14 and 4-15 show the simulated experimental and theoretical dispersion curves for this profile.

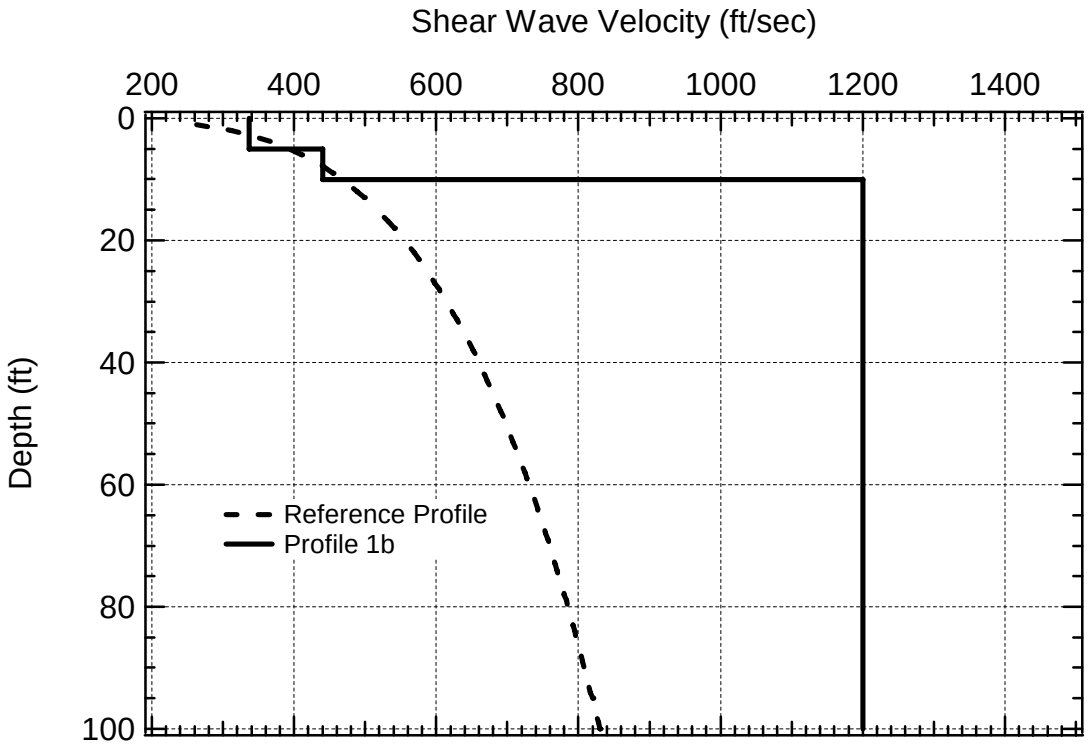

Figure 4-11 Profile 1b shown with the reference profile.

Table 4-3 Individual layer characteristics for Profile 1b.

Layer	Thickness (ft)	V_S (ft/sec)	ν	Unit Weight (pcf)
1	5	337	0.25	120
2	5	440	0.25	120
3	Halfspace	1200	0.25	120

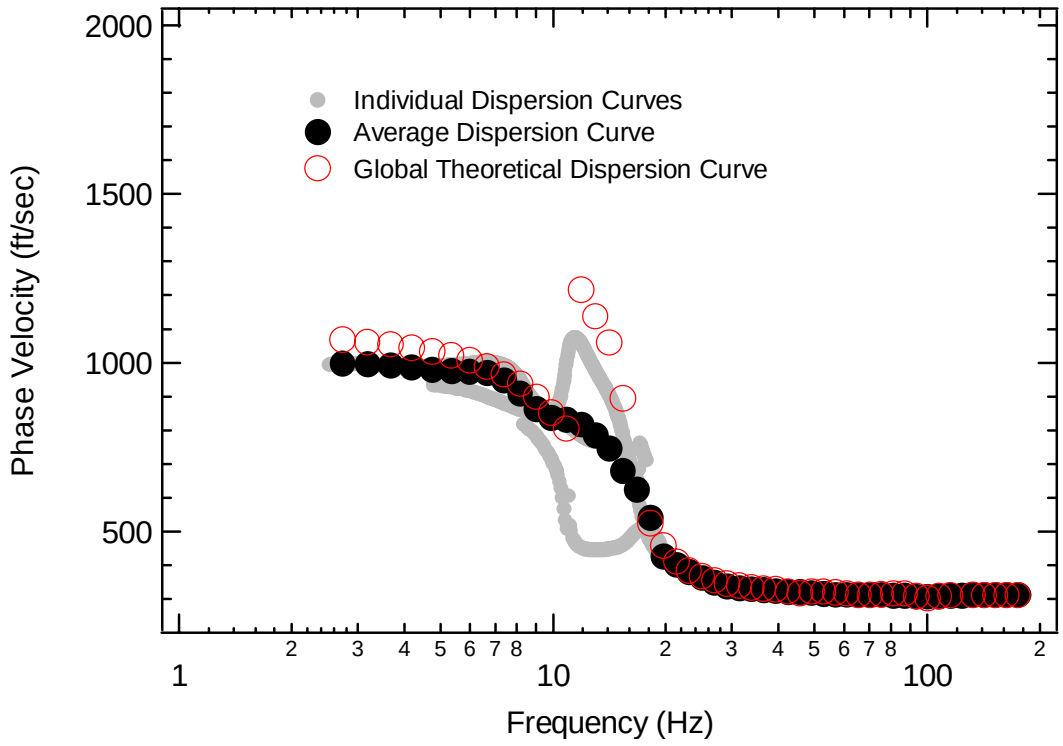

Figure 4-12 **Simulated experimental dispersion curves (individual and global average) versus global theoretical dispersion curve, plotted versus frequency for Profile 1b.**

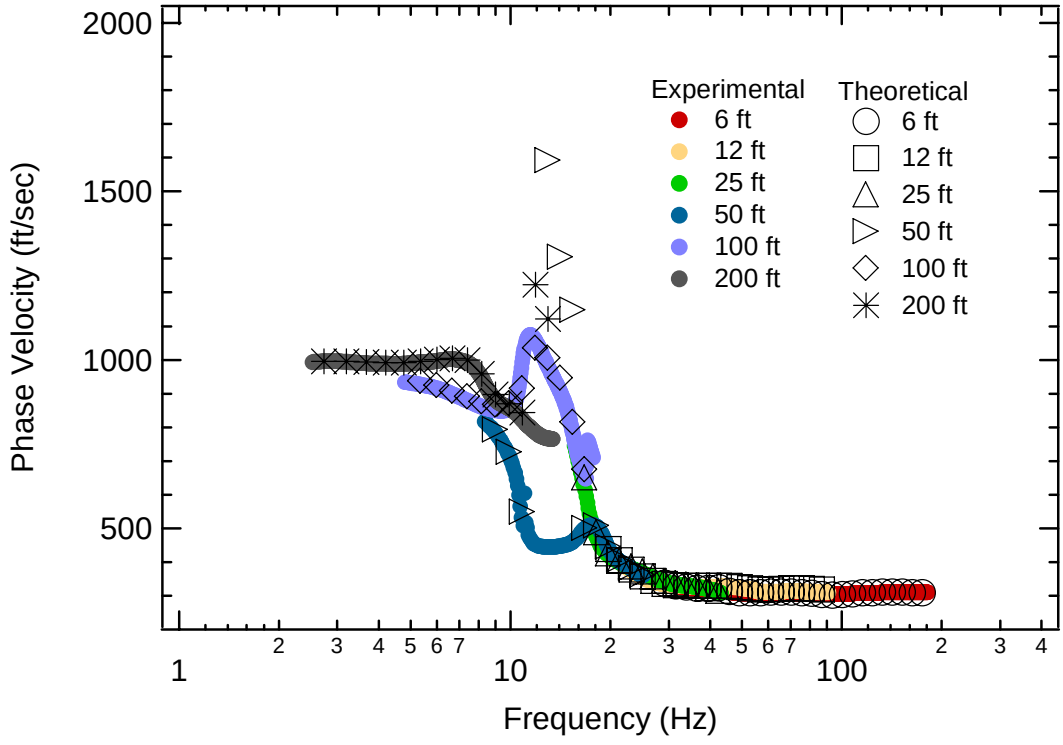

Figure 4-13 **Individual experimental dispersion curves and array theoretical dispersion curves plotted versus frequency for Profile 1b.**

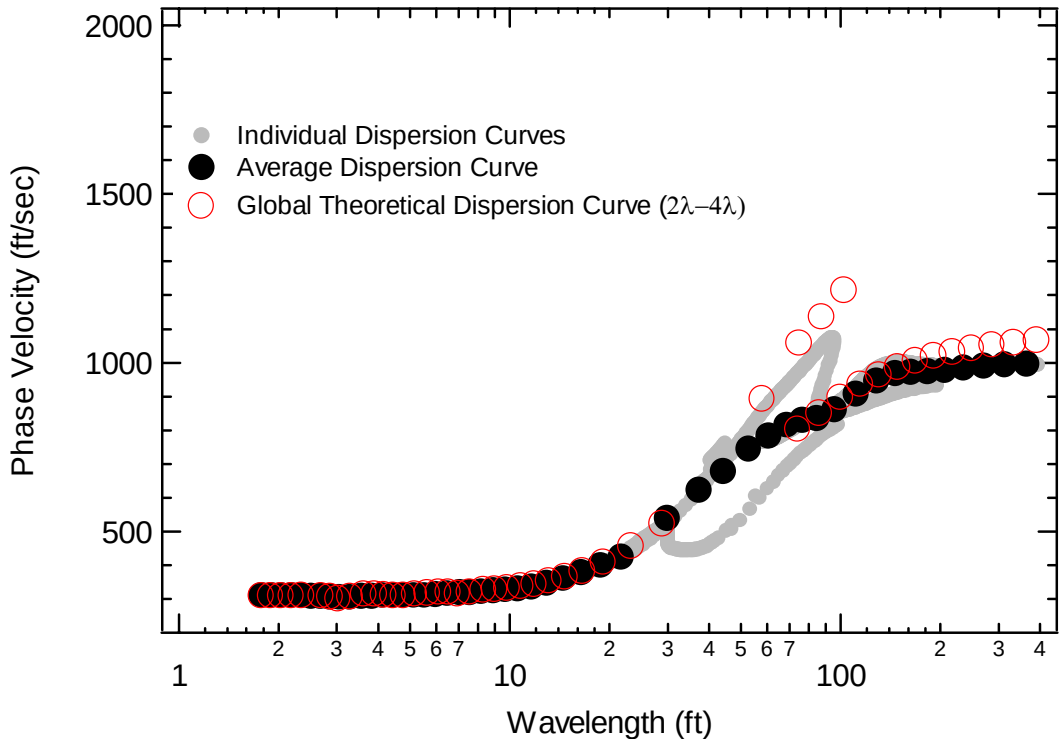

Figure 4-14 **Simulated experimental dispersion curves (individual and global average) versus global theoretical dispersion curve, plotted versus wavelength for Profile 1b.**

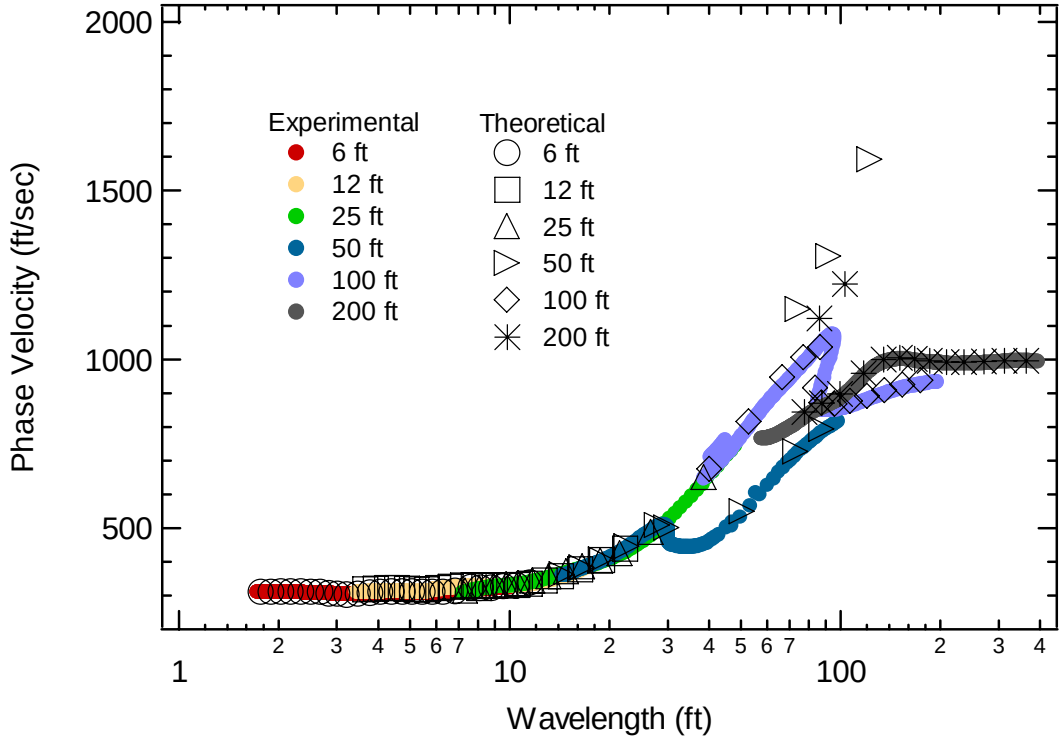

Figure 4-15 **Individual experimental and array theoretical dispersion curves plotted versus wavelength for Profile 1b.**

4.3.3 Profile 1c

Profile 1c is presented in Figure 4-16. Table 4-4 shows the individual layer characteristics for Profile 1c. Figures 4-17, 4-18, 4-19 and 4-20 show the simulated experimental and theoretical dispersion curves for this profile.

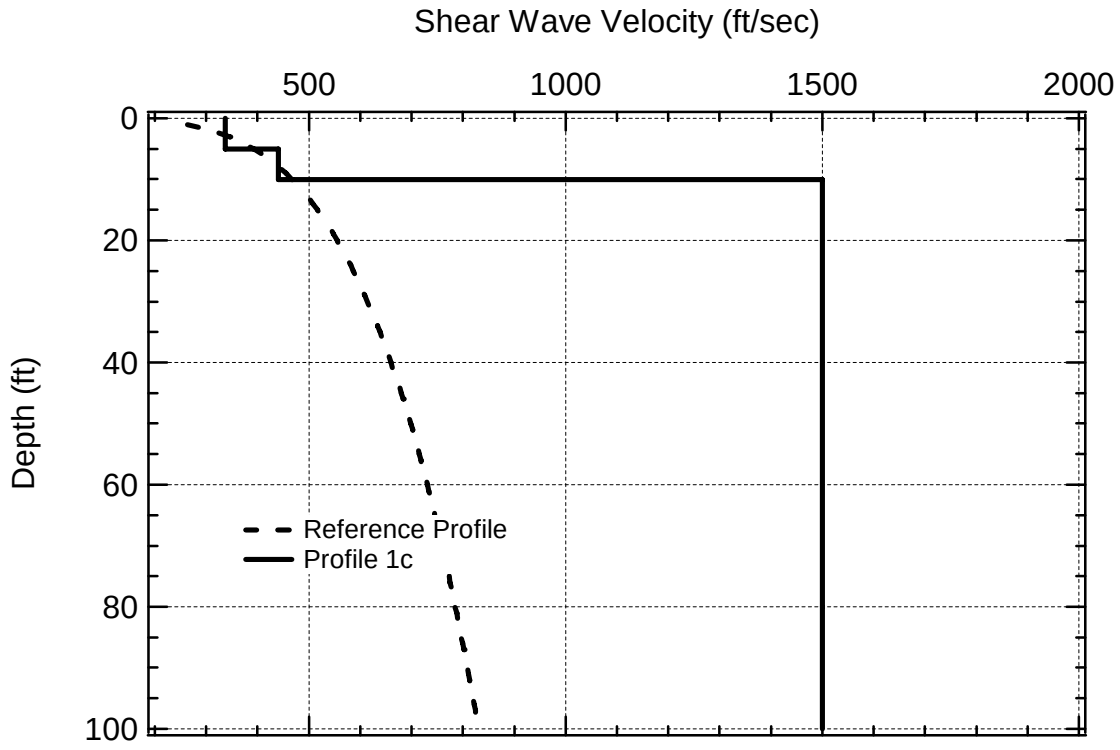

Figure 4-16 Profile 1c shown with the reference profile.

Table 4-4 Individual layer characteristics for Profile 1c.

Layer	Thickness (ft)	V_S (ft/sec)	ν	Unit Weight (pcf)
1	5	337	0.25	120
2	5	440	0.25	120
3	Halfspace	1500	0.25	120

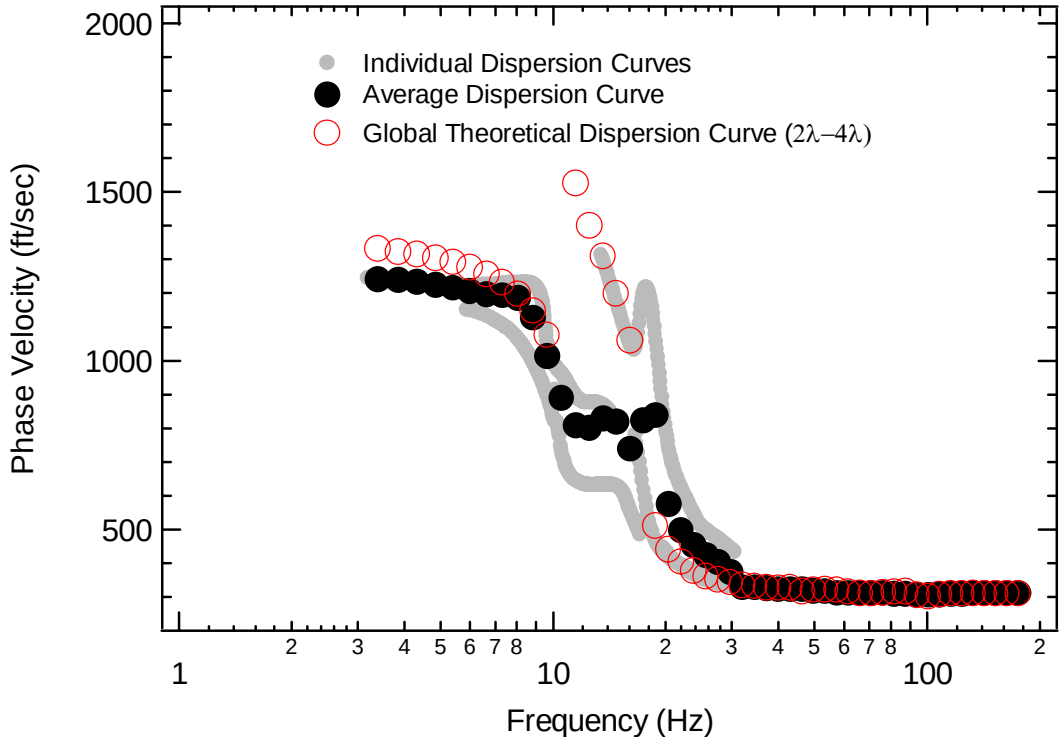

Figure 4-17 **Simulated experimental dispersion curves (individual and global average) versus global theoretical dispersion curve, plotted versus frequency for Profile 1c.**

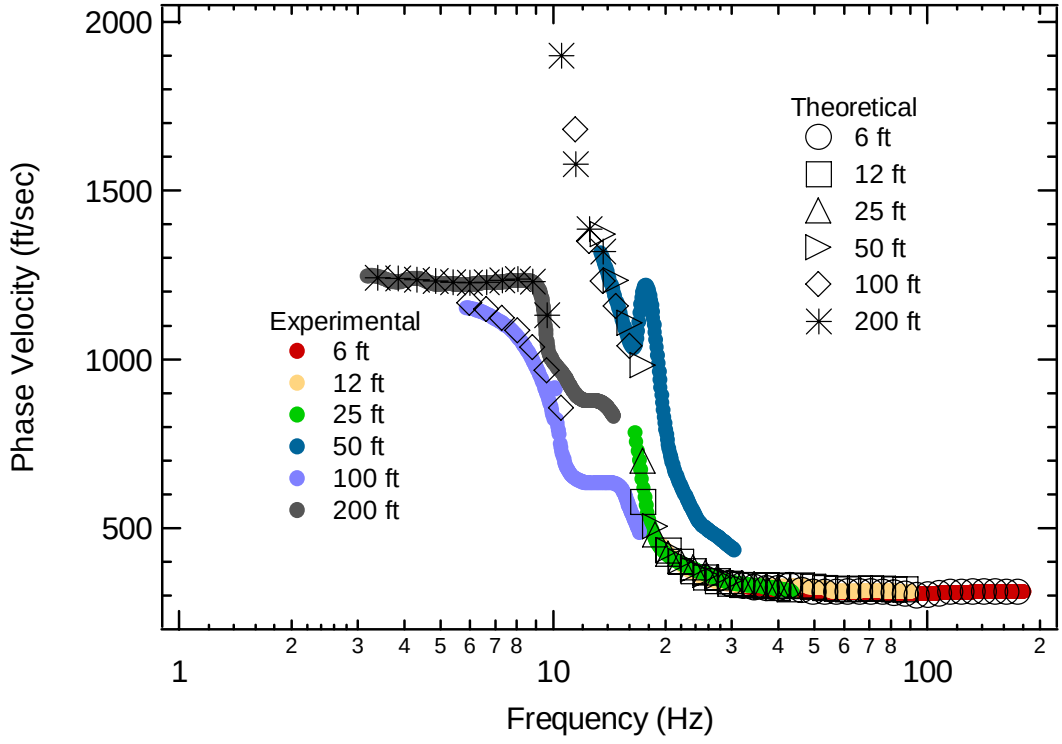

Figure 4-18 **Individual experimental and array theoretical dispersion curves plotted versus frequency for Profile 1c.**

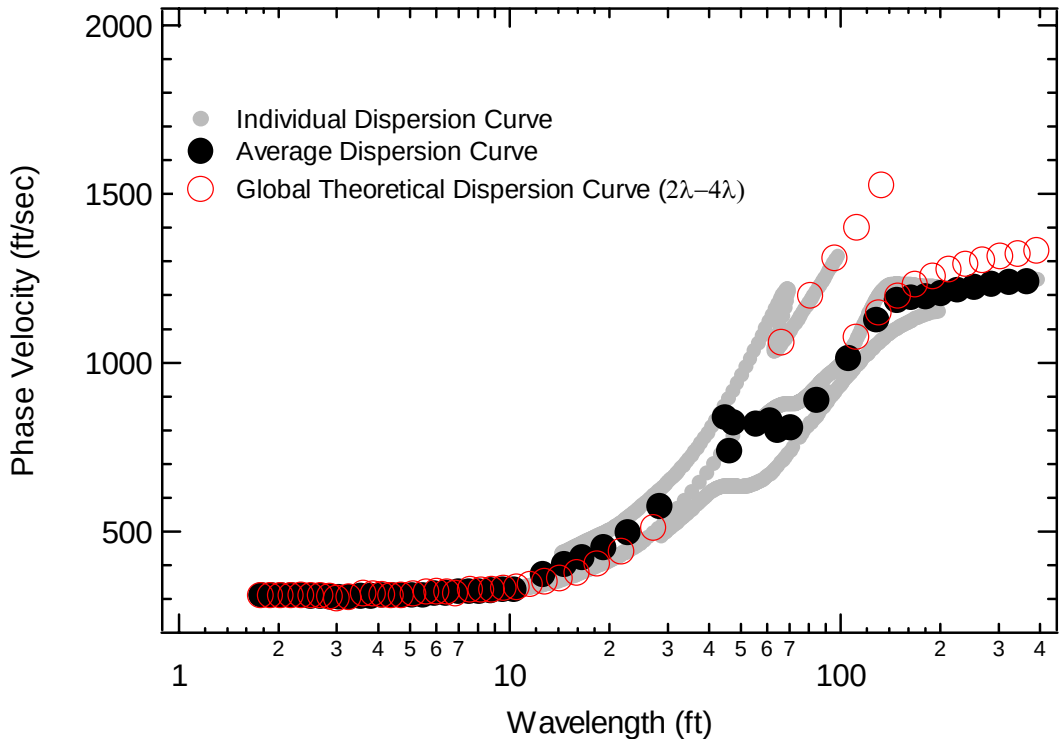

Figure 4-19 **Simulated experimental dispersion curves (individual and global average) versus global theoretical dispersion curve, plotted versus wavelength for Profile 1c.**

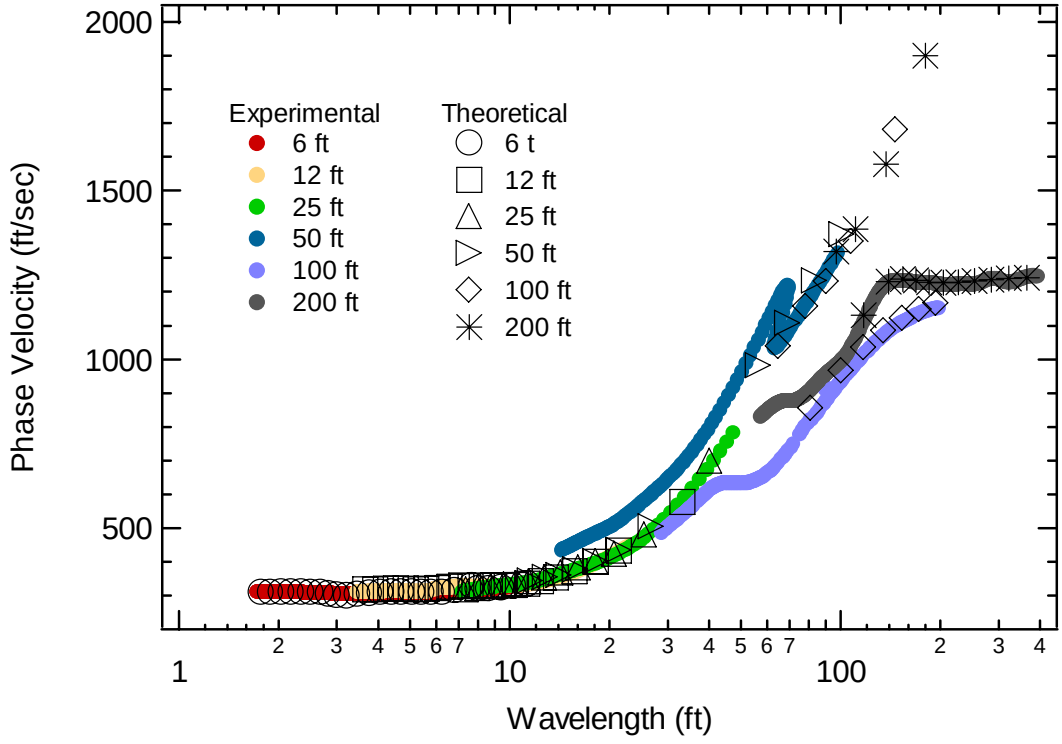

Figure 4-20 **Individual experimental and array theoretical dispersion curves plotted versus wavelength for Profile 1c.**

4.3.4 Profile 2a

Profile 2a is presented in Figure 4-21. Table 4-5 shows the individual layer characteristics for Profile 2a. Figures 4-22, 4-23, 4-24 and 4-25 show the simulated experimental and theoretical dispersion curves for this profile.

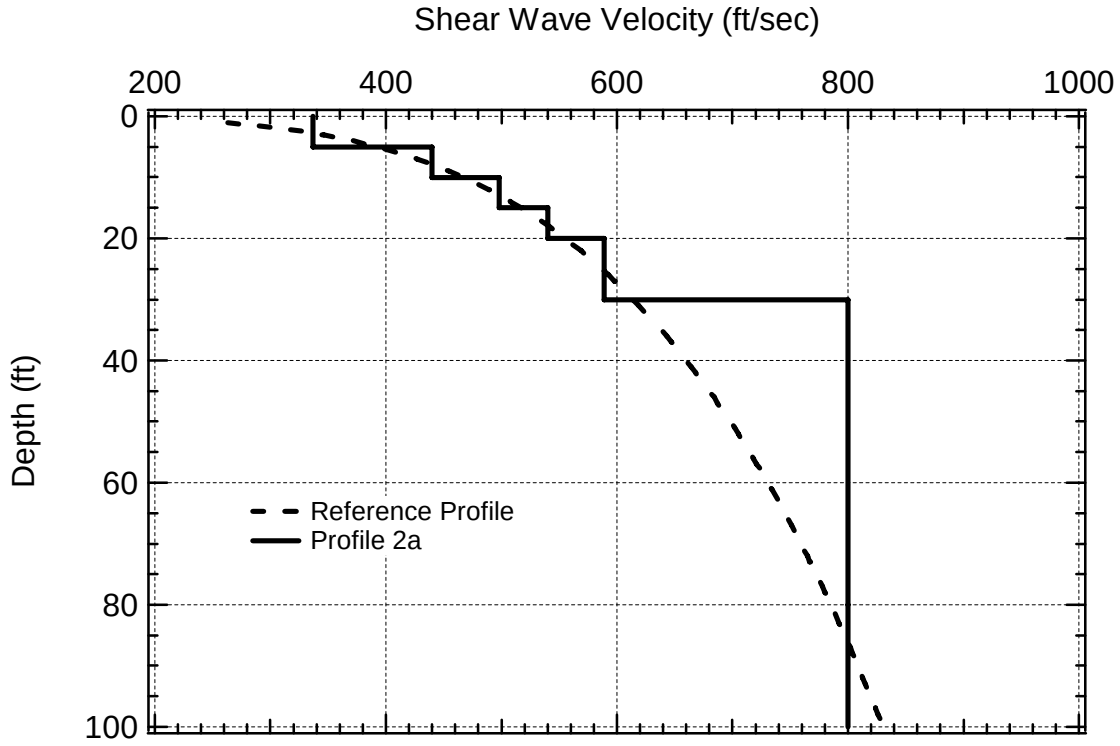

Figure 4-21 Profile 2a shown with the reference profile.

Table 4-5 Individual layer characteristics for Profile 2a.

Layer	Thickness (ft)	V_S (ft/sec)	ν	Unit Weight (pcf)
1	5	337	0.25	120
2	5	440	0.25	120
3	5	498	0.25	120
4	5	540	0.25	120
5	10	589	0.25	120
6	Halfspace	800	0.25	120

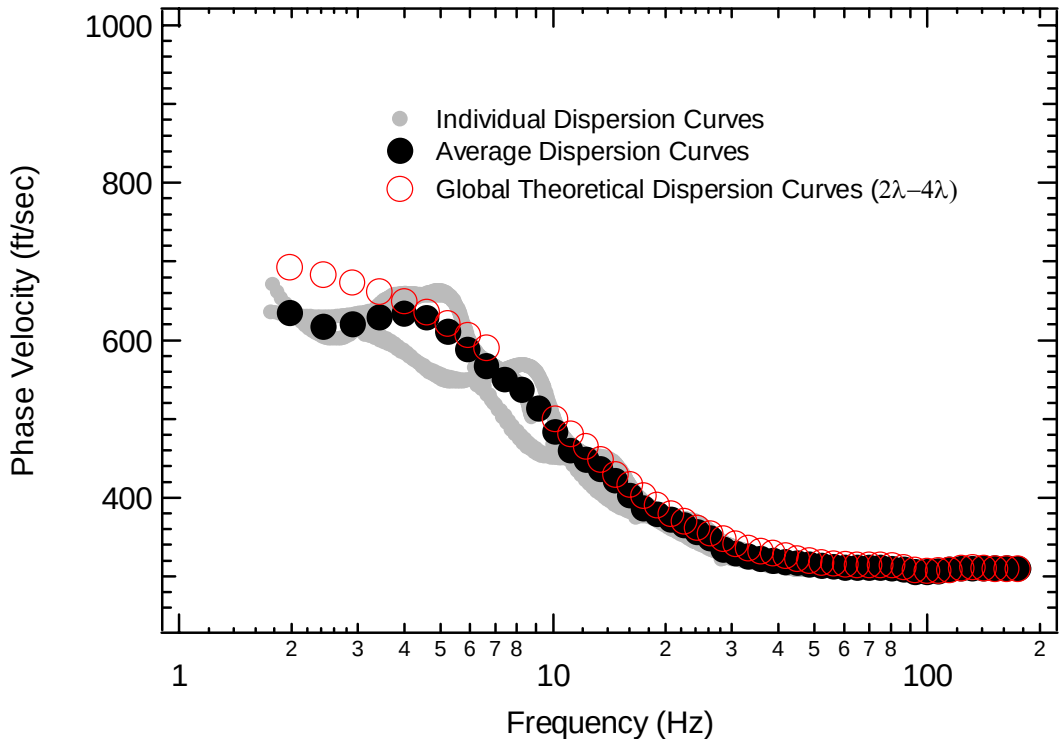

Figure 4-22 **Simulated experimental dispersion curves (individual and global average) versus global theoretical dispersion curve, plotted versus frequency for Profile 2a.**

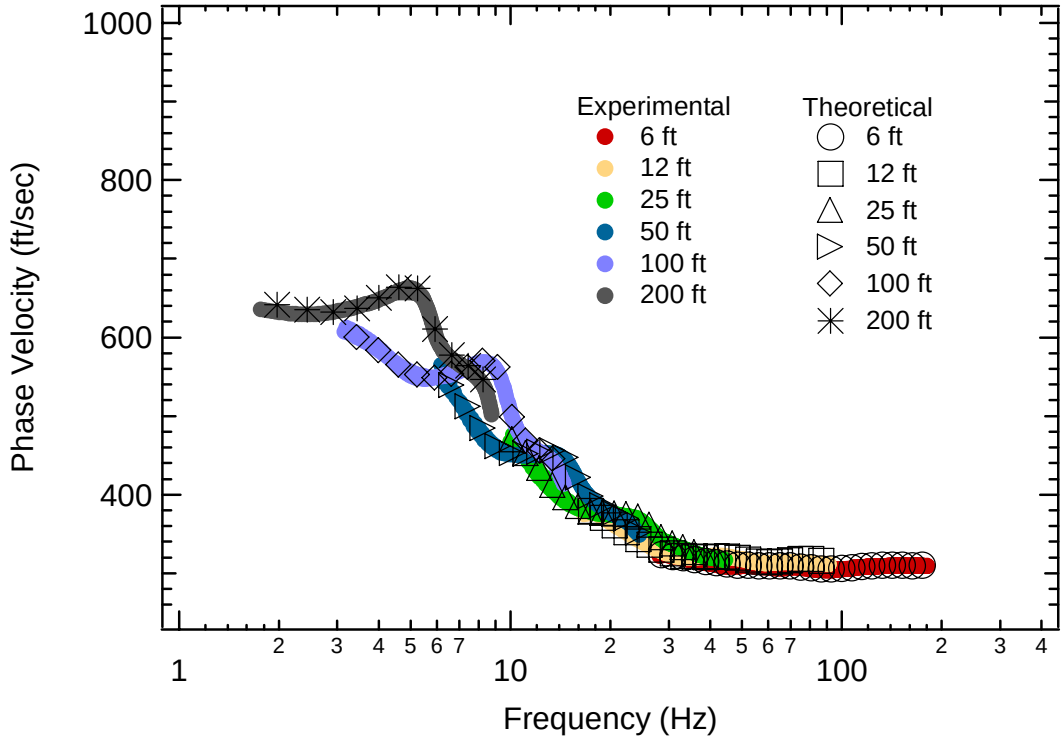

Figure 4-23 **Individual experimental and array theoretical dispersion curves plotted versus frequency for Profile 2a.**

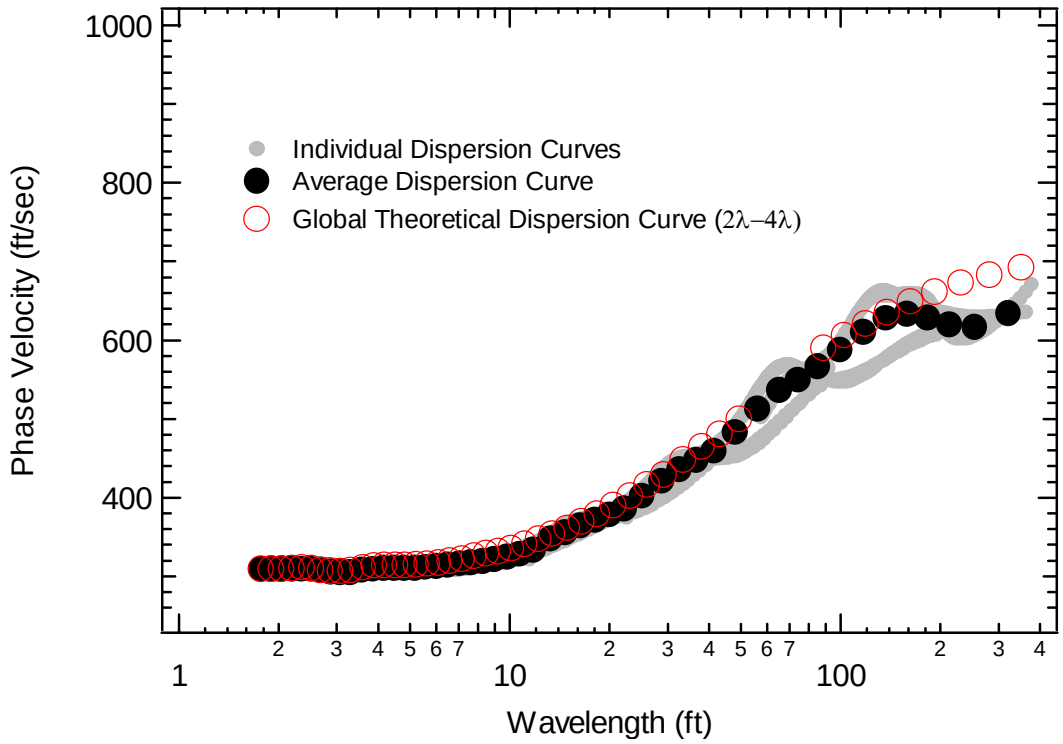

Figure 4-24 **Simulated experimental dispersion curves (individual and global average) versus global theoretical dispersion curve, plotted versus wavelength for Profile 2a.**

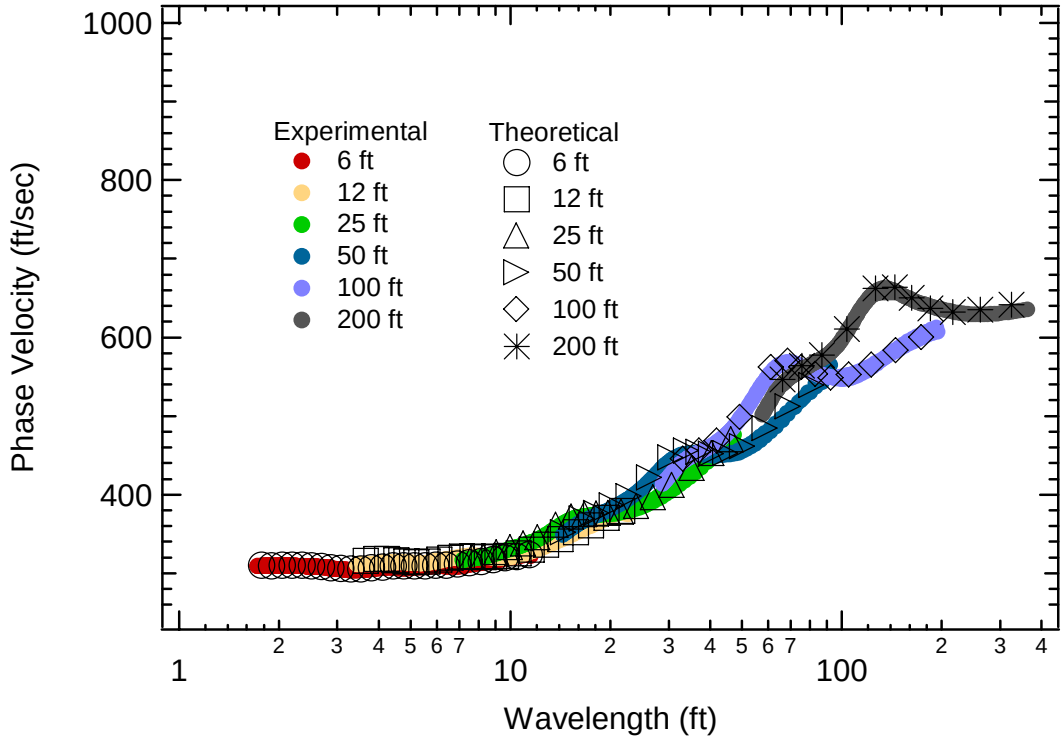

Figure 4-25 **Individual experimental and array theoretical dispersion curves plotted versus wavelength for Profile 2a.**

4.3.5 Profile 2b

Profile 2b is presented in Figure 4-26. Table 4-6 shows the individual layer characteristics for Profile 2b. Figures 4-27, 4-28, 4-29 and 4-30 show the simulated experimental and theoretical dispersion curves for this profile.

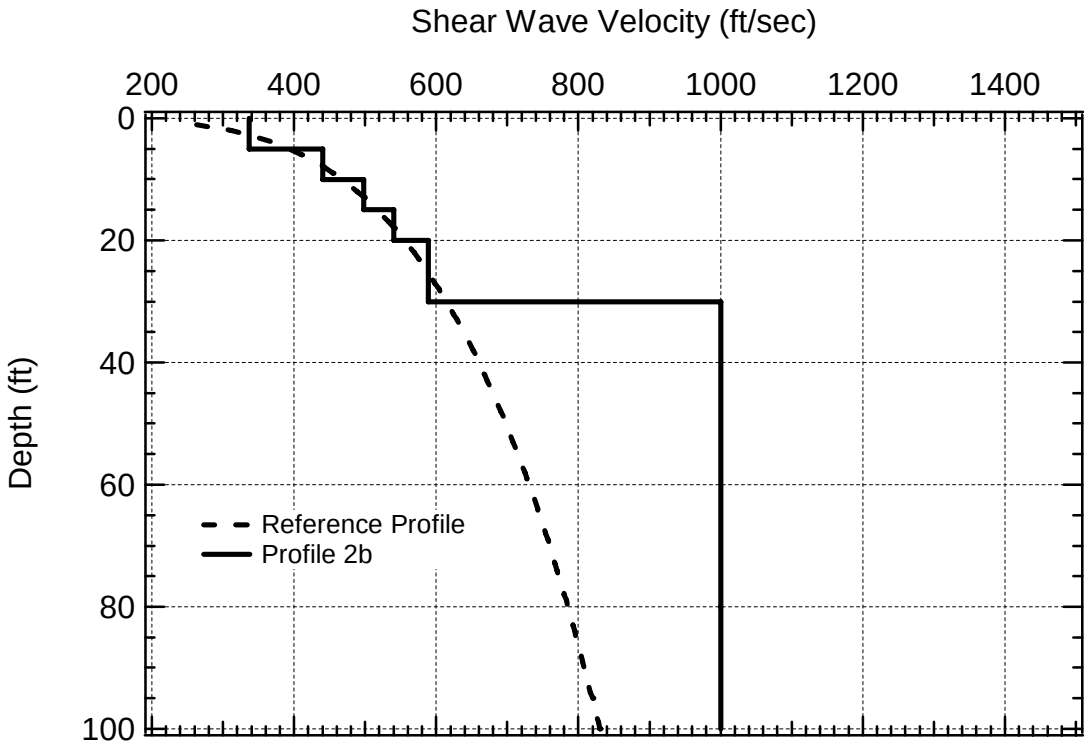

Figure 4-26 Profile 2b shown with the reference profile.

Table 4-6 Individual layer characteristics for Profile 2b.

Layer	Thickness (ft)	V_S (ft/sec)	ν	Unit Weight (pcf)
1	5	337	0.25	120
2	5	440	0.25	120
3	5	498	0.25	120
4	5	540	0.25	120
5	10	589	0.25	120
6	Halfspace	1000	0.25	120

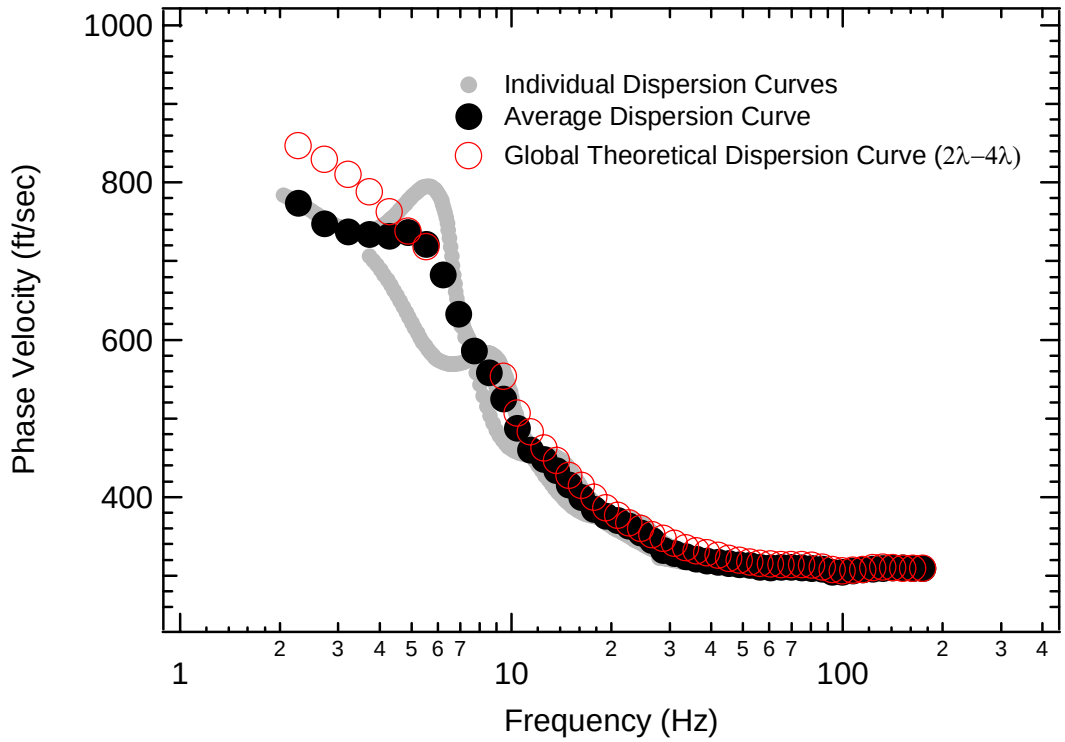

Figure 4-27 **Simulated experimental dispersion curves (individual and global average) versus global theoretical dispersion curve, plotted versus frequency for Profile 2b.**

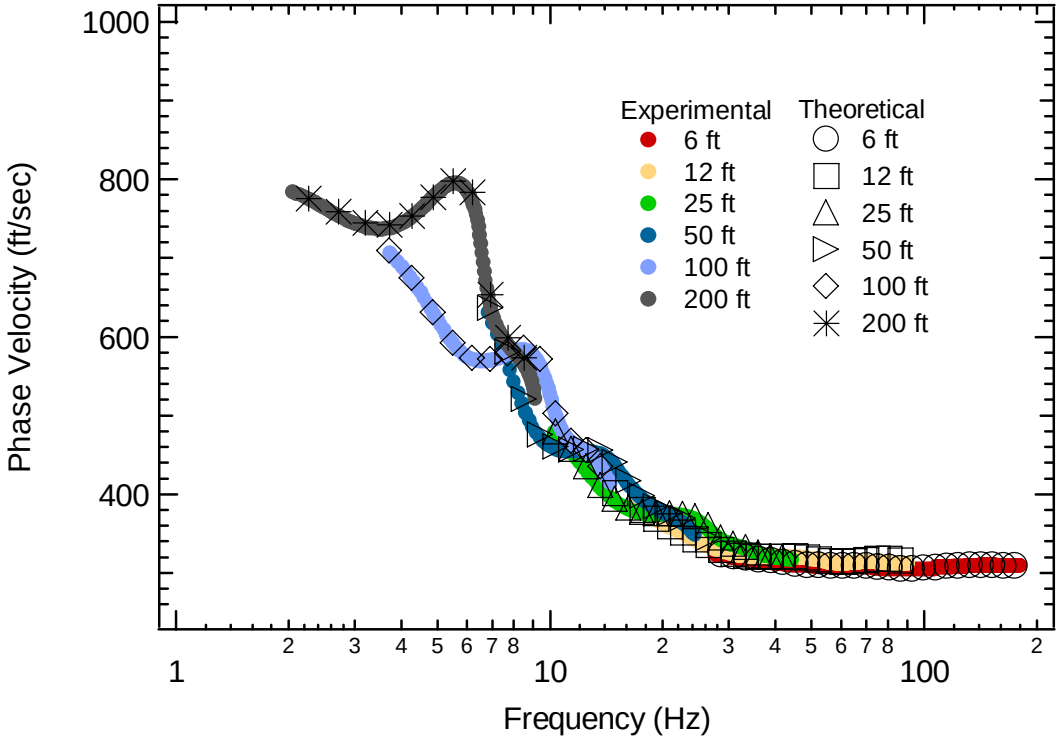

Figure 4-28 **Individual experimental and array theoretical dispersion curves plotted versus frequency for Profile 2b.**

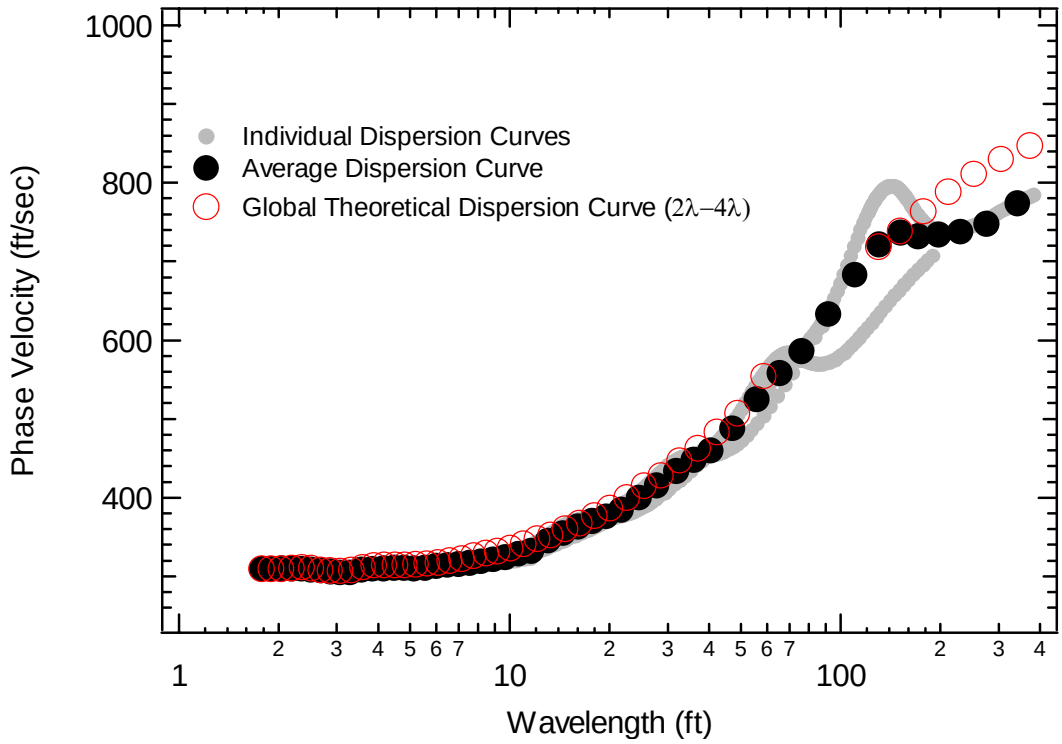

Figure 4-29 **Simulated experimental dispersion curves (individual and global average) versus global theoretical dispersion curve, plotted versus wavelength for Profile 2b.**

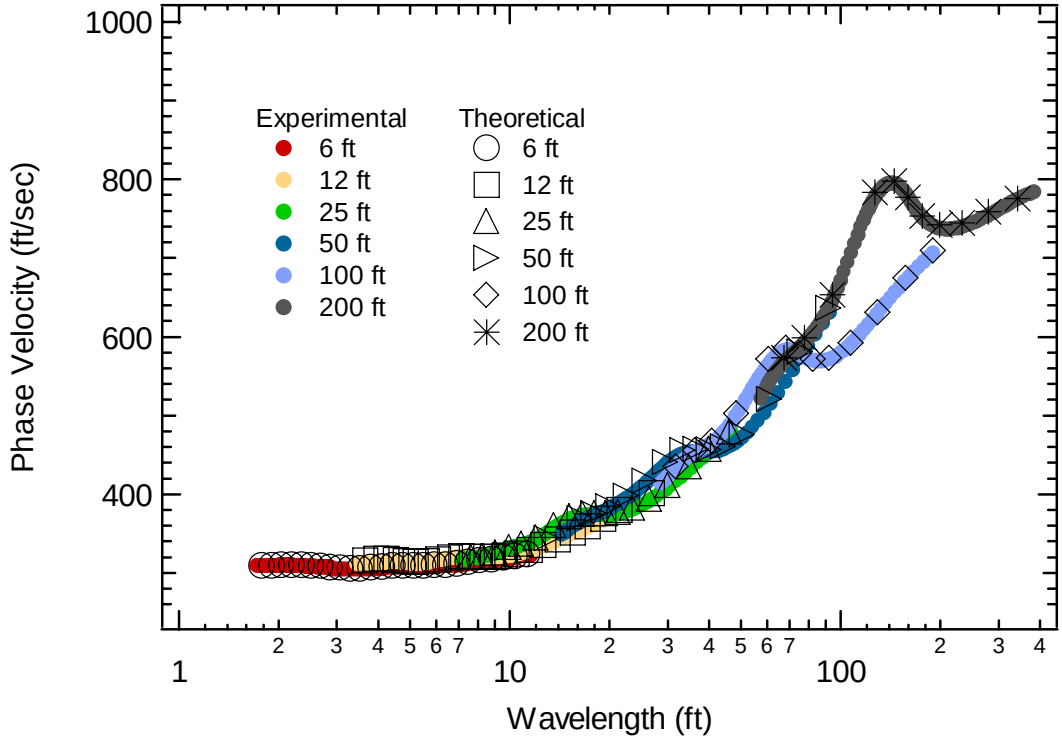

Figure 4-30 **Individual and global average experimental dispersion curves and global theoretical dispersion curve plotted versus wavelength for Profile 2b.**

4.3.6 Profile 2c

Profile 2c is presented in Figure 4-31. Table 4-7 shows the individual layer characteristics for Profile 2c. Figures 4-32, 4-33, 4-34 and 4-35 show the simulated experimental and theoretical dispersion curves for this profile.

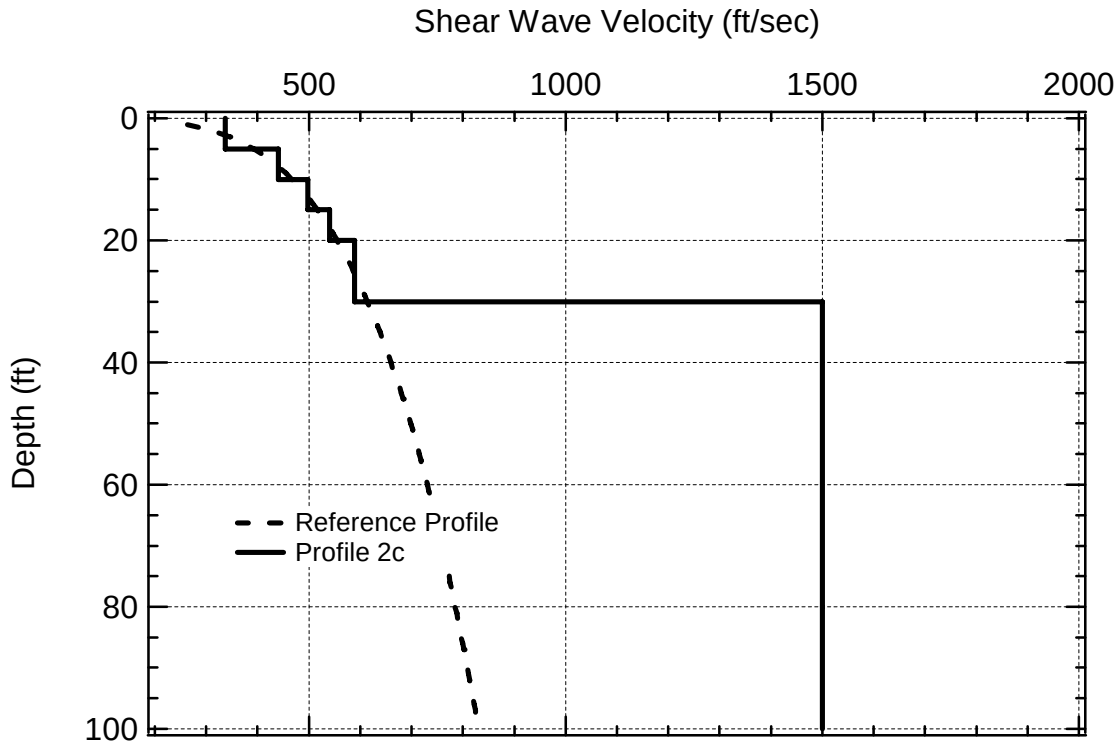

Figure 4-31 Profile 2c shown with the reference profile.

Table 4-7 Individual layer characteristics for Profile 2c.

Layer	Thickness (ft)	V_S (ft/sec)	ν	Unit Weight (pcf)
1	5	337	0.25	120
2	5	440	0.25	120
3	5	498	0.25	120
4	5	540	0.25	120
5	10	589	0.25	120
6	Halfspace	1500	0.25	120

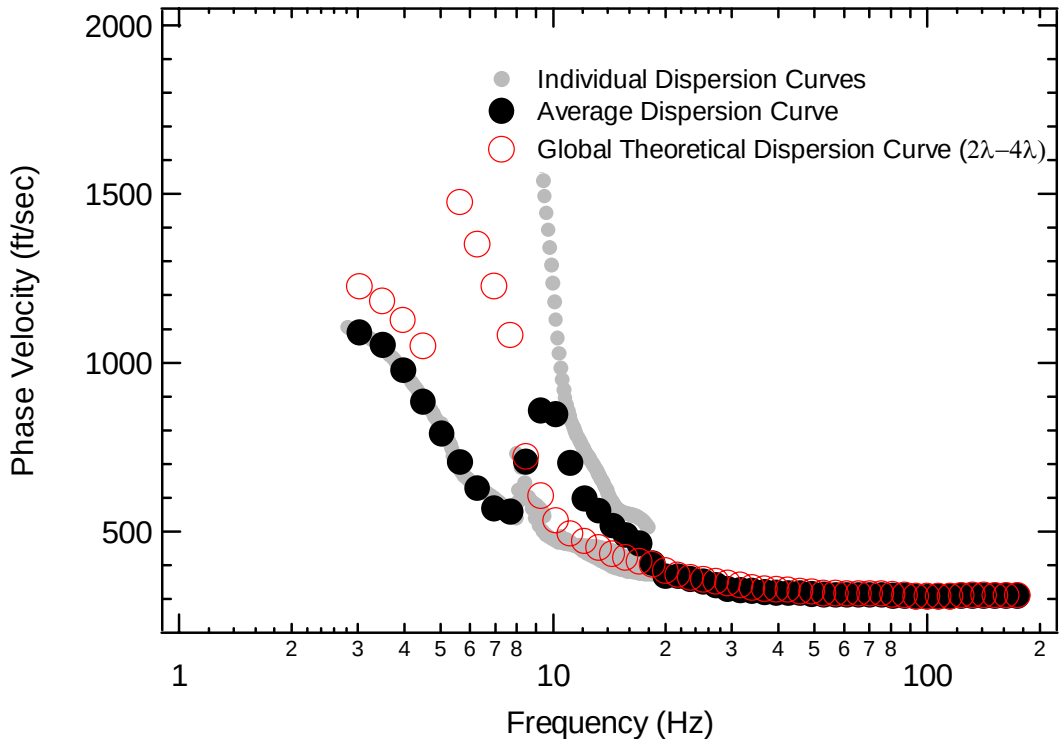

Figure 4-32 **Simulated experimental dispersion curves (individual and global average) versus global theoretical dispersion curve, plotted versus frequency for Profile 2c.**

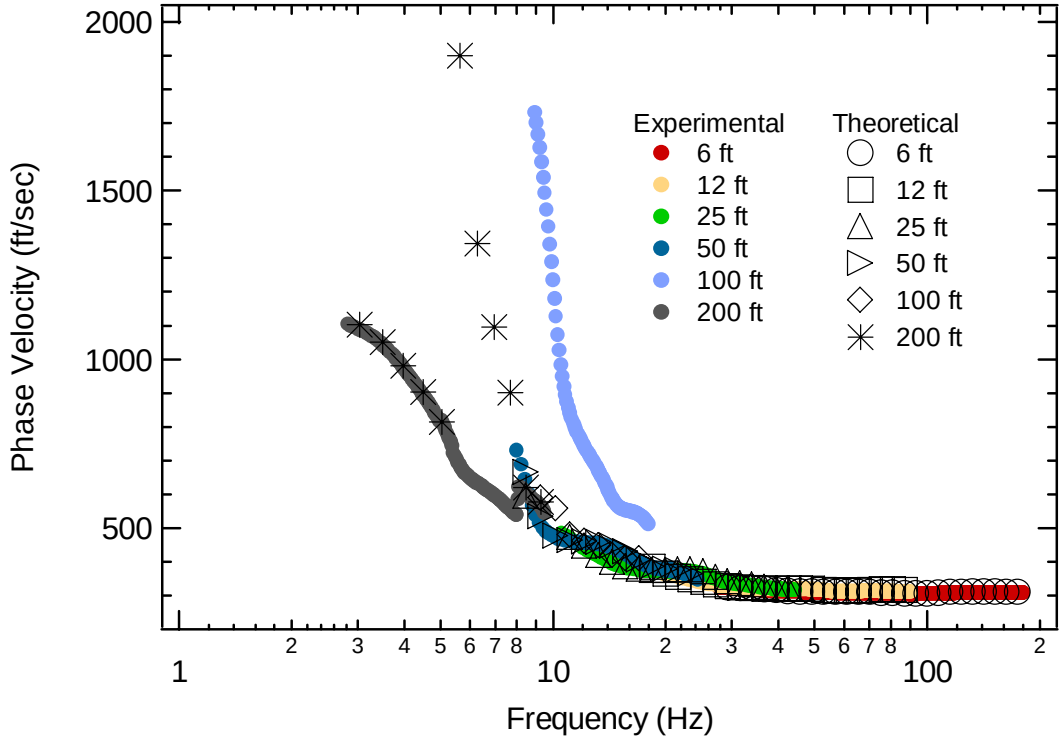

Figure 4-33 **Individual experimental and array theoretical dispersion curves plotted versus frequency for Profile 2c.**

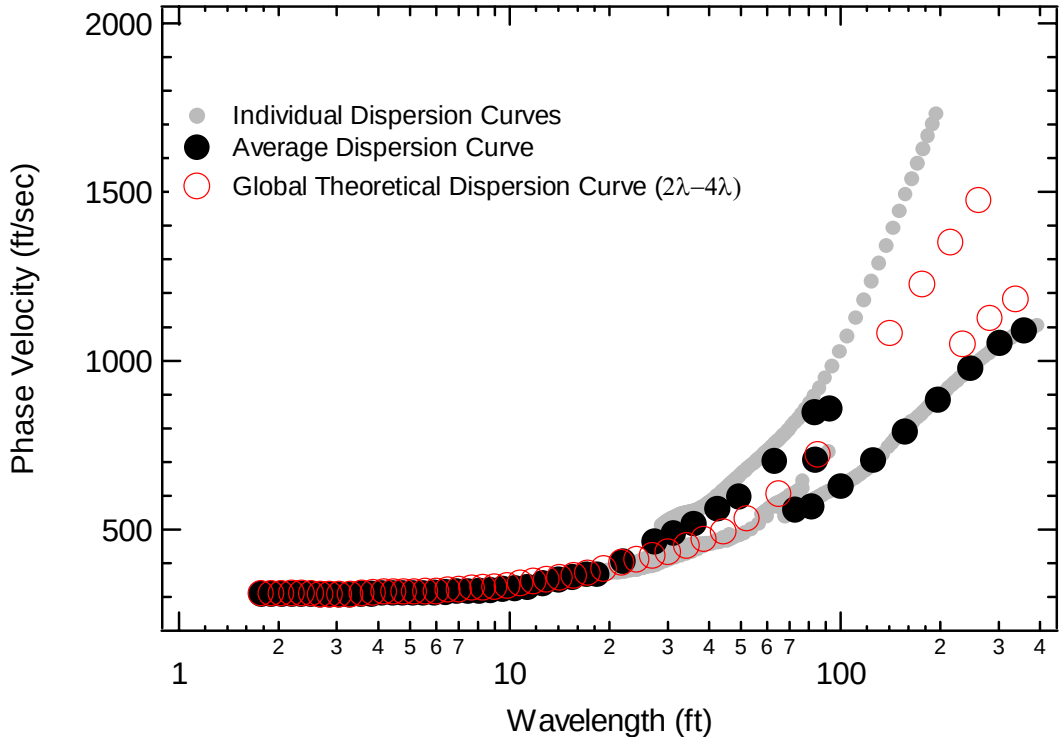

Figure 4-34 **Simulated experimental dispersion curves (individual and global average) versus global theoretical dispersion curve, plotted versus wavelength for Profile 2c.**

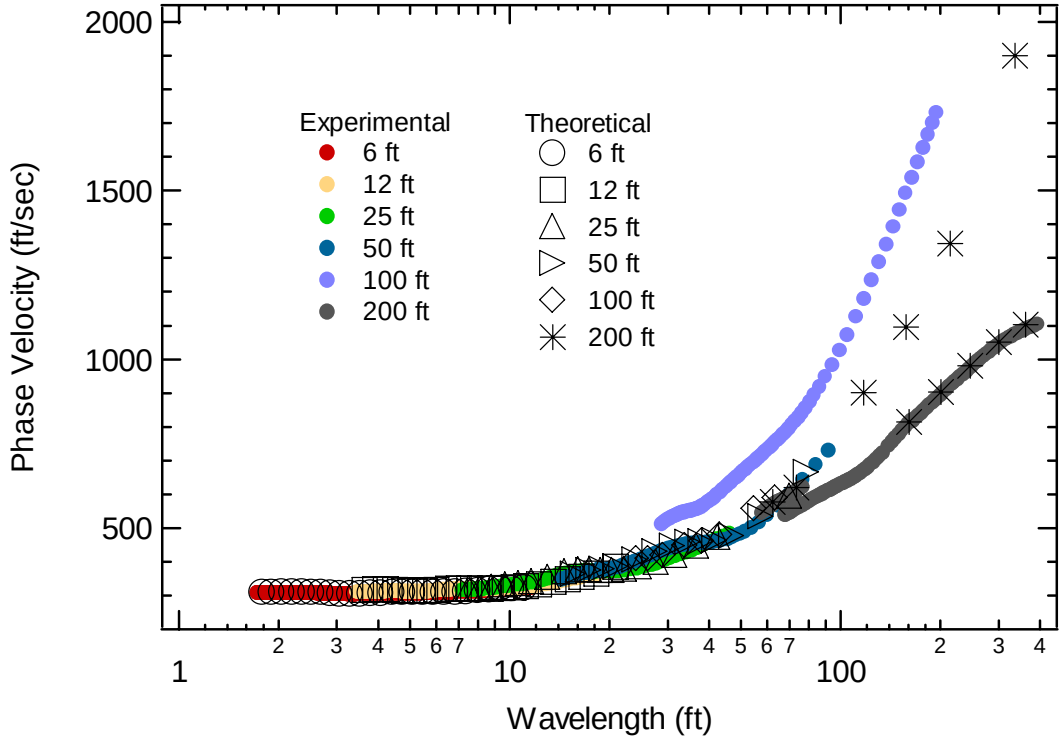

Figure 4-35 **Individual experimental and array theoretical dispersion curves plotted versus wavelength for Profile 2c.**

4.3.7 Profile 2d

Profile 2d is presented in Figure 4-36. Table 4-8 shows the individual layer characteristics for Profile 2d. Figures 4-37, 4-38, 4-39 and 4-40 show the simulated experimental and theoretical dispersion curves for this profile.

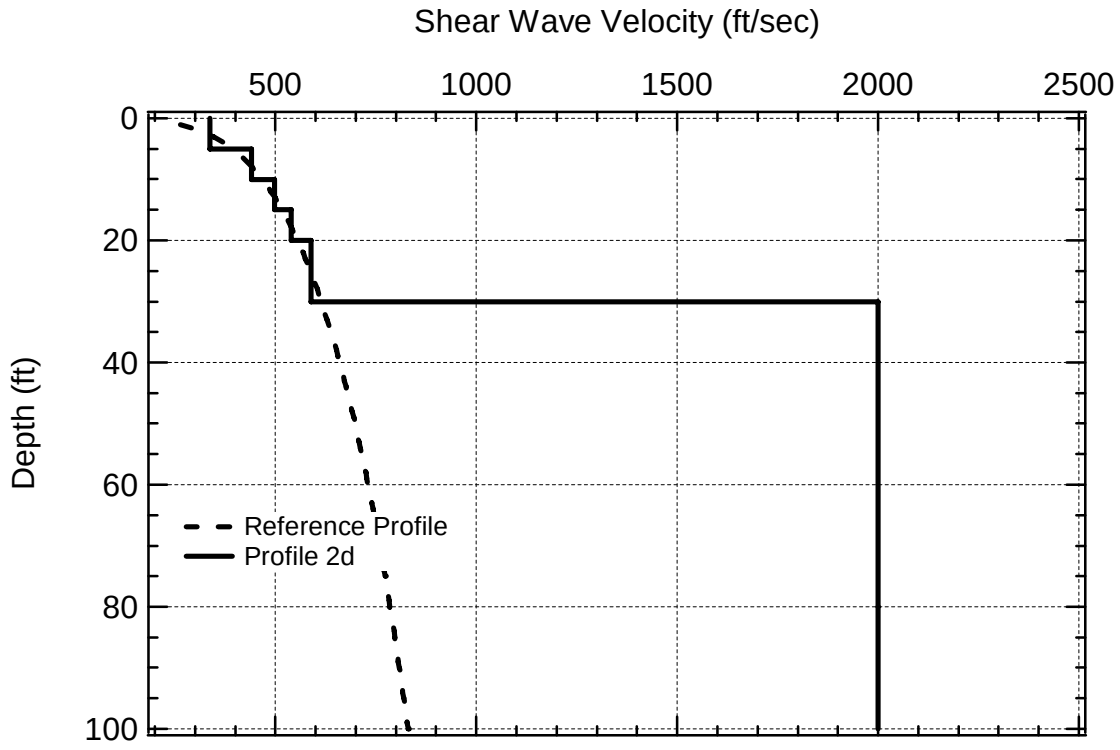

Figure 4-36 Profile 2d shown with the reference profile.

Table 4-8 Individual layer characteristics for Profile 2d.

Layer	Thickness (ft)	V_S (ft/sec)	ν	Unit Weight (pcf)
1	5	337	0.25	120
2	5	440	0.25	120
3	5	498	0.25	120
4	5	540	0.25	120
5	10	589	0.25	120
6	Halfspace	2000	0.25	120

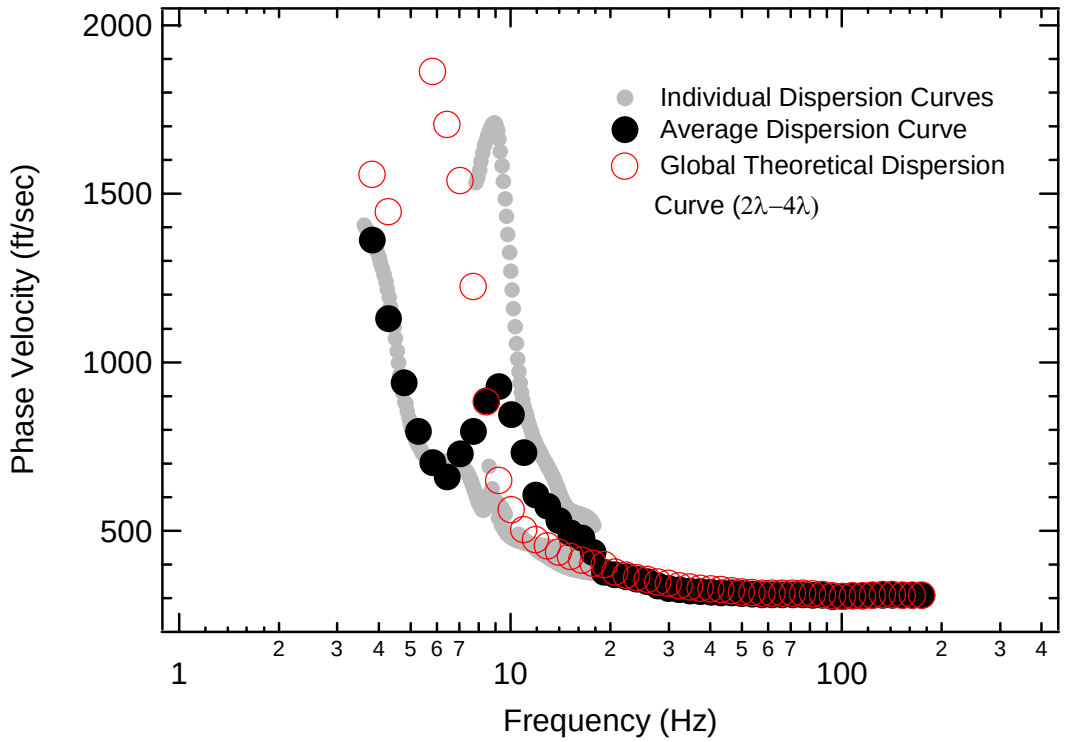

Figure 4-37 **Simulated experimental dispersion curves (individual and global average) versus global theoretical dispersion curve, plotted versus frequency for Profile 2d.**

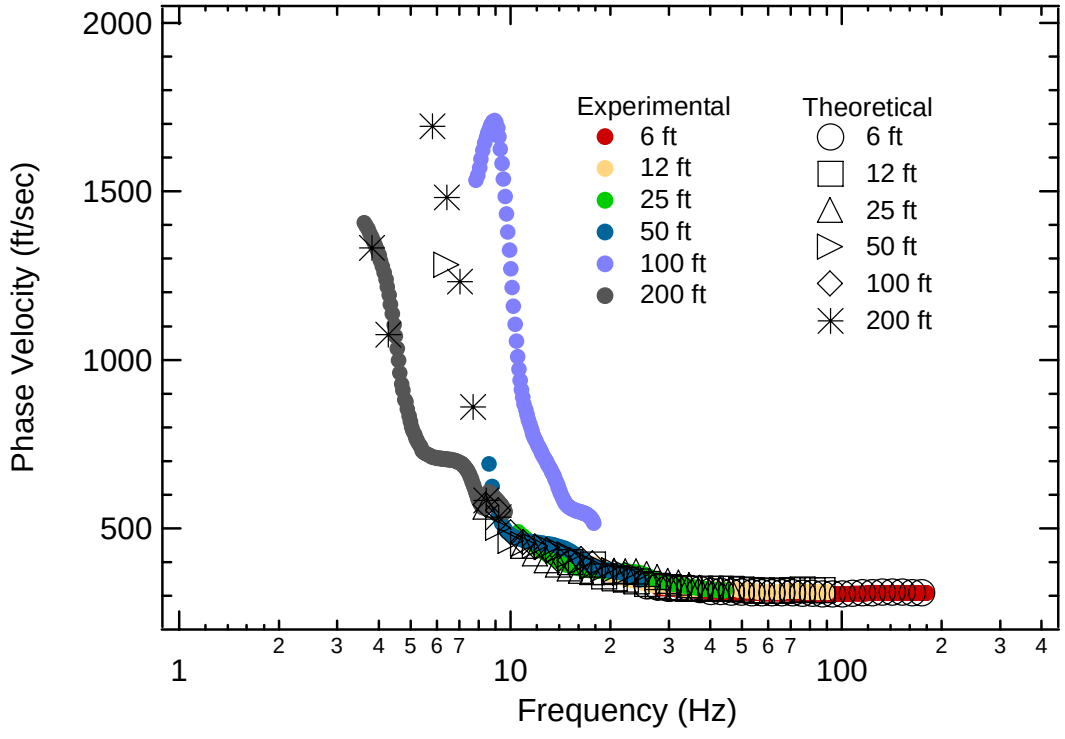

Figure 4-38 **Individual experimental and array theoretical dispersion curves plotted versus frequency for Profile 2d.**

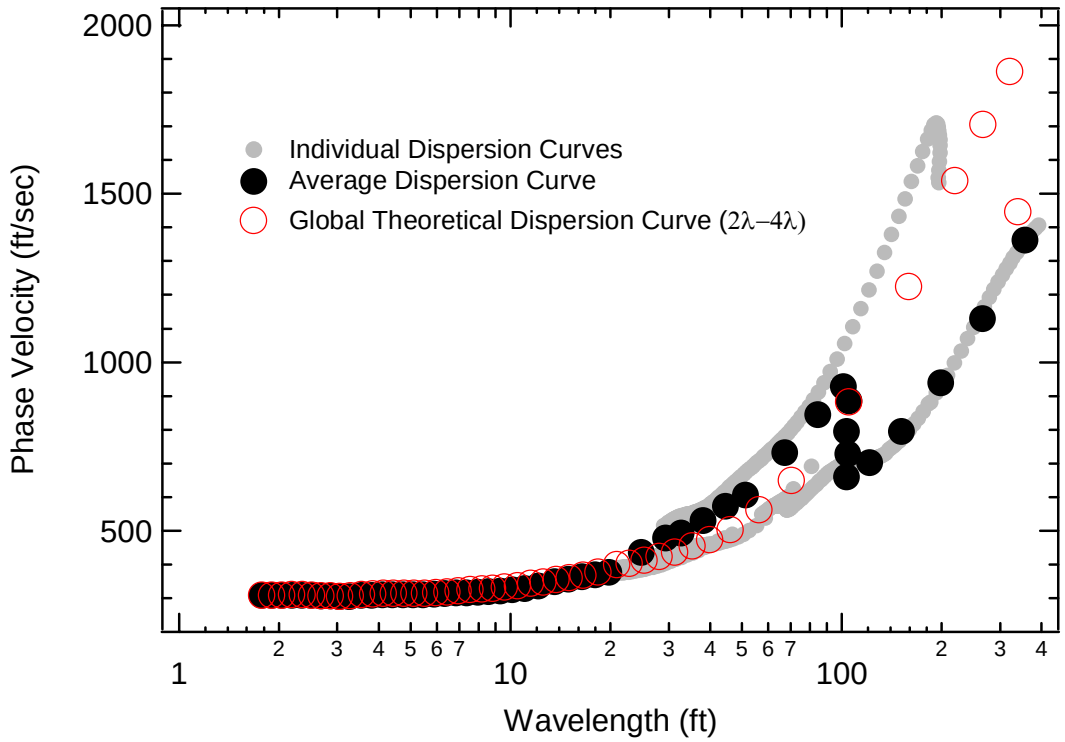

Figure 4-39 **Simulated experimental dispersion curves (individual and global average) versus global theoretical dispersion curve, plotted versus wavelength for Profile 2d.**

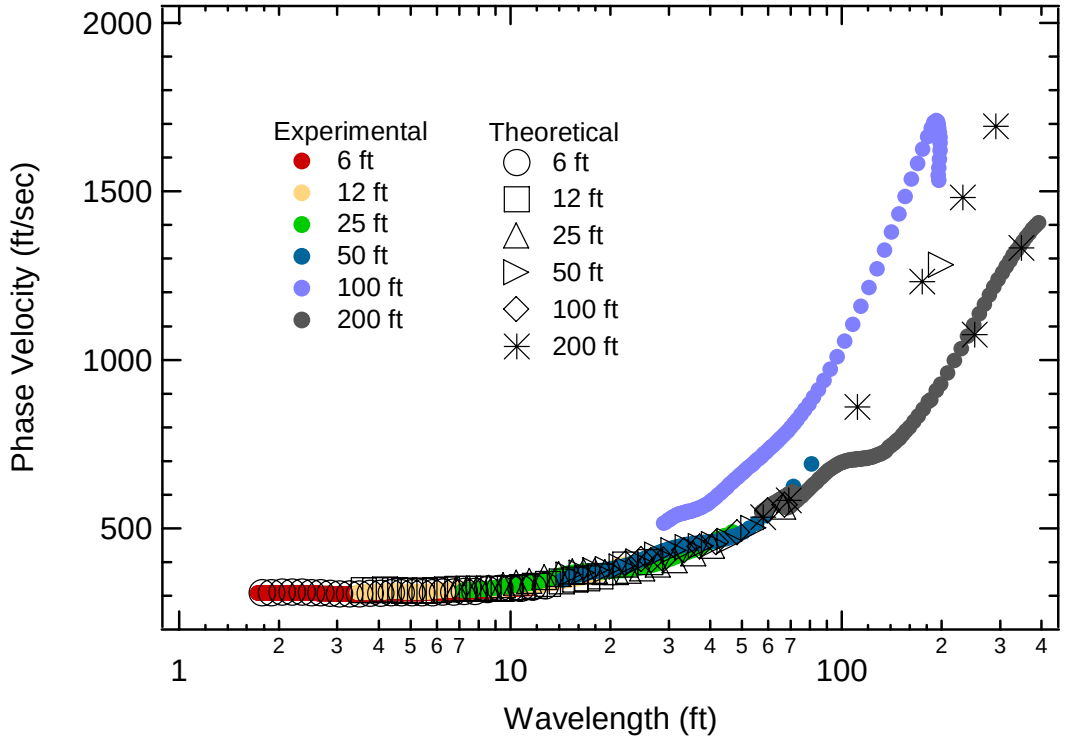

Figure 4-40 **Individual experimental and array theoretical dispersion curves plotted versus wavelength for Profile 2d.**

4.4 Stiff-over-Soft Profiles

4.4.1 Profile 3a

Profile 3a is presented in Figure 4-41. Table 4-9 shows the individual layer characteristics for Profile 3a. Figures 4-42, 4-43, 4-44 and 4-45 show the simulated experimental and theoretical dispersion curves for this profile.

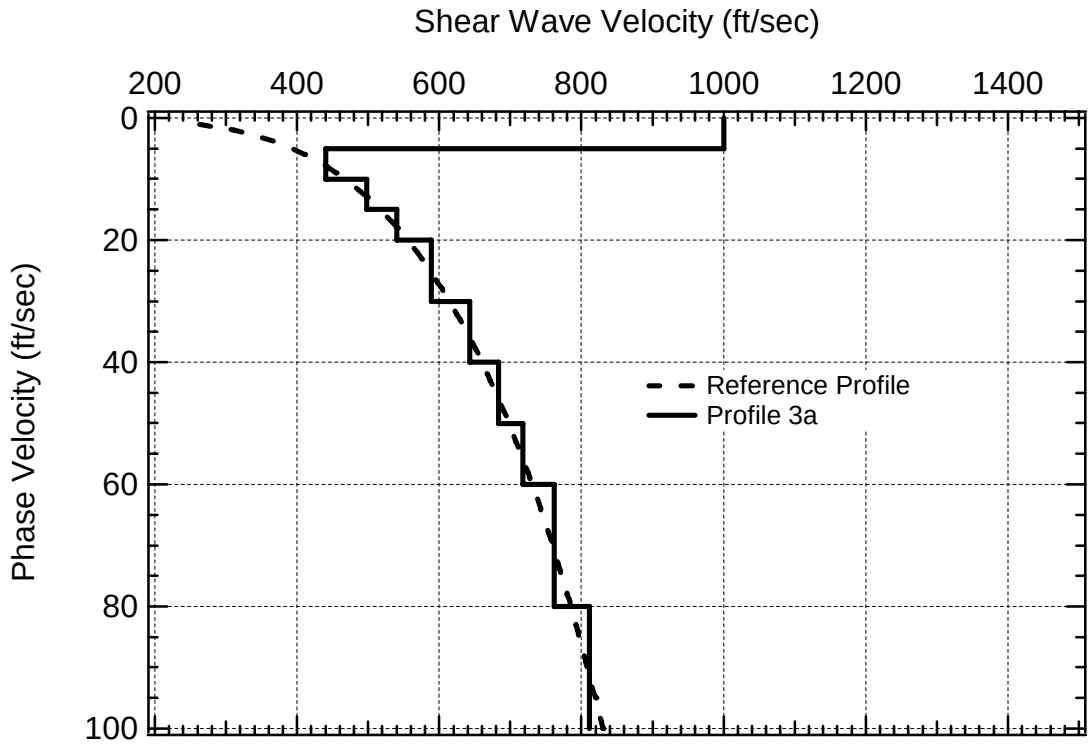

Figure 4-41 Profile 3a shown with the reference profile.

Table 4-9 Individual layer characteristics for Profile 3a.

Layer	Thickness (ft)	V_S (ft/sec)	ν	Unit Weight (pcf)
1	5	1000	0.25	120
2	5	440	0.25	120
3	5	498	0.25	120
4	5	540	0.25	120
5	10	589	0.25	120
6	10	643	0.25	120
7	10	683	0.25	120
8	10	718	0.25	120
9	20	762	0.25	120
10	Halfspace	811	0.25	120

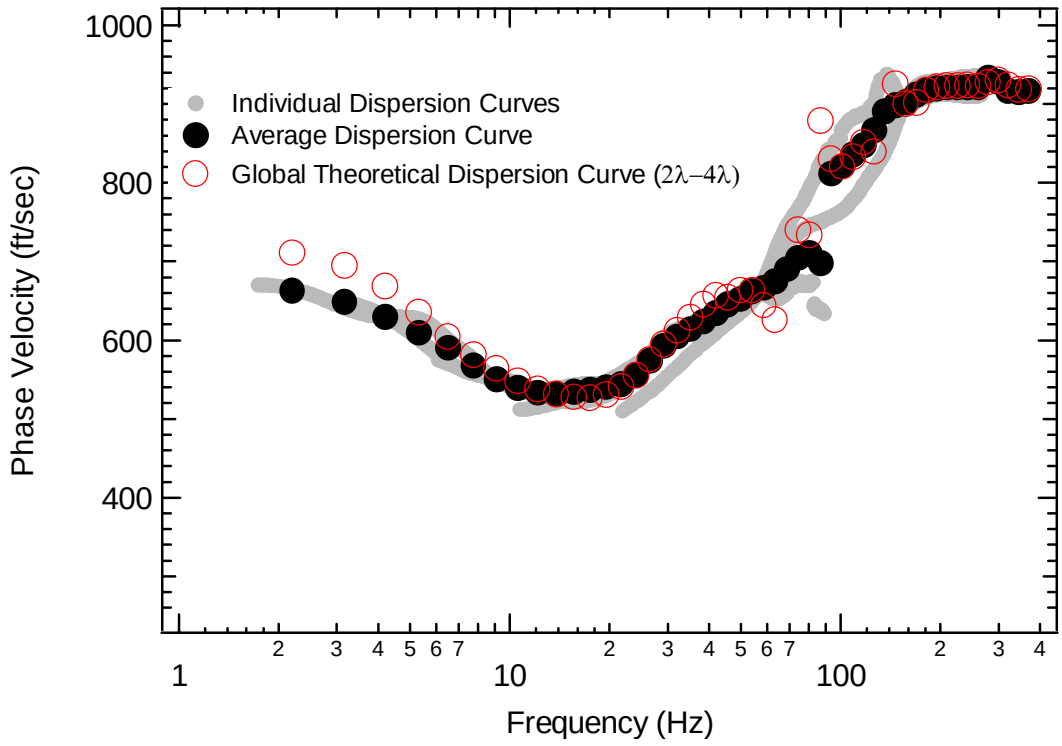

Figure 4-42 **Simulated experimental dispersion curves (individual and global average) versus global theoretical dispersion curve, plotted versus frequency for Profile 3a.**

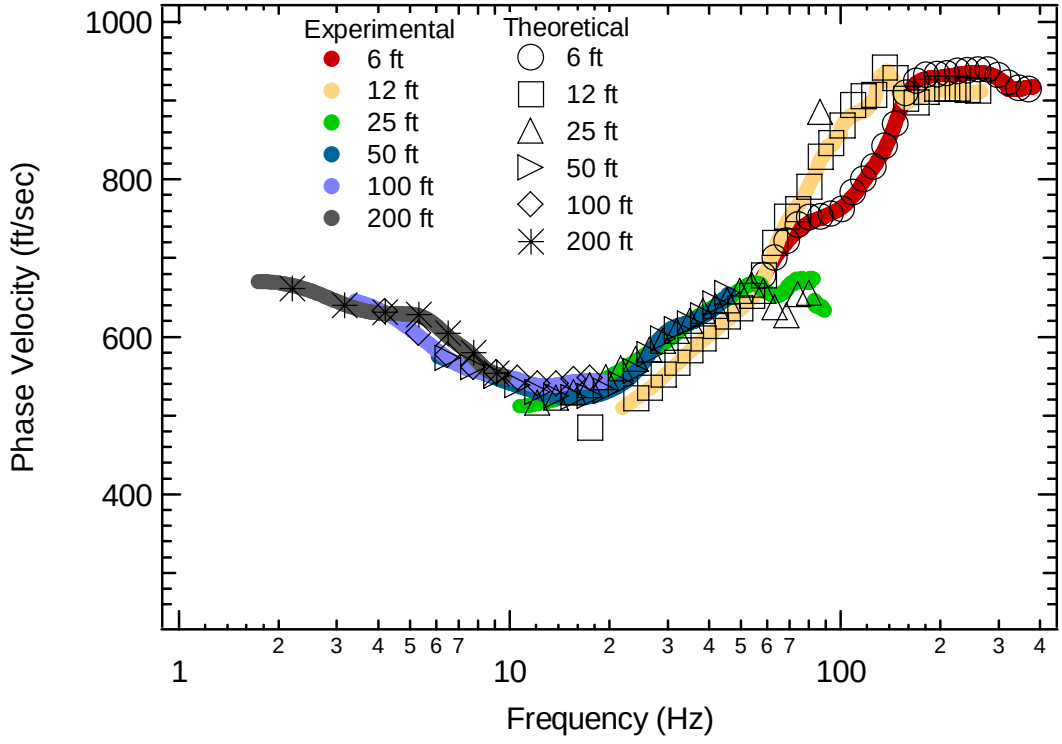

Figure 4-43 **Individual experimental and array theoretical dispersion curves plotted versus frequency for Profile 3a.**

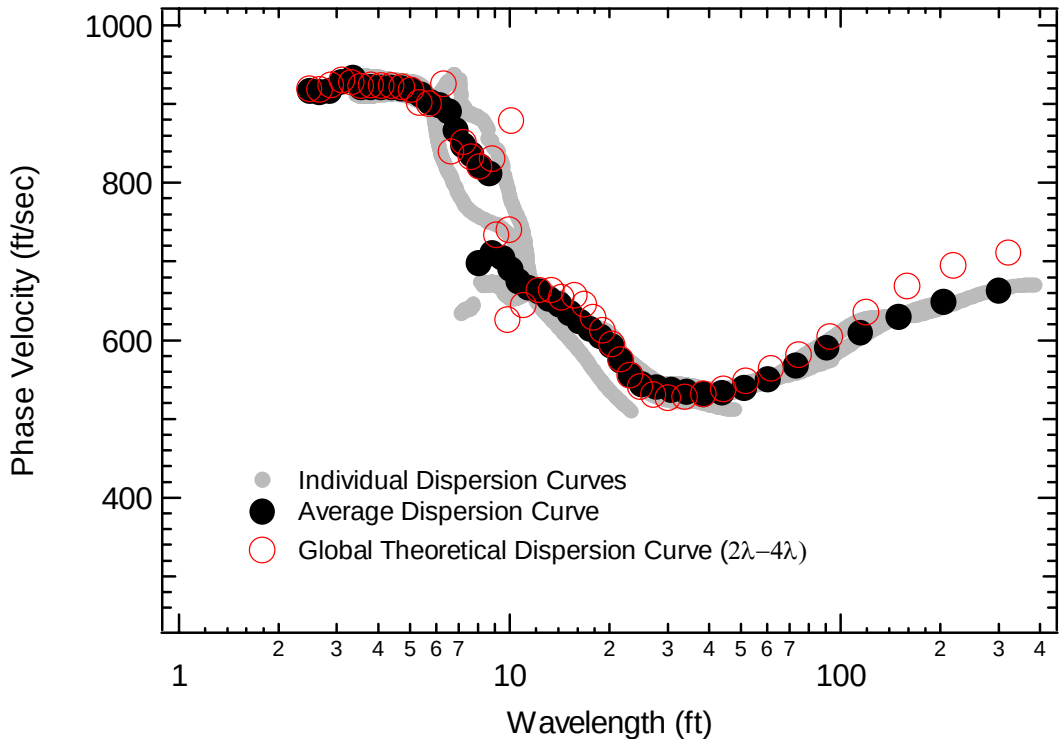

Figure 4-44 **Simulated experimental dispersion curves (individual and global average) versus global theoretical dispersion curve, plotted versus wavelength for Profile 3a.**

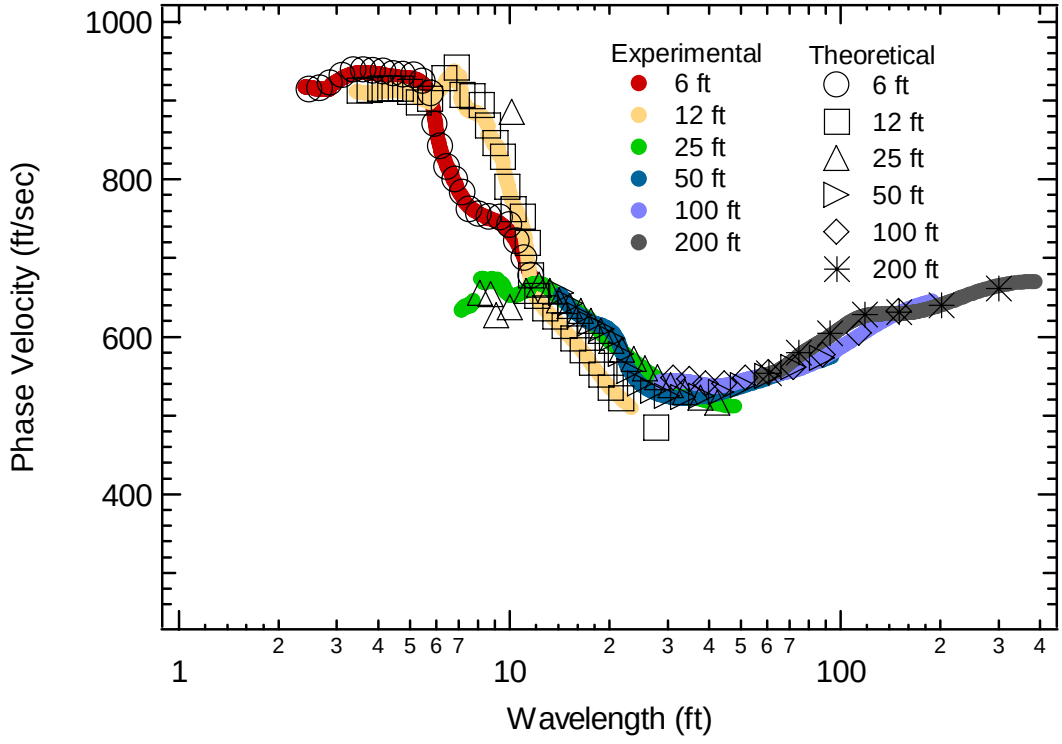

Figure 4-45 **Individual experimental and array theoretical dispersion curves plotted versus wavelength for Profile 3a.**

4.4.2 Profile 3b

Profile 3b is presented in Figure 4-46. Table 4-10 shows the individual layer characteristics for Profile 3b. Figures 4-47, 4-48, 4-49 and 4-50 show the simulated experimental and theoretical dispersion curves for this profile.

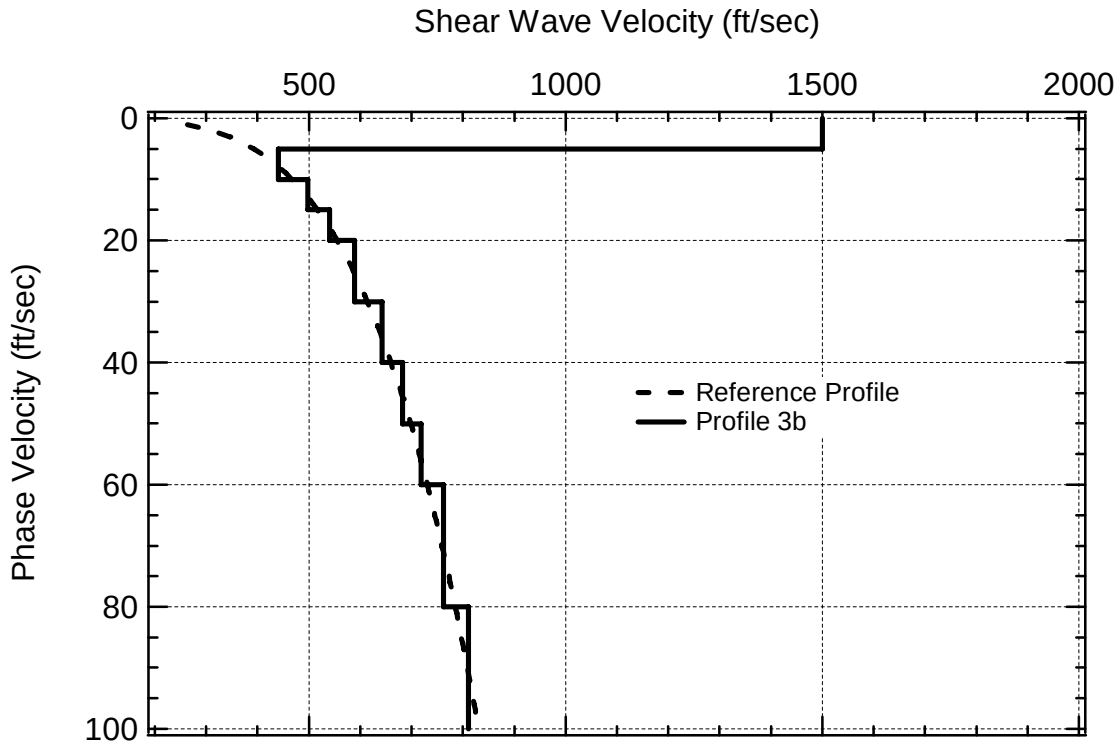

Figure 4-46 Profile 3b shown with the reference profile.

Table 4-10 Individual layer characteristics for Profile 3b.

Layer	Thickness (ft)	V_S (ft/sec)	ν	Unit Weight (pcf)
1	5	1500	0.25	120
2	5	440	0.25	120
3	5	498	0.25	120
4	5	540	0.25	120
5	10	589	0.25	120
6	10	643	0.25	120
7	10	683	0.25	120
8	10	718	0.25	120
9	20	762	0.25	120
10	Halfspace	811	0.25	120

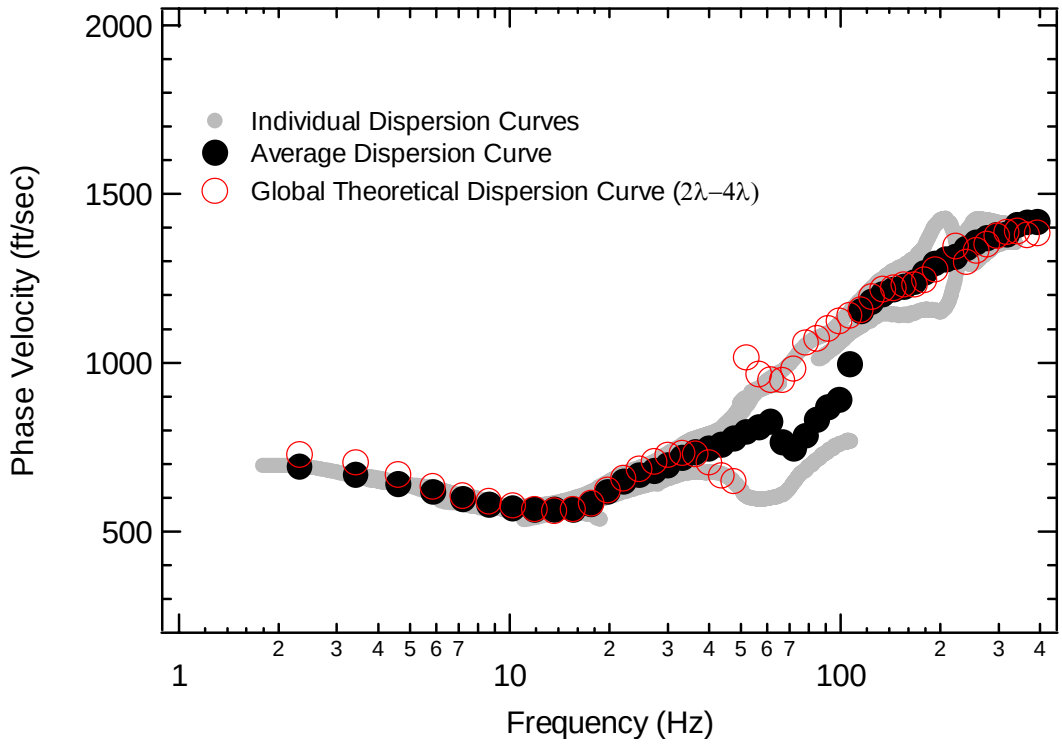

Figure 4-47 **Simulated experimental dispersion curves (individual and global average) versus global theoretical dispersion curve, plotted versus frequency for Profile 3b.**

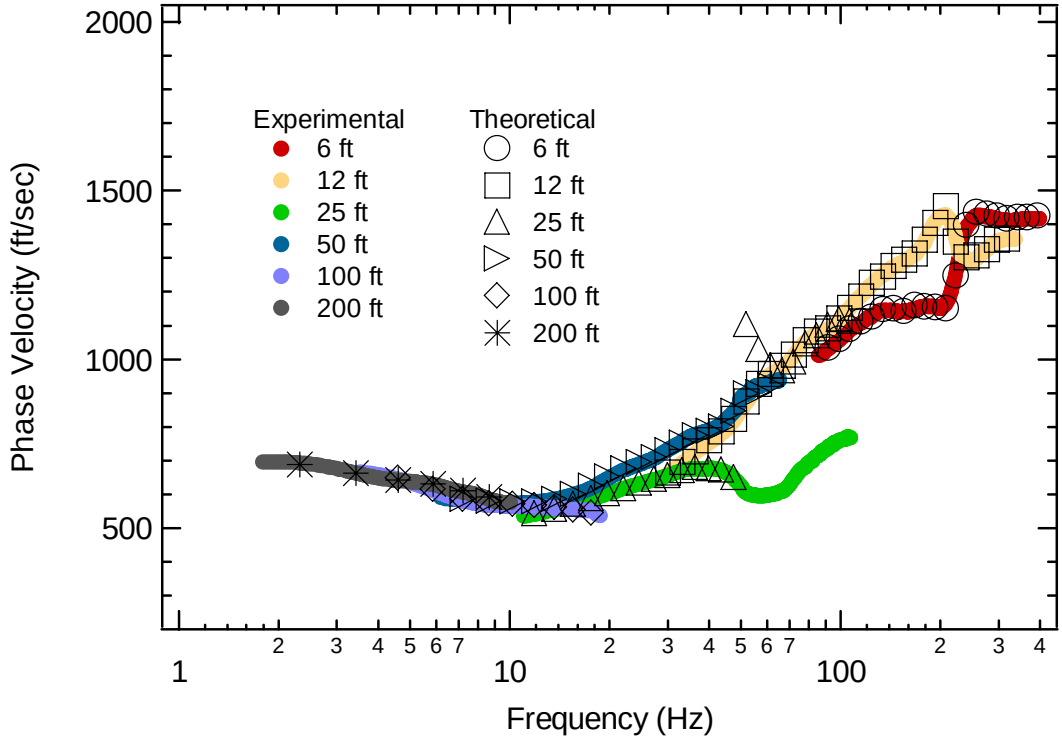

Figure 4-48 **Individual experimental and array theoretical dispersion curves plotted versus frequency for Profile 3b.**

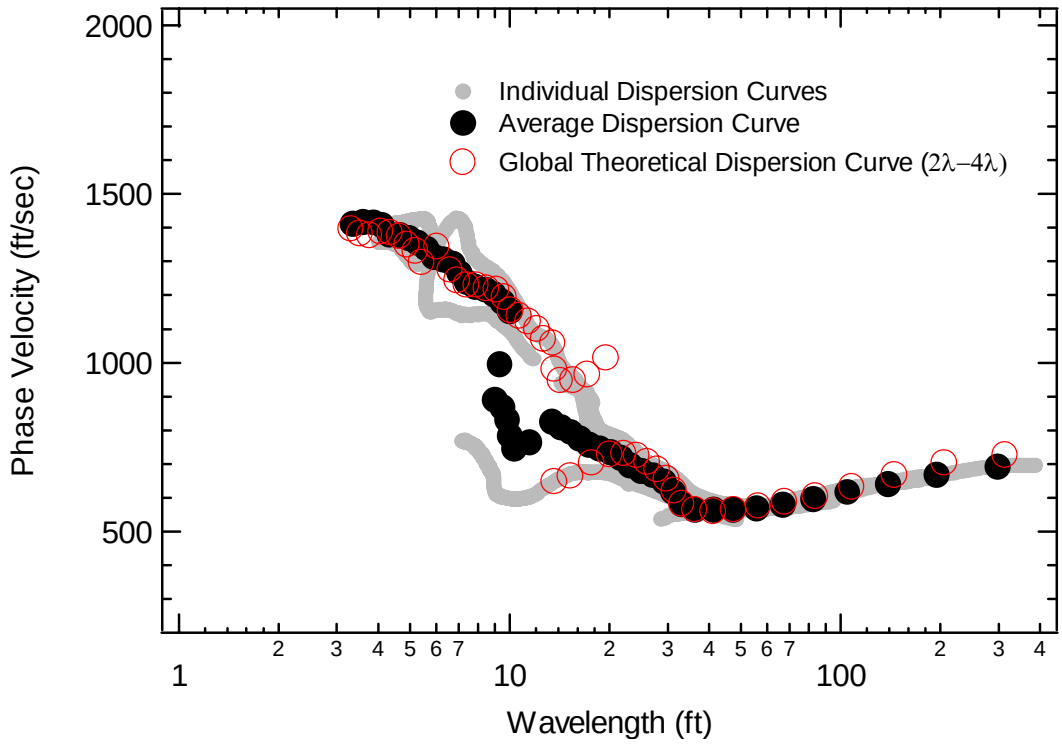

Figure 4-49 **Simulated experimental dispersion curves (individual and global average) versus global theoretical dispersion curve, plotted versus wavelength for Profile 3b.**

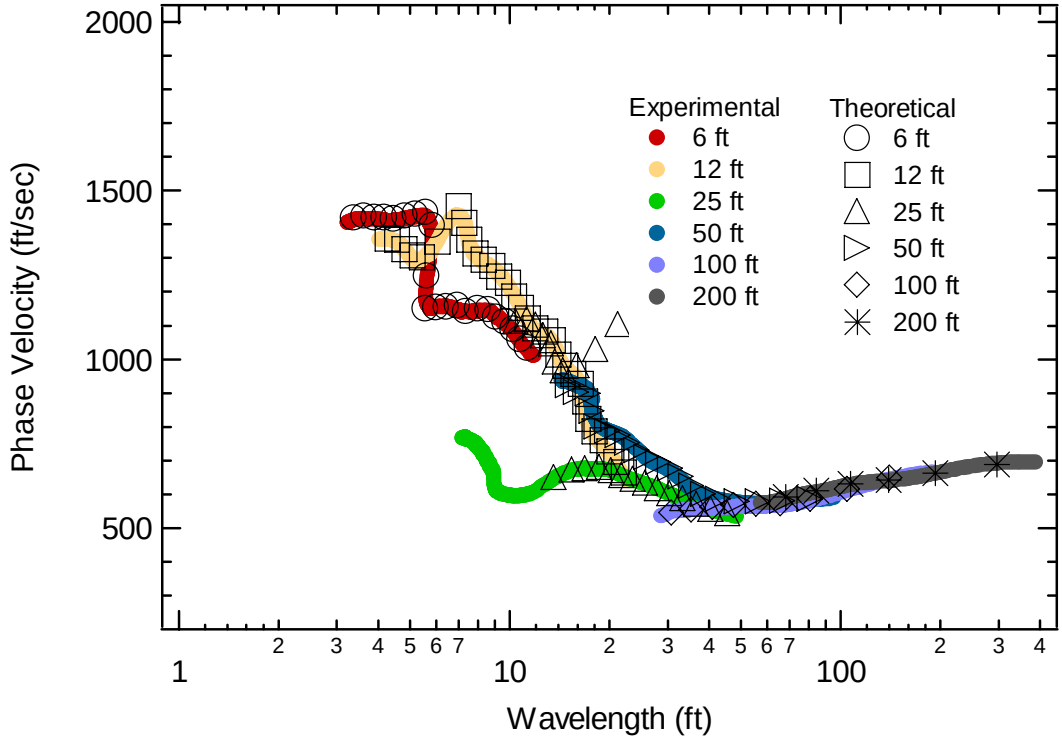

Figure 4-50 **Individual experimental and array theoretical dispersion curves plotted versus wavelength for Profile 3b.**

4.4.3 Profile 3c

Profile 3c is presented in Figure 4-51. Table 4-11 shows the individual layer characteristics for Profile 3c. Figures 4-52, 4-53, 4-54 and 4-55 show the simulated experimental and theoretical dispersion curves for this profile.

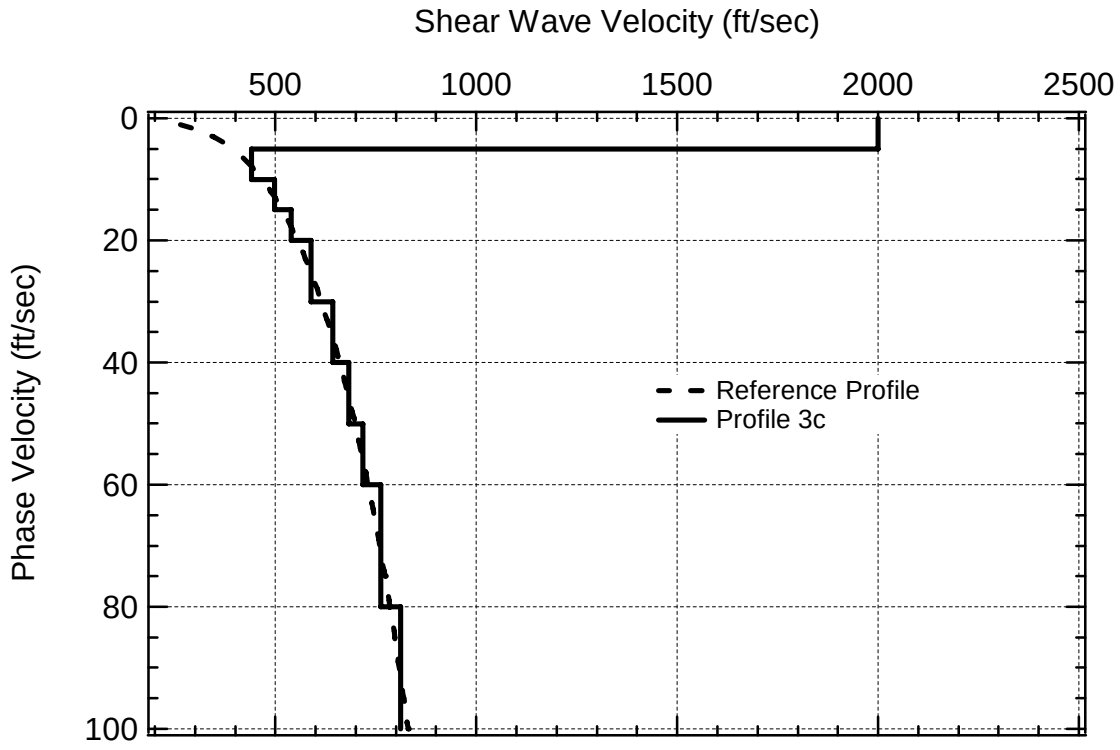

Figure 4-51 Profile 3c shown with the reference profile.

Table 4-11 Individual layer characteristics for Profile 3c.

Layer	Thickness (ft)	V_S (ft/sec)	ν	Unit Weight (pcf)
1	5	2000	0.25	120
2	5	440	0.25	120
3	5	498	0.25	120
4	5	540	0.25	120
5	10	589	0.25	120
6	10	643	0.25	120
7	10	683	0.25	120
8	10	718	0.25	120
9	20	762	0.25	120
10	Halfspace	811	0.25	120

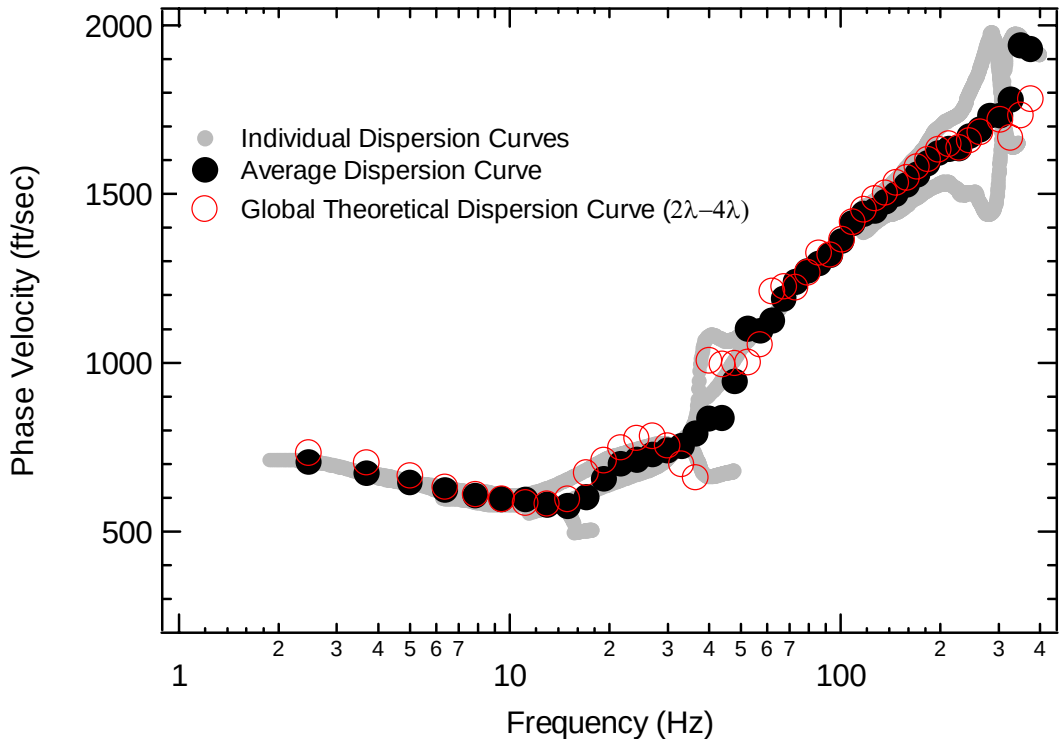

Figure 4-52 **Simulated experimental dispersion curves (individual and global average) versus global theoretical dispersion curve, plotted versus frequency for Profile 3c.**

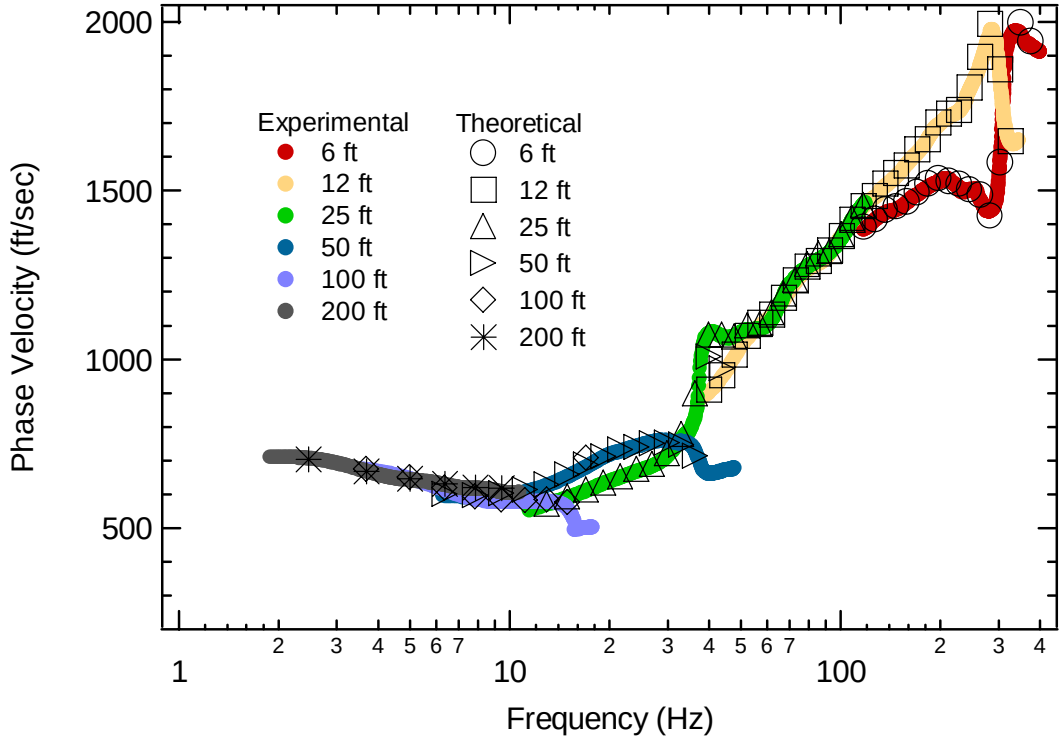

Figure 4-53 **Individual experimental and array theoretical dispersion curves plotted versus frequency for Profile 3c.**

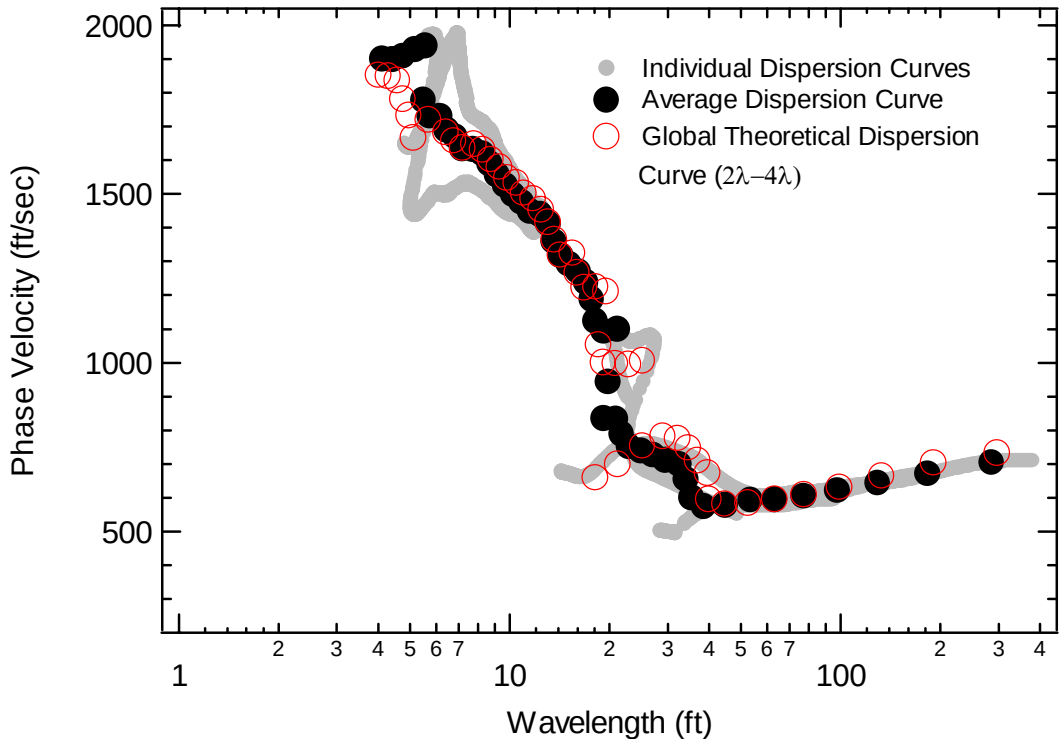

Figure 4-54 **Simulated experimental dispersion curves (individual and global average) versus global theoretical dispersion curve, plotted versus wavelength for Profile 3c.**

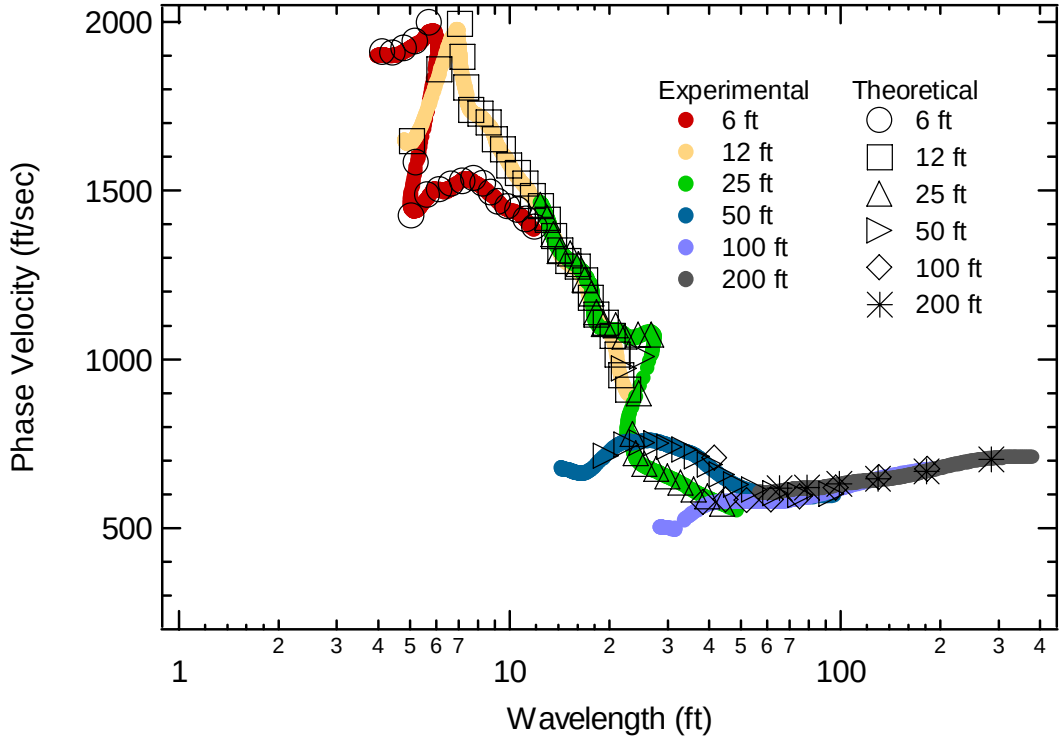

Figure 4-55 **Individual experimental and array theoretical dispersion curves plotted versus wavelength for Profile 3c.**

4.4.4 Profile 4a

Profile 4a is presented in Figure 4-56. Table 4-12 shows the individual layer characteristics for Profile 4a. Figures 4-57, 4-58, 4-59 and 4-60 show the simulated experimental and theoretical dispersion curves for this profile.

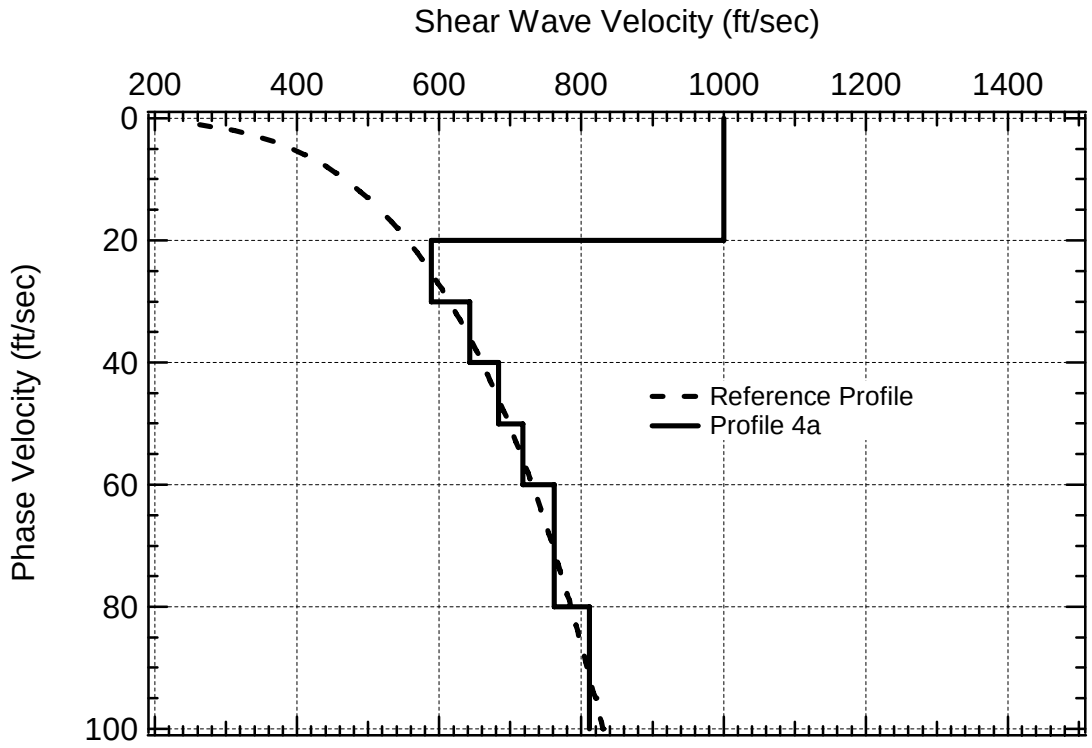

Figure 4-56 Profile 4a shown with the reference profile.

Table 4-12 Individual layer characteristics for Profile 4a.

Layer	Thickness (ft)	V_S (ft/sec)	ν	Unit Weight (pcf)
1	20	1000	0.25	120
2	10	589	0.25	120
3	10	643	0.25	120
4	10	683	0.25	120
5	10	718	0.25	120
6	20	762	0.25	120
7	Halfspace	811	0.25	120

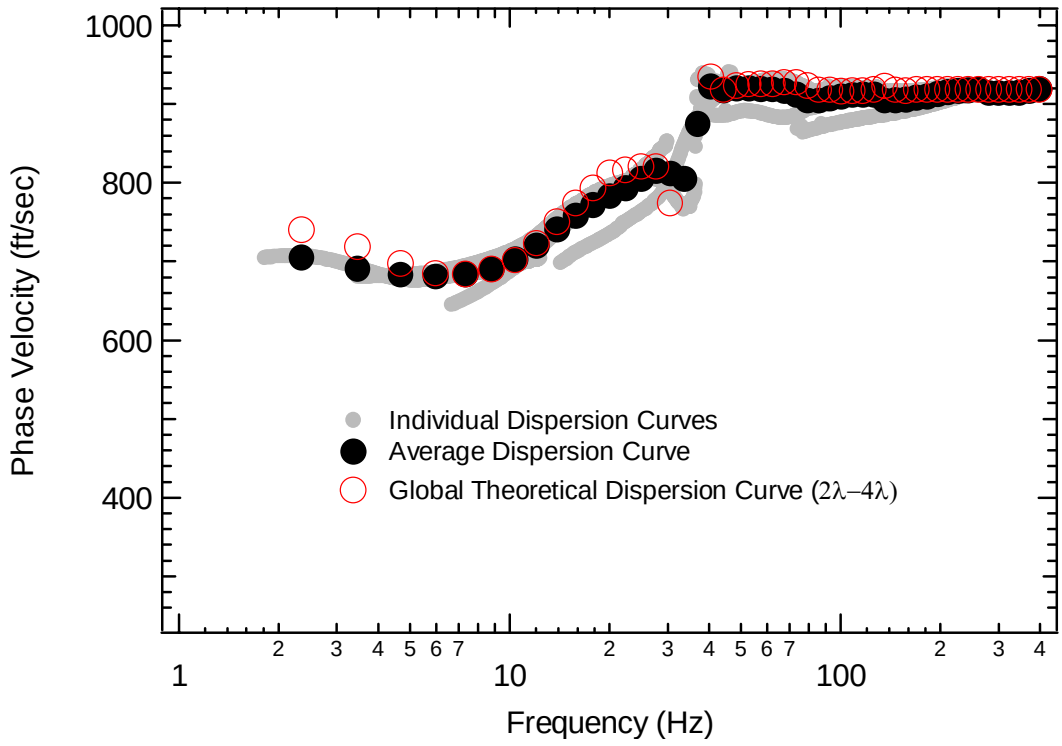

Figure 4-57 **Simulated experimental dispersion curves (individual and global average) versus global theoretical dispersion curve, plotted versus frequency for Profile 4a.**

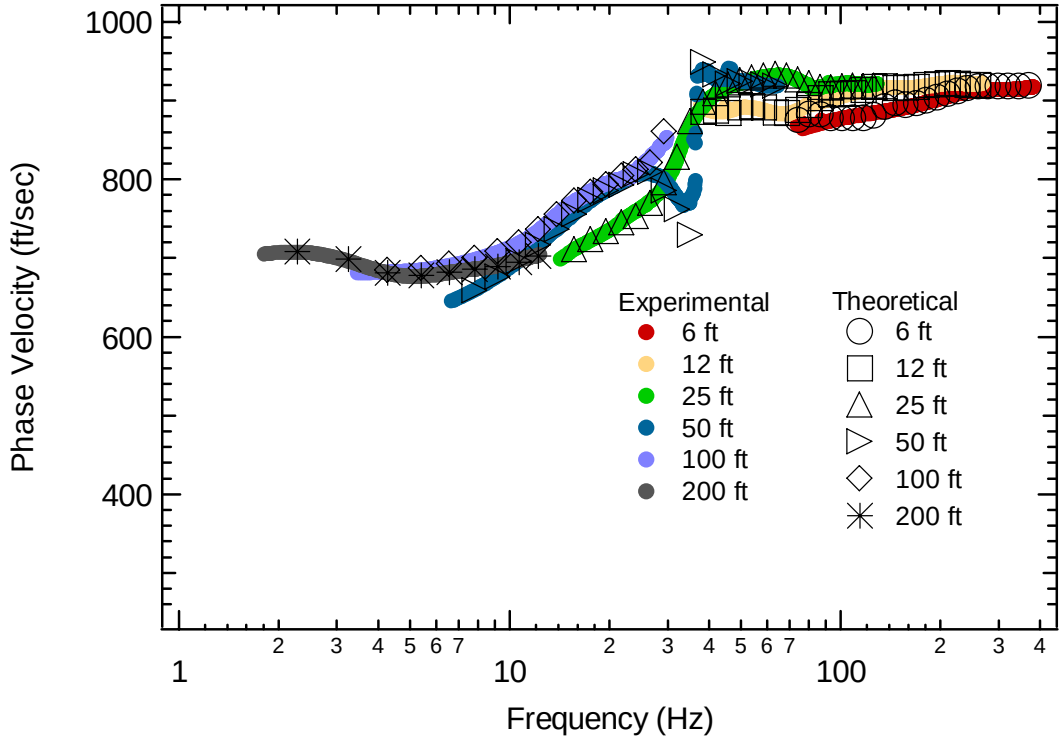

Figure 4-58 **Individual experimental and array theoretical dispersion curves plotted versus frequency for Profile 4a.**

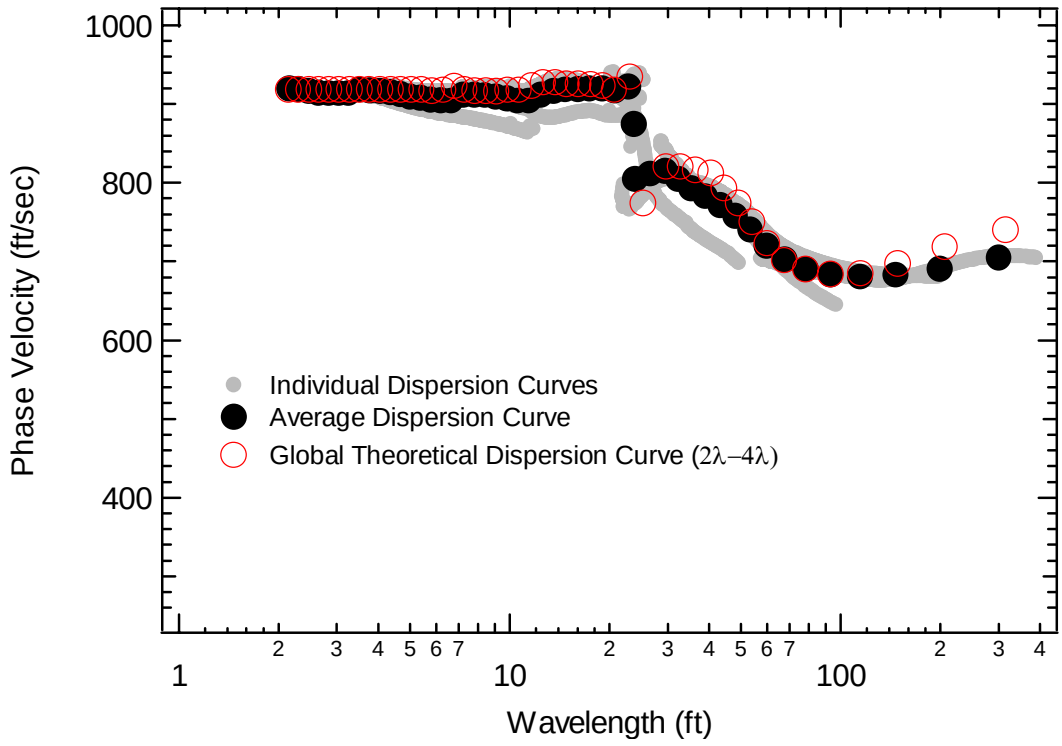

Figure 4-59 **Simulated experimental dispersion curves (individual and global average) versus global theoretical dispersion curve, plotted versus wavelength for Profile 4a.**

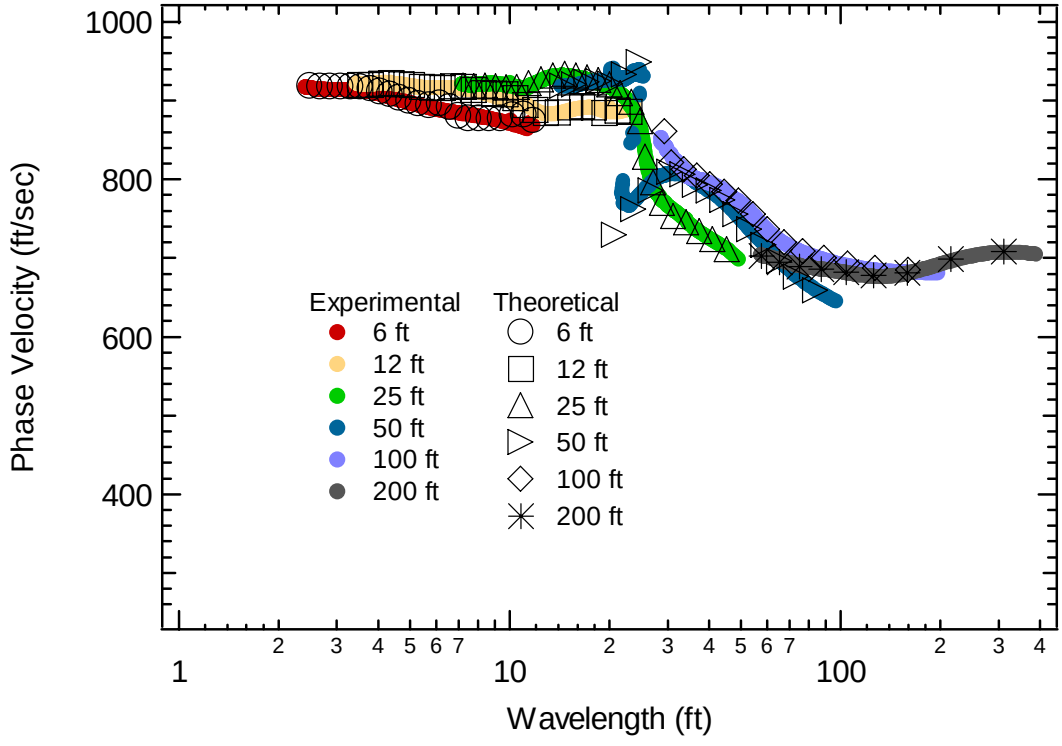

Figure 4-60 **Individual experimental and array theoretical dispersion curves plotted versus wavelength for Profile 4a.**

4.4.5 Profile 4b

Profile 4b is presented in Figure 4-61. Table 4-13 shows the individual layer characteristics for Profile 4b. Figures 4-62, 4-63, 4-64 and 4-65 show the simulated experimental and theoretical dispersion curves for this profile.

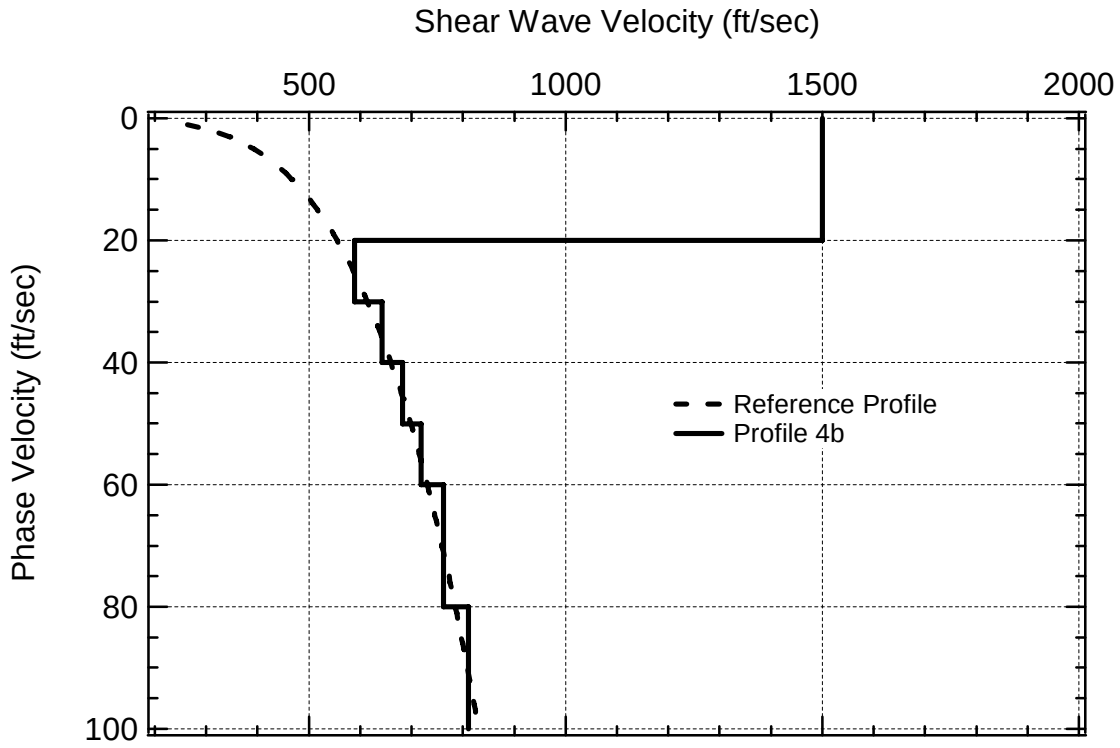

Figure 4-61 Profile 4b shown with the reference profile.

Table 4-13 Individual layer characteristics for Profile 4b.

Layer	Thickness (ft)	V_S (ft/sec)	ν	Unit Weight (pcf)
1	20	1500	0.25	120
2	10	589	0.25	120
3	10	643	0.25	120
4	10	683	0.25	120
5	10	718	0.25	120
6	20	762	0.25	120
7	Halfspace	811	0.25	120

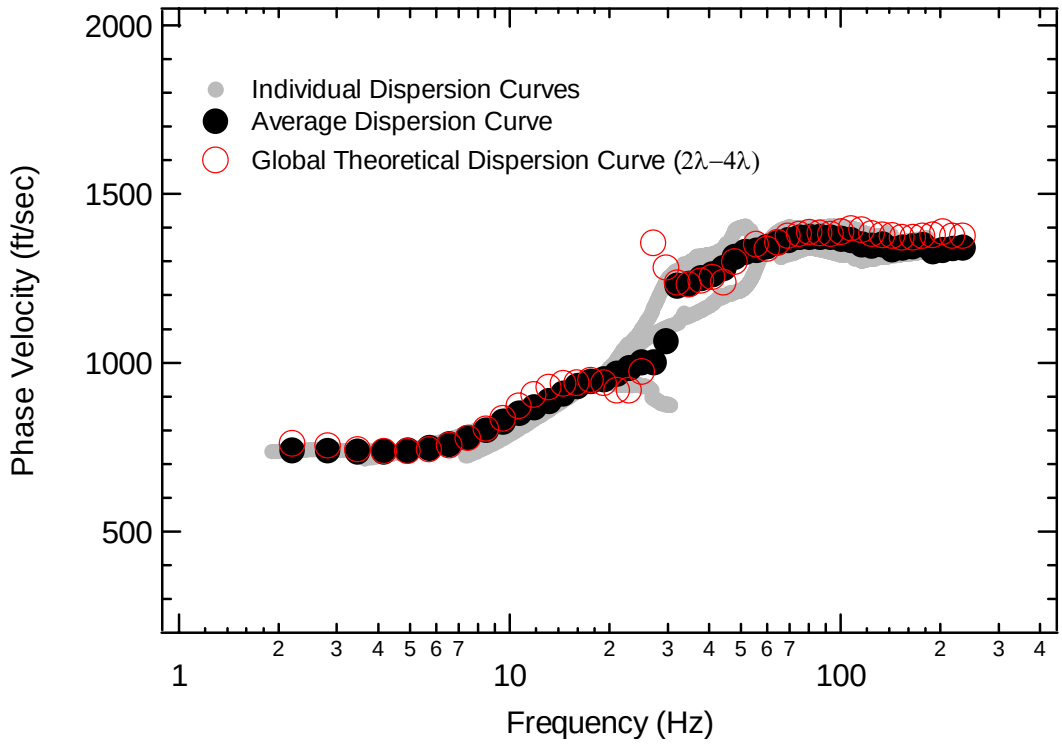

Figure 4-62 **Simulated experimental dispersion curves (individual and global average) versus global theoretical dispersion curve, plotted versus frequency for Profile 4b.**

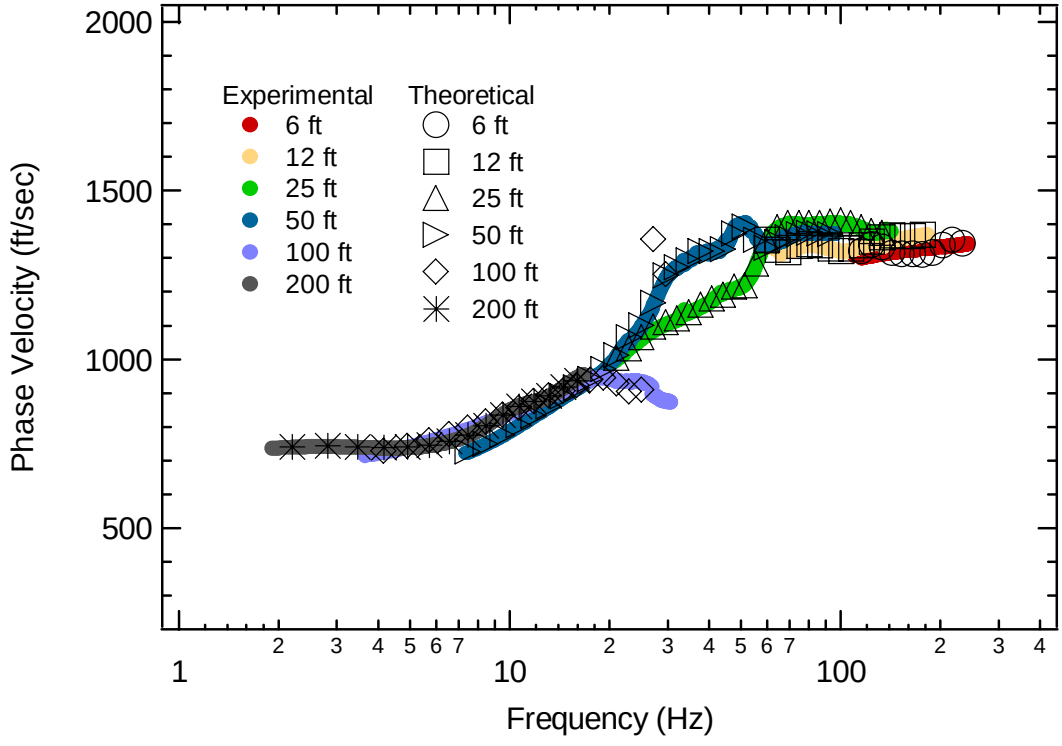

Figure 4-63 **Individual experimental and array theoretical dispersion curves plotted versus frequency for Profile 4b.**

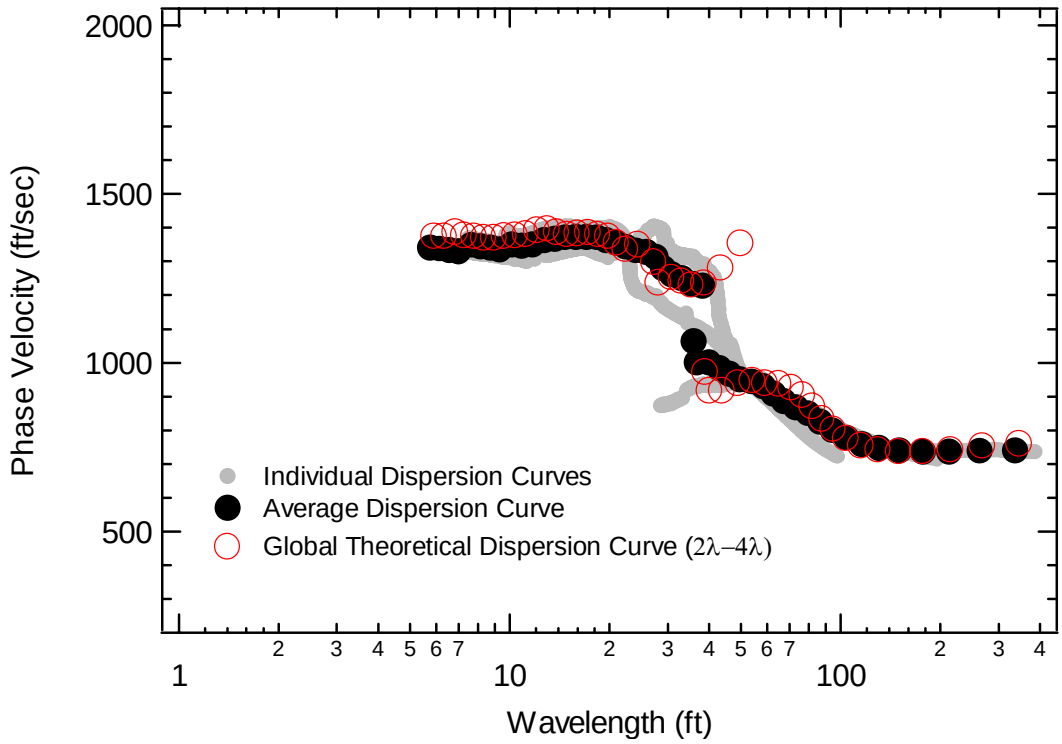

Figure 4-64 **Simulated experimental dispersion curves (individual and global average) versus global theoretical dispersion curve, plotted versus wavelength for Profile 4b.**

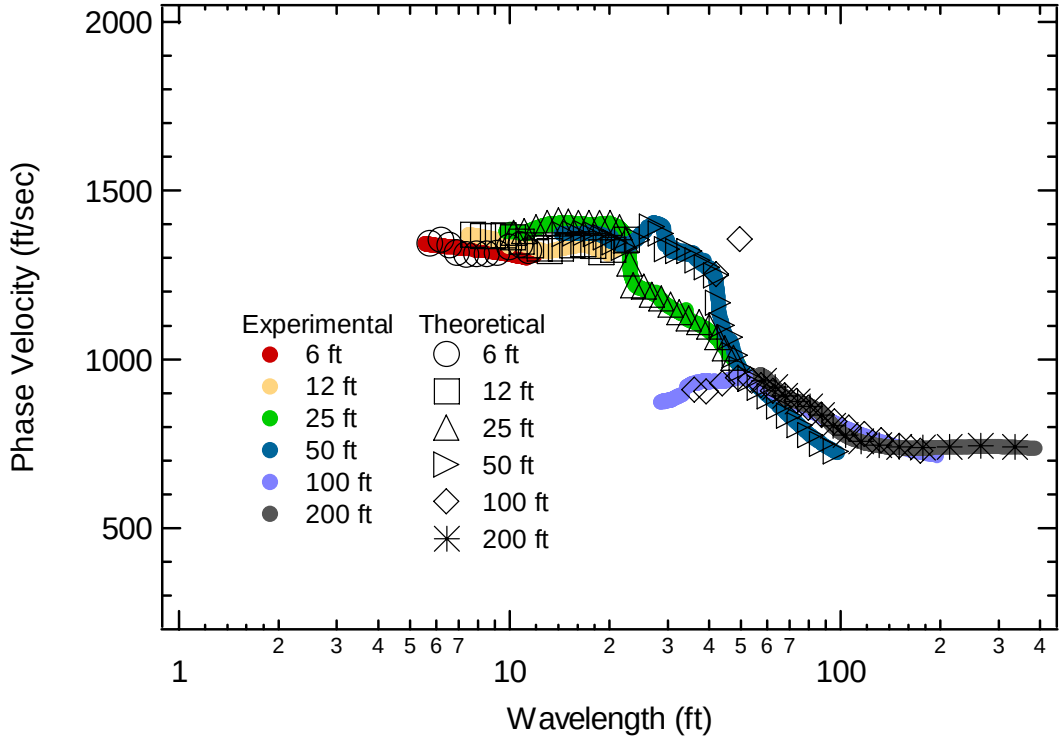

Figure 4-65 **Individual experimental and array theoretical dispersion curves plotted versus wavelength for Profile 4b.**

4.4.6 Profile 4c

Profile 4c is presented in Figure 4-66. Table 4-14 shows the individual layer characteristics for Profile 4c. Figures 4-67, 4-68, 4-69 and 4-70 show the simulated experimental and theoretical dispersion curves for this profile.

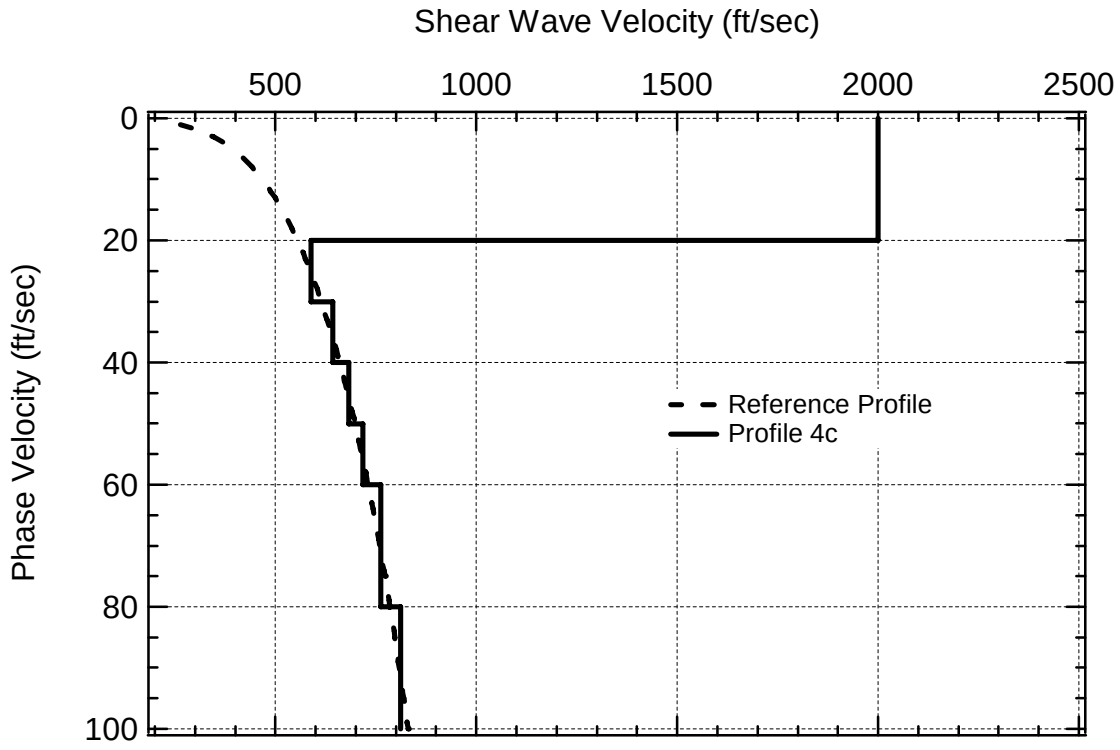

Figure 4-66 Profile 4c shown with the reference profile.

Table 4-14 Individual layer characteristics for Profile 4c.

Layer	Thickness (ft)	V_S (ft/sec)	ν	Unit Weight (pcf)
1	20	2000	0.25	120
2	10	589	0.25	120
3	10	643	0.25	120
4	10	683	0.25	120
5	10	718	0.25	120
6	20	762	0.25	120
7	Halfspace	811	0.25	120

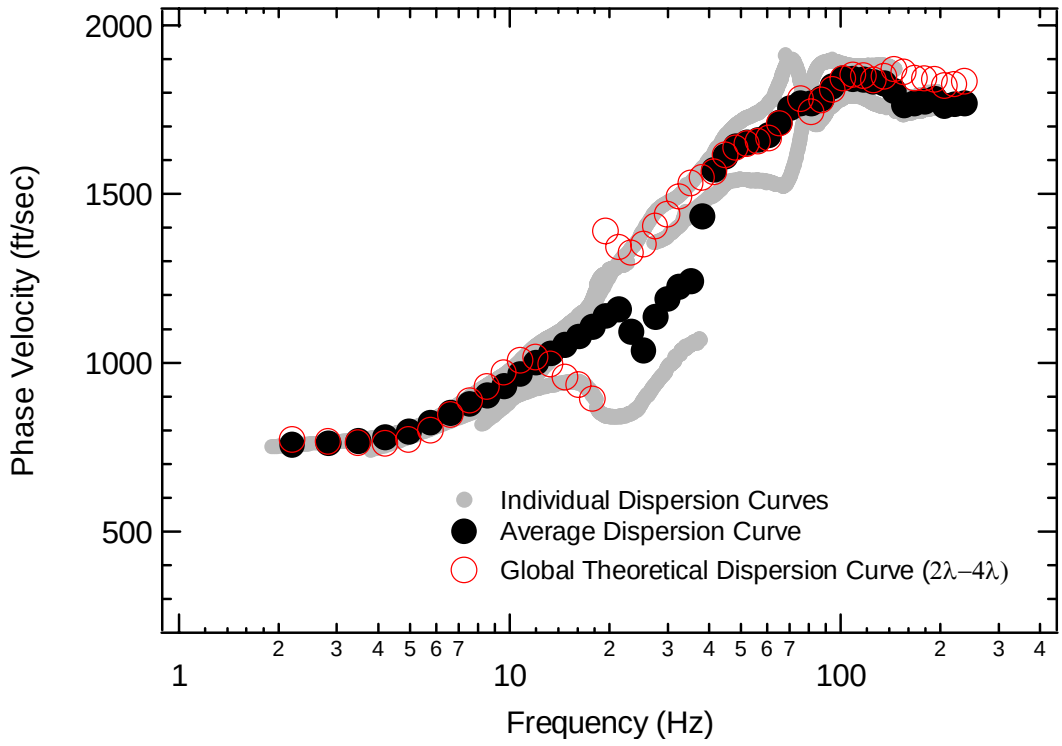

Figure 4-67 **Simulated experimental dispersion curves (individual and global average) versus global theoretical dispersion curve, plotted versus frequency for Profile 4c.**

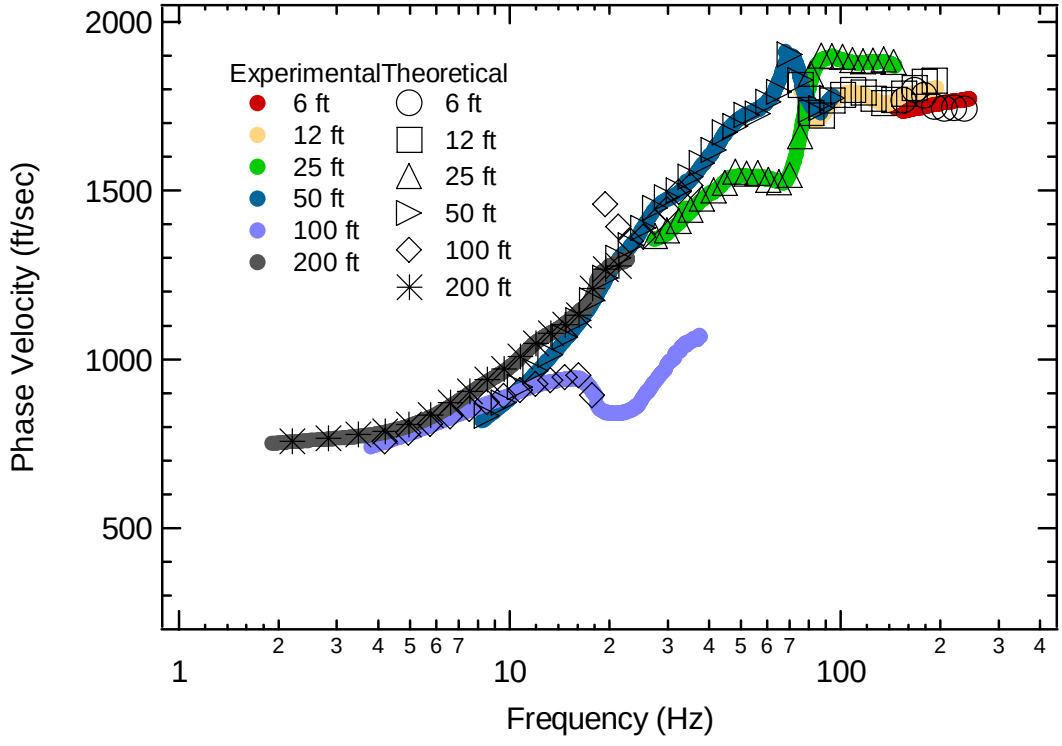

Figure 4-68 **Individual experimental and array theoretical dispersion curves plotted versus frequency for Profile 4c.**

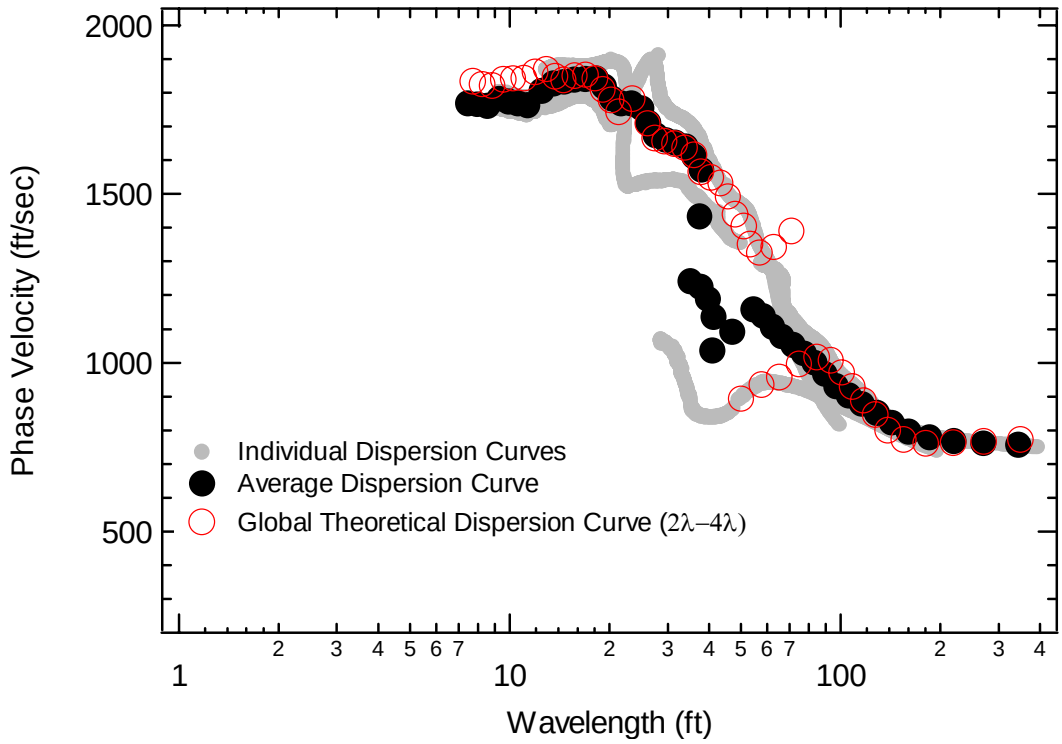

Figure 4-69 **Simulated experimental dispersion curves (individual and global average) versus global theoretical dispersion curve, plotted versus wavelength for Profile 4c.**

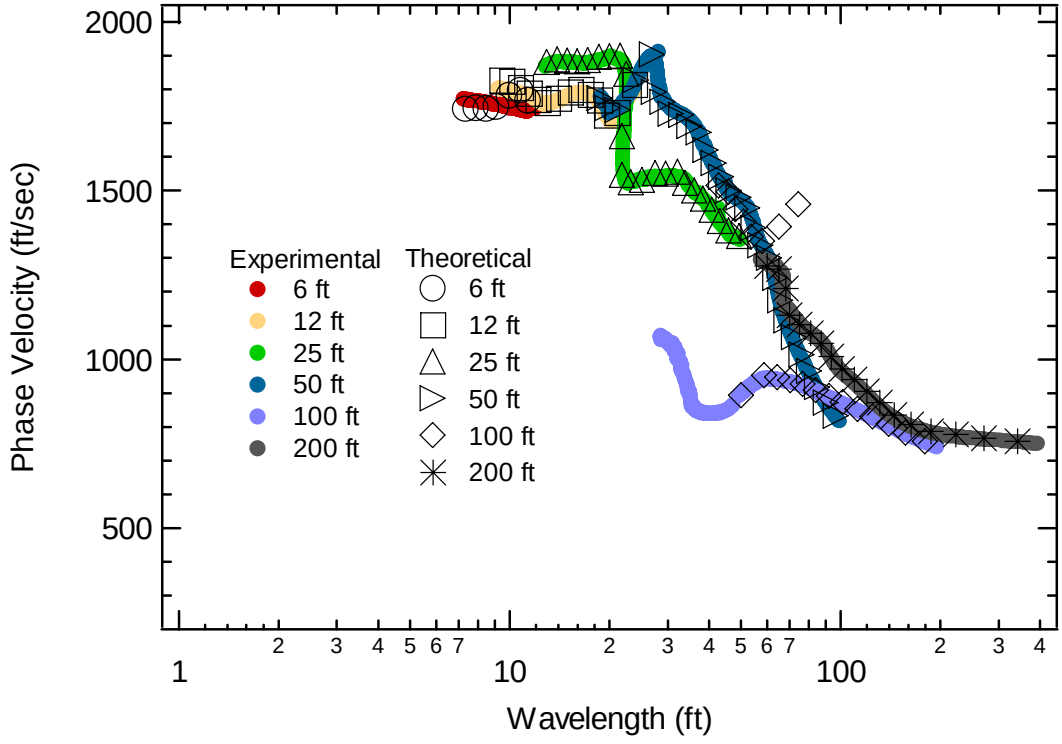

Figure 4-70 **Individual experimental and array theoretical dispersion curves plotted versus wavelength for Profile 4c.**

4.5 Embedded Stiff Layer

4.5.1 Profile 5a

Profile 5a is presented in Figure 4-71. Table 4-15 shows the individual layer characteristics for Profile 5a. Figures 4-72, 4-73, 4-74 and 4-75 show the simulated experimental and theoretical dispersion curves for this profile.

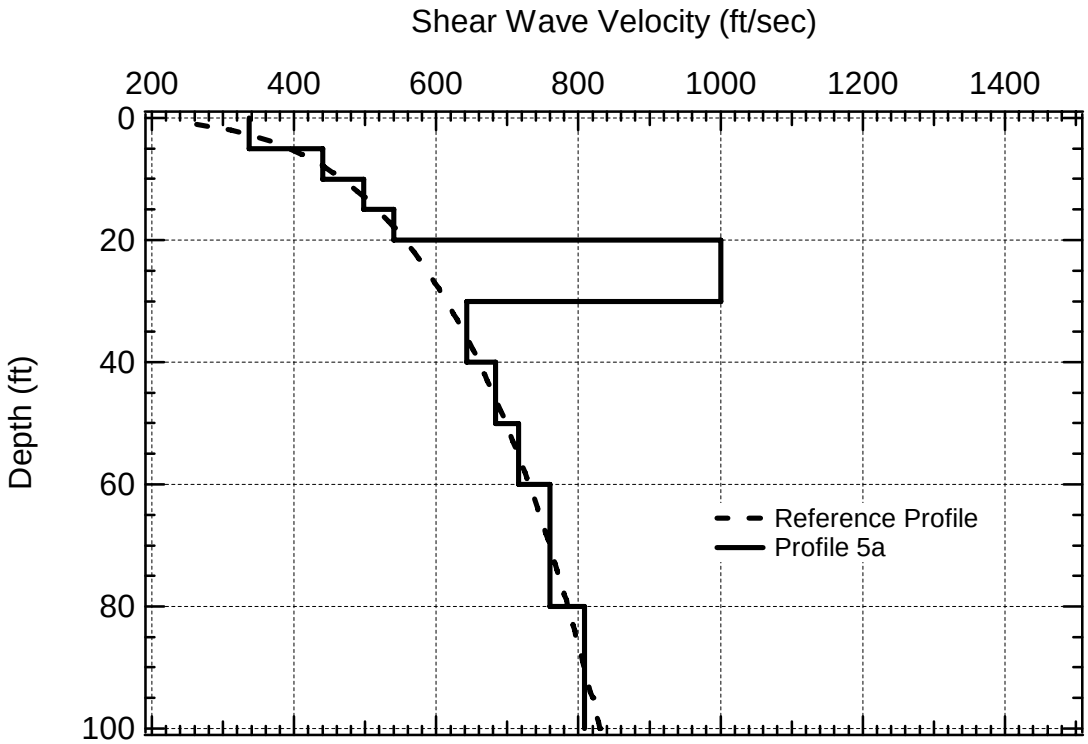

Figure 4-71 Profile 5a shown with the reference profile.

Table 4-15 Individual layer characteristics for Profile 5a.

Layer	Thickness (ft)	V_S (ft/sec)	ν	Unit Weight (pcf)
1	5	337	0.25	120
2	5	440	0.25	120
3	5	498	0.25	120
4	5	540	0.25	120
5	10	1000	0.25	120
6	10	643	0.25	120
7	10	683	0.25	120
8	10	718	0.25	120
9	20	762	0.25	120
10	Halfspace	811	0.25	120

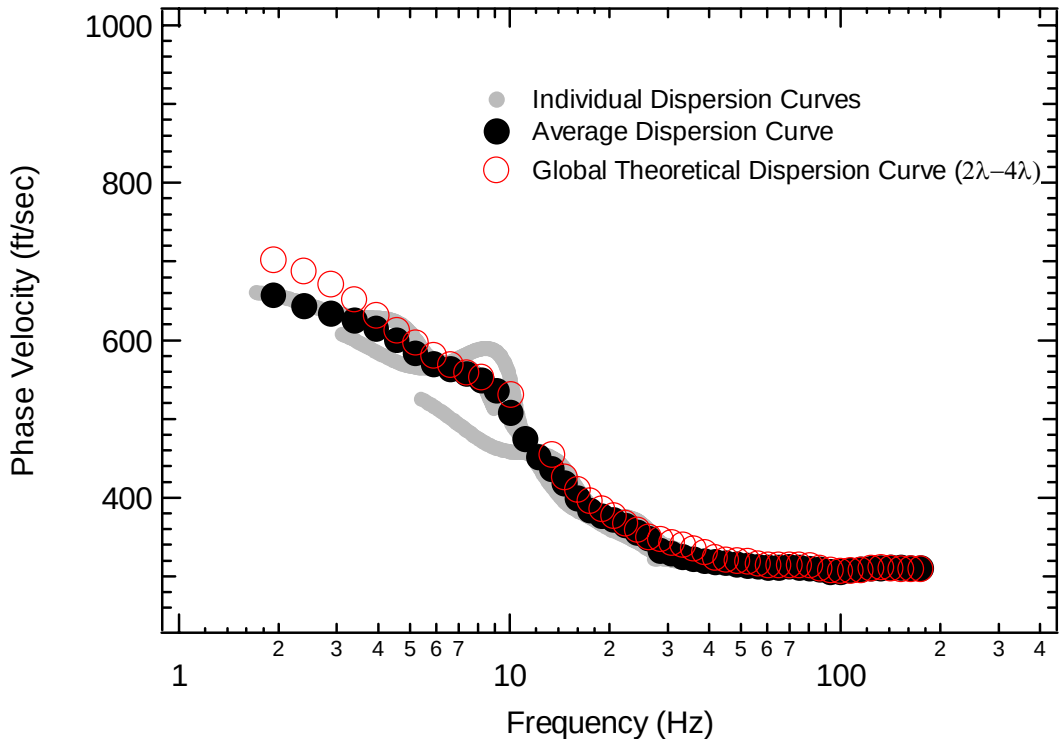

Figure 4-72 **Simulated experimental dispersion curves (individual and global average) versus global theoretical dispersion curve, plotted versus frequency for Profile 5a.**

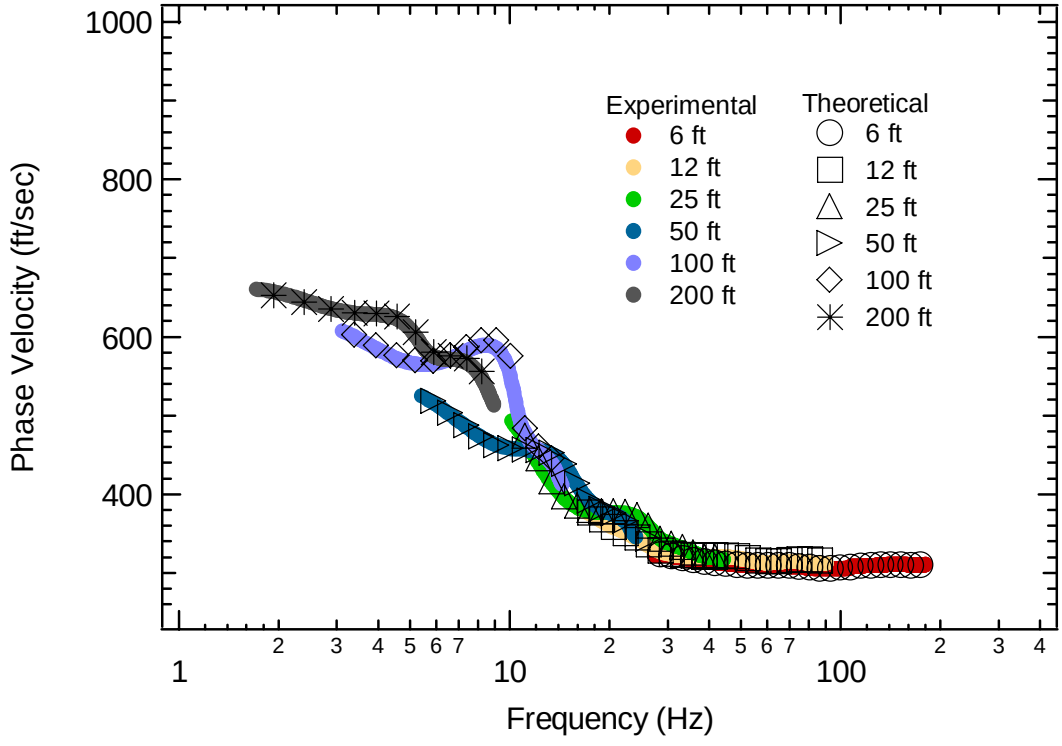

Figure 4-73 **Individual experimental and array theoretical dispersion curves plotted versus frequency for Profile 5a.**

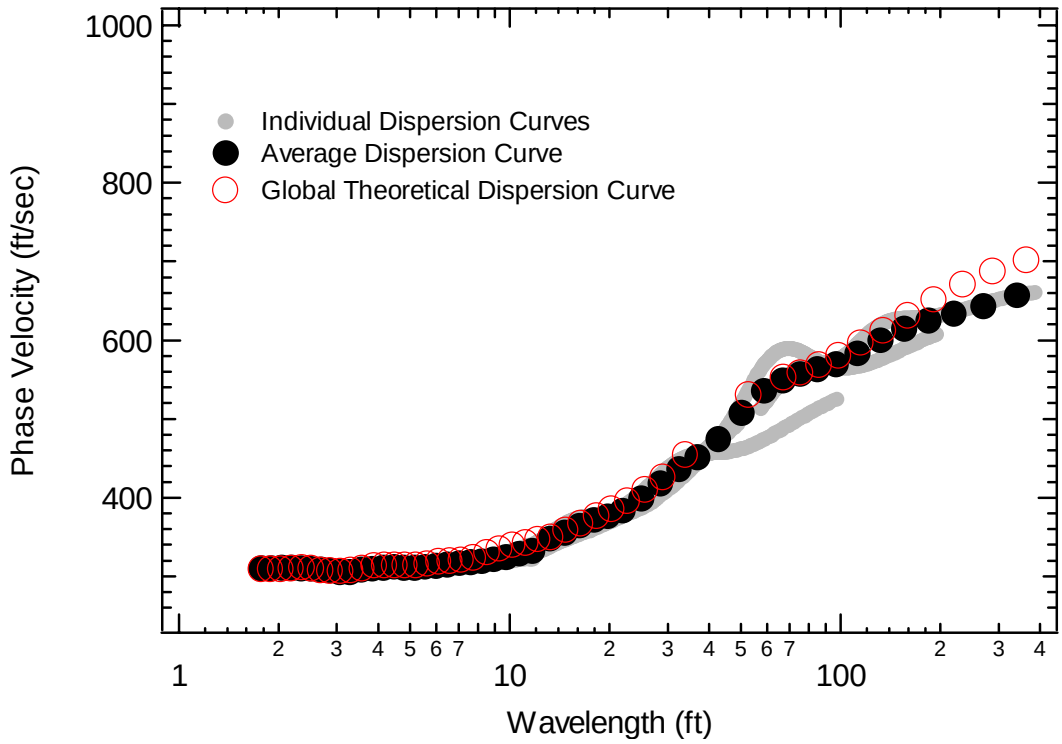

Figure 4-74 **Simulated experimental dispersion curves (individual and global average) versus global theoretical dispersion curve, plotted versus wavelength for Profile 5a.**

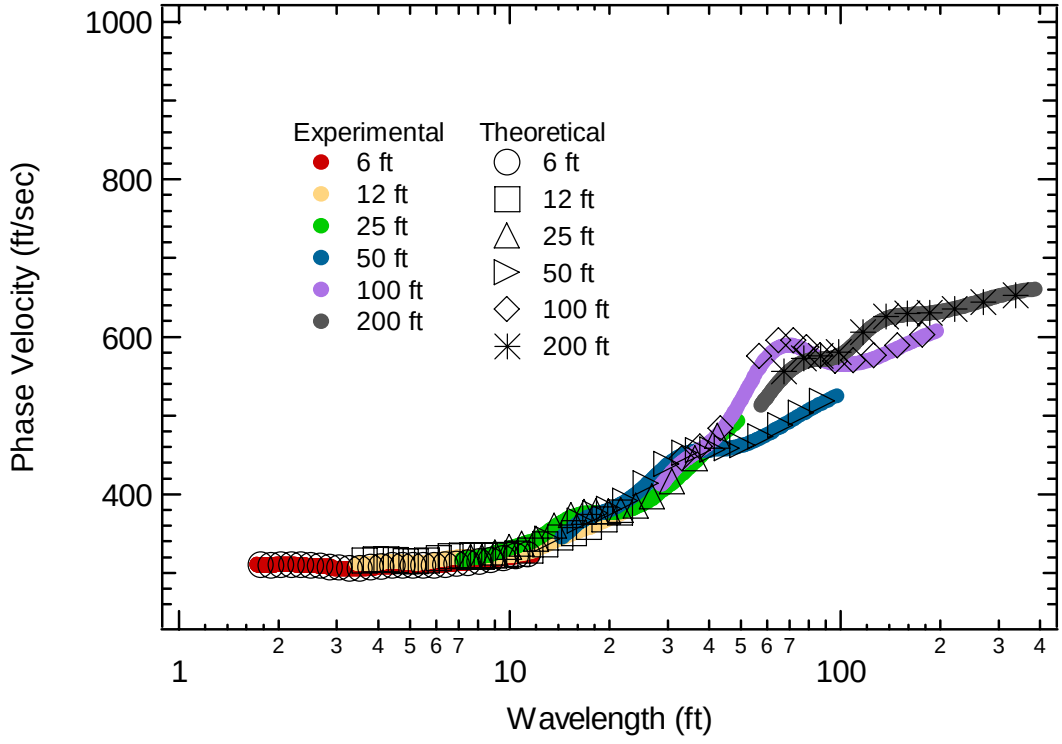

Figure 4-75 **Individual experimental and array theoretical dispersion curves plotted versus wavelength for Profile 5a.**

4.5.2 Profile 5b

Profile 5b is presented in Figure 4-76. Table 4-16 shows the individual layer characteristics for Profile 5b. Figures 4-77, 4-78, 4-79 and 4-80 show the simulated experimental and theoretical dispersion curves for this profile.

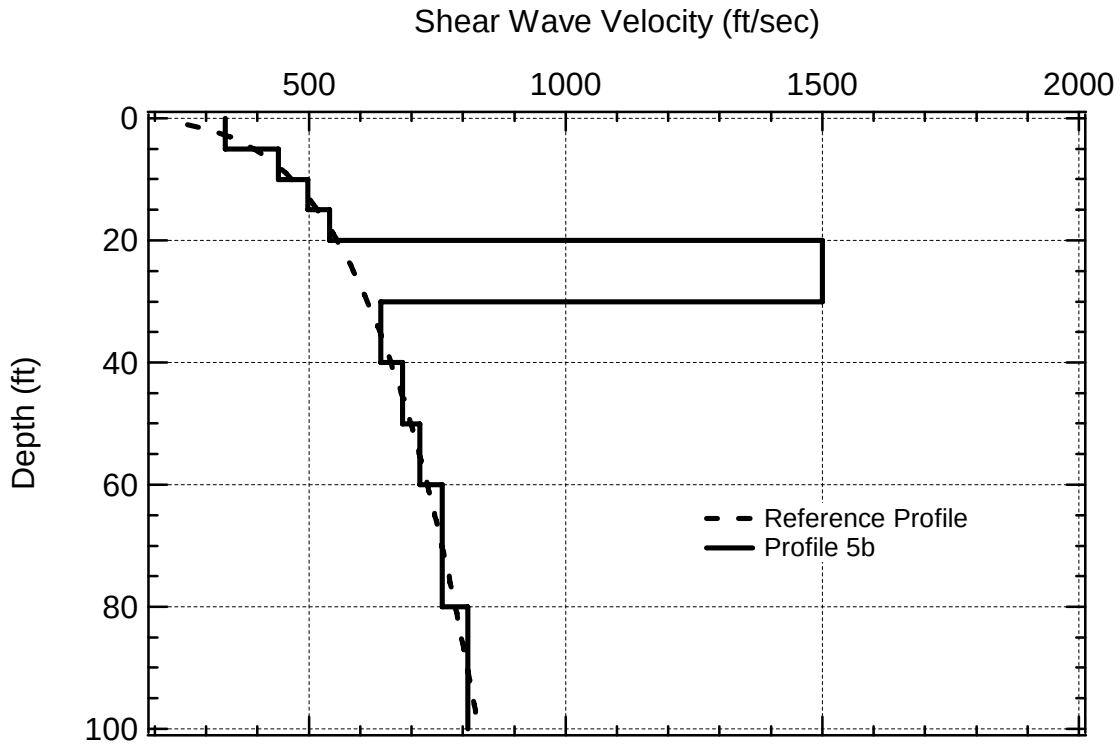

Figure 4-76 Profile 5b shown with the reference profile.

Table 4-16 Individual layer characteristics for Profile 5b.

Layer	Thickness (ft)	V_S (ft/sec)	ν	Unit Weight (pcf)
1	5	337	0.25	120
2	5	440	0.25	120
3	5	498	0.25	120
4	5	540	0.25	120
5	10	1500	0.25	120
6	10	643	0.25	120
7	10	683	0.25	120
8	10	718	0.25	120
9	20	762	0.25	120
10	Halfspace	811	0.25	120

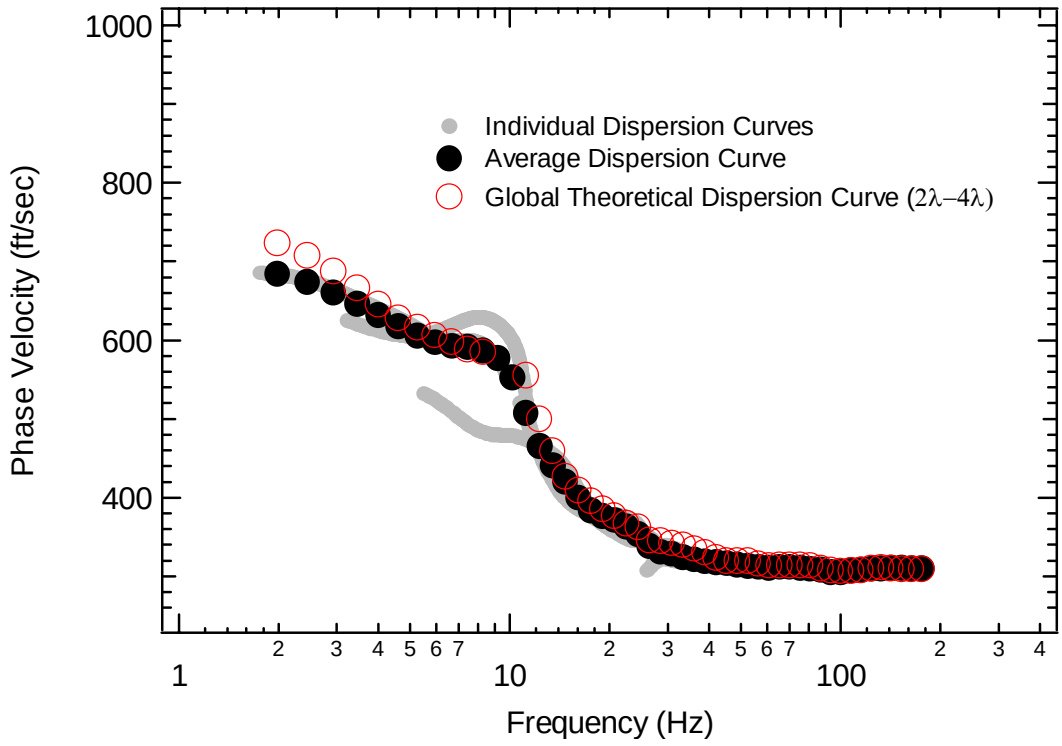

Figure 4-77 **Simulated experimental dispersion curves (individual and global average) versus global theoretical dispersion curve, plotted versus frequency for Profile 5b.**

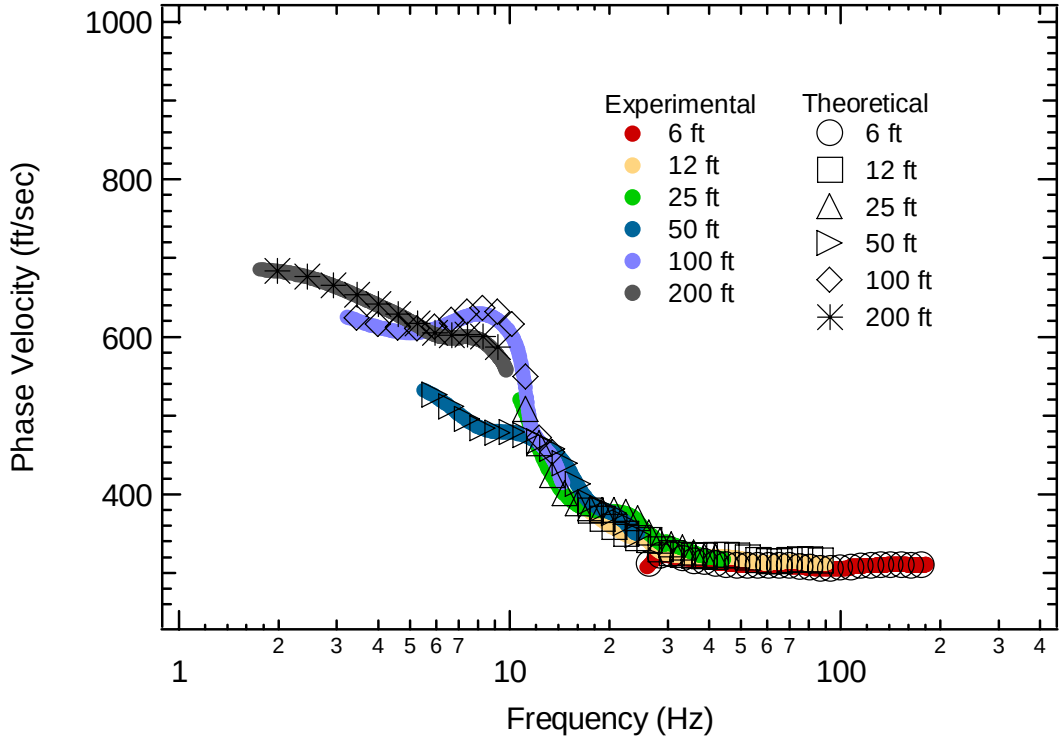

Figure 4-78 **Individual experimental and array theoretical dispersion curves plotted versus frequency for Profile 5b.**

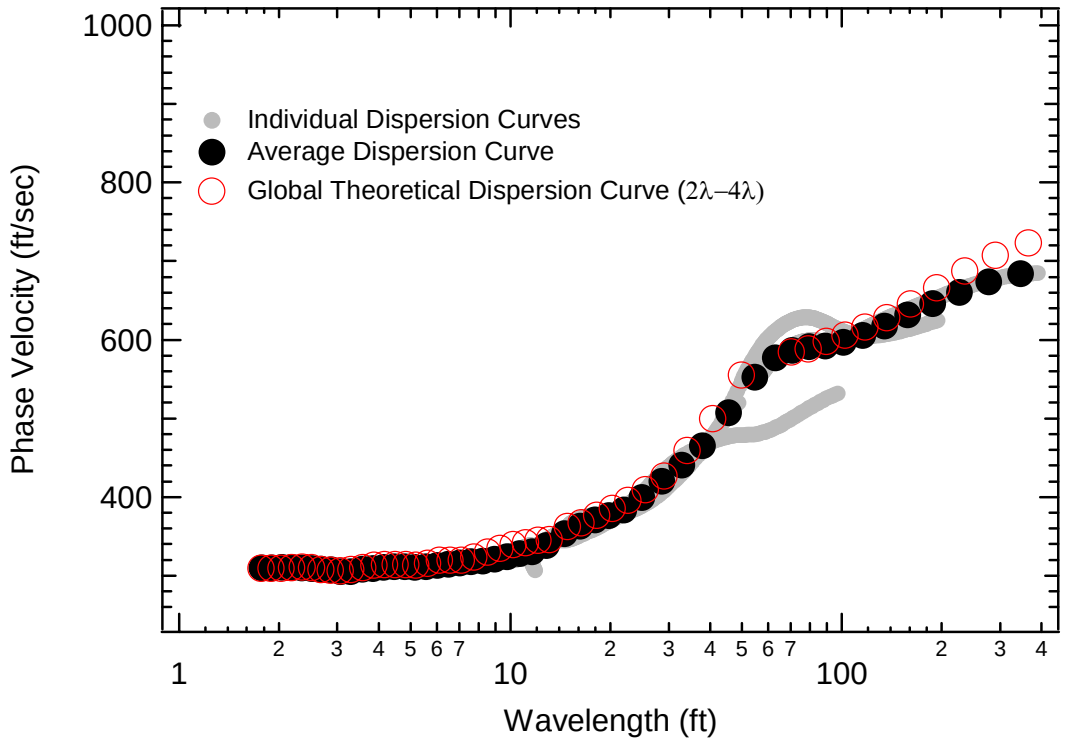

Figure 4-79 **Simulated experimental dispersion curves (individual and global average) versus global theoretical dispersion curve, plotted versus wavelength for Profile 5b.**

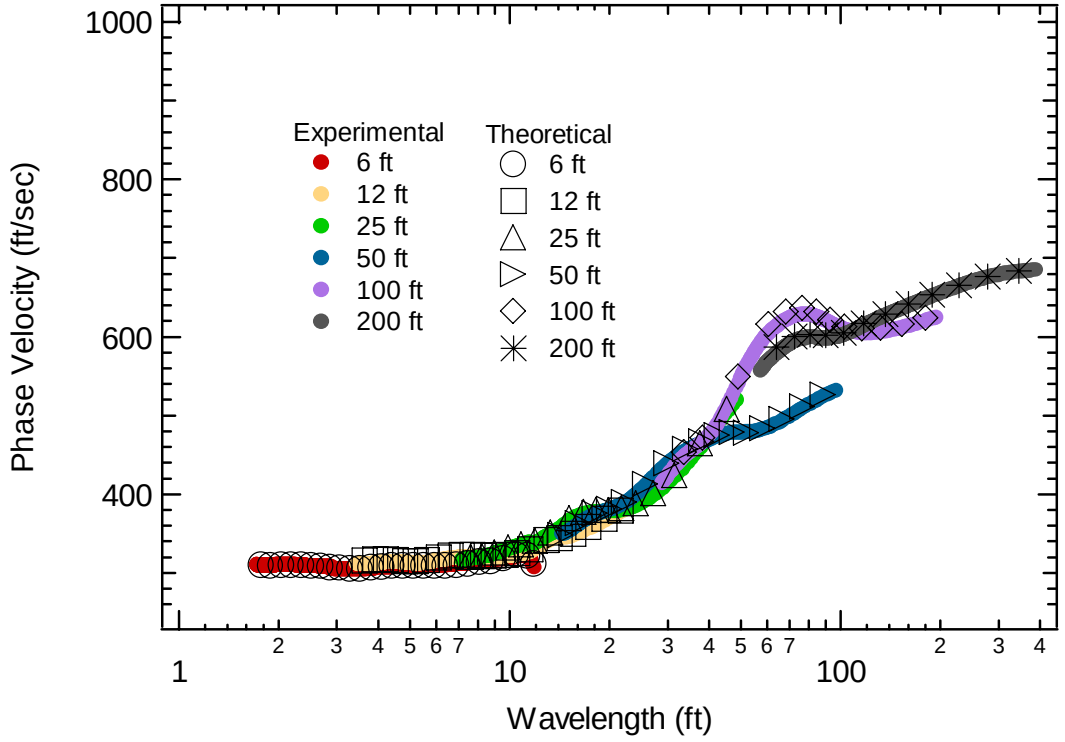

Figure 4-80 **Individual experimental and array theoretical dispersion curves plotted versus wavelength for Profile 5b.**

4.5.3 Profile 5c

Profile 5c is presented in Figure 4-81. Table 4-17 shows the individual layer characteristics for Profile 5c. Figures 4-82, 4-83, 4-84 and 4-85 show the simulated experimental and theoretical dispersion curves for this profile.

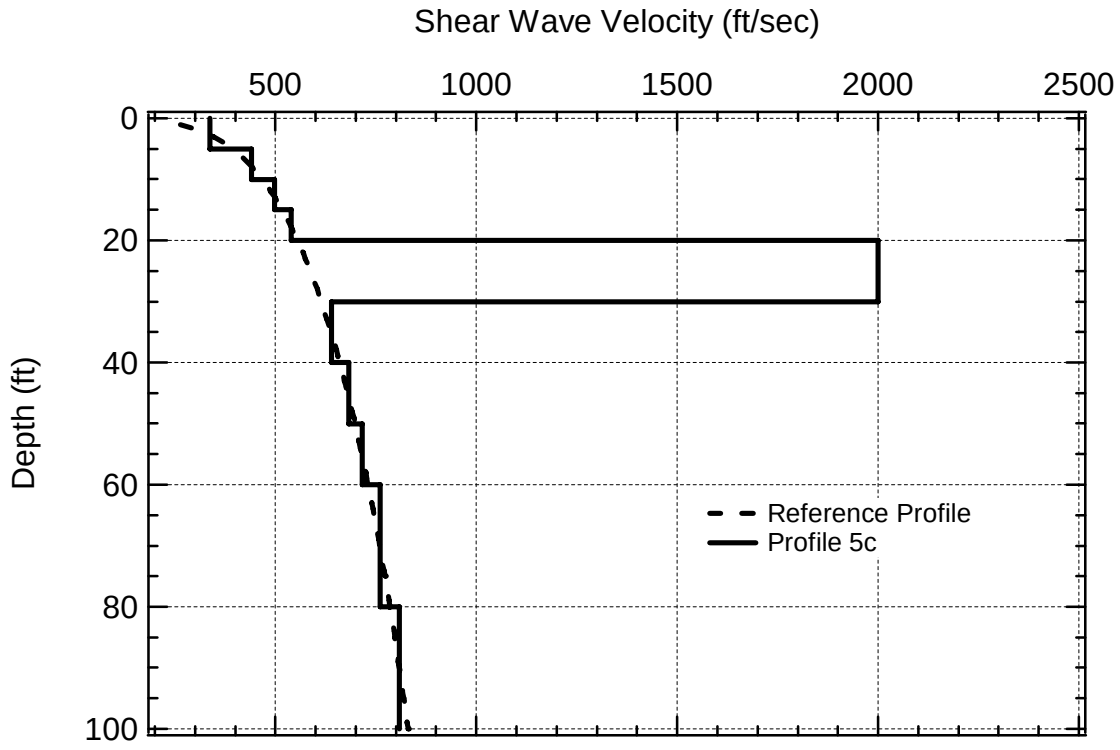

Figure 4-81 Profile 5c shown with the reference profile.

Table 4-17 Individual layer characteristics for Profile 5c.

Layer	Thickness (ft)	V_S (ft/sec)	ν	Unit Weight (pcf)
1	5	337	0.25	120
2	5	440	0.25	120
3	5	498	0.25	120
4	5	540	0.25	120
5	10	2000	0.25	120
6	10	643	0.25	120
7	10	683	0.25	120
8	10	718	0.25	120
9	20	762	0.25	120
10	Halfspace	811	0.25	120

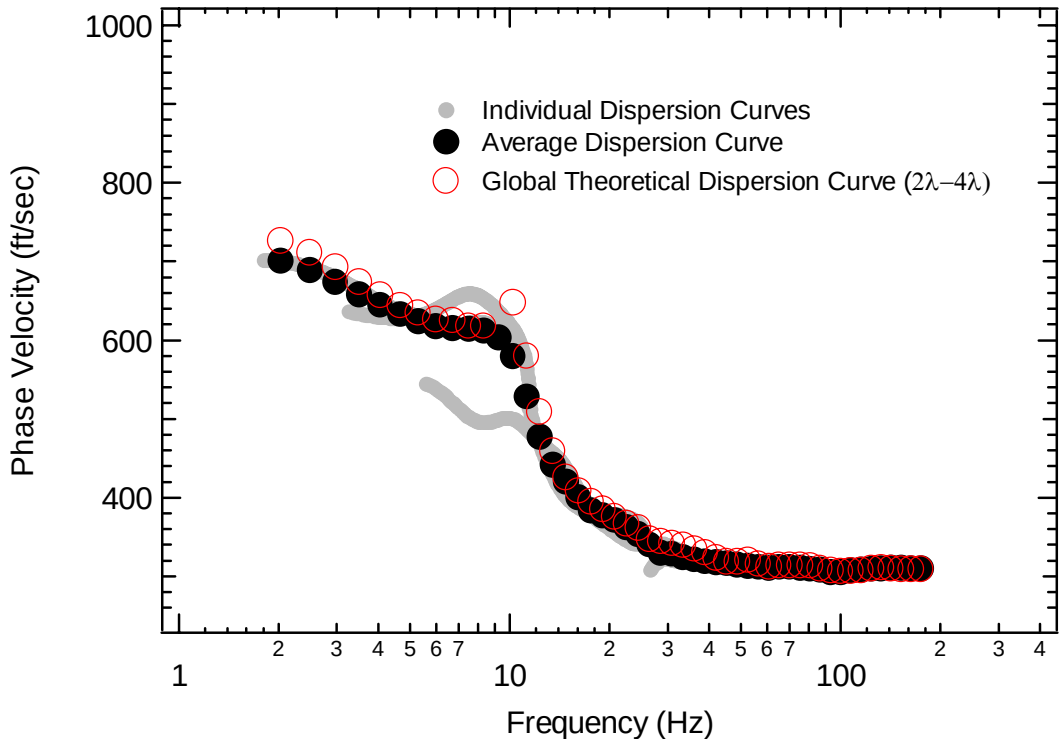

Figure 4-82 **Simulated experimental dispersion curves (individual and global average) versus global theoretical dispersion curve, plotted versus frequency for Profile 5c.**

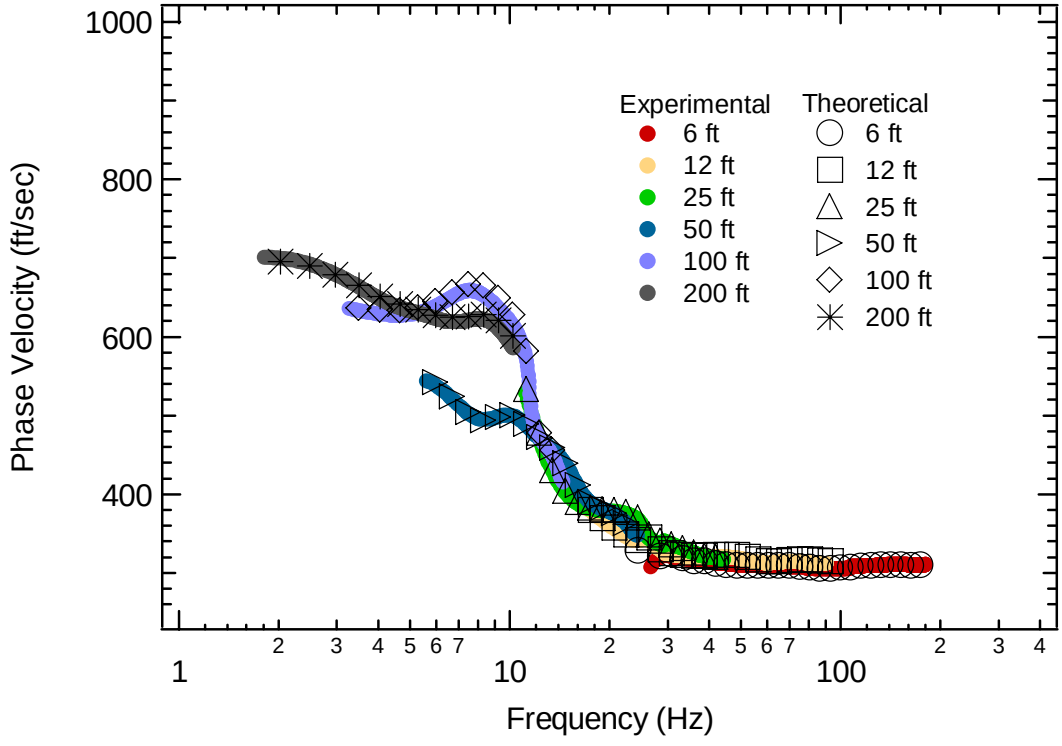

Figure 4-83 **Individual experimental and array theoretical dispersion curves plotted versus frequency for Profile 5c.**

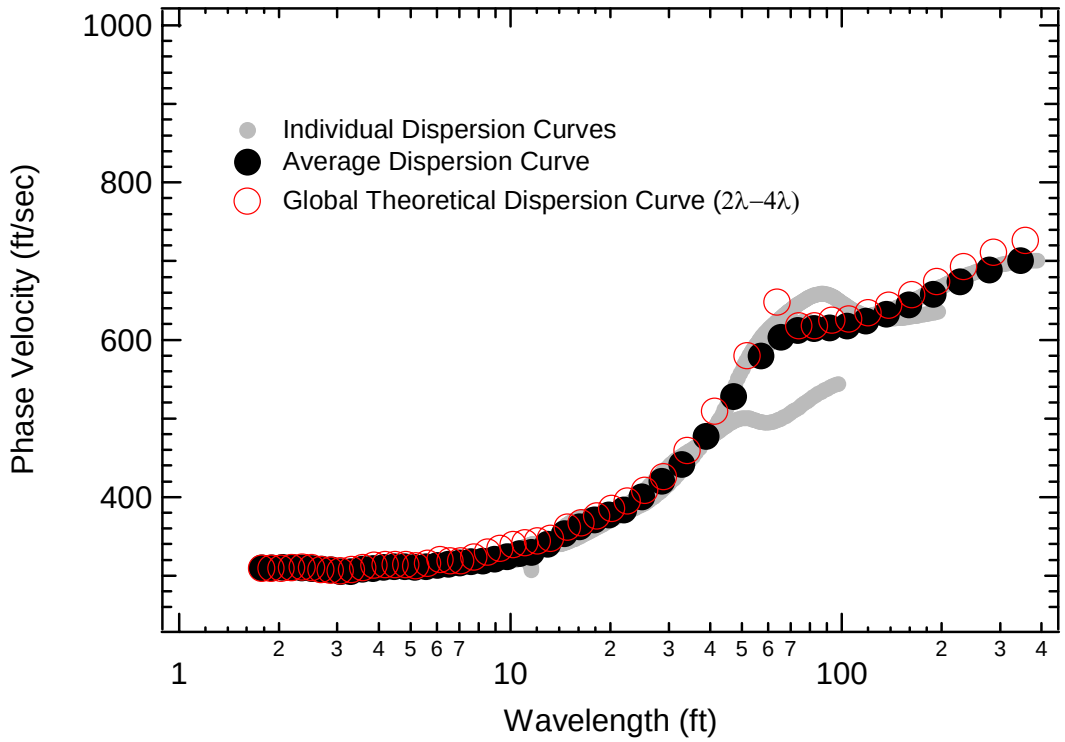

Figure 4-84 **Simulated experimental dispersion curves (individual and global average) versus global theoretical dispersion curve, plotted versus wavelength for Profile 5c.**

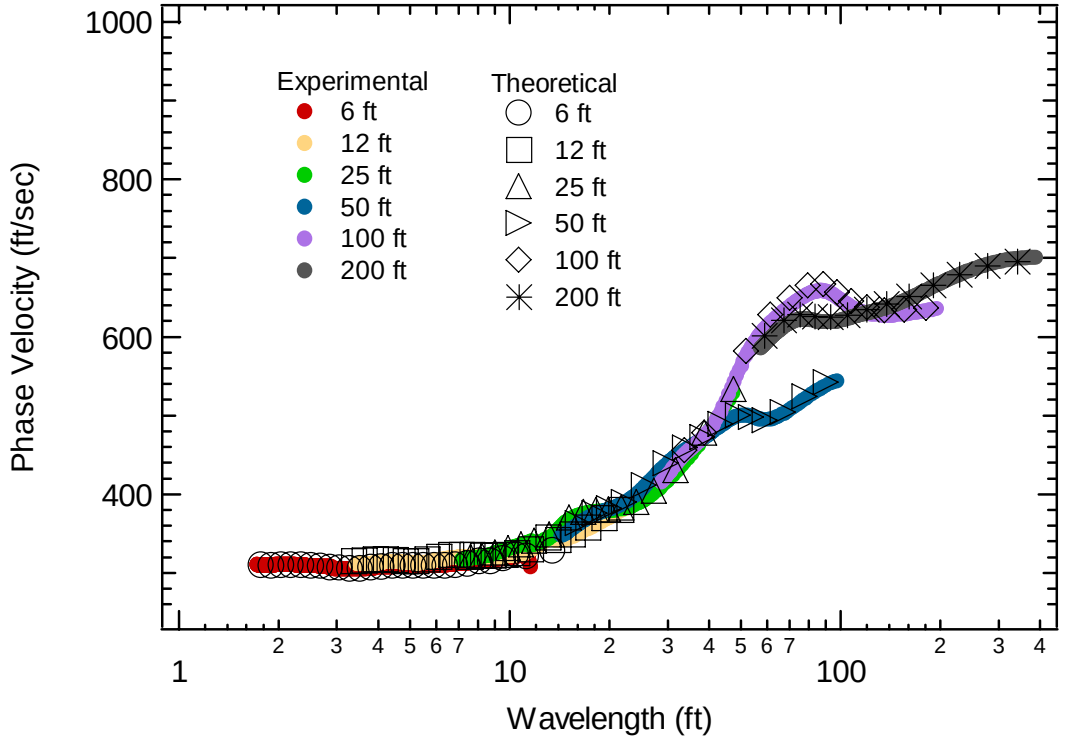

Figure 4-85 **Individual experimental and array theoretical dispersion curves plotted versus wavelength for Profile 5c.**

4.5.4 Profile 6a

Profile 6a is presented in Figure 4-86. Table 4-18 shows the individual layer characteristics for Profile 6a. Figures 4-87, 4-88, 4-89 and 4-90 show the simulated experimental and theoretical dispersion curves for this profile.

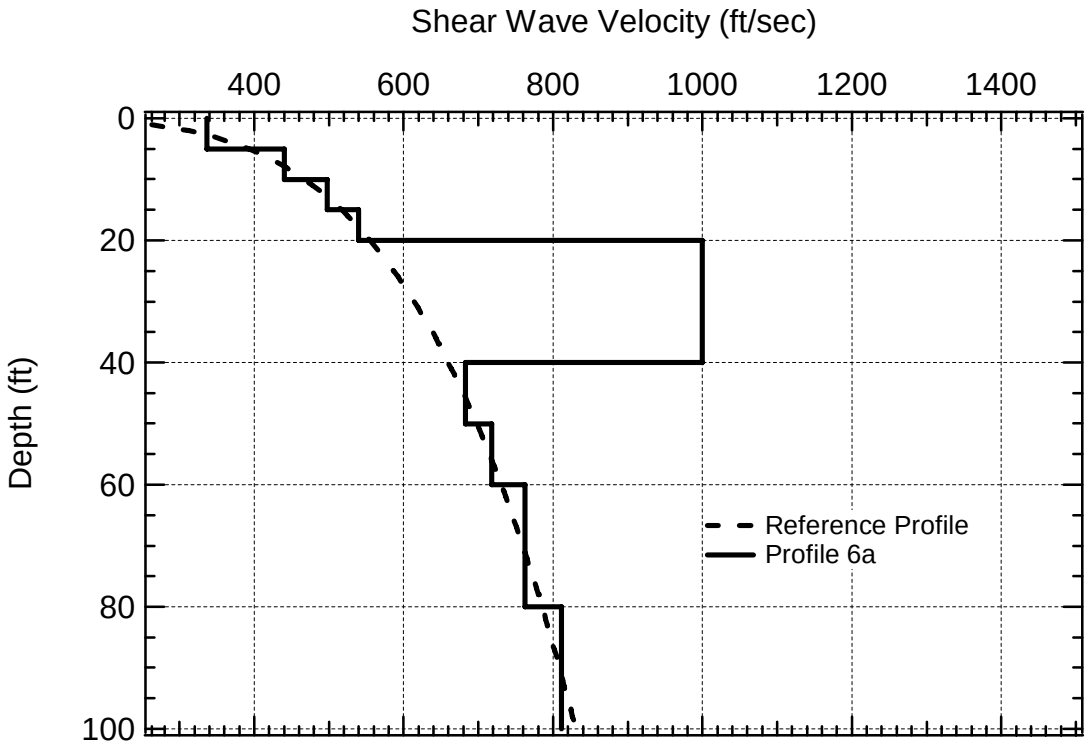

Figure 4-86 Profile 6a shown with the reference profile.

Table 4-18 Individual layer characteristics for Profile 6a.

Layer	Thickness (ft)	V_S (ft/sec)	ν	Unit Weight (pcf)
1	5	337	0.25	120
2	5	440	0.25	120
3	5	498	0.25	120
4	5	540	0.25	120
5	20	1000	0.25	120
6	10	683	0.25	120
7	10	718	0.25	120
8	20	762	0.25	120
9	Halfspace	811	0.25	120

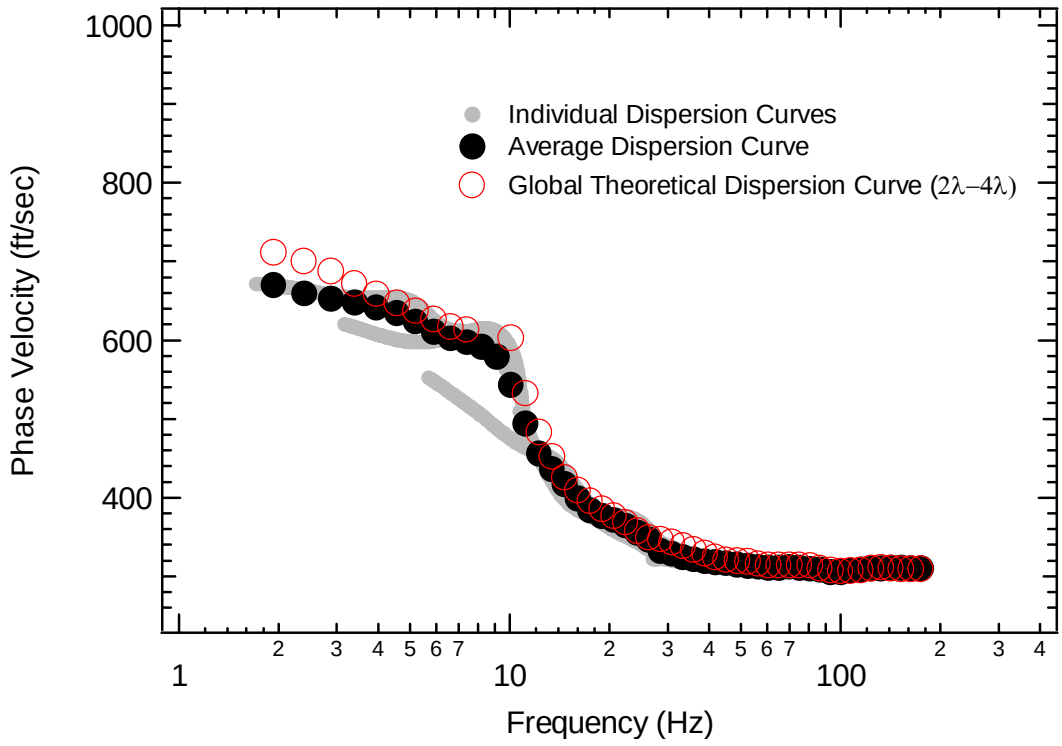

Figure 4-87 **Simulated experimental dispersion curves (individual and global average) versus global theoretical dispersion curve, plotted versus frequency for Profile 6a.**

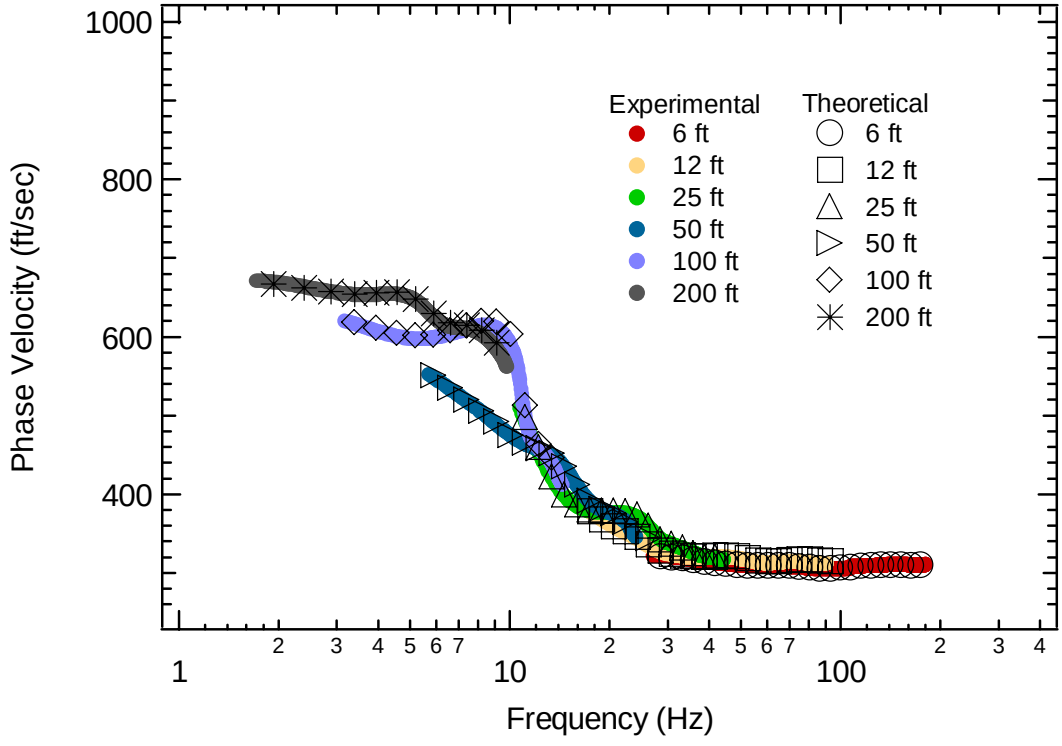

Figure 4-88 **Individual experimental and array theoretical dispersion curves plotted versus frequency for Profile 6a.**

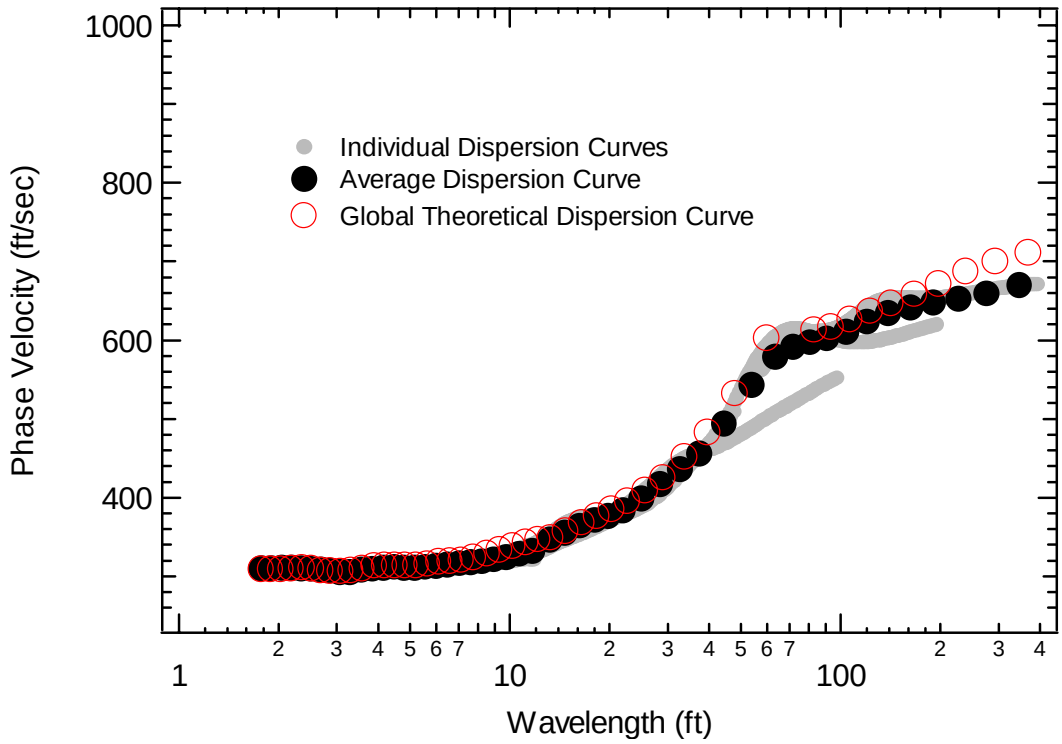

Figure 4-89 **Simulated experimental dispersion curves (individual and global average) versus global theoretical dispersion curve, plotted versus wavelength for Profile 6a.**

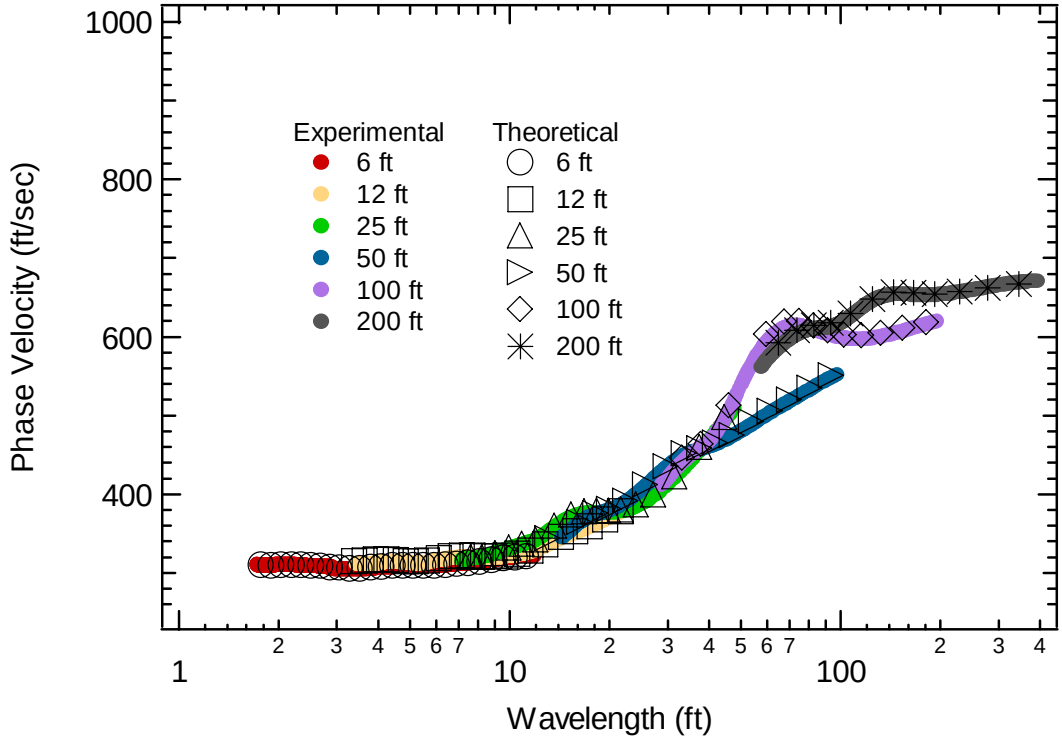

Figure 4-90 **Individual experimental and array theoretical dispersion curves plotted versus wavelength for Profile 6a.**

4.5.5 Profile 6b

Profile 6b is presented in Figure 4-91. Table 4-19 shows the individual layer characteristics for Profile 6b. Figures 4-92, 4-93, 4-94 and 4-95 show the simulated experimental and theoretical dispersion curves for this profile.

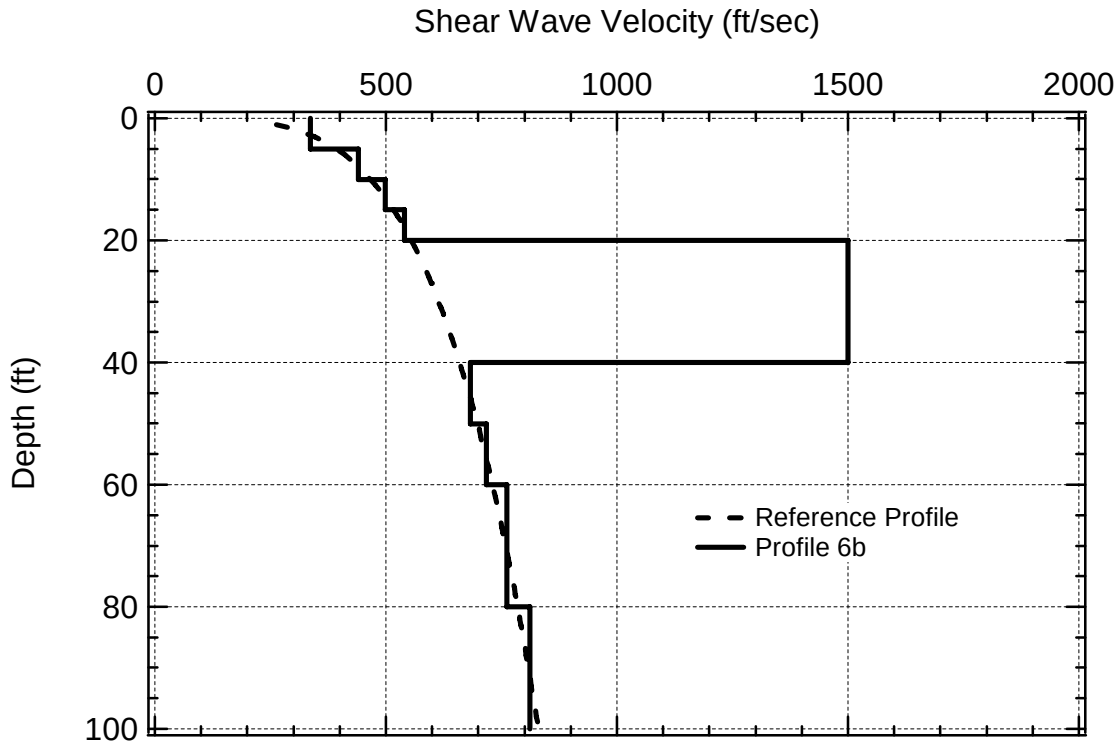

Figure 4-91 Profile 6b shown with the reference profile.

Table 4-19 Individual layer characteristics for Profile 6b.

Layer	Thickness (ft)	V_S (ft/sec)	ν	Unit Weight (pcf)
1	5	337	0.25	120
2	5	440	0.25	120
3	5	498	0.25	120
4	5	540	0.25	120
5	20	1500	0.25	120
6	10	683	0.25	120
7	10	718	0.25	120
8	20	762	0.25	120
9	Halfspace	811	0.25	120

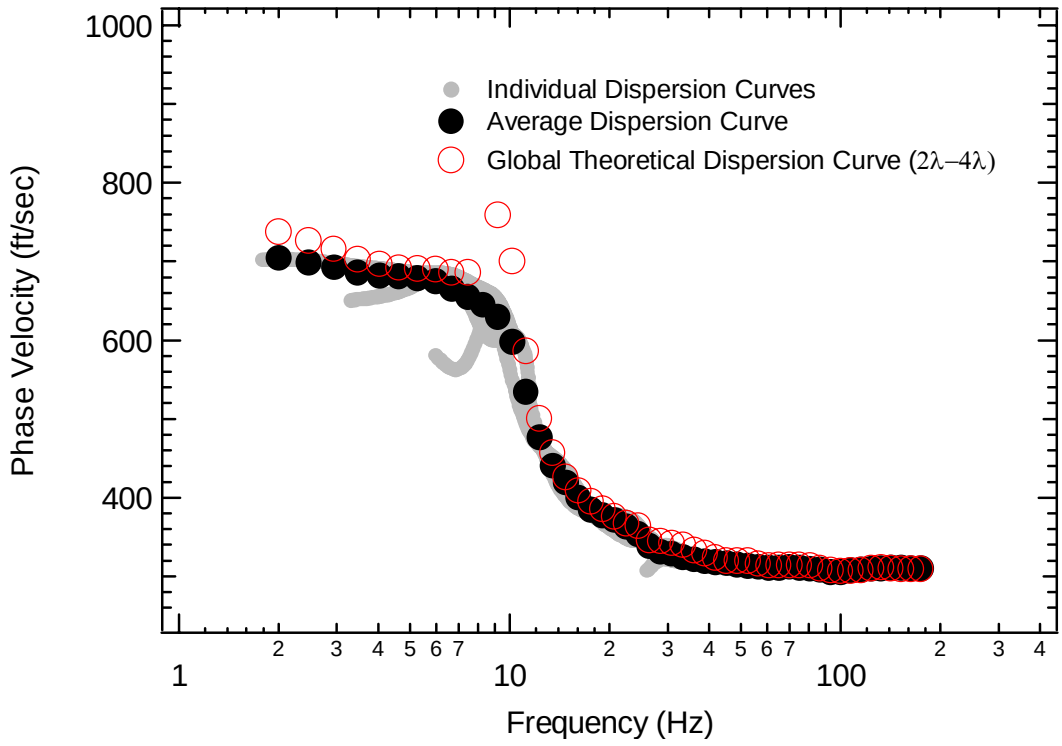

Figure 4-92 **Simulated experimental dispersion curves (individual and global average) versus global theoretical dispersion curve, plotted versus frequency for Profile 6b.**

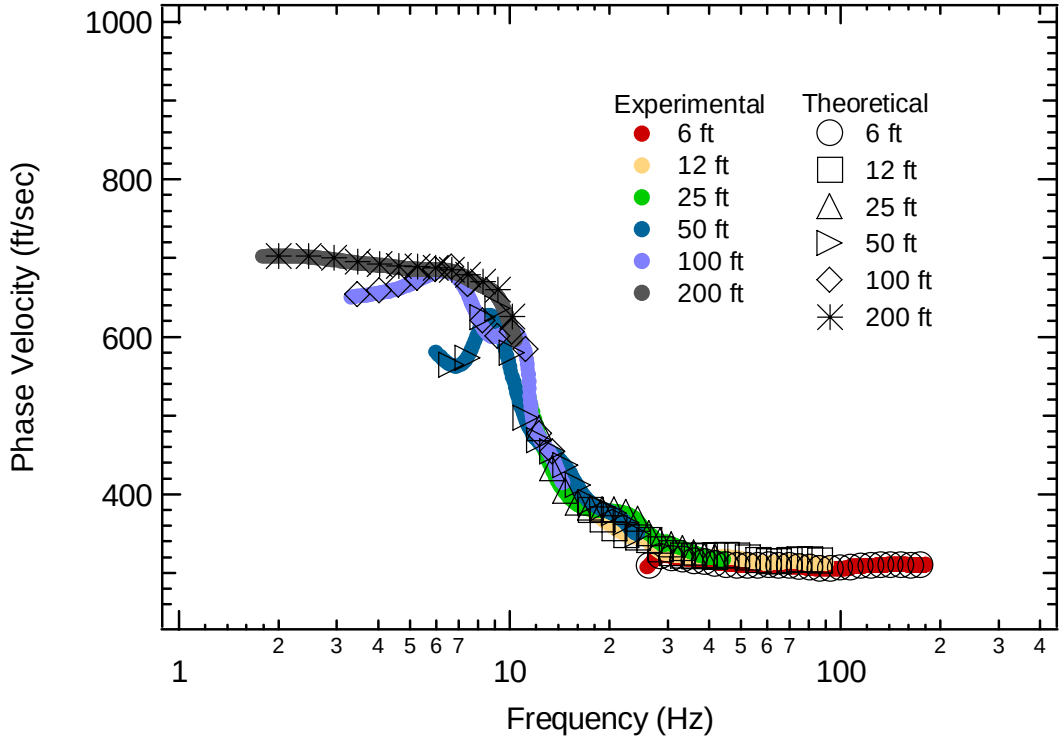

Figure 4-93 **Individual experimental and array theoretical dispersion curves plotted versus frequency for Profile 6b.**

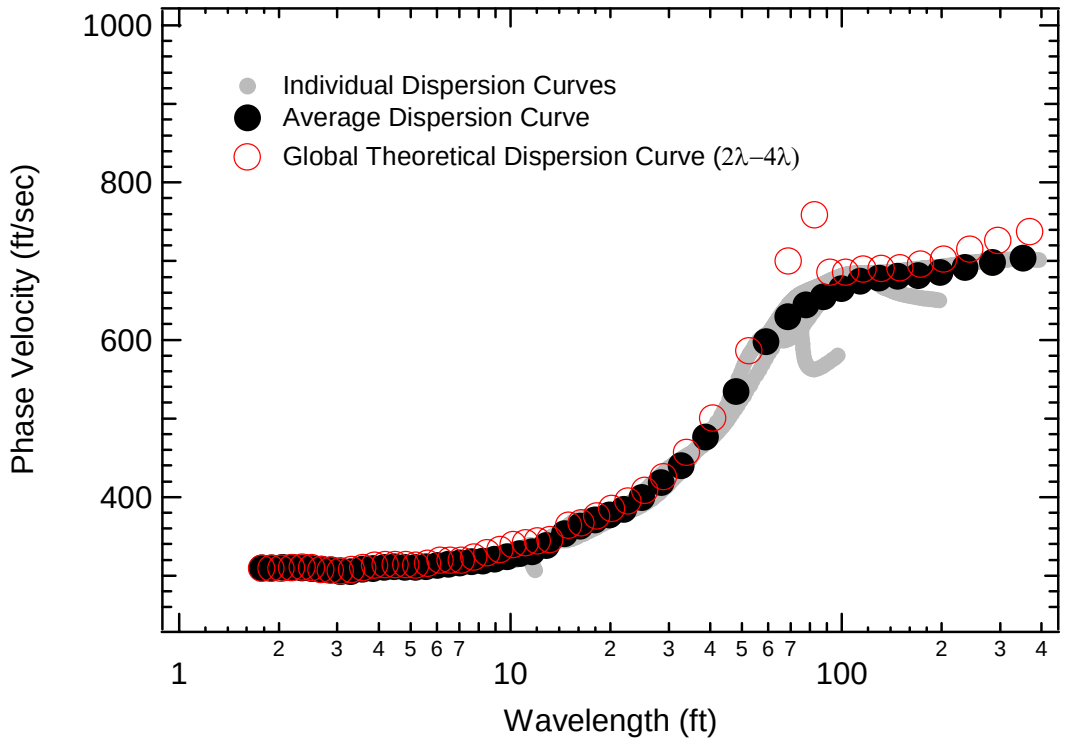

Figure 4-94 **Simulated experimental dispersion curves (individual and global average) versus global theoretical dispersion curve, plotted versus wavelength for Profile 6b.**

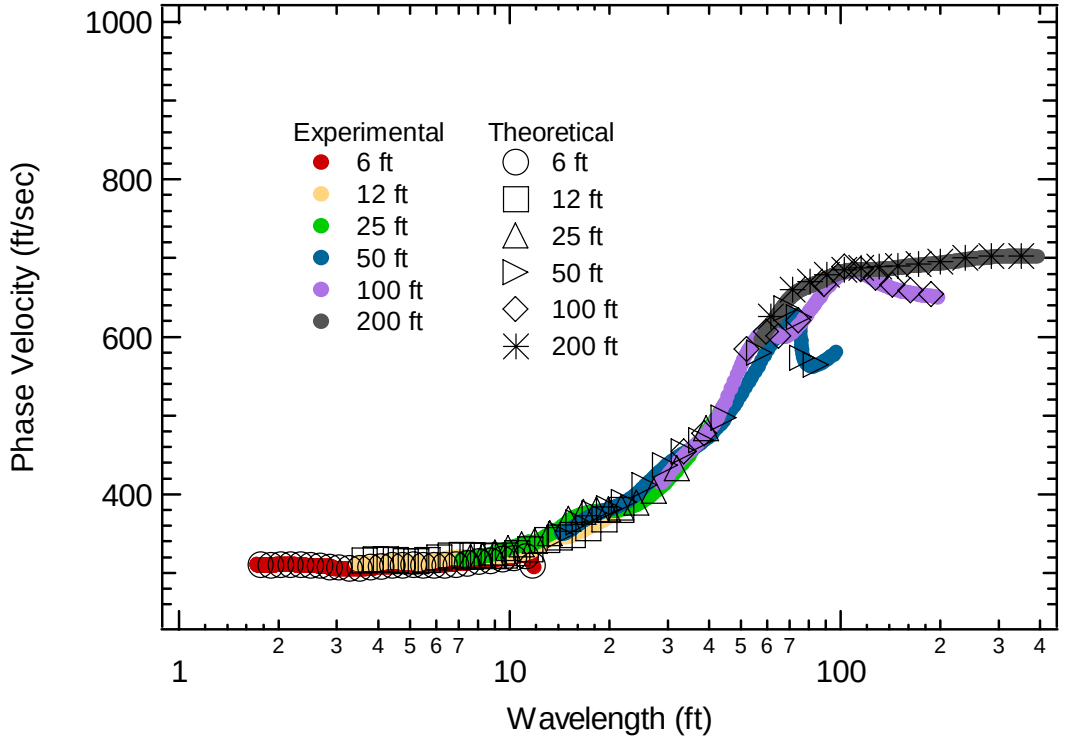

Figure 4-95 **Individual experimental and array theoretical dispersion curves plotted versus wavelength for Profile 6b.**

4.5.6 Profile 6c

Profile 6c is presented in Figure 4-96. Table 4-20 shows the individual layer characteristics for Profile 6c. Figures 4-97, 4-98, 4-99 and 4-100 show the simulated experimental and theoretical dispersion curves for this profile.

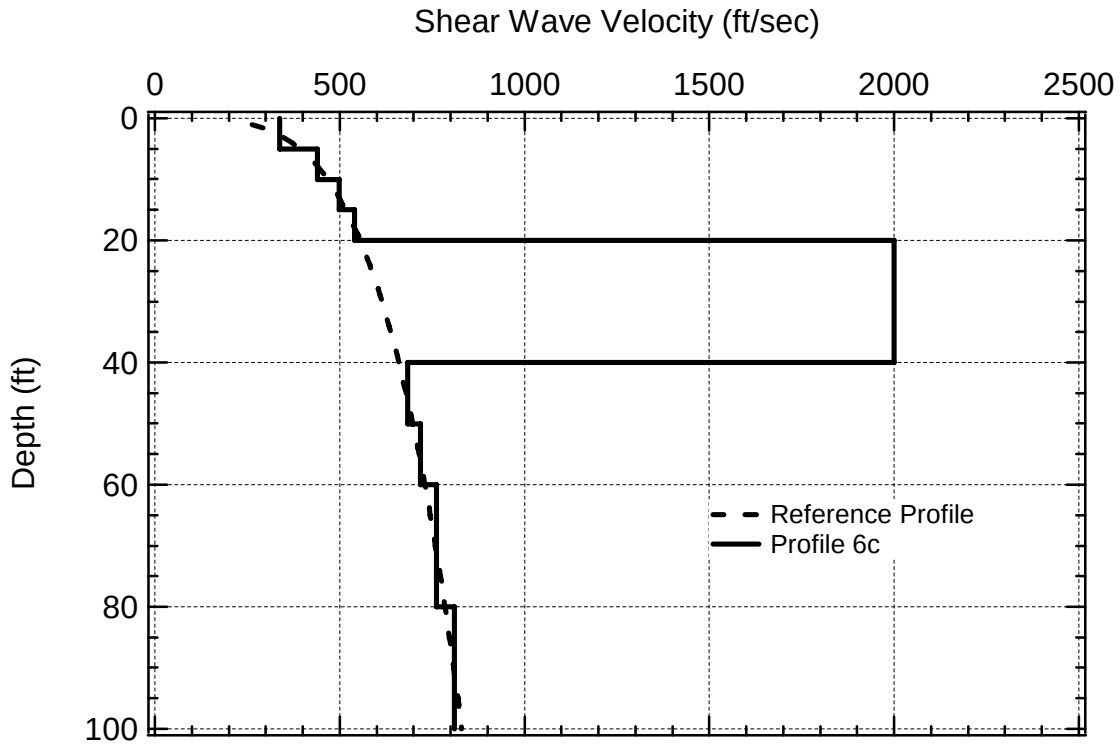

Figure 4-96 Profile 6c shown with the reference profile.

Table 4-20 Individual layer characteristics for Profile 6c.

Layer	Thickness (ft)	V_S (ft/sec)	ν	Unit Weight (pcf)
1	5	337	0.25	120
2	5	440	0.25	120
3	5	498	0.25	120
4	5	540	0.25	120
5	20	2000	0.25	120
6	10	683	0.25	120
7	10	718	0.25	120
8	20	762	0.25	120
9	Halfspace	811	0.25	120

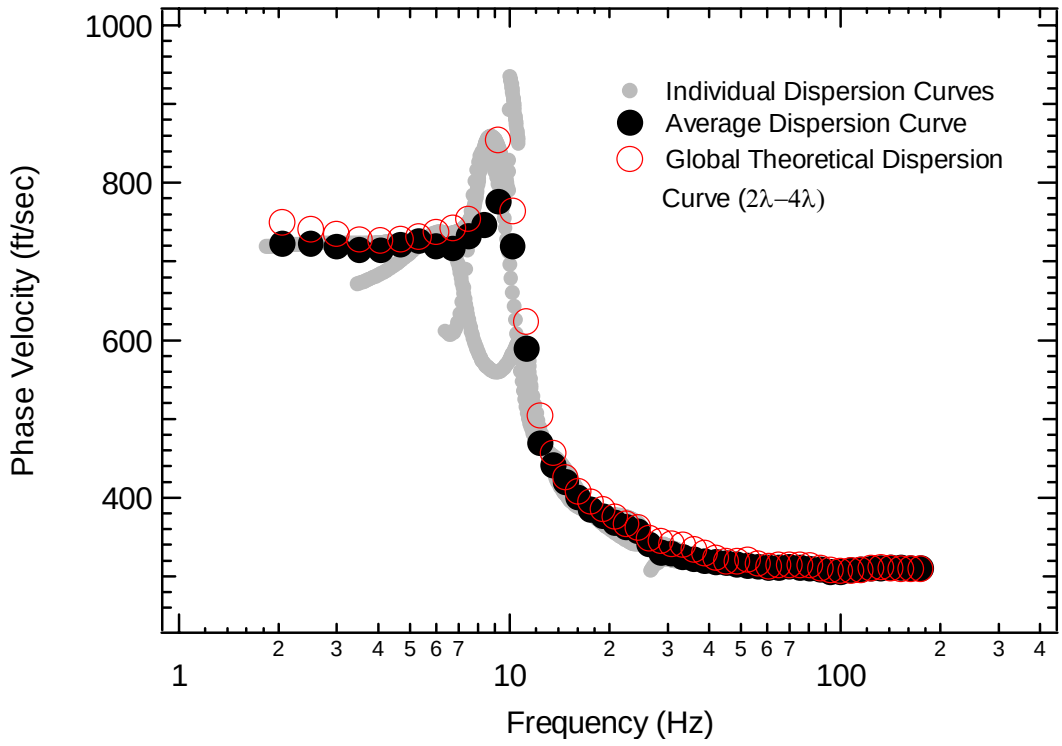

Figure 4-97 **Simulated experimental dispersion curves (individual and global average) versus global theoretical dispersion curve, plotted versus frequency for Profile 6c.**

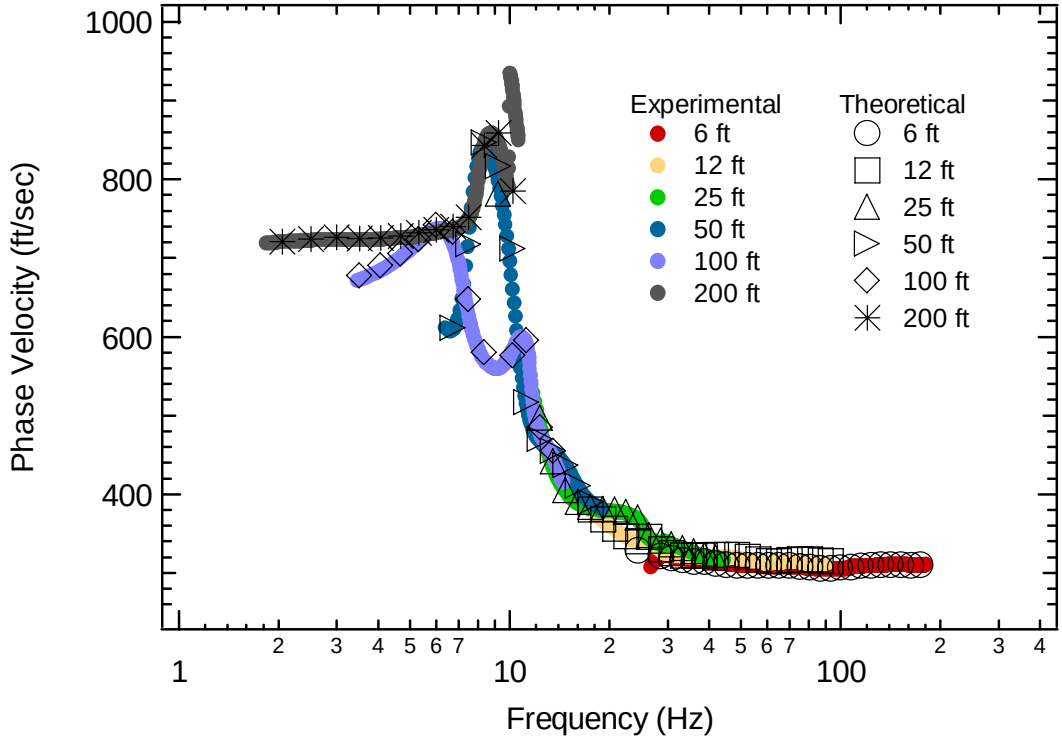

Figure 4-98 **Individual experimental and array theoretical dispersion curves plotted versus frequency for Profile 6c.**

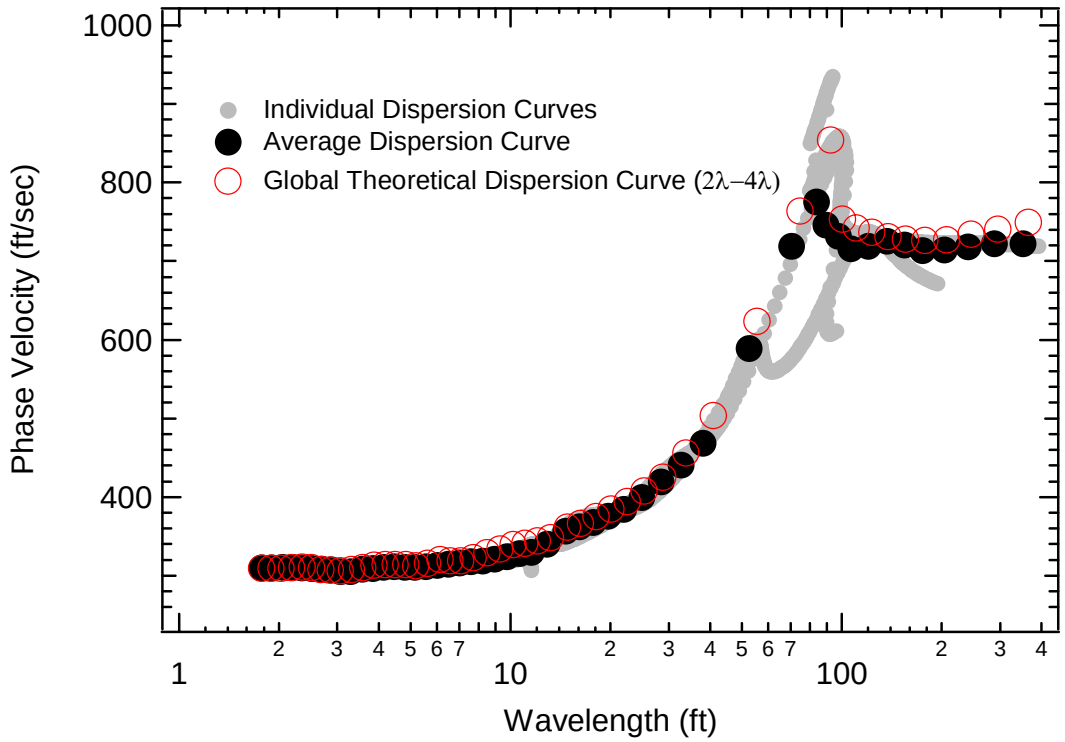

Figure 4-99 **Simulated experimental dispersion curves (individual and global average) versus global theoretical dispersion curve, plotted versus wavelength for Profile 6c.**

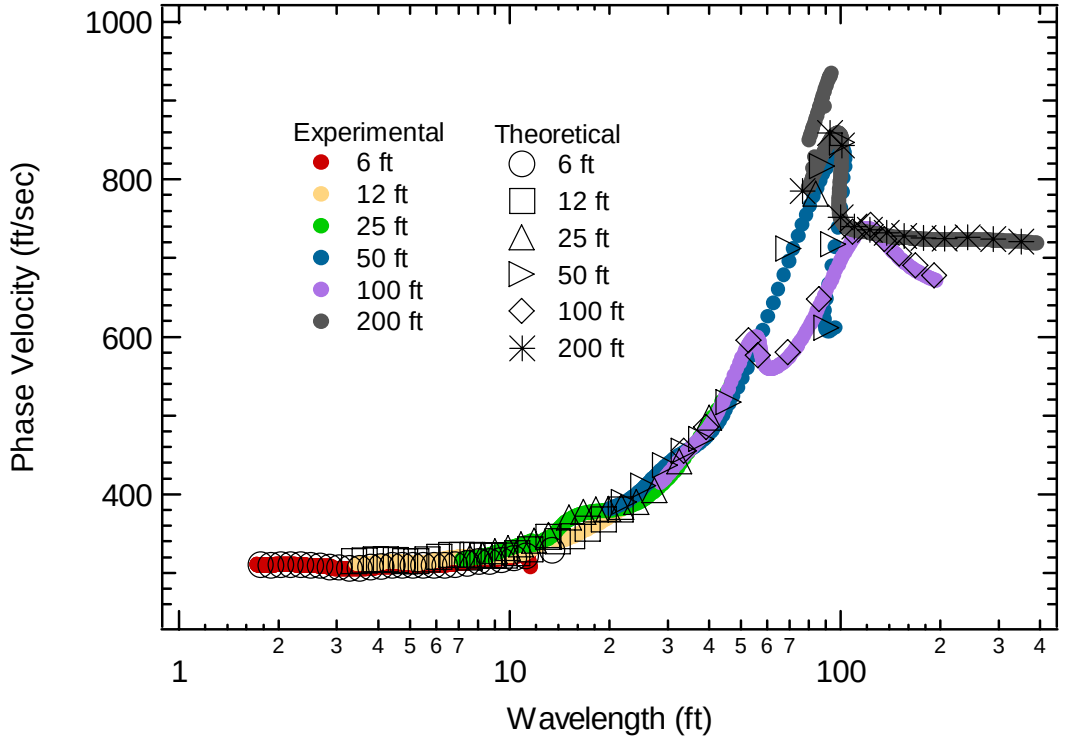

Figure 4-100 **Individual experimental and array theoretical dispersion curves plotted versus wavelength for Profile 6c.**

4.6 Profiles with Embedded Soft Layer

4.6.1 Profile 7a

Profile 7a is presented in Figure 4-101. Table 4-21 shows the individual layer characteristics for Profile 7a. Figures 4-102, 4-103, 4-104 and 4-105 show the simulated experimental and theoretical dispersion curves for this profile.

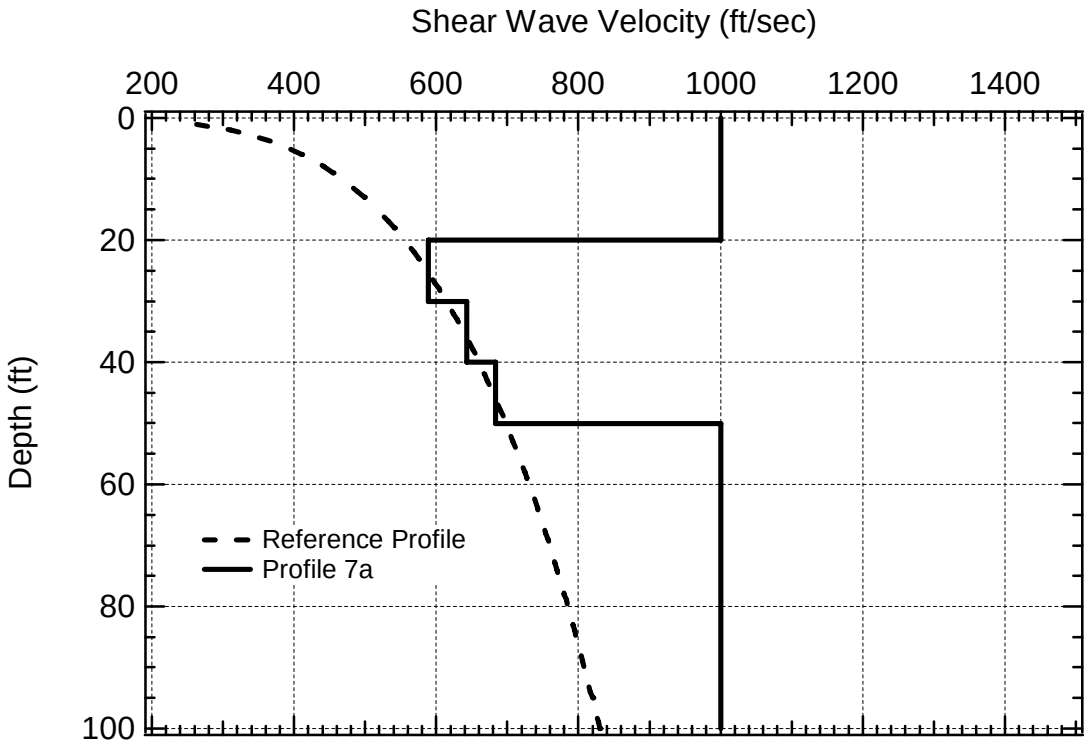

Figure 4-101 Profile 7a shown with the reference profile.

Table 4-21 Individual layer characteristics for Profile 7a.

Layer	Thickness (ft)	V_S (ft/sec)	ν	Unit Weight (pcf)
1	20	1000	0.25	120
2	10	589	0.25	120
3	10	643	0.25	120
4	10	683	0.25	120
5	Halfspace	1000	0.25	120

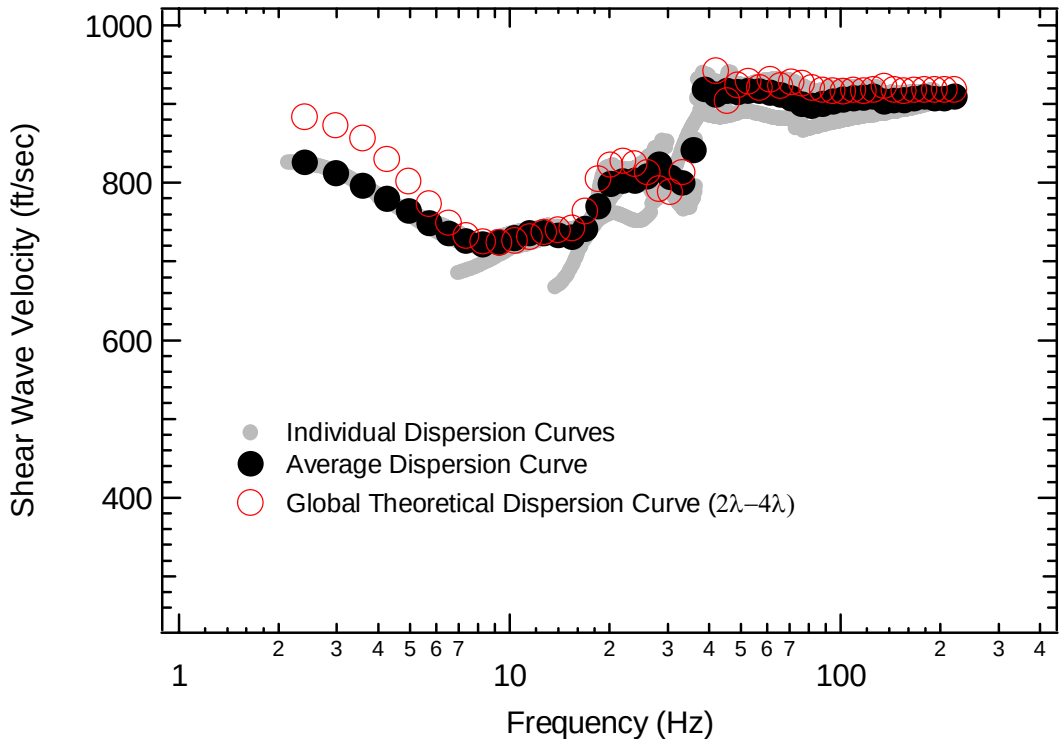

Figure 4-102 **Simulated experimental dispersion curves (individual and global average) versus global theoretical dispersion curve, plotted versus frequency for Profile 7a.**

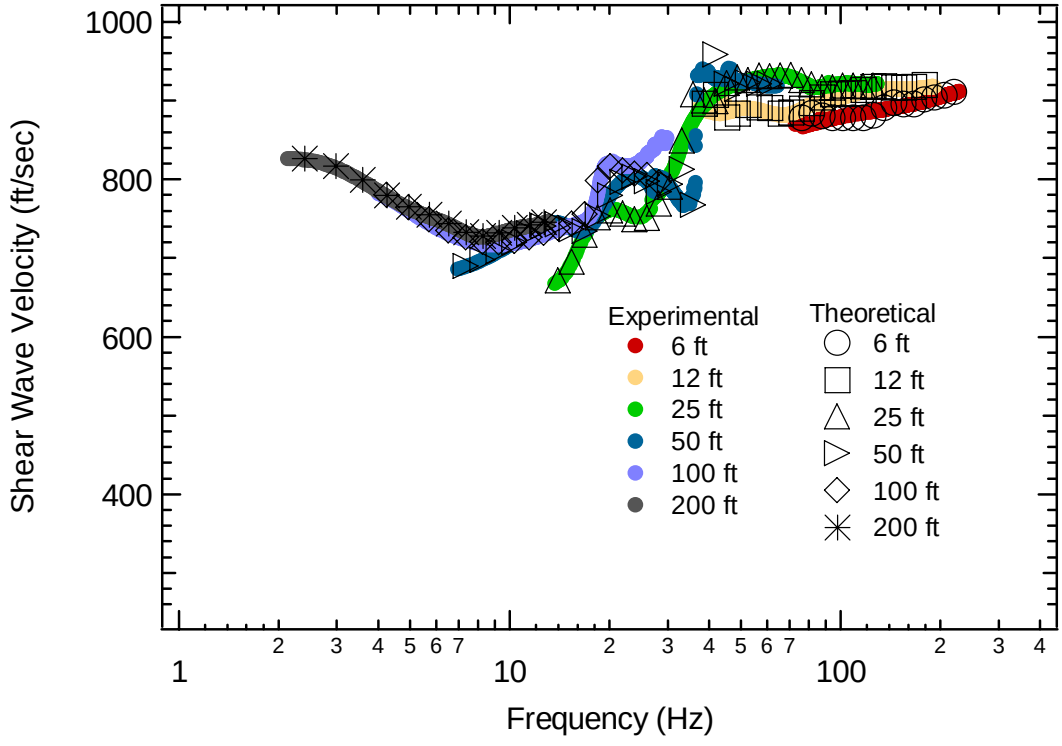

Figure 4-103 **Individual experimental and array theoretical dispersion curves plotted versus frequency for Profile 7a.**

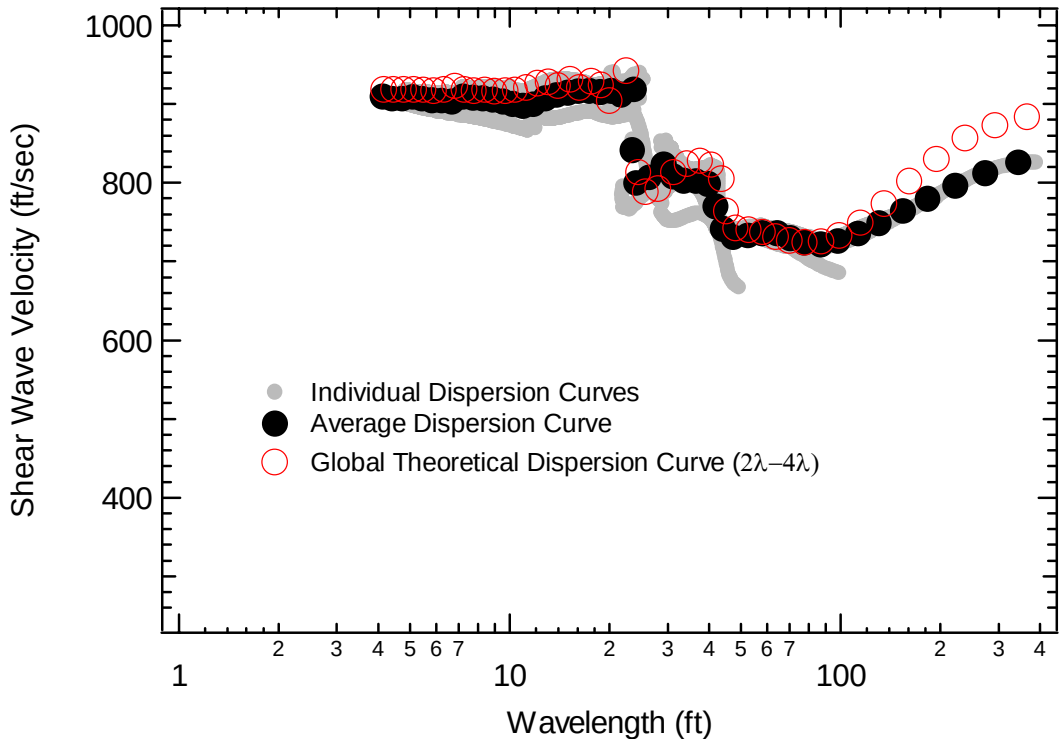

Figure 4-104 **Simulated experimental dispersion curves (individual and global average) versus global theoretical dispersion curve, plotted versus wavelength for Profile 7a.**

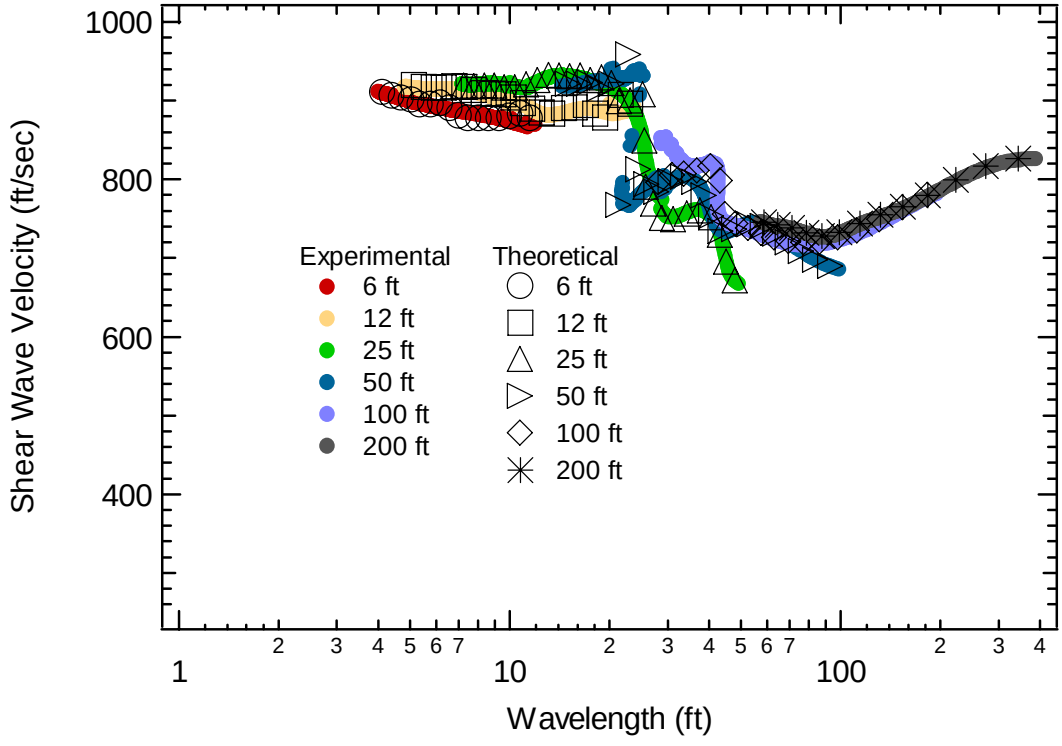

Figure 4-105 **Individual experimental and array theoretical dispersion curves plotted versus wavelength for Profile 7a.**

4.6.2 Profile 7b

Profile 7b is presented in Figure 4-106. Table 4-22 shows the individual layer characteristics for Profile 7b. Figures 4-107, 4-108, 4-109 and 4-110 show the simulated experimental and theoretical dispersion curves for this profile.

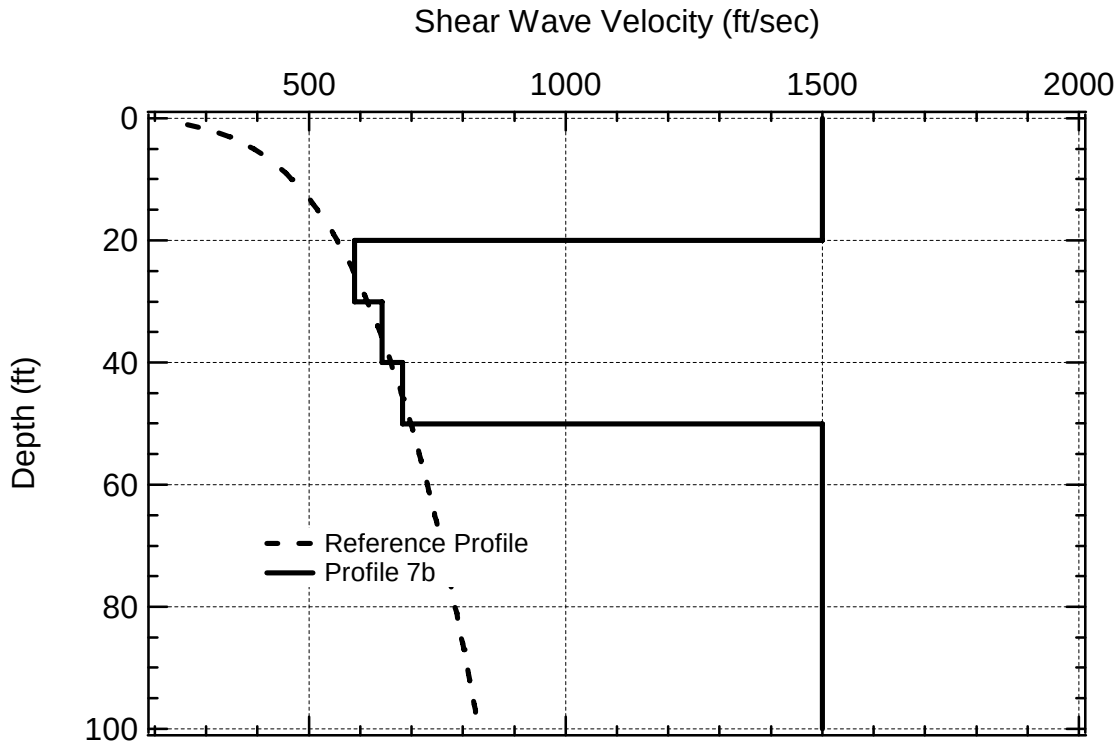

Figure 4-106 Profile 7b shown with the reference profile.

Table 4-22 Individual layer characteristics for Profile 7b.

Layer	Thickness (ft)	V_S (ft/sec)	ν	Unit Weight (pcf)
1	20	1500	0.25	120
2	10	589	0.25	120
3	10	643	0.25	120
4	10	683	0.25	120
5	Halfspace	1500	0.25	120

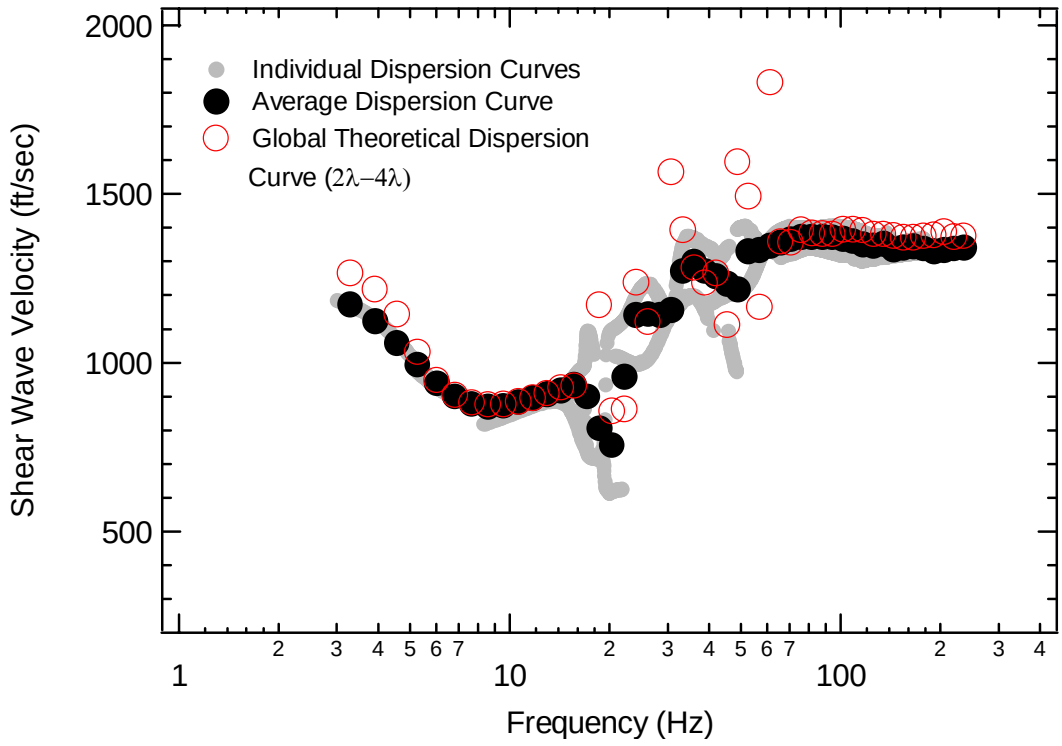

Figure 4-107 **Simulated experimental dispersion curves (individual and global average) versus global theoretical dispersion curve, plotted versus frequency for Profile 7b.**

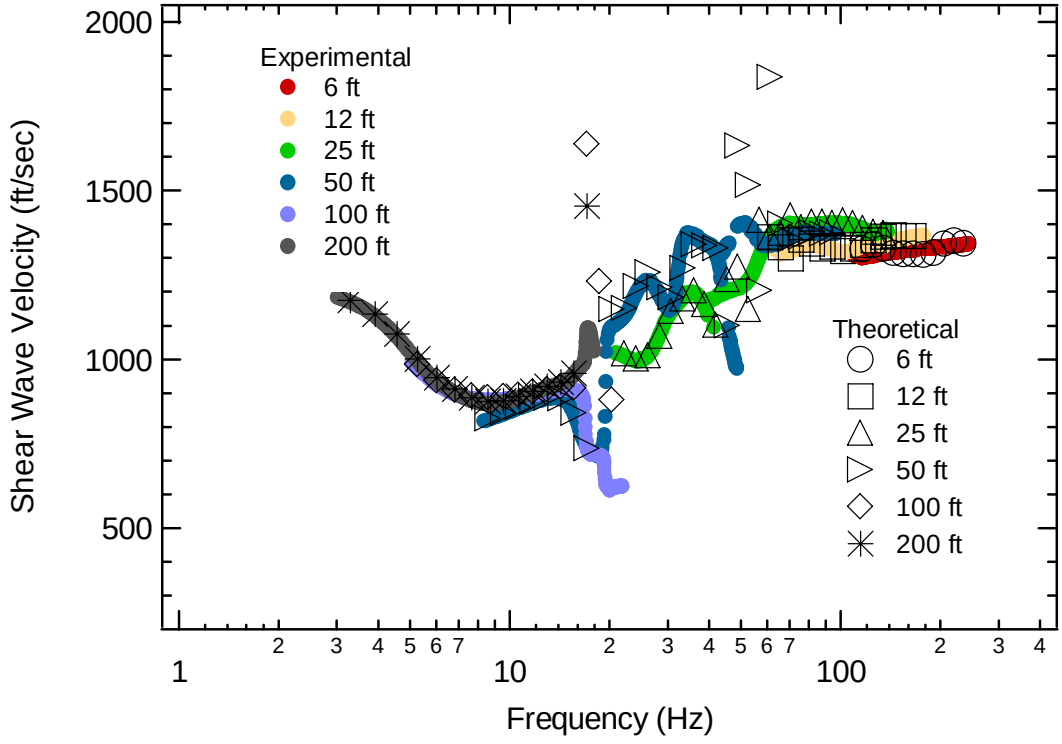

Figure 4-108 **Individual experimental and array theoretical dispersion curves plotted versus frequency for Profile 7b.**

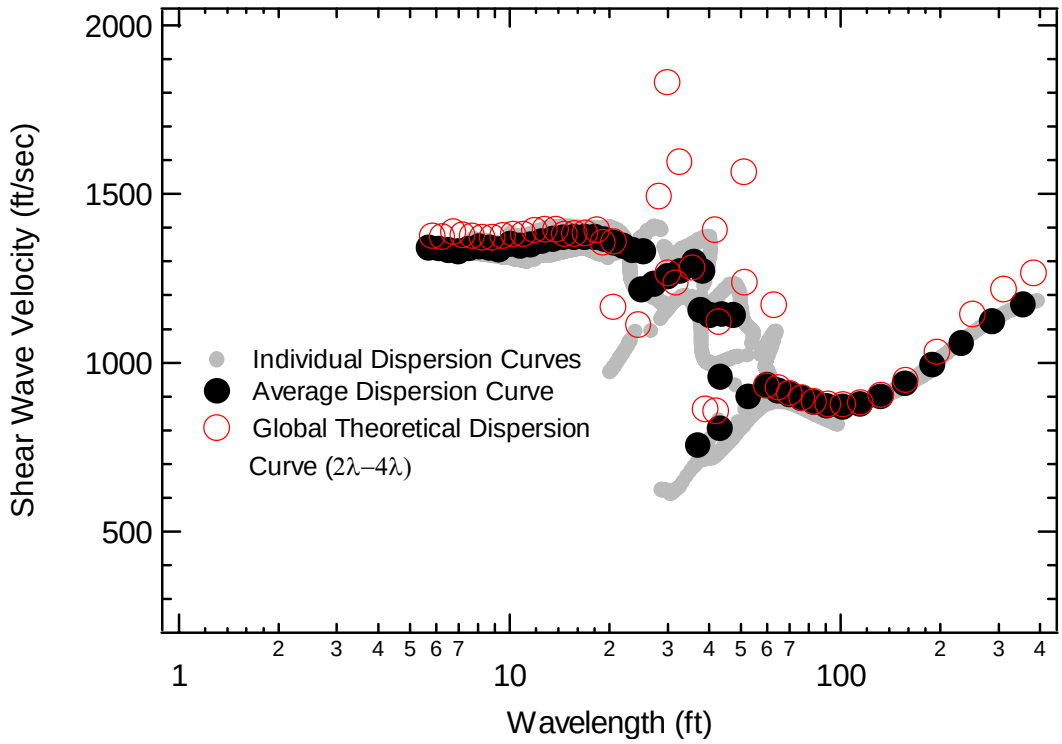

Figure 4-109 **Simulated experimental dispersion curves (individual and global average) versus global theoretical dispersion curve, plotted versus wavelength for Profile 7b.**

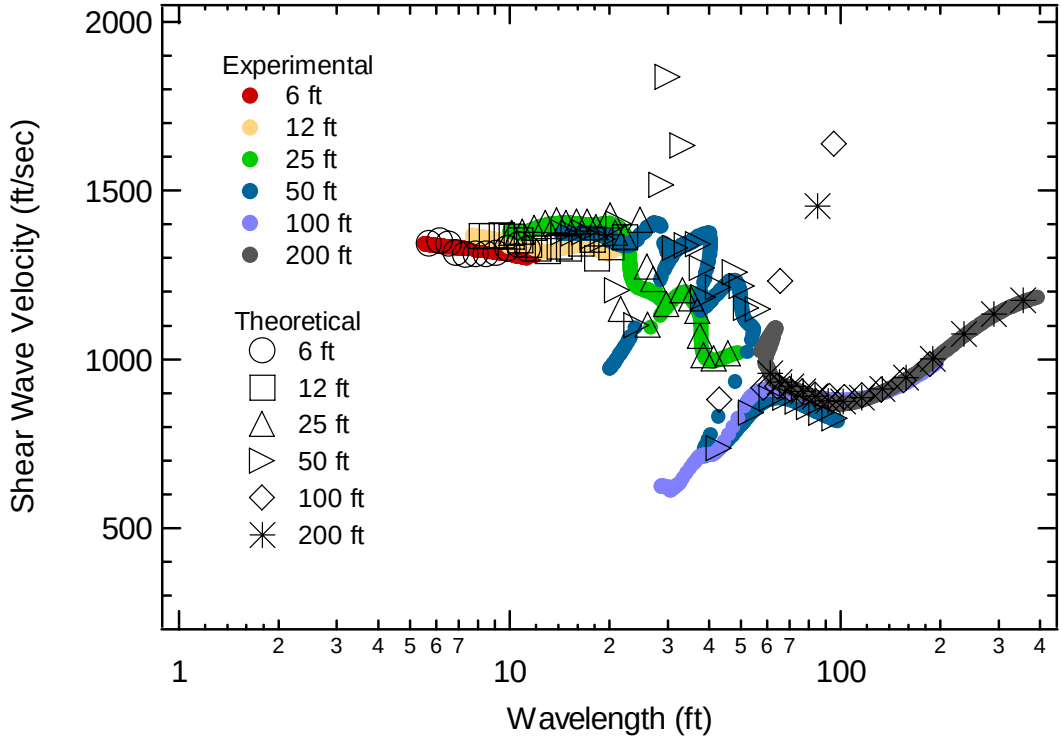

Figure 4-110 **Individual experimental and array theoretical dispersion curves plotted versus wavelength for Profile 7b.**

4.6.3 Profile 7c

Profile 7c is presented in Figure 4-111. Table 4-23 shows the individual layer characteristics for Profile 7c. Figures 4-112, 4-113, 4-114 and 4-115 show the simulated experimental and theoretical dispersion curves for this profile.

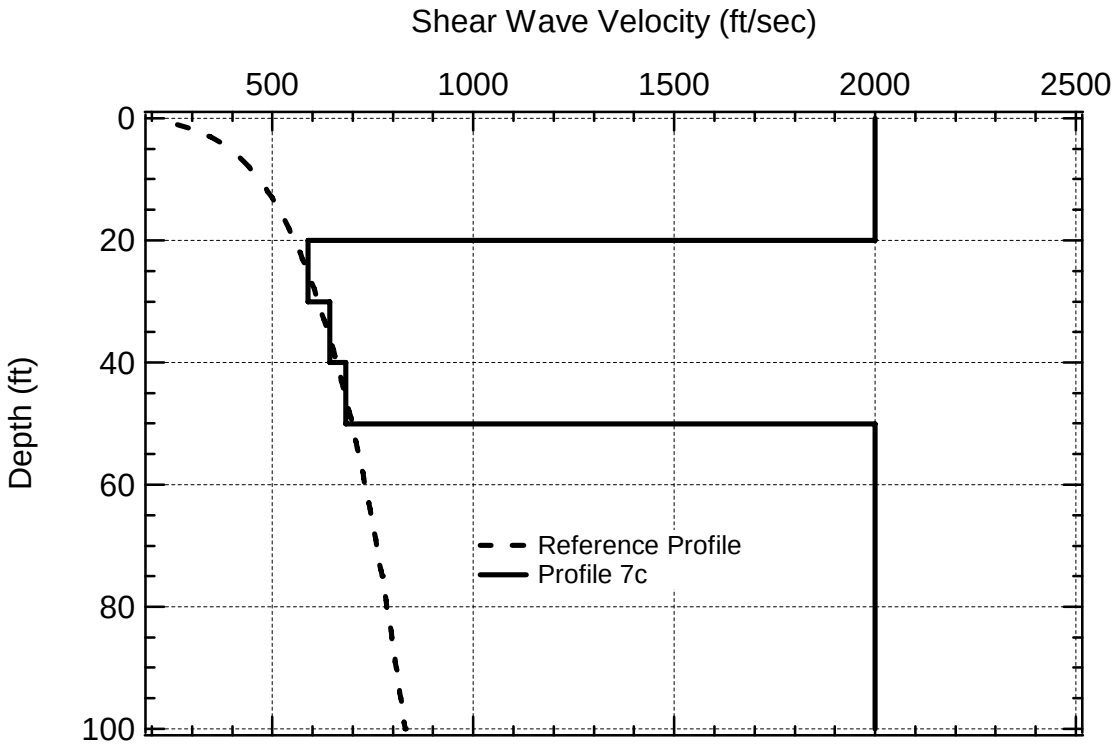

Figure 4-111 Profile 7c shown with the reference profile.

Table 4-23 Individual layer characteristics for Profile 7c.

Layer	Thickness (ft)	V_S (ft/sec)	ν	Unit Weight (pcf)
1	20	2000	0.25	120
2	10	589	0.25	120
3	10	643	0.25	120
4	10	683	0.25	120
5	Halfspace	2000	0.25	120

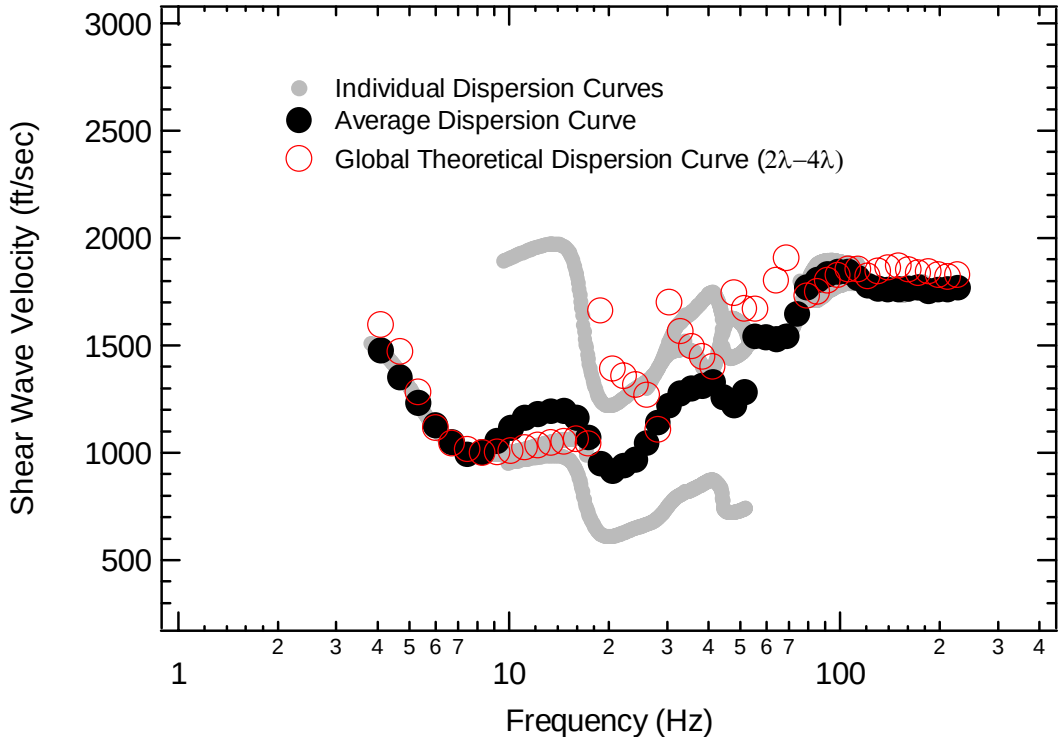

Figure 4-112 **Simulated experimental dispersion curves (individual and global average) versus global theoretical dispersion curve, plotted versus frequency for Profile 7c.**

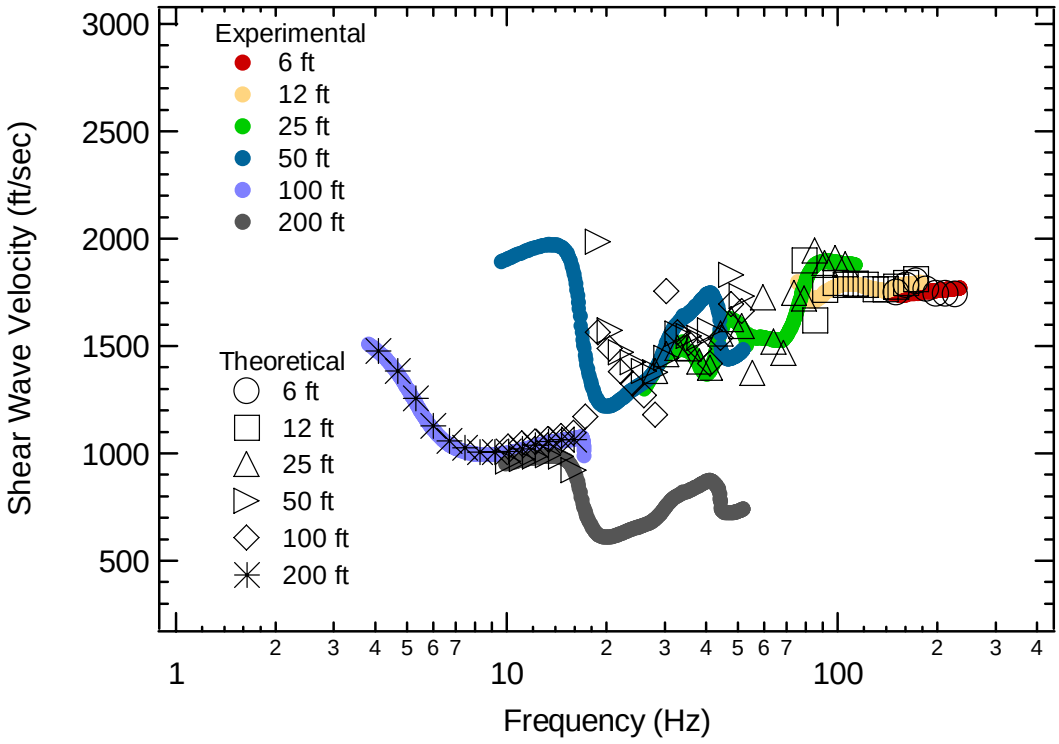

Figure 4-113 **Individual experimental and array theoretical dispersion curves plotted versus frequency for Profile 7c.**

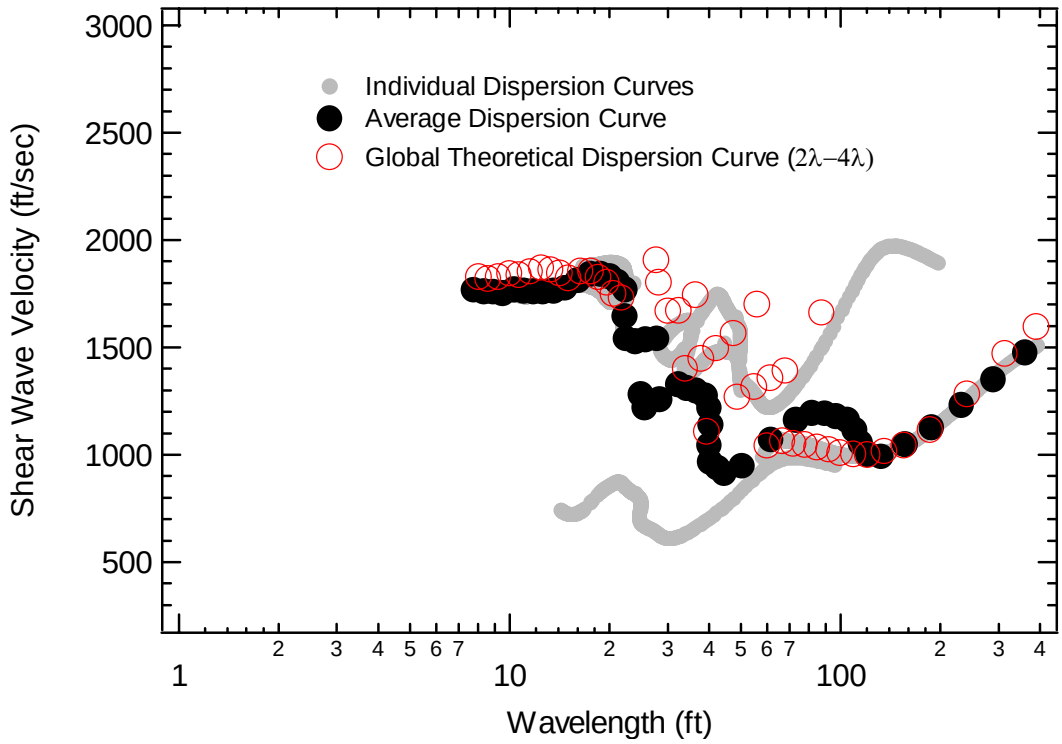

Figure 4-114 **Simulated experimental dispersion curves (individual and global average) versus global theoretical dispersion curve, plotted versus wavelength for Profile 7c.**

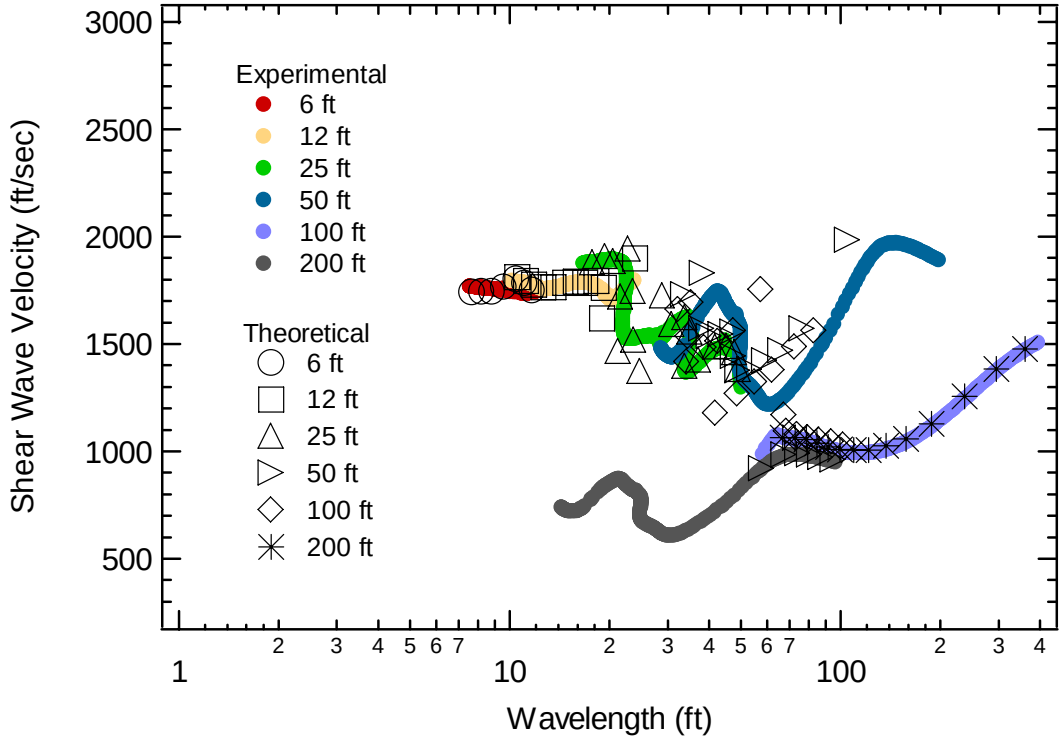

Figure 4-115 **Individual experimental and array theoretical dispersion curves plotted versus wavelength for Profile 7c.**

Chapter 5 Discussion and Analysis

5.1 Introduction

In this chapter the results presented in Chapter 4 for the simulated global and array analysis of the V_S profiles are discussed and analyzed. The chapter is divided into separate sections for each of the general soil profile conditions that were simulated, starting with the reference profile from which the other 22 profiles were generated. The influence of changes in profile conditions such as layer stiffness and depth on the global and array analysis is discussed. Modal dispersion curves are presented for some of the cases to assist in understanding the trends observed in the simulated effective dispersion curves. In addition, the influence of changes in Poisson's ratio on the results of this study is presented and discussed. Lastly, the practical implications of the findings from this study are discussed.

5.2 Reference Profile

The results from the SASW simulations for the reference profile can be found in Section 4.2, of Chapter 4. The effectiveness of the global and array analysis for this profile is discussed below.

Global Analysis:

The results from the simulation of the reference profile show that over most of the frequency or wavelength range of interest the simulated dispersion curve follows a consistent trend. Figure 5.1 presents a comparison of the average dispersion curve generated from the simulated data, the global

theoretical dispersion curve, and the first three modal dispersion curves for this site. In this case, the theoretical effective phase velocity (global theoretical dispersion curve) follows the fundamental mode over the wavelength range of interest. The average global experimental dispersion follows this same trend over much of the wavelength range, but deviates by as much as 15% from the trend at long wavelengths.

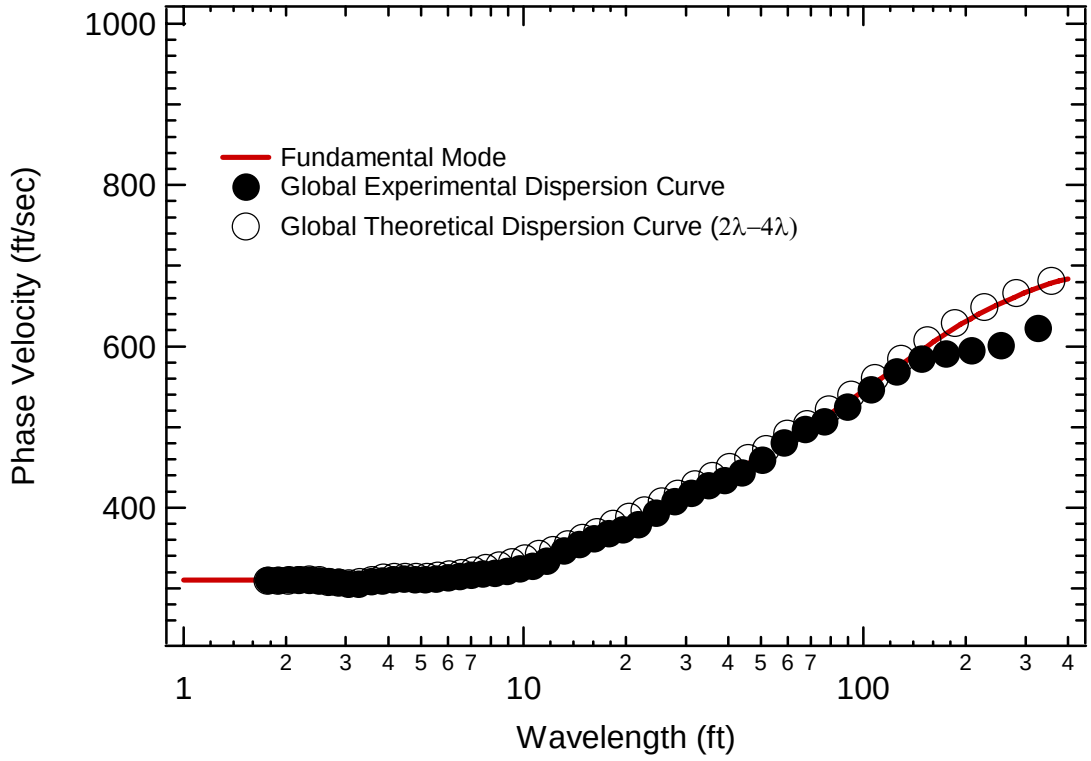

Figure 5-1 **Modal dispersion curve shown with the global experimental and theoretical dispersion curves for the reference profile.**

This deviation can be attributed to near-field effects. The theoretical global dispersion curve was calculated at 2λ and 4 λ from the source for every frequency. At these distances from the source, the cylindrically spreading wavefront begins to behave more like a plane wave. The experimental dispersion curve, on the other hand, was generated from receiver locations as

close as 0.5λ to the source. This near field effect is minimized where data from adjacent receiver spacings overlap, because the near-field portion of the longer spacing is averaged with the far-field portion of the closer spacing. At the longest receiver spacing, however, the effect is significant. In practice, it is often not possible to obtain good quality data at long wavelengths where receivers are located at least 2λ from the source. The ultimate effect of this inconsistency in that the final V_S profile will predict a halfspace velocity that is lower than the true velocity.

Array Analysis:

To overcome this inconsistency between the global experimental and theoretical dispersion curves, the array analysis uses the actual receiver locations to generate dispersion curves for each of the receiver pairs. The array analysis for the reference profile yielded results that are in perfect agreement between the theoretically calculated dispersion curves and the experimentally determined dispersion curves, as shown in Figure 5-2. This is expected, because the theoretical solution models a cylindrically spreading wave at the same spatial locations it is recorded at in the field. The near-field problem observed in the global analysis is, therefore, not an issue in this analysis.

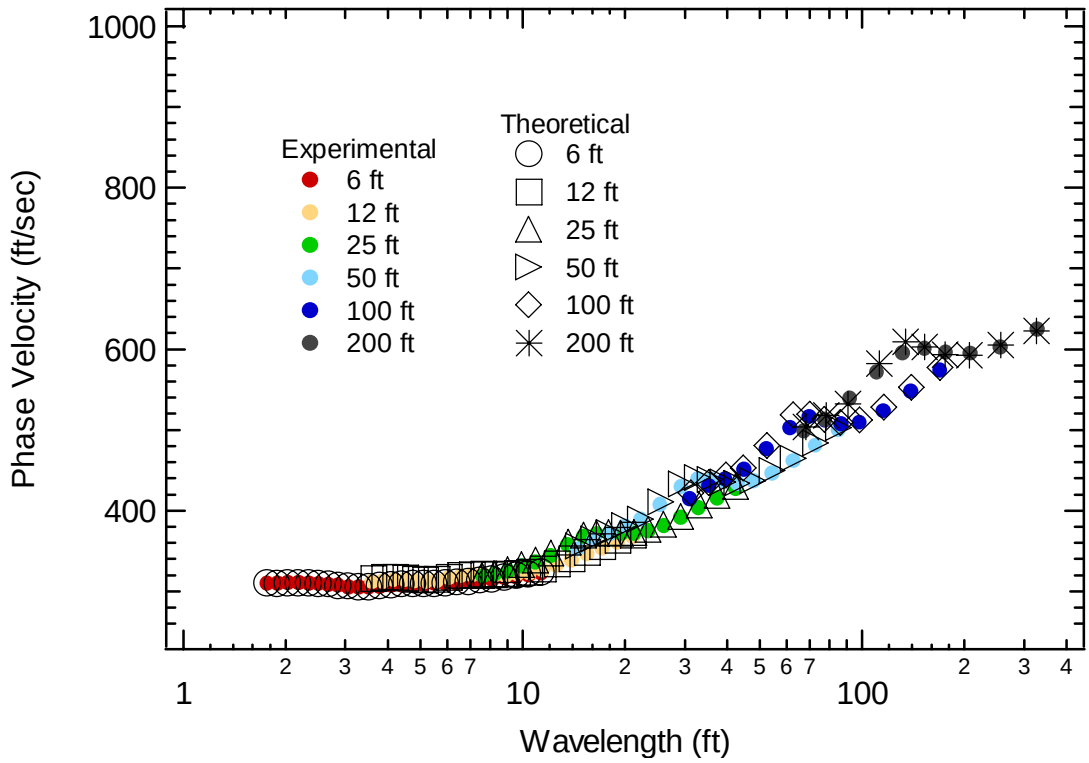

Figure 5-2 **Experimental and theoretical dispersion curves from the array analysis generated for the reference profile.**

5.3 Soft-over-Stiff Profiles

All of the results from simulations of the soft-over-stiff profiles can be found in Section 4.3, of Chapter 4. The effectiveness of the global and array approaches is discussed below. Surprisingly, this profile condition was the most problematic for both global and array analysis and is, therefore, analyzed and discussed in greater detail in Section 5-7.

Global Analysis:

The effectiveness of the global analysis of the soft-over-stiff condition was highly dependent on the contrast between the surface layers and the stiffer halfspace. For Profile 1a, the results from the global analysis are quite similar to

the reference profile case, with good agreement over most of the wavelength range, but deviations at the longest wavelengths, as shown in Figure 5-3. The individual dispersion curves do not overlap as well as in the reference profile case (as shown in the wavelength range of 30 to 100 ft in Figure 4-9) but the average dispersion curve is still consistent with the 2λ-4 λ global curve (except at the longest wavelengths). This behavior is also evident for Profiles 2a (Figures 4-22 and 4-24) and Profile 2b (Figures 4-27 and 4-29). As in the case of the reference profile, the impact of the use of a global analysis would be an underprediction of the halfspace velocity.

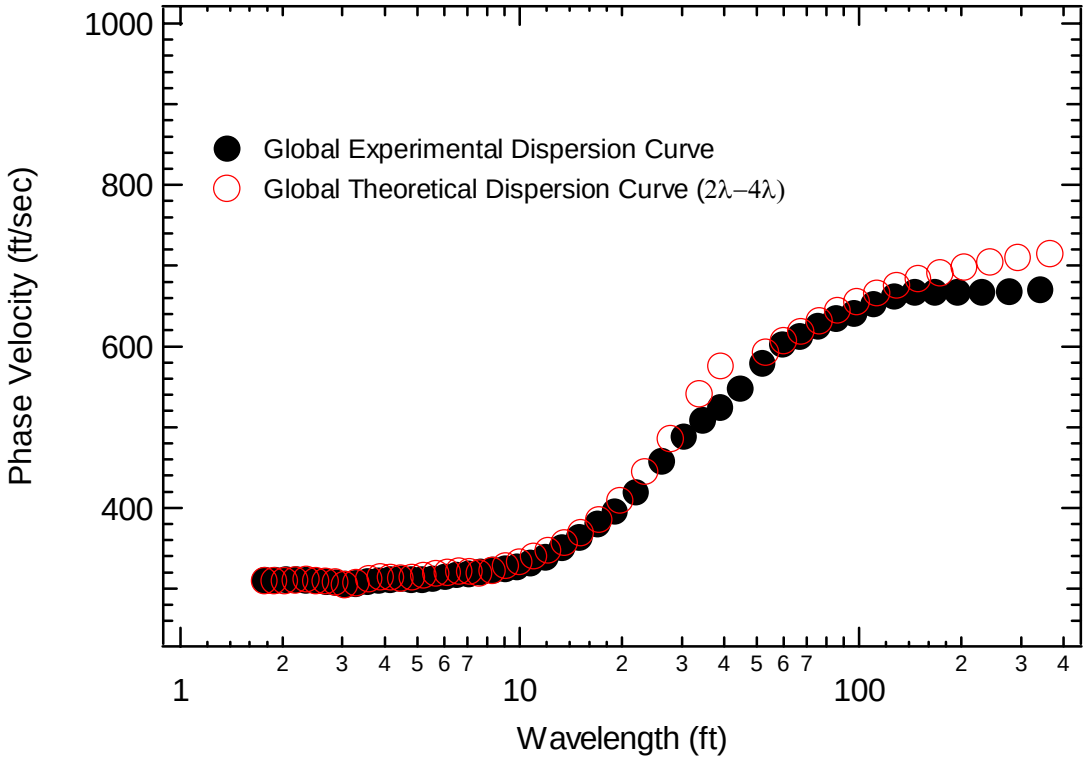

Figure 5-3 Global experimental and theoretical dispersion curves for Profile 1a.

As the halfspace velocity increased in the simulations (Profiles 1b and 1c, and Profiles 2c and 2d) the deviations between the individual dispersion curves

become greater, and the theoretical curve was significantly different than the average curve over much of the wavelength range, as shown, for example, in Figure 5-4 for Profile 2c. Additional figures displaying similar behavior for Profiles 1b (Figure 4-12), 1c (Figure 4-17), and 2d (Figures 4-37 and 4-39) are presented in Chapter 4. In these cases, the effectiveness of the global approach is clearly limited due to the gross inconsistencies between the experimental and theoretical dispersion curves.

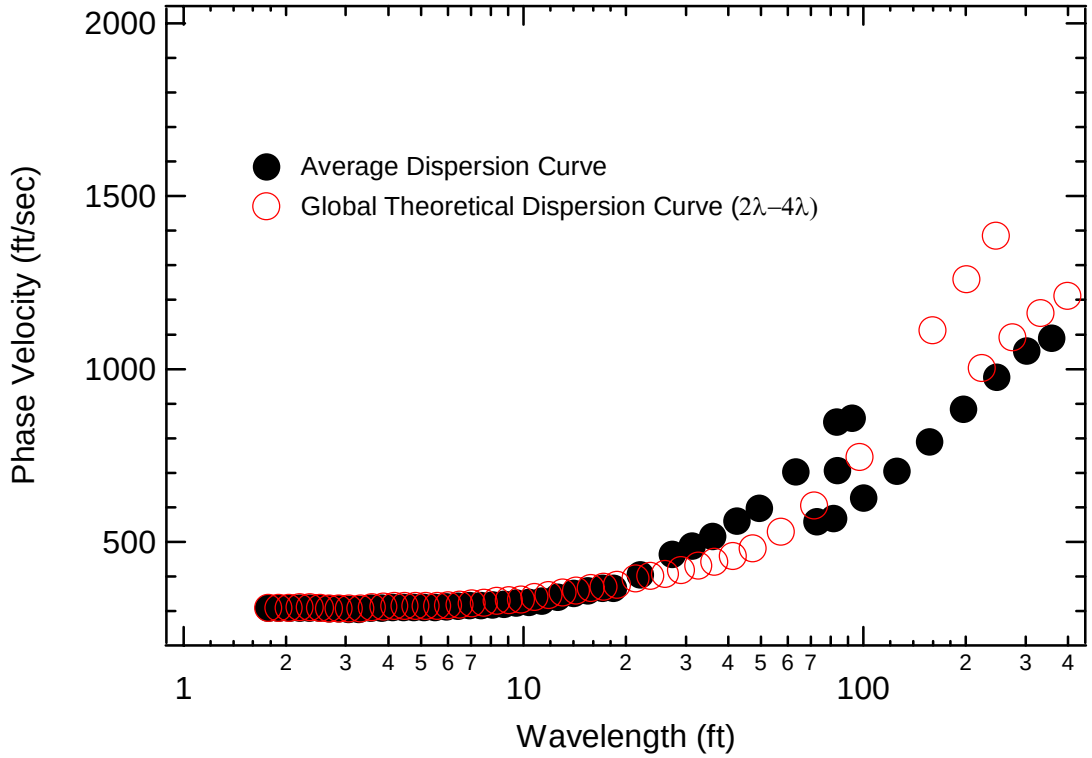

Figure 5-4 Global experimental and theoretical dispersion curve for Profile 2c.

Array Analysis:

It was surprising to discover that the array approach, which models the experimental set-up, can produce erroneous results in some cases. For the soft-over-stiff condition, the experimental and theoretical array results are consistent

when the halfspace velocity is low (Profile 1a, 2a and 2b). Figure 5-5 shows a comparison between the average experimental and array theoretical dispersion curves for Profile 1a. This pattern of behavior can also be recognized in Figures 4-23, 4-25, 4-28 and 4-29 for Profile 2a and 2b.

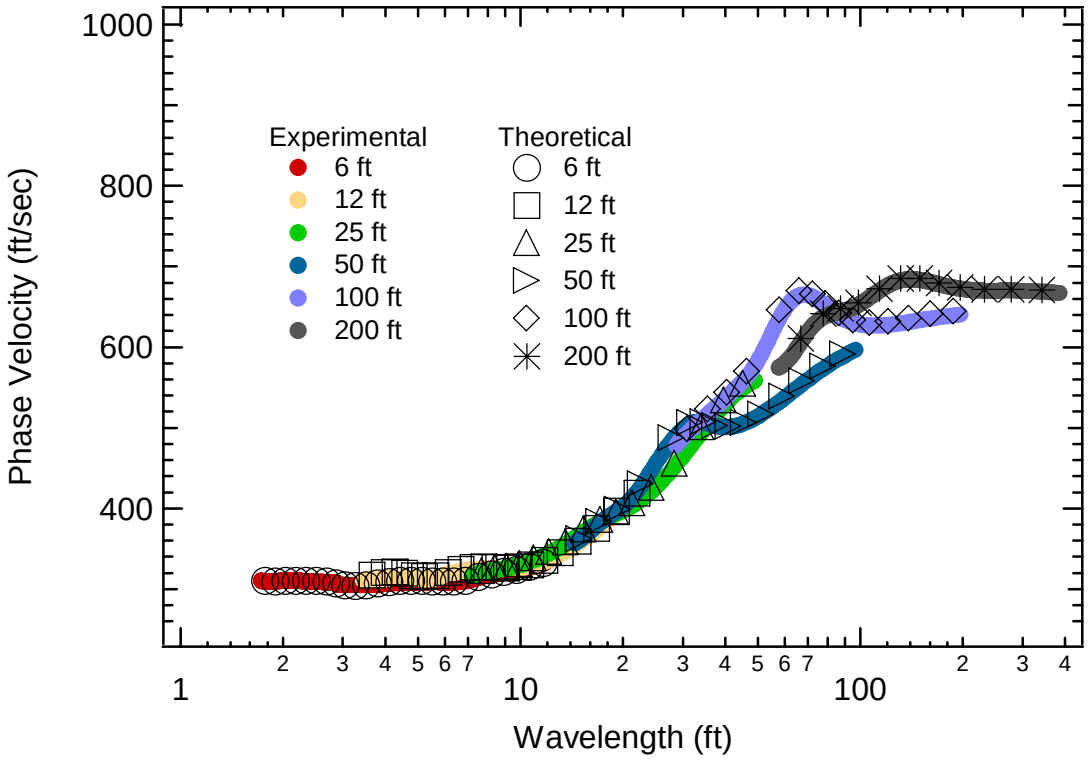

Figure 5-5 Array experimental and theoretical dispersion curves for Profile 1a.

As the halfspace velocity was increased, the model results show differences between the simulated experimental dispersion curves and the theoretical dispersion curves. The differences become more pronounced as the halfspace velocity increases. An example of this is shown in Figure 5-6 for Profile 1c and Figure 5-7 for Profile 2c. Similar results were found for Profile 1b (Figures 4-13 and 4-15) and Profile 2d (Figures 4-38 and 4-40). These results indicate a problem with the phase unwrapping procedures used in SASW testing.

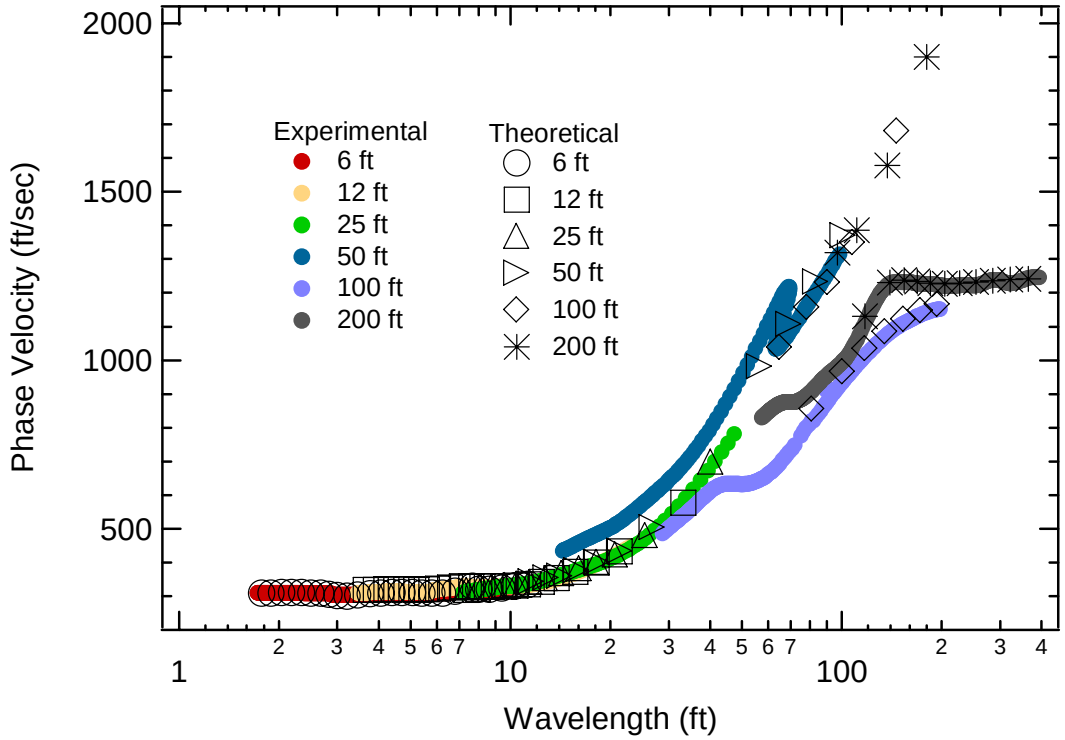

Figure 5-6 **Array experimental and theoretical dispersion curves for Profile 1c.**

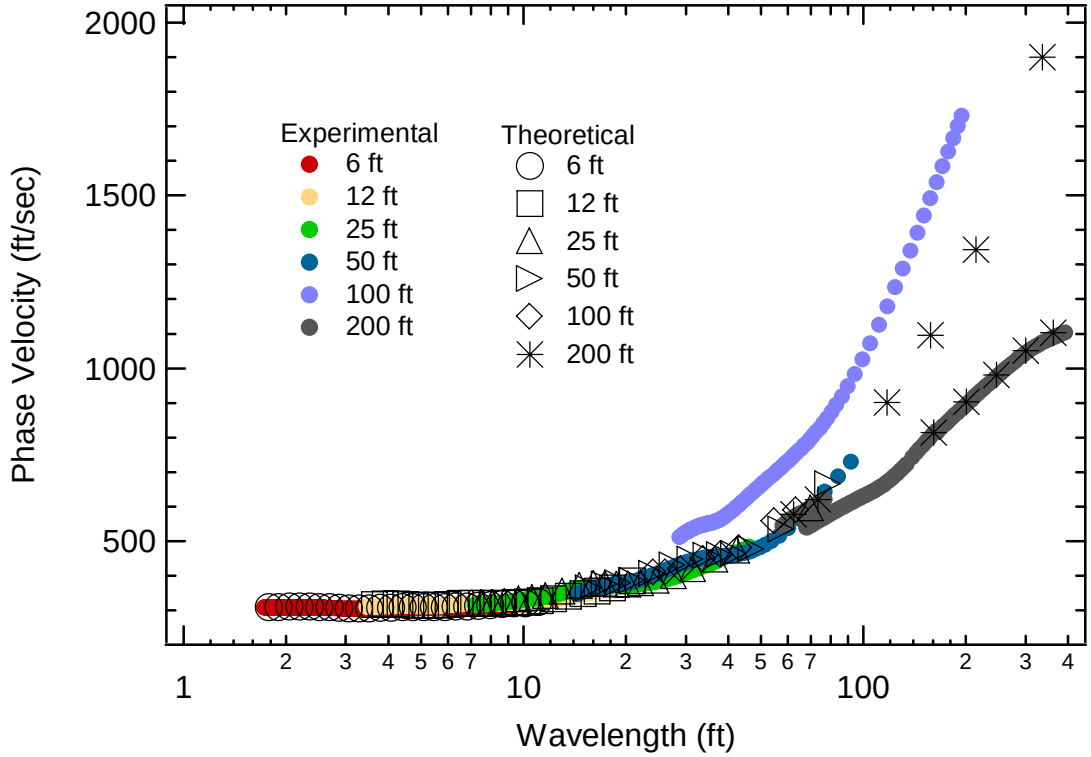

Figure 5-7 **Array experimental and theoretical dispersion curves for Profile 2c.**

It is interesting to compare the effective dispersion curve to the modal dispersion curves for these cases. For example, Figure 5-8 presents the modal and effective dispersion curves for Profile 1c. In this case, the effective dispersion curve follows the fundamental mode at short and long wavelengths, but unlike the reference profile case, the effective velocity dispersion curve abruptly transitions to the second mode over an intermediate wavelength range and then returns to the fundamental mode at longer wavelengths. The effect of this phenomenon on the experimental dispersion curves is discussed in greater detail in Section 5.7.

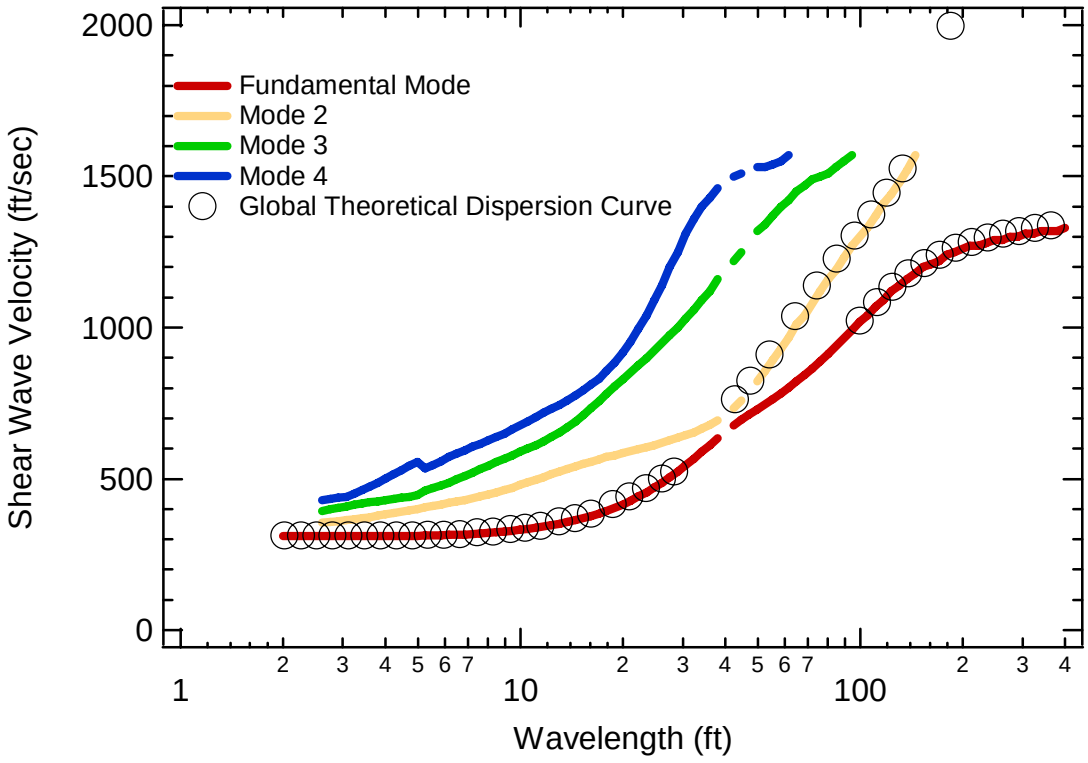

Figure 5-8 **Modal dispersion curves and global theoretical dispersion curves for Profile 1c.**

5.4 Stiff-over-Soft

All of the results of the stiff-over-soft profiles can be found in Section 4.4 of Chapter 4. The effectiveness of the global and array approach for this profile condition is discussed below.

Global Analysis:

The global approach was effective for most of the stiff-over-soft profiles that were simulated. The analysis works best when the contrast between the stiffness of the surface layer and the soft layer is low (Profile 3a and 4a). However, even when the contrast is large there is general consistency between the global experimental and theoretical dispersion curves (Profiles 3c and 4c). Figures 5-9 and 5-10 present comparisons between the global theoretical and experimental dispersion curves for Profiles 3a and 3c, respectively. For these cases, the average experimental curve follows the global theoretical curve with some scatter evident. As in the reference profile case, at long wavelengths, the global theoretical solution is greater than the average experimental curve. In general, as the velocity of the surface layer increases, the deviations between the experimental and theoretical curves become more pronounced over a greater range of wavelengths. Based on these results it appears that the global SASW approach can provide realistic results at sites with stiff layers over softer layers .

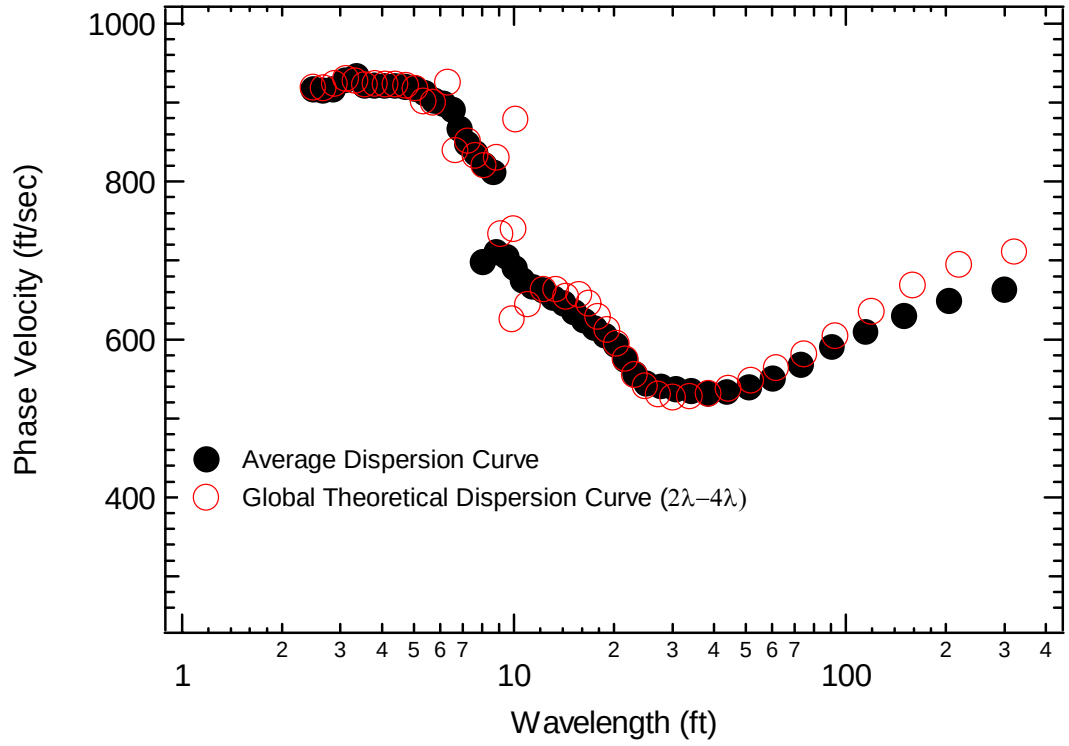

Figure 5-9 Global theoretical and experimental dispersion curve for Profile 3a.

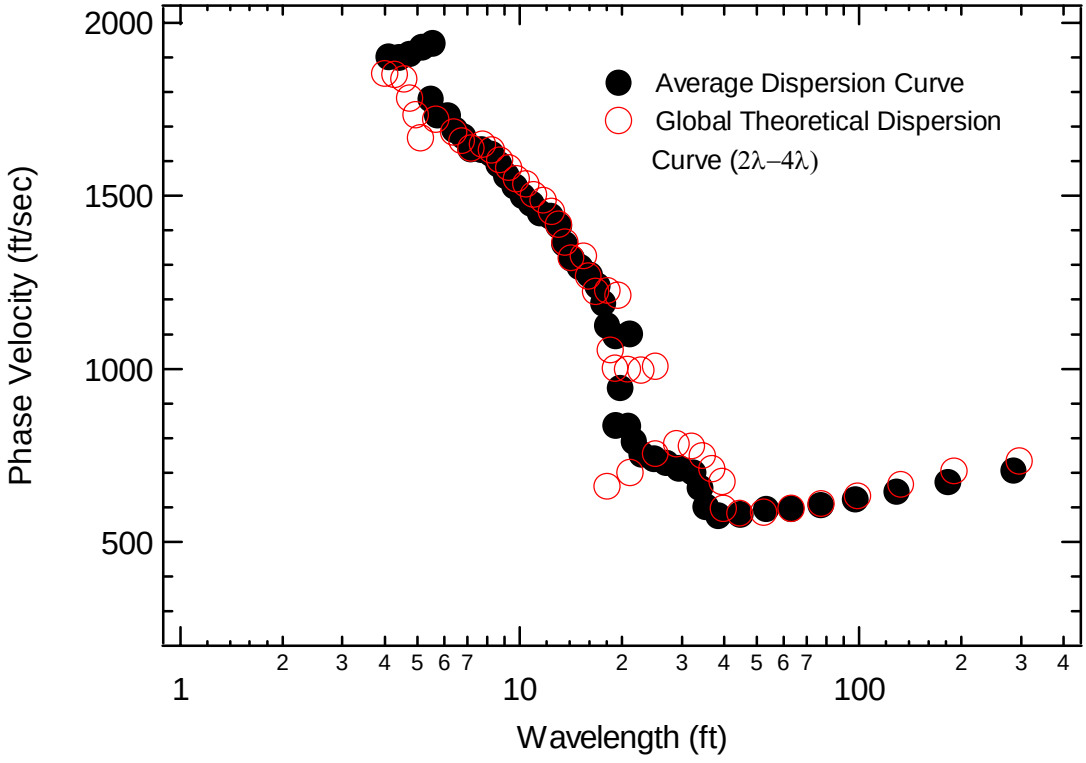

Figure 5-10 Global theoretical and experimental dispersion curve for Profile 3c.

Array Analysis:

For nearly all stiff-over-soft cases that were simulated, the individual and the array theoretical dispersion curves agree very well. The exceptions are the 25-ft spacing for Profile 3b and the 100-ft spacing for Profile 4c. Figures 5-11 and 5-12 are plots of the experimental and theoretical dispersion curves for Profiles 3b and 4c, respectively. Portions of the experimental dispersion curves are not consistent with the theoretical curves and deviated significantly from the general trend of the data. As in the soft-over-stiff case, this indicates a problem with the phase unwrapping procedures used in the SASW method. In these cases, most of the receiver spacings yielded consistent results, so the impact is minimal.

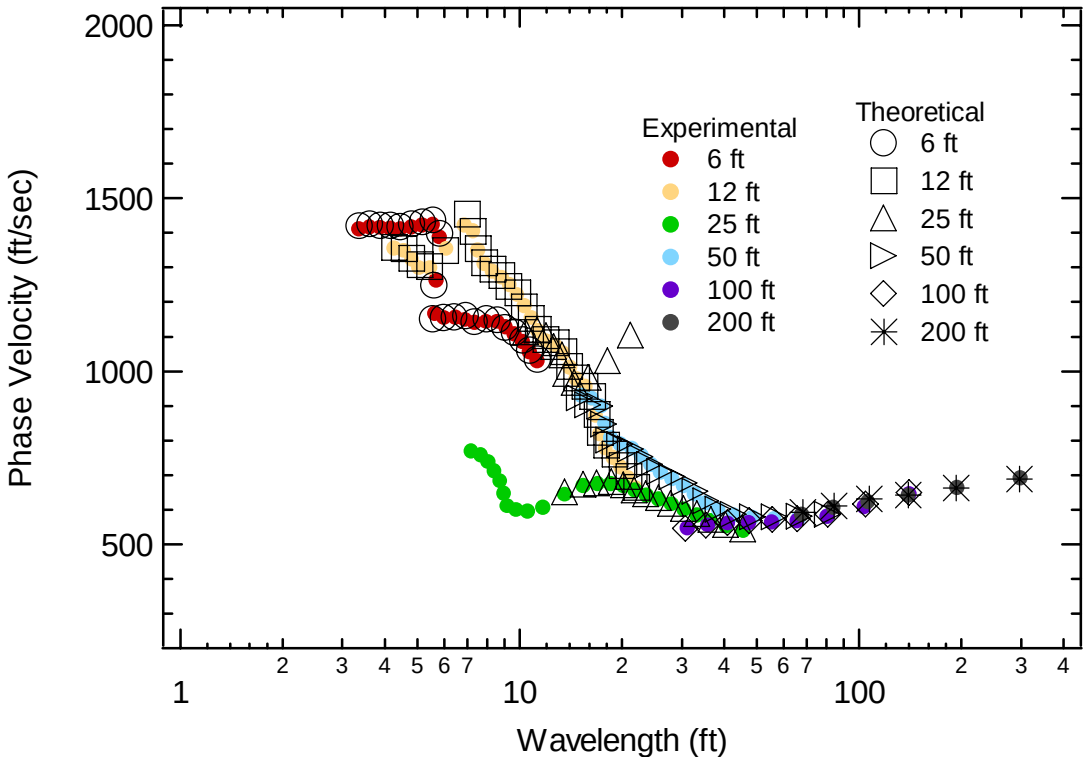

Figure 5-11 Array experimental and theoretical dispersion curves for Profile 3b.

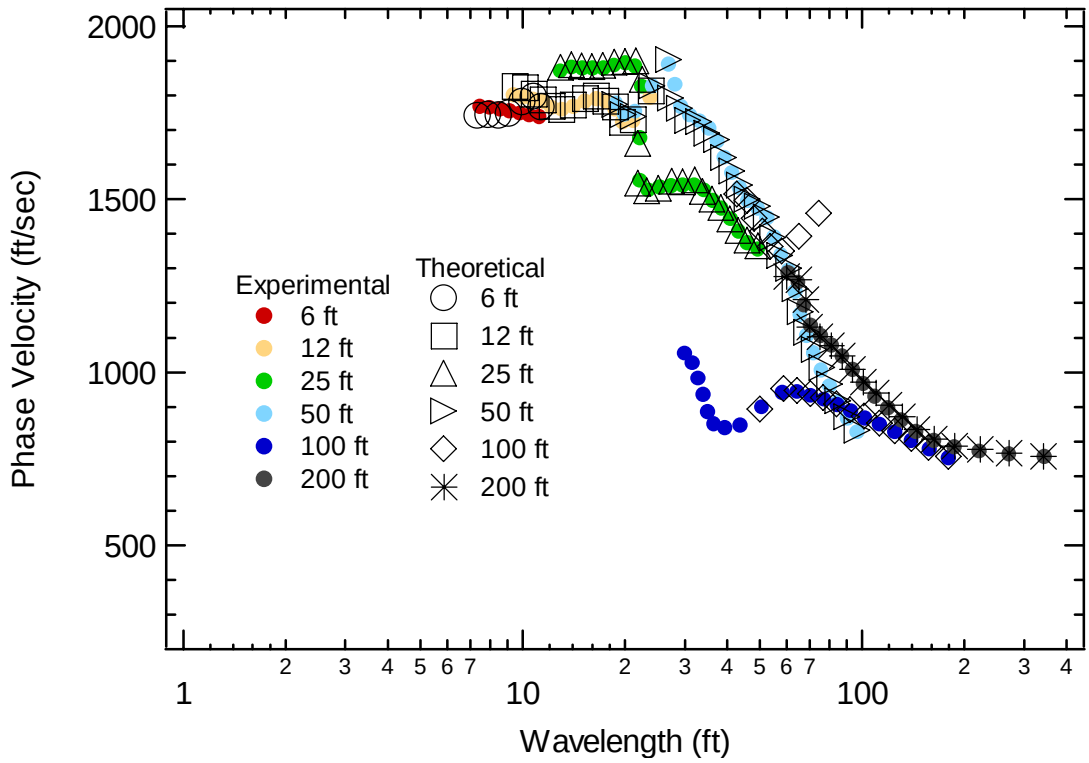

Figure 5-12 Array experimental and theoretical dispersion curves for Profile 4c.

It is interesting to compare the modal dispersion curves for this profile condition to the effective velocity (global) dispersion curve. Figure 5-13 presents the modal and effective dispersion curves for Profile 3a. In this case, it is clear that the effective dispersion curve follows the fundamental mode up to a frequency of approximately 20 Hz. Above this frequency the effective velocity dispersion curve does not follow a single mode but follows a continuous curve that is a superposition of modes. In this case, use of a fundamental mode solution would not provide the correct theoretical dispersion curve.

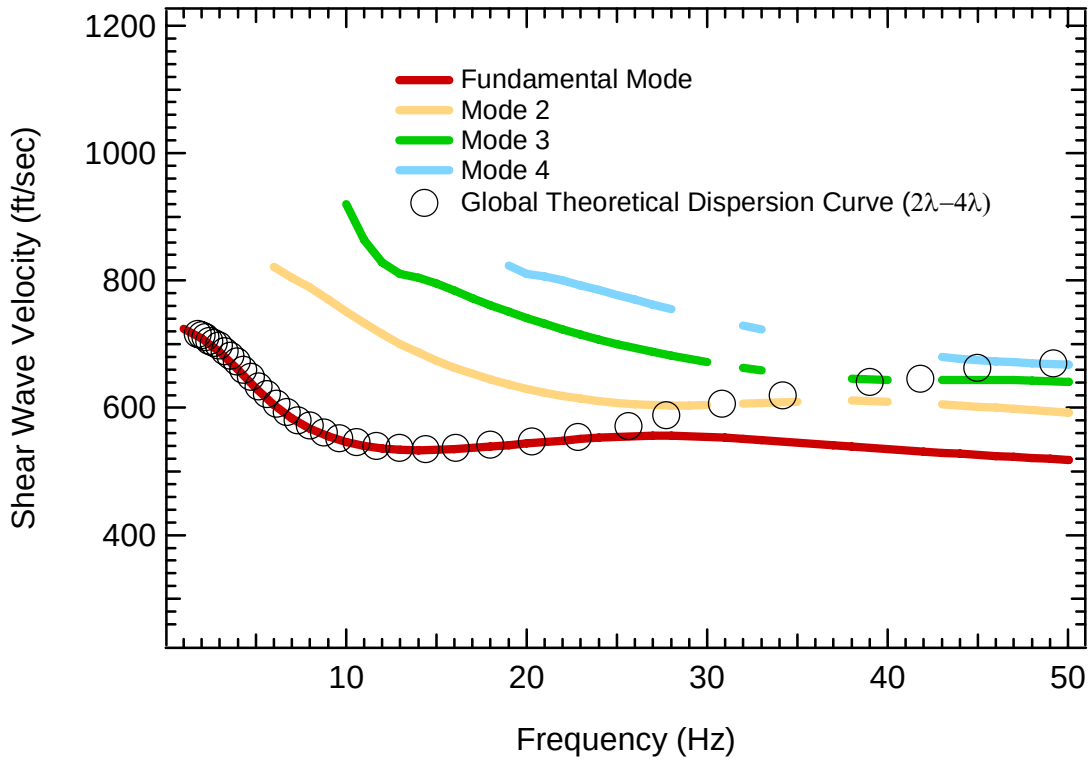

Figure 5-13 **Modal dispersion curve with the global theoretical dispersion curve for Profile 3a.**

5.5 Profiles with a Embedded Stiff Layer

All of the results of the embedded-stiff-layer profiles can be found in Section 4.5 of Chapter 4. The effectiveness of the global and array approach for this profile condition is discussed below.

Global Analysis:

The results of the global analysis of the profiles with an embedded stiff layer show good agreement between the average and theoretical dispersion curves. For example, the dispersion curves resulting from a global analysis of Profile 6c are shown in Figure 5-14. Although this profile includes a 20-ft thick

layer with a V_S of over three times the average profile $V_{S,}$ the experimental and theoretical dispersion data are in good agreement. For most of these cases, at long wavelengths the global theoretical dispersion curve tends to deviate from the experimental dispersion curves in a manner consistent with what was observed for the reference profile. Increasing the values of velocity and thickness of the embedded stiff layer had little effect on the agreement between the experimental and theoretical solutions. The results indicate that the conventional global SASW approach can deal effectively with an embedded stiff layer. It should be noted that this study did not examine the ability to resolve the size or stiffness of the layer, only the consistency between the measured experimental dispersion curve and the global theoretical solution.

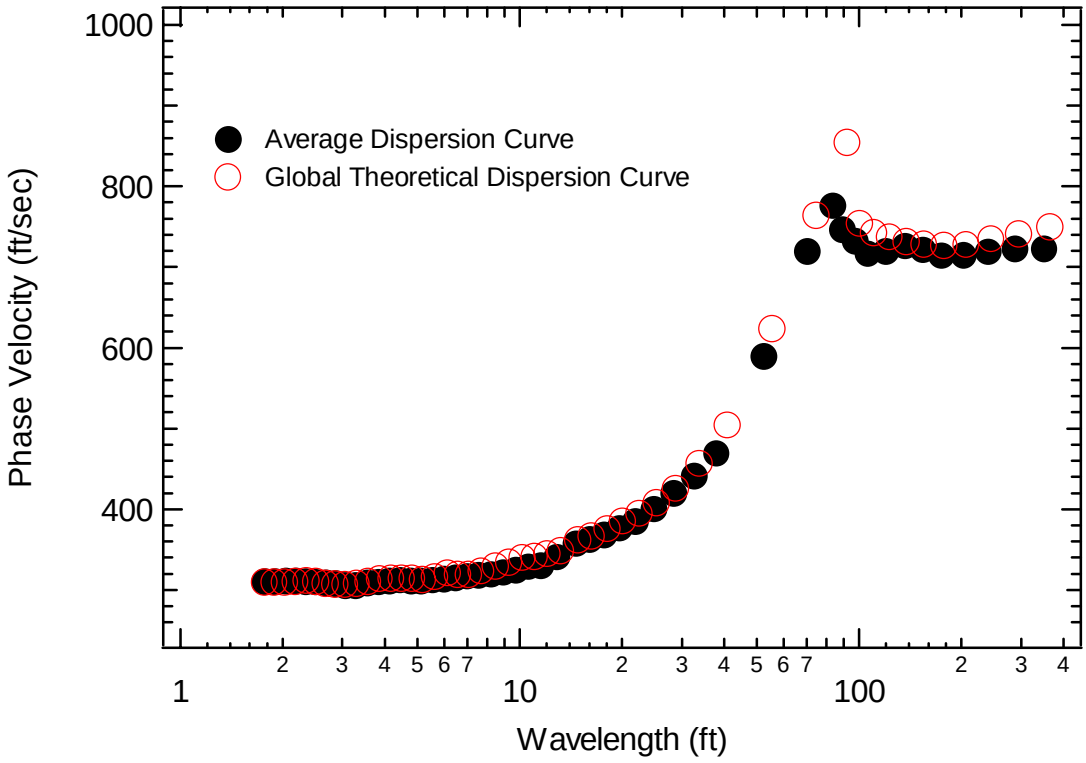

Figure 5-14 Global experimental and theoretical dispersion curve for Profile 6c.

Array Analysis:

The array analysis performed on profiles with embedded stiff layers yielded experimental dispersion curves that are in very good agreement with the theoretical dispersion curves. It is interesting to note that the non-overlapping segments of the dispersion curve observed in Figure 4-93, for example, are consistent with the theoretical solution. Figure 5-15 shows the consistency between the experimental and theoretical dispersion curves for Profile 6c.

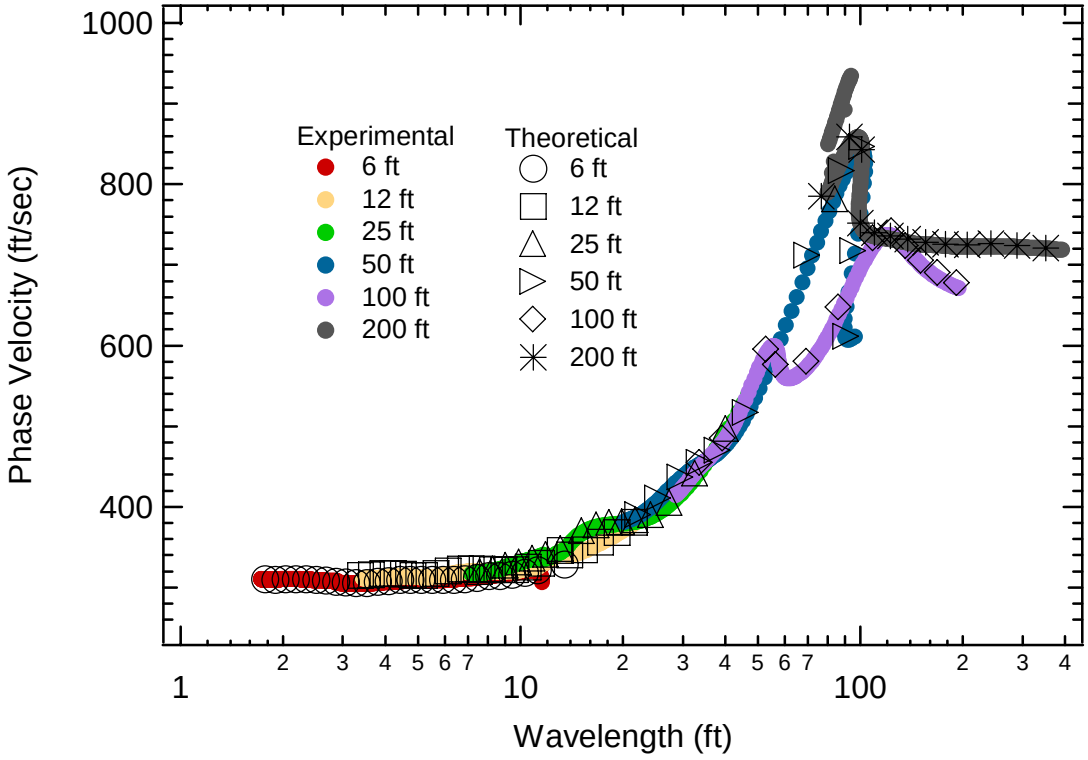

Figure 5-15 Array experimental and theoretical dispersion curve for Profile 6c.

5.6 Profiles with an Embedded Soft Layer

All of the results of the embedded-soft-layer profiles can be found in Section 4.6 of Chapter 4. The effectiveness of the global and array approach for this profile condition is discussed below.

Global Analysis:

For Profile 7a, the global analysis results are consistent with the average individual dispersion curves, as shown in Figure 5-16. As the velocity values of the stiff layers were increased (Profile 7c, for example), the theoretical solution scattered significantly beginning at wavelengths approximately equal to the surface layer thickness, as is shown in Figure 5-17. These results indicate that a global analysis will not be effective where very large stiffness contrasts are present. The wavelength range where the average experimental dispersion curve deviates from a smooth trend (20 to 50 ft) is the same depth range of the soft velocity layer. Additional figures regarding the global analysis of Profile 7a (4-102 and 4-104), 7b (4-107 and 4-109) and 7c (4-112 and 4-114) are shown in Chapter 4.

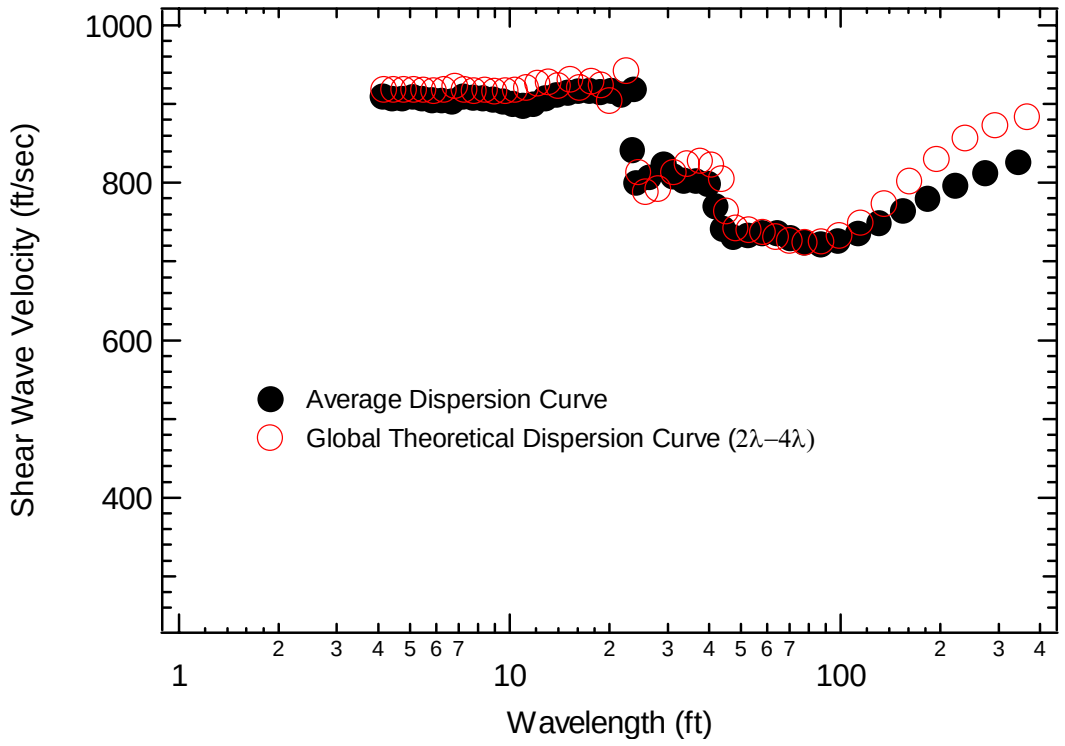

Figure 5-16 **Global experimental and theoretical dispersion curves for Profile 7a.**

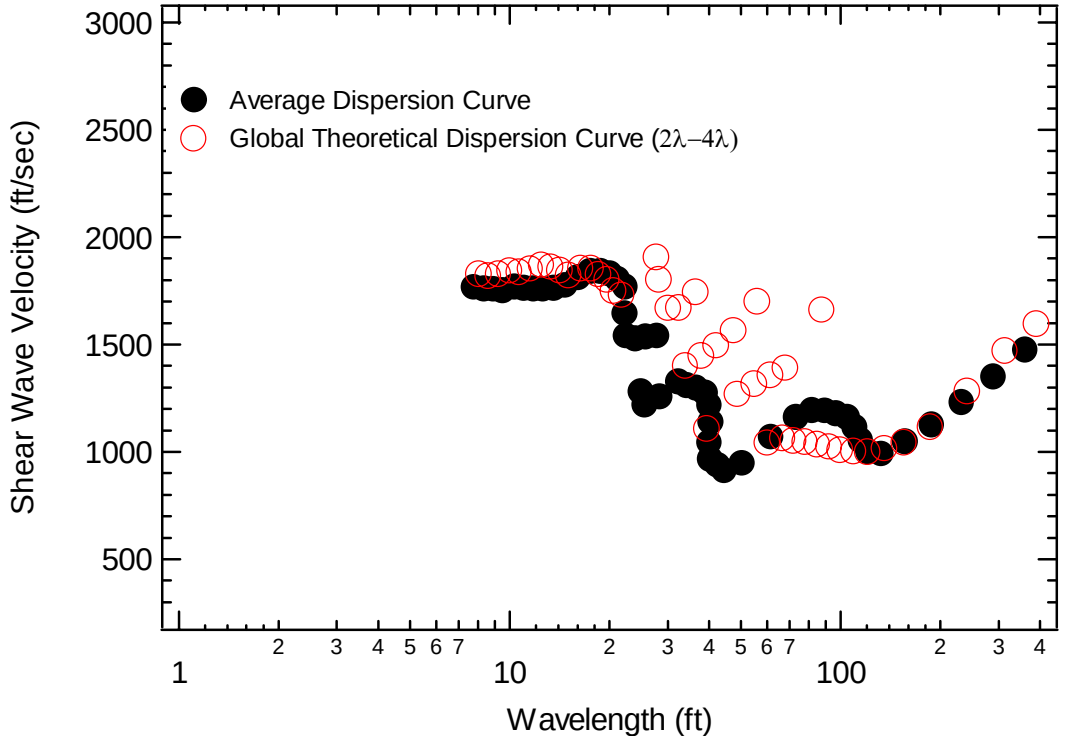

Figure 5-17 **Global experimental and theoretical dispersion curves for Profile 7c.**

The modal dispersion curves are shown with the effective dispersion curve in Figure 5-18 for Profile 7c. From this figure it can be seen that at short and long wavelengths the effective dispersion curve follows the fundamental mode, but over a wavelength range of approximately 20 to 50 ft the effective dispersion curves show distinct jumps to one or more higher modes.

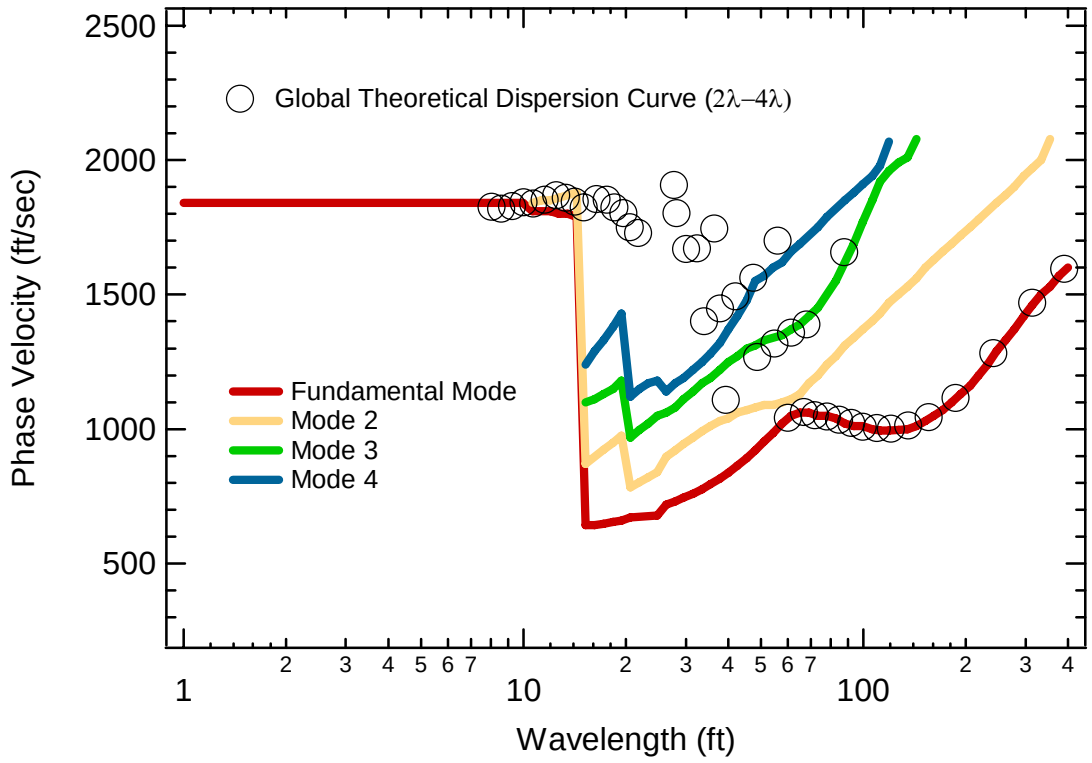

Figure 5-18 Modal and array theoretical dispersion curve for Profile 7c.

Array Analysis:

The array analysis produced consistent experimental and theoretical dispersion curves for cases with small shear wave velocity inversions. Figure 5-19 shows the agreement between the dispersion curves for Profile 7a. When the velocity contrasts become larger, however, the experimental and theoretical

dispersion curves become more inconsistent. Figure 5-20 show the array experimental and theoretical dispersion curves for Profiles 7c where the stiffness inversion is large. An array analysis at a site with a large velocity inversion would not be able to determine a single V_S profile that provided a match to all of the individual experimental dispersion curves. This example again indicates a problem with the phase unwrapping procedures used in the SASW analysis for some V_S profile conditions.

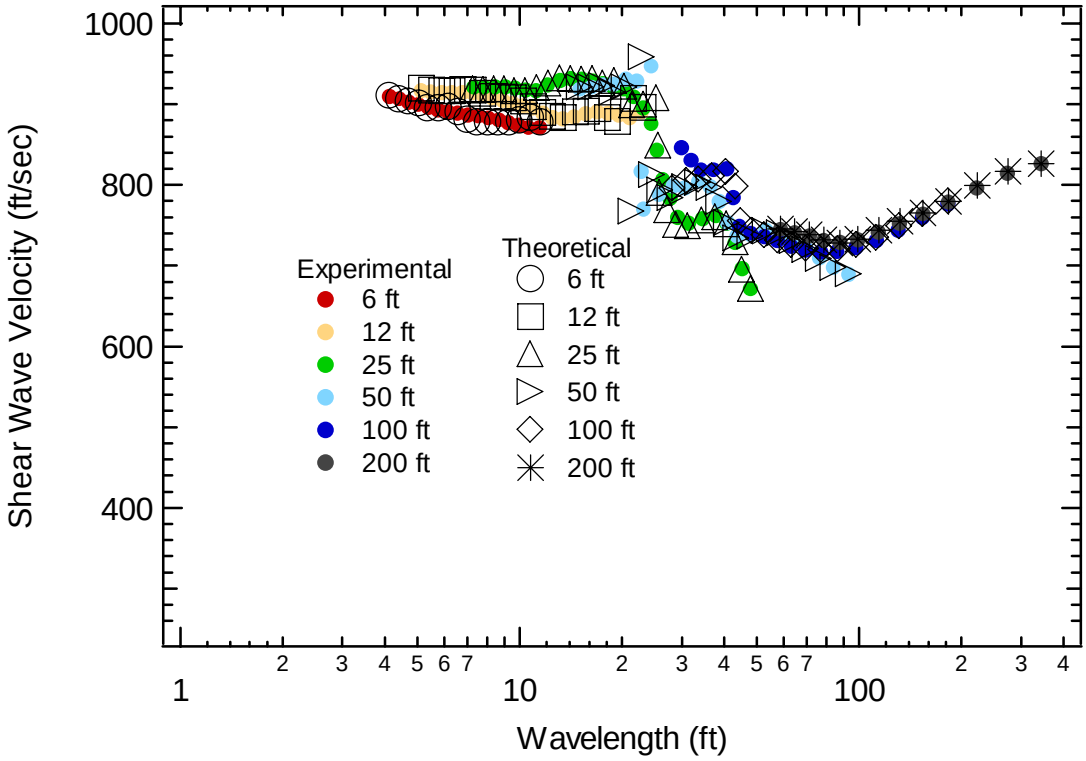

Figure 5-19 Array experimental and theoretical dispersion curves for Profile 7a.

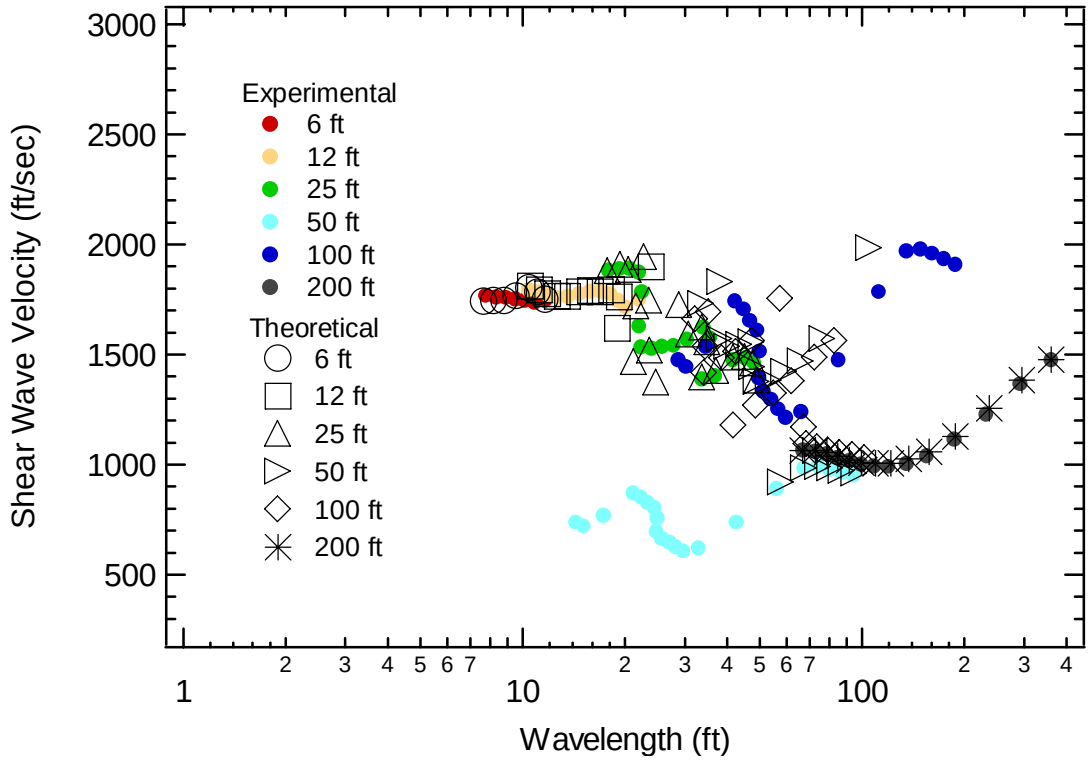

Figure 5-20 Array experimental and theoretical dispersion curves for Profile 7c.

5.7 Further Analysis of Soft-over-Stiff

Among the general profile conditions that were studied, the soft-over-stiff profiles proved to be the most problematic when the velocity of the halfspace was sufficiently large. For Profile 1, there is no jump to a higher mode when the halfspace velocity is equal to 800 ft/sec. As the halfspace velocity increases to 1200 and 1500 ft/sec, there is an abrupt jump to the 2nd mode over an intermediate range of frequencies, as shown in Figure 5-21.

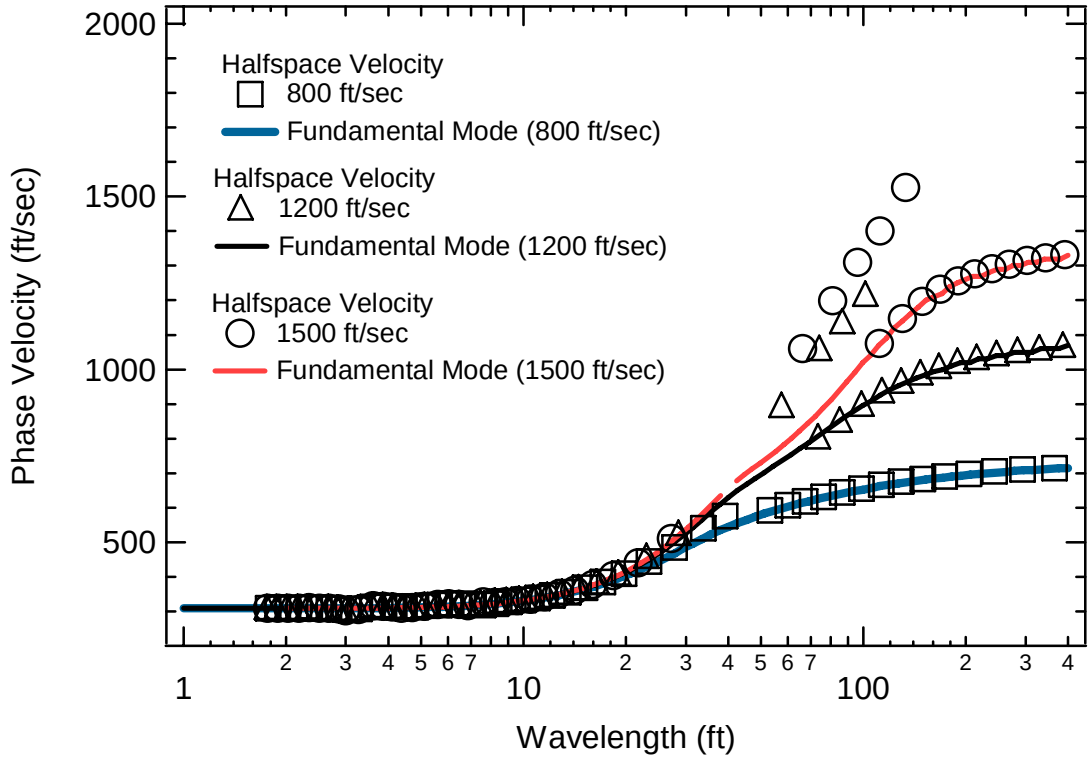

Figure 5-21 **Global theoretical and fundamental mode dispersion curves for Profiles 1a, 1b and 1c.**

The frequency range at which the mode jump occurred varied with the depth of the halfspace. Figure 5-22 is a plot of the global theoretical dispersion curve for the soft-over-stiff profiles with the depth of the halfspace at 10, 30, 50 and 80 ft. As is shown in Figure 5-22, as the depth to the halfspace increases the frequency and range of frequencies over which the jump occurs decreases. At a halfspace depth of 80 ft, there is no jump to a higher mode over the frequencies of interest.

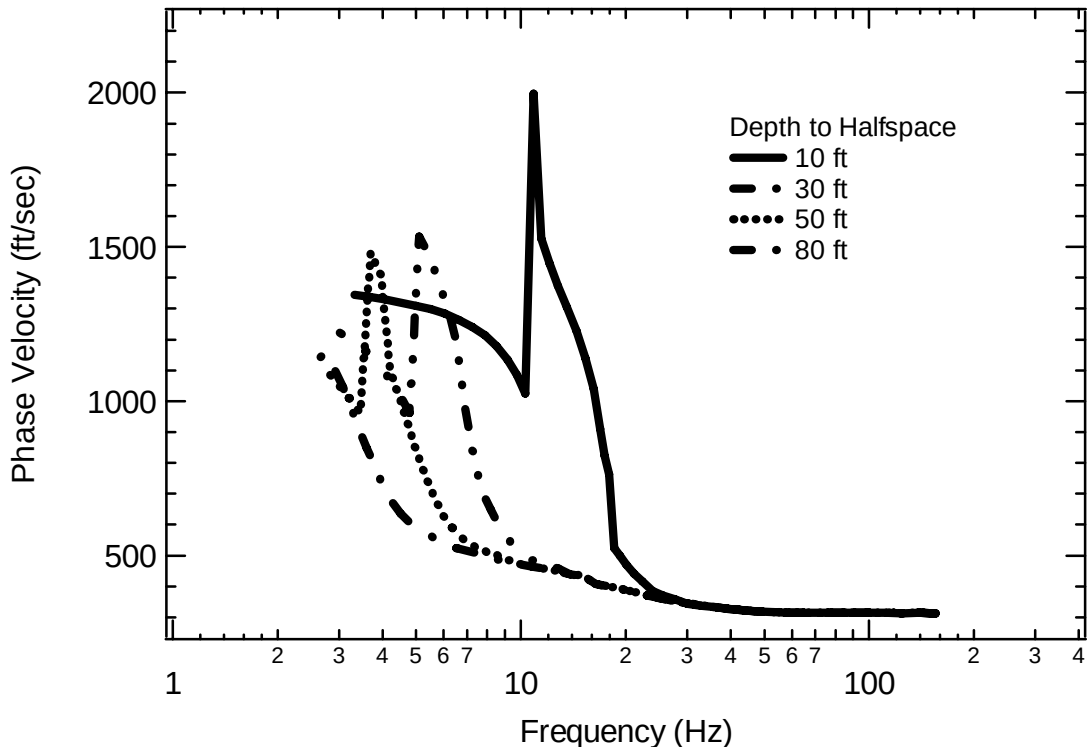

Figure 5-22 Theoretical global dispersion curves with a halfspace of 1500 ft/sec at a depth of 10, 30, 50 and 80 ft.

The abrupt jump to a higher mode is the cause of the dispersion inconsistencies observed for Profiles 1b and 1c and Profiles 2c and 2d. This is demonstrated for Profile 2d where the half-space was located at a depth of 30 ft. Figure 4-40 shows that the 100 ft and 200 ft experimental dispersion curves are not consistent with the theoretical dispersion curves even though the exact receiver locations were modeled in the theoretical solution. Figures 5-23 and 5-24 present the wrapped phase plots from the 100 and 200-ft receiver spacings. In the SASW method these phase plots are unwrapped by identifying 360-degree jumps in the phase plot. The locations of these jumps used to generate the simulated experimental dispersion curves are indicated in Figures 5-23 and 5-24

Figure 5.25 presents the effective velocity dispersion curves and modal dispersion curves for Profile 2d. Figure 5-25 demonstrates that the effective velocity dispersion curve for Profile 2d abruptly transitions to a higher mode over a frequency range of about 4.5 to 8 Hz. Due to this abrupt transition, it is not valid to unwrap the phase plot as a single continuous dispersion curve. Instead, the phase plot must be treated as two separate modes. Figure 5-26 shows the correct phase unwrapping for the portion of the phase plot that comes from the fundamental mode, and Figure 5-27 shows the correct phase unwrapping for the portion of the phase plot that comes from the higher mode. When this interpretation of the phase plot is used, the experimental dispersion curve is in perfect agreement with the theoretical dispersion curve, as shown in Figure 5-28. The problem is that it is not apparent or known beforehand that multiple, distinct modes are present in the phase plot. Therefore, it is not possible to correctly unwrap the phase plots.

This inconsistency is due to the fact that the theoretical analysis solves for the phase difference separately for each frequency from the phase difference calculated in the spatial domain, while the experimental procedure relies on unwrapping phase plots in the temporal domain to determine the phase difference at a given frequency. The result of this inconsistency can have serious consequences on the shear wave velocity profiles that are interpreted at a site, as discussed in Section 5.9. In the following section, the effect of Poisson's ratio is briefly examined and discussed.

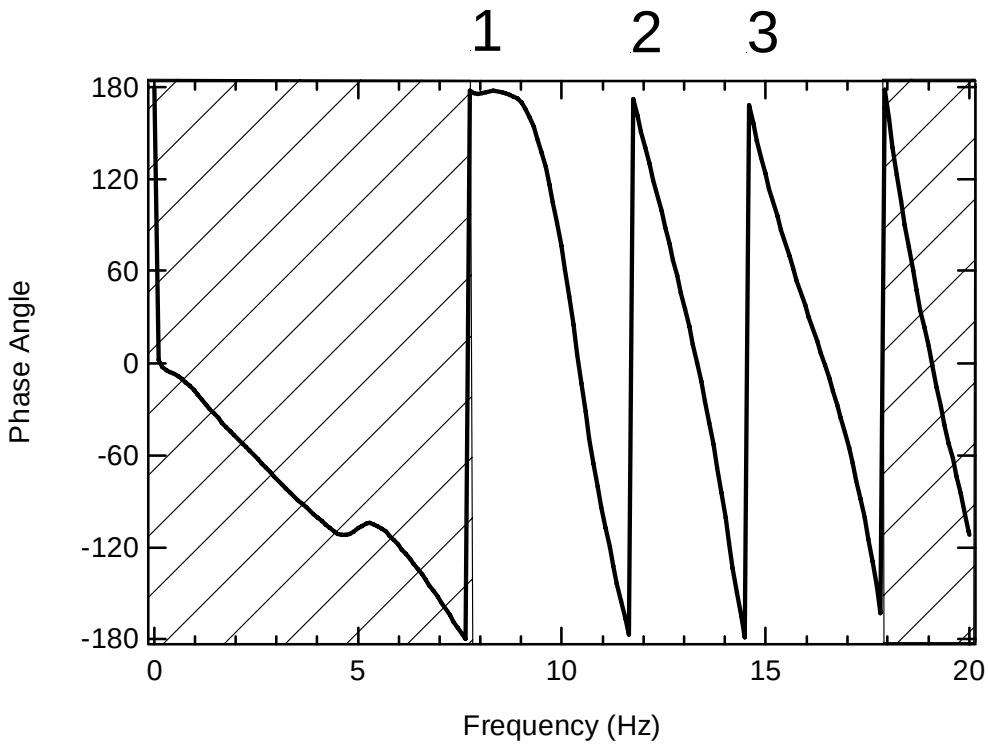

Figure 5-23 Conventional phase unwrapping of the 100 ft spacing for Profile 2d.

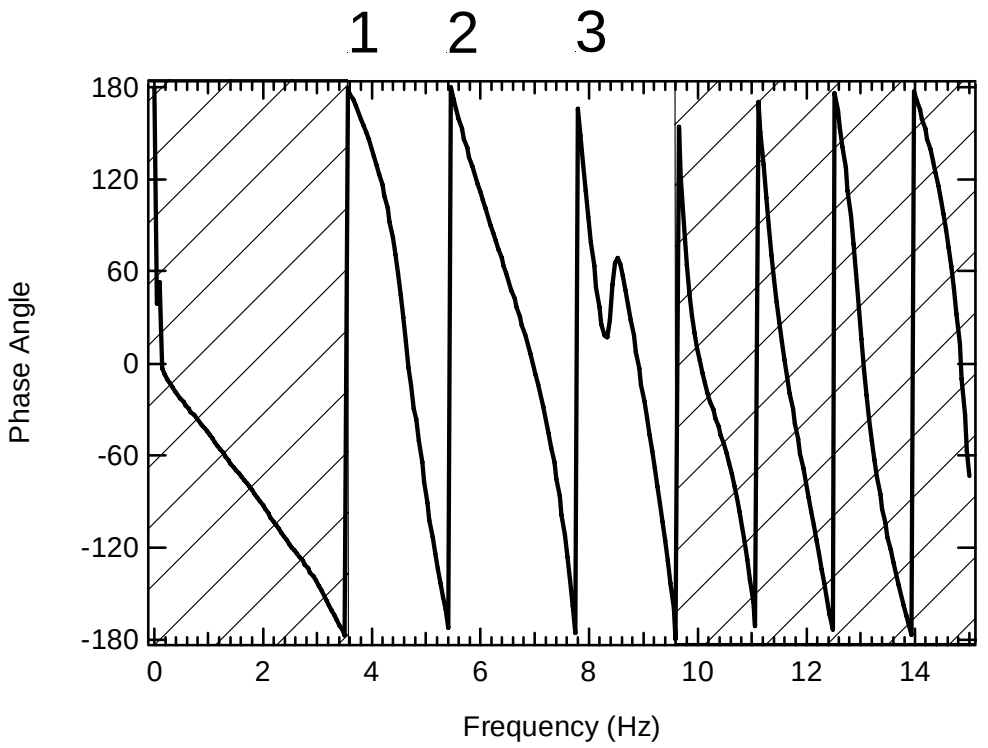

Figure 5-24 Conventional phase unwrapping of the 200 ft spacing for Profile 2d.

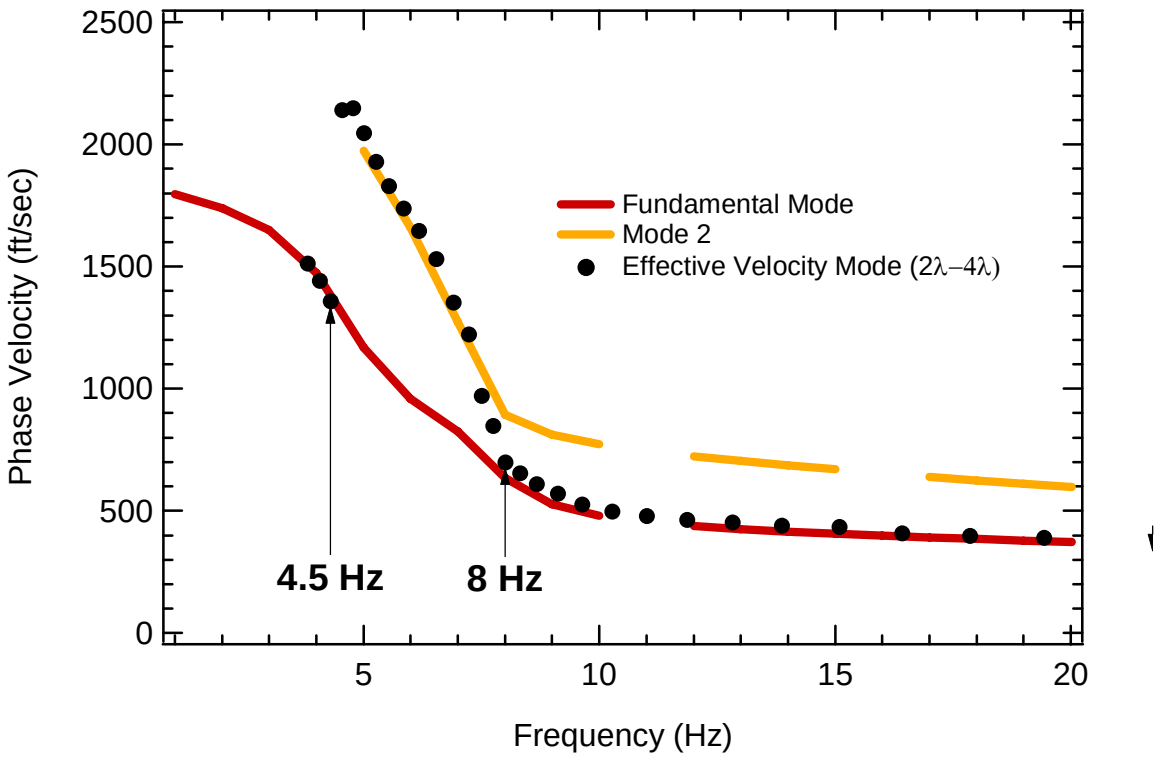

Figure 5-25 **Effective velocity and modal dispersion curves for Profile 2d.**

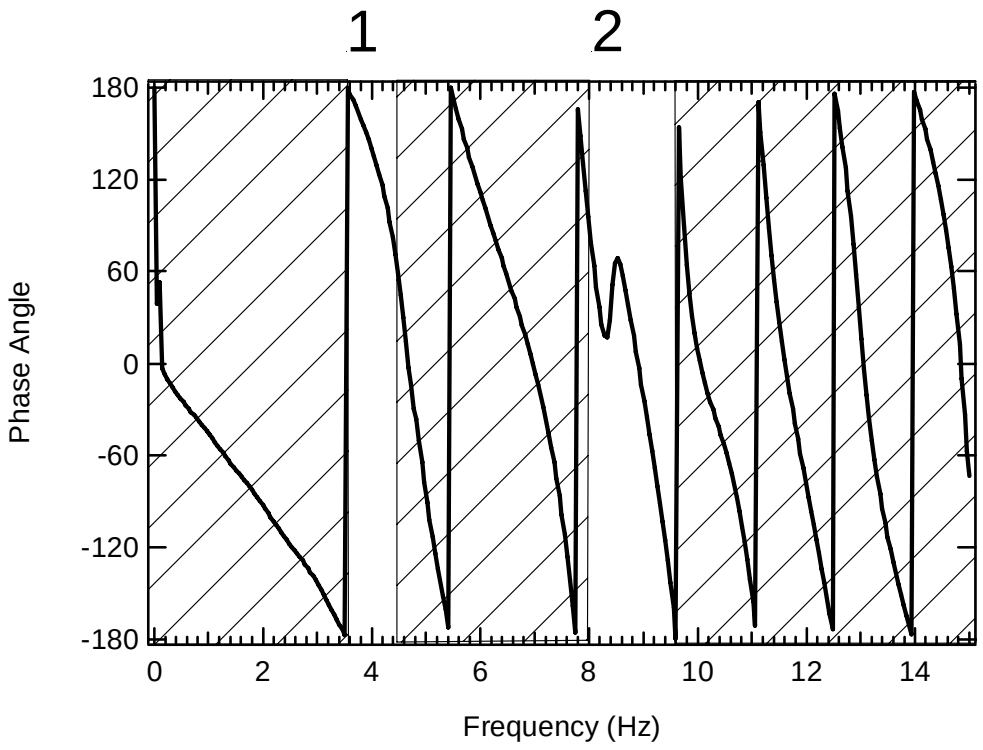

Figure 5-26 **Masking procedure to account for the fundamental mode for Profile 2d, 100 ft spacing.**

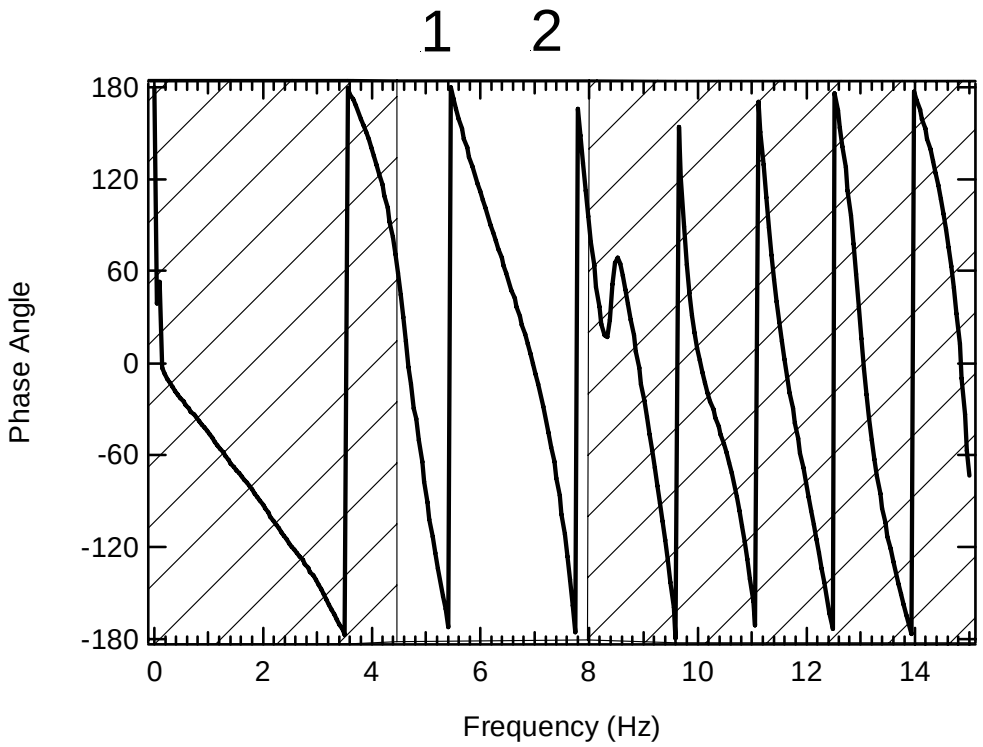

Figure 5-27 **Masking to account for jump to higher mode for Profile 2d, 200 ft spacing.**

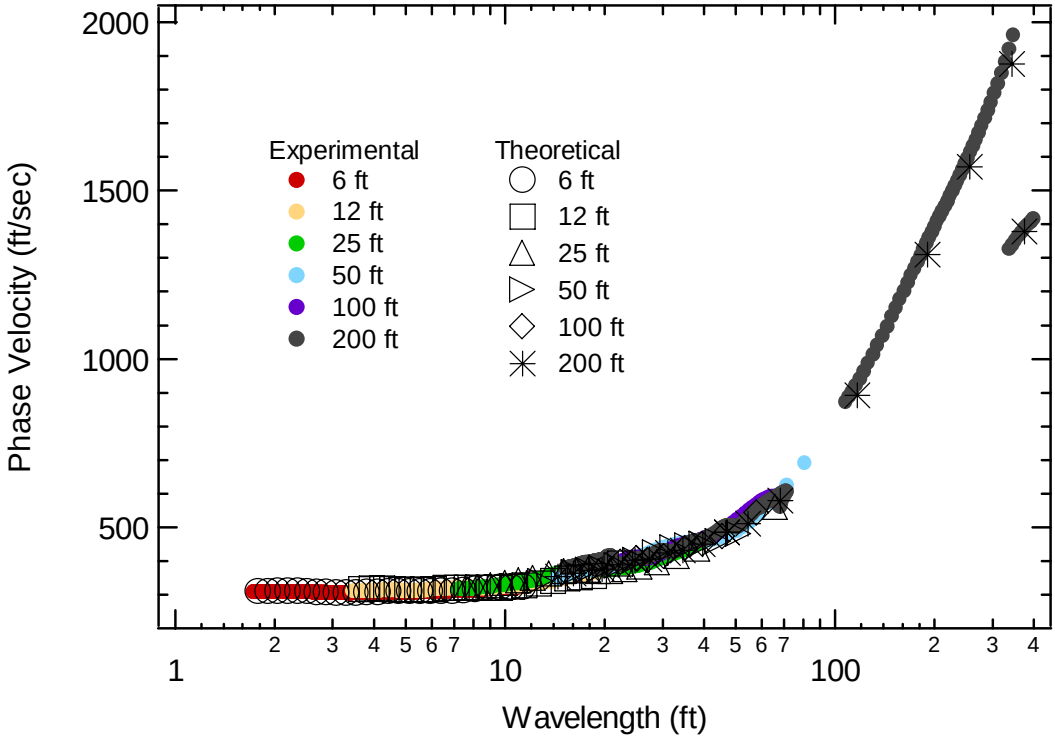

Figure 5-28 **Individual experimental and array theoretical dispersion curves created through amended masking procedures for Profile 2d.**

5.8 Effect of Poisson's Ratio on Dispersion Curves at Soft-over-Stiff Sites

The soft-over-stiff Profile 2c was analyzed further by generating synthetic time records with Poisson's ratio equal to 0.35 and 0.45. Figure 5-29 shows the individual experimental dispersion curve with the array theoretical dispersion curve. From this figure it can be seen that Poisson's ratio has a significant impact on the dispersion curves. Although the 200-ft experimental dispersion curve does not follow the theoretical solution, in general there is much better agreement between the curves than was seen when Poisson's ratio was equal to 0.25.

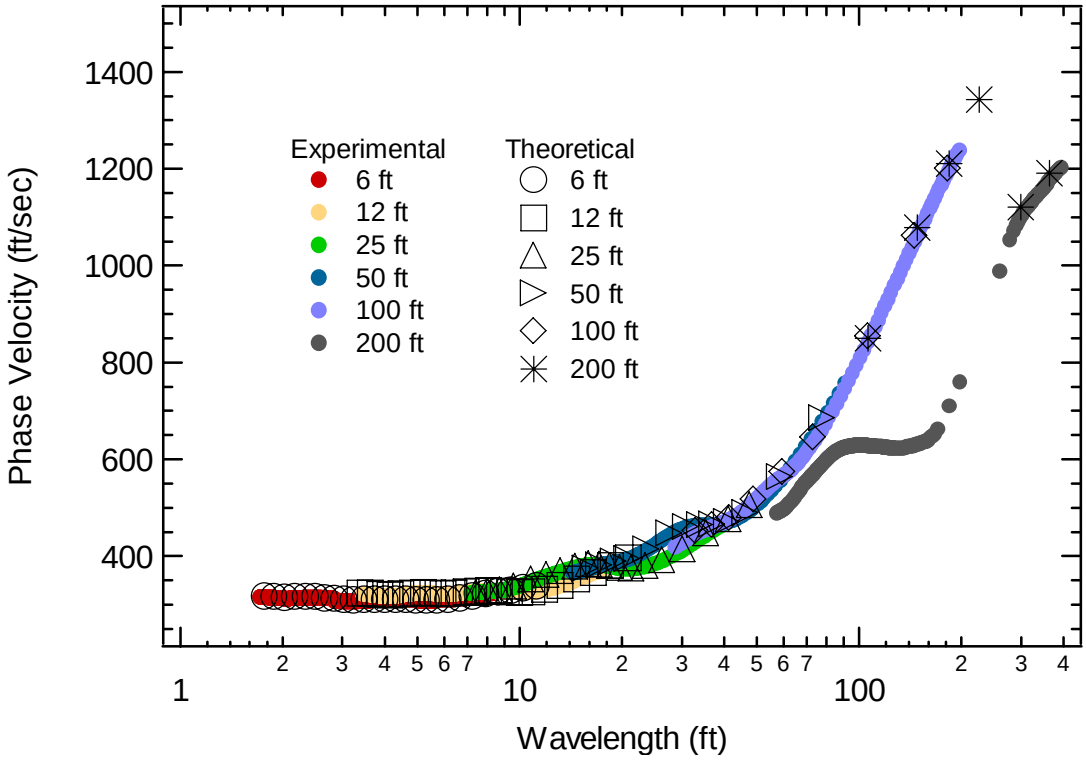

Figure 5-29 Individual experimental and array theoretical dispersion curves for Profile 2c with Poisson's ratio equal to 0.35.

Figure 5-30 shows the individual experimental and array theoretical dispersion curves for Profile 2c with Poisson's ratio equal to 0.45. The

experimental curve is drastically different than what was observed in Figure 4-34 when Poisson's ratio was equal to 0.25. In this case the experimental dispersion curve was a perfect match to the theoretical dispersion curve for all receiver spacings.

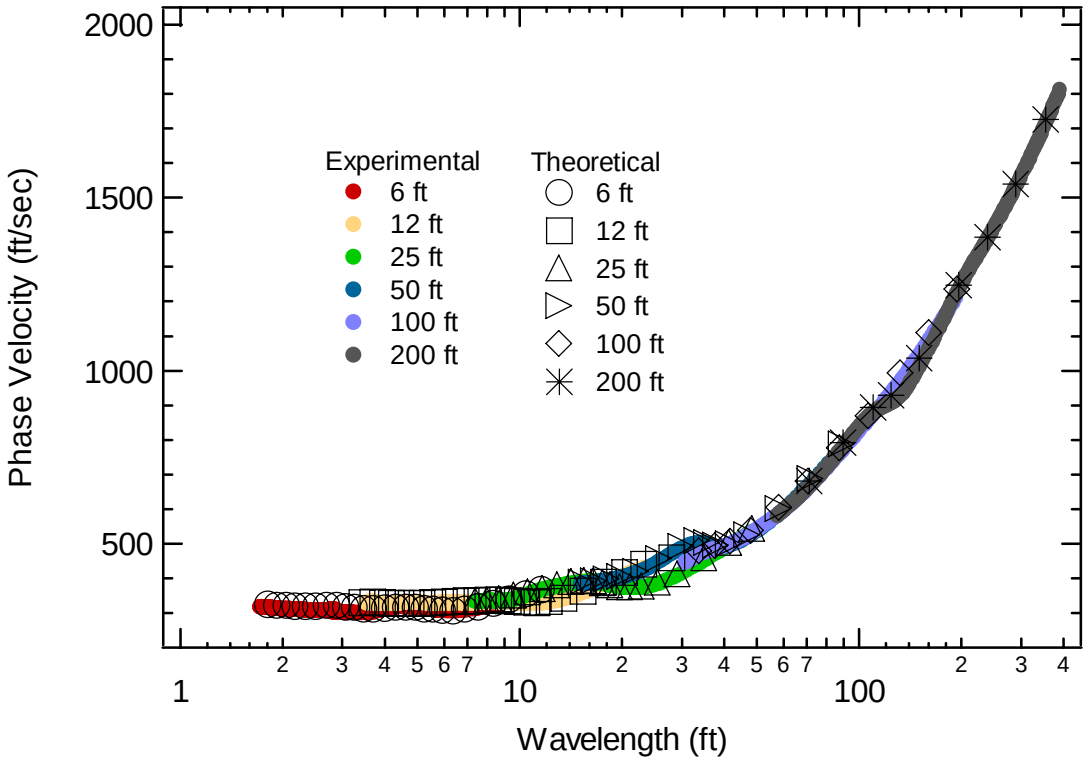

Figure 5-30 Individual experimental and array theoretical dispersion curve for Profile 2c with poisson's ration equal to 0.45.

Figure 5-30 indicates that the soft-over-stiff profiles may not be as problematic when Poisson's ratio is high, as is the case at saturated sites. This may help explain why these problems have not been as prevalent at soft-over-stiff sites. This issue needs to be examined in greater depth.

5.9 Practical Implications of Conventional SASW Interpretation at Soft-over-Stiff Sites

The SASW simulations of stiff-over-soft sites demonstrated that higher mode energy had a large impact on the dispersion curves for cases where there was a large impedance contrast. Conventional phase unwrapping of the phase spectrum from these profiles produced an erroneous dispersion curve. To demonstrate the potential implications of this problem, inversion of the simulated dispersion curve from Profile 2d was performed using an array analysis, global analysis, and fundamental mode analysis. Only the portions of the dispersion curve that appeared continuous were used (the 100 ft spacing was not included). Figure 5-31a shows the dispersion curve for Profile 2d with the 100-ft receiver spacing data removed. Neither the array nor global analysis inversion could provide a reasonable match to the simulated dispersion curve. However, when the fundamental mode solution was used, good agreement could be achieved between the simulated and theoretical dispersion curves, as shown in Figure 5-31b. The resulting V_S profile is compared to the actual profile used to generate the simulated time records in Figure 5-32. In this case, the erroneous dispersion curve and use of a fundamental mode solution resulted in a predicted V_S profile that was as much as 50% less than the actual profile.

This problem is particularly important in cases where the SASW method is used for assigning V_{S30} (average V_S in top 30 m) which is used for earthquake site classification in the International Building Code (IBC). A misinterpretation as was demonstrated in Figure 5-32 could result in an erroneous site classification.

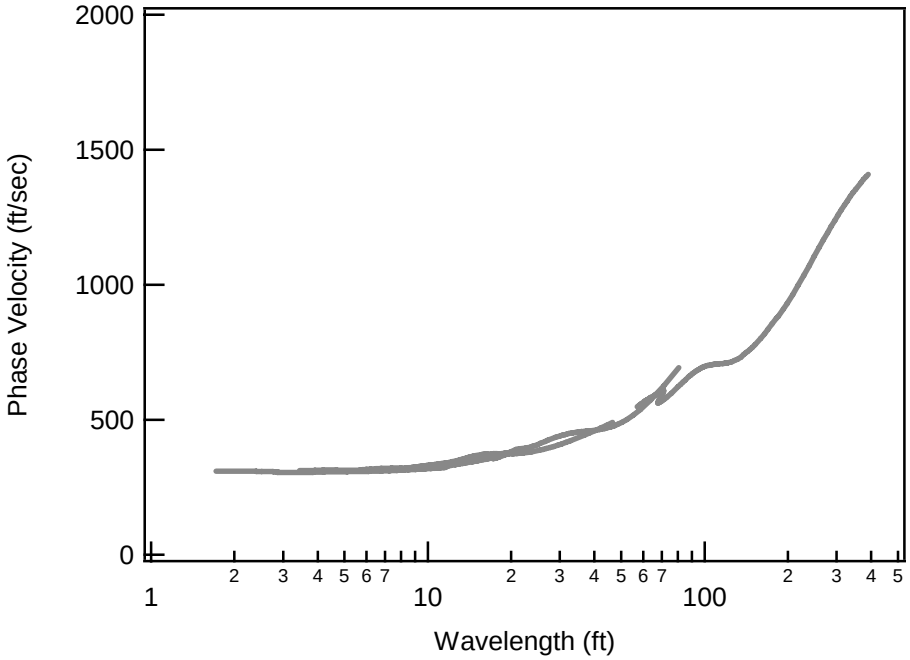

a. Simulated dispersion curve from Profile 2d with 100 ft spacing data removed

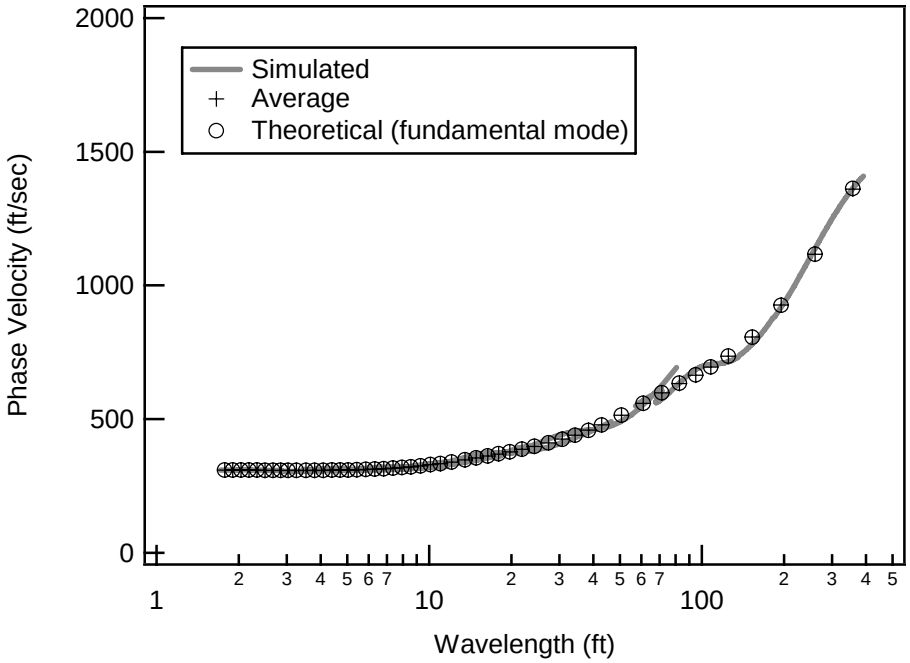

a. Match achieved from inversion analysis between fundamental mode theoretical dispersion curve and average simulated dispersion curve from Profile 2d

Figure 5-31 Simulated and theoretical dispersion curves from Profile 2d.

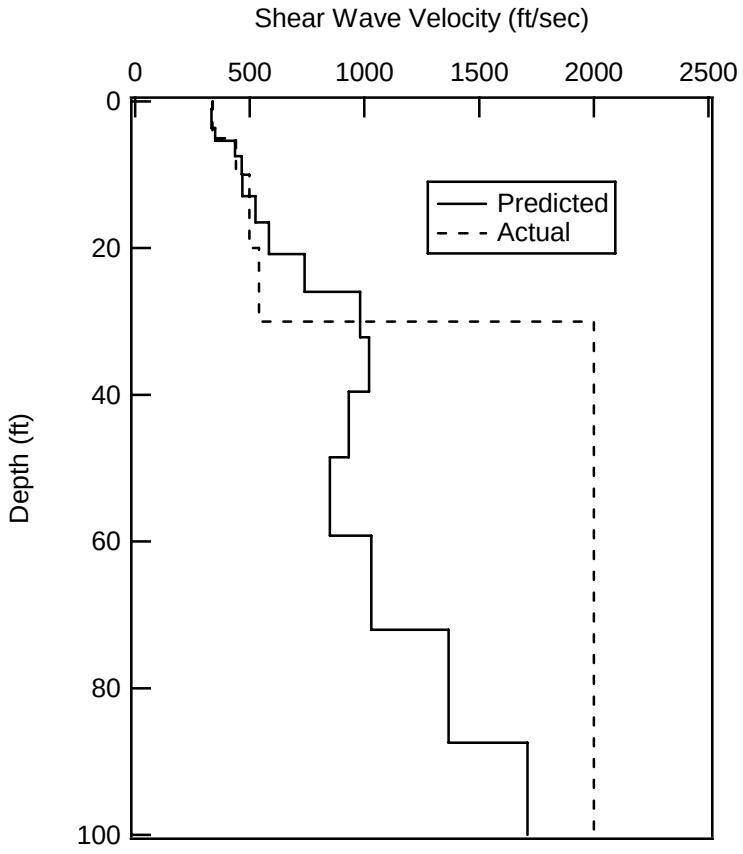

Figrue 5-32 Comparison between predicted V_S profile from fundamental mode inversion analysis and actual V_S profile for profile 2d

5.10 Summary

In this chapter the results from SASW simulations presented in Chapter 4 were discussed and analyzed. It was found that the soft-over-stiff profiles were the most problematic when using conventional phase unwrapping procedures due to distinct jumps to higher modes. The potential error that would be caused by assuming that the phase plot is continuous was demonstrated for a soft-over-stiff with a high velocity contrast case. Most of the other soil profiles were accurately resolved using conventional phase unwrapping because the

fundamental mode dominated or the theoretical solution followed a gradual and continuous path through higher mode energy. It was also shown in this chapter that Poisson's ratio can have a significant effect on the development of the experimental dispersion curve at soft-over-stiff sites.

Chapter 6 Conclusions

6.1 Conclusion

The SASW surface wave methodology was analyzed by performing analytical simulations of surface wave measurements for a variety of realistic geotechnical conditions. Simulations were performed for a total of 23 shear wave velocity profiles which were developed from a single reference profile. The general profile conditions that were analyzed included: 1. gradually increasing V_S with depth, 2. soft-over-stiff conditions, 3. stiff-over-soft conditions, 4. embedded stiff layer, and 5. embedded soft layer. Conventional phase unwrapping procedures were applied to the synthetic data and both array and global analyses were conducted. The major conclusions obtained from this research are:

1. The global analysis produced theoretical dispersion curves which closely follow the experimental dispersion curves at short wavelengths for the reference profile, soft-over-stiff profiles with small velocity contrasts, stiff-over-soft profiles, profiles with an embedded stiff layer and profiles with an embedded soft layer with low velocity contrast. At longer wavelengths, typically greater than 150 ft. (for the cases that were simulated), the theoretical dispersion curve deviates from the average experimental dispersion curve by as much as 15%. This deviation can be attributed to near-field effects. The global analysis involves calculating a theoretical dispersion curve with receivers spaced 2λ and 4λ from the source, while

the experimental dispersion curve was calculated as close as 0.5 λ to the source over the same frequencies. This effect is minimized when adjacent receiver spacings overlap, but at the longest spacing the effect is significant. The effect of this inconsistency between the theoretical and experimental dispersion curves would be underprediction of the V_S values of the deepest layers.

2. The array analysis for the reference profile, soft-over-stiff profiles with small velocity contrasts, stiff-over-soft profiles, profiles with an embedded stiff layer and profiles with an embedded soft layer with low velocity contrasts yielded results that are consistent between the theoretical and experimental dispersion curves for the entire wavelength range. This result was expected since the theoretical dispersion curves are calculated at the same locations from the source as the experimental curves.
3. For most of the cases, the global averaging procedures produced experimental dispersion curves which are generally consistent with the experimental dispersion curves, with the exception of the long wavelength data as noted above. The array averaging procedures were also effective at providing a representative experimental dispersion curve for these profiles in most cases. The exceptions were the cases of profiles with very large velocity inversions and the soft-over-stiff conditions, as discussed below.
4. In some cases, notably the soft-over-stiff profiles and profiles with an embedded soft layer with higher velocity contrasts, simulations show large

deviations between the global and array experimental dispersion curves and the theoretical dispersion curves for the site. In these cases, the effective dispersion curve primarily follows the fundamental mode but abruptly transitions to a higher mode over a narrow frequency range when the velocity contrast was set sufficiently large. This behavior is unlike the continuous effective dispersion curves observed for other profile conditions. This transition to a higher mode caused the conventional SASW phase unwrapping procedures to produce an experimental dispersion curve that was inconsistent with the theoretical dispersion curve for the site. Subsequent fitting of a theoretical dispersion curve to the erroneous experimental dispersion curve produced a predicted V_S profile that was greatly in error.

5. The effective dispersion curve for the stiff-over-soft profiles and the profiles with an embedded soft layer does not follow the fundamental mode over the entire frequency range simulated. The effective dispersion curve follows a generally smooth and continuous transition from the fundamental to a superposition of modes. The continuous nature of the effective dispersion curves allowed the phase unwrapping procedure to produce an experimental dispersion curve that is consistent with the theoretical dispersion curves.
6. Changing the velocity contrast and depth of the stiff layer for the soft-over-stiff profiles had a significant effect on the effective and modal dispersion curve. The effective dispersion curve has a distinct jump to a

higher mode and the frequency range over which this occurred increased with increasing velocity contrast. As the depth of the stiff layer was increased the frequencies and frequency range over which the jump to the higher mode occurred decreased.

7. For the soft-over-stiff profiles with large velocity contrasts and Poisson's ratio (ν) equal to 0.25, conventional phase unwrapping procedures produced an erroneous dispersion curve and significant errors in the predicted V_S profile. Additional simulations of this profile were conducted with ν equal to 0.35 and 0.45 . For the case of ν =0.35, similar results were found as in the ν=0.25 case. However, for the case of ν=0.45, conventional phase unwrapping procedures produced an experimental dispersion curve that is consistent with the theoretical dispersion curve. This suggests that at saturated or near-saturated soft-over-stiff soil sites where ν=0.45 or greater, the conventional SASW approach may provide reliable results.

6.2 Recommendations

The study covered a broad range of soil conditions in order to identify conditions where the potential exists for erroneous results from the SASW procedure. This study did not look in depth at the causes or possible remedies to the problems that were identified. The following are recommendations for future studies.

1. Verify the observations from this analytical study by conducting field measurements at geotechnical sites with complex stiffness profiles.

2. Perform additional simulations of the soft-over-stiff profiles with changes in the stiffness geometry to understand better the influence of velocity contrasts and the depth of profile layers.
3. Perform additional simulations of the general profile conditions using a range of Poisson's ratio values to understand better the effect of this soil property.
4. Perform inversion analysis procedures to evaluate the effectiveness of automated curve fitting programs at complex geotechnical sites.
5. Perform simulations of these same sites using a multi-channel wavefield transformation approach to develop the experimental surface wave dispersion curves.

Appendix A:

Masked Phase Plots

Reference Profile

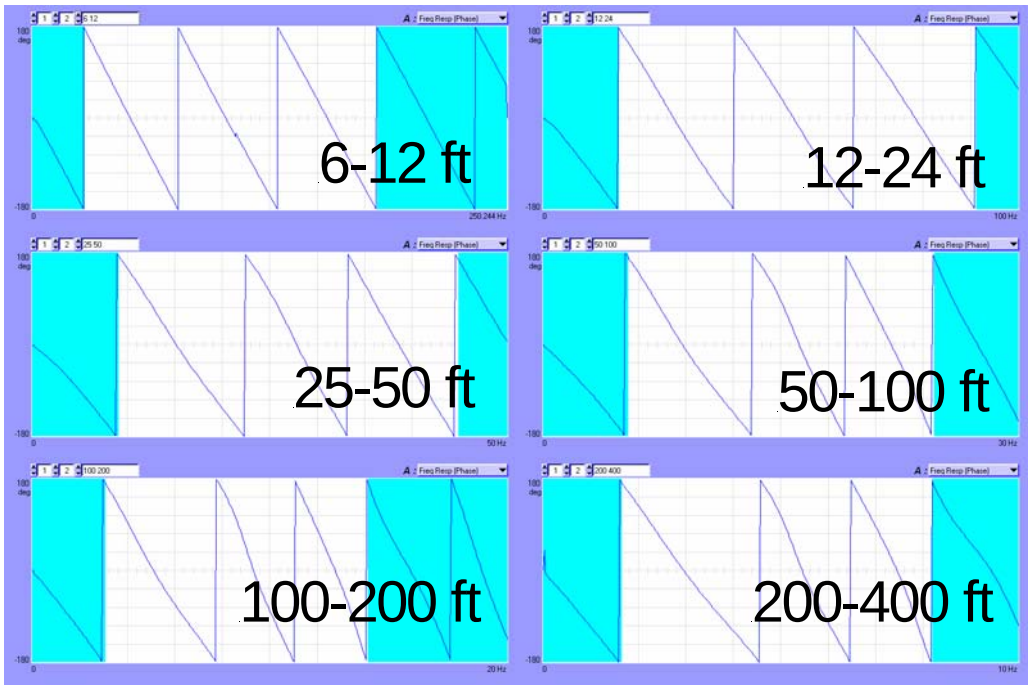

Figure A-1 **Masked phase plots for receiver spacing of 6, 12, 25, 50, 100 and 200 ft for the Reference Profile.**

Baseline Profile 1a

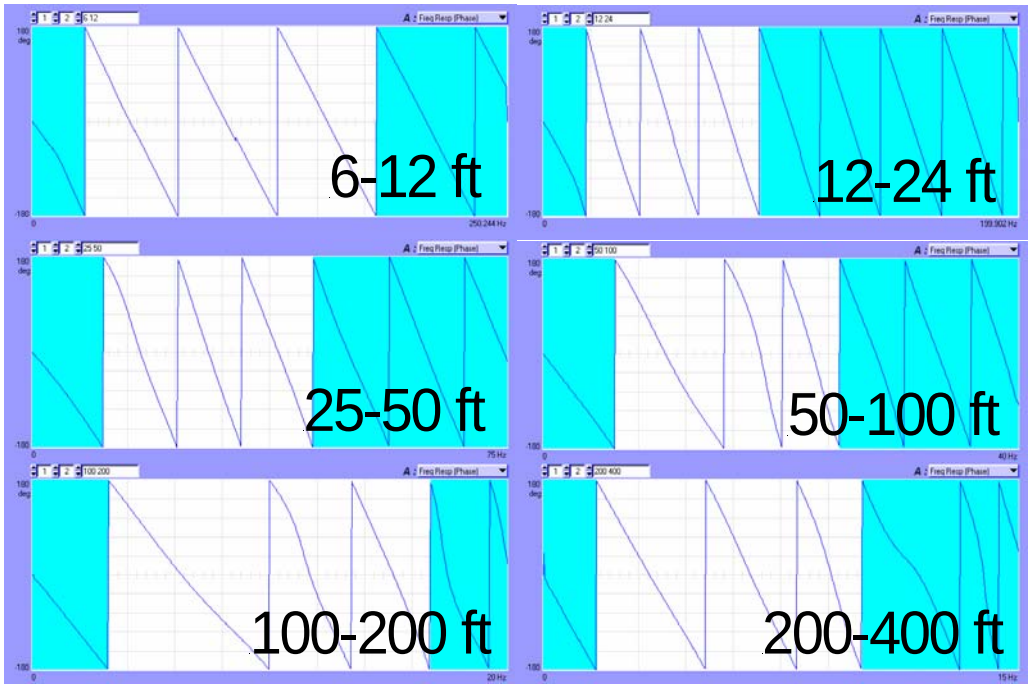

Figure A-2 **Masked phase plots for receiver spacing of 6, 12, 25, 50, 100 and 200 ft for the Baseline Profile 1a.**

Baseline Profile 1b

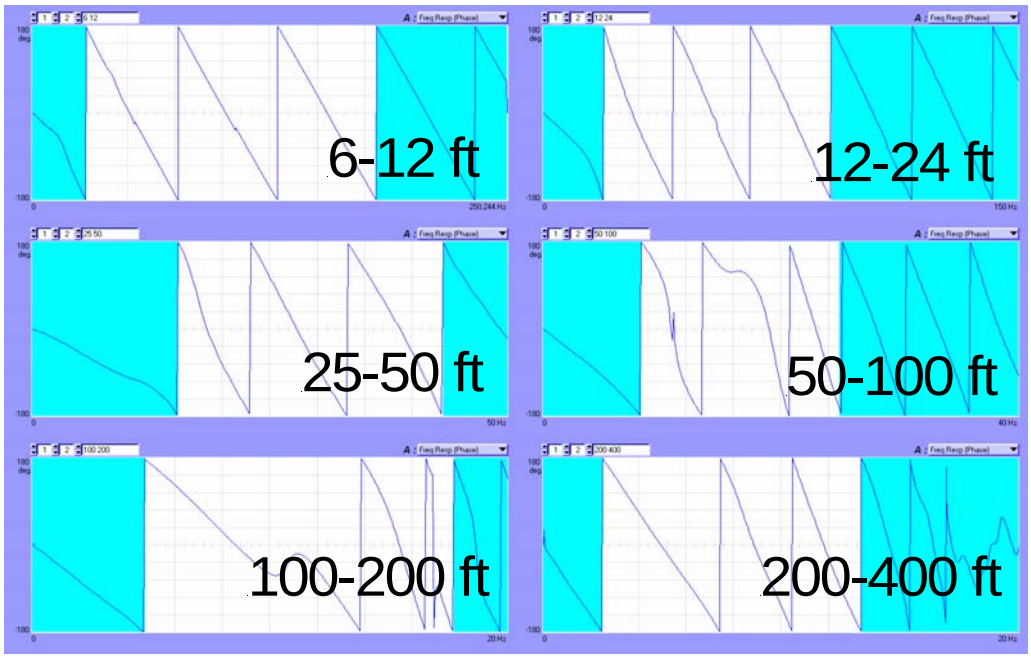

Figure A-3 **Masked phase plots for receiver spacing of 6, 12, 25, 50, 100 and 200 ft for the Baseline Profile 1b.**

Baseline Profile 1c

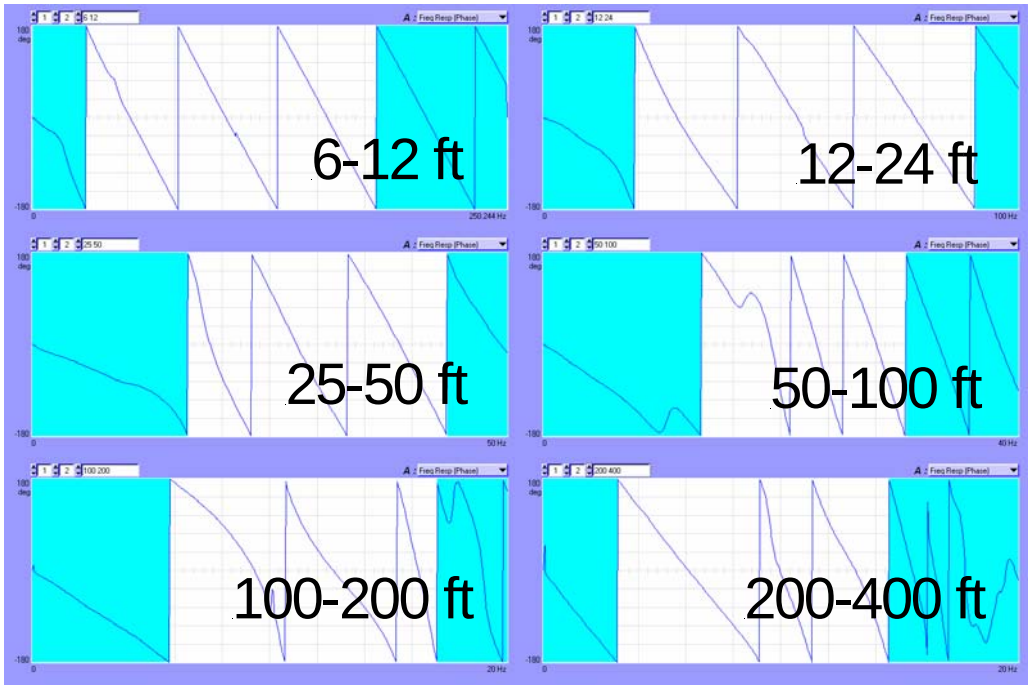

Figure A-4 **Masked phase plots for receiver spacing of 6, 12, 25, 50, 100 and 200 ft for the Baseline Profile 1c.**

Baseline Profile 2a

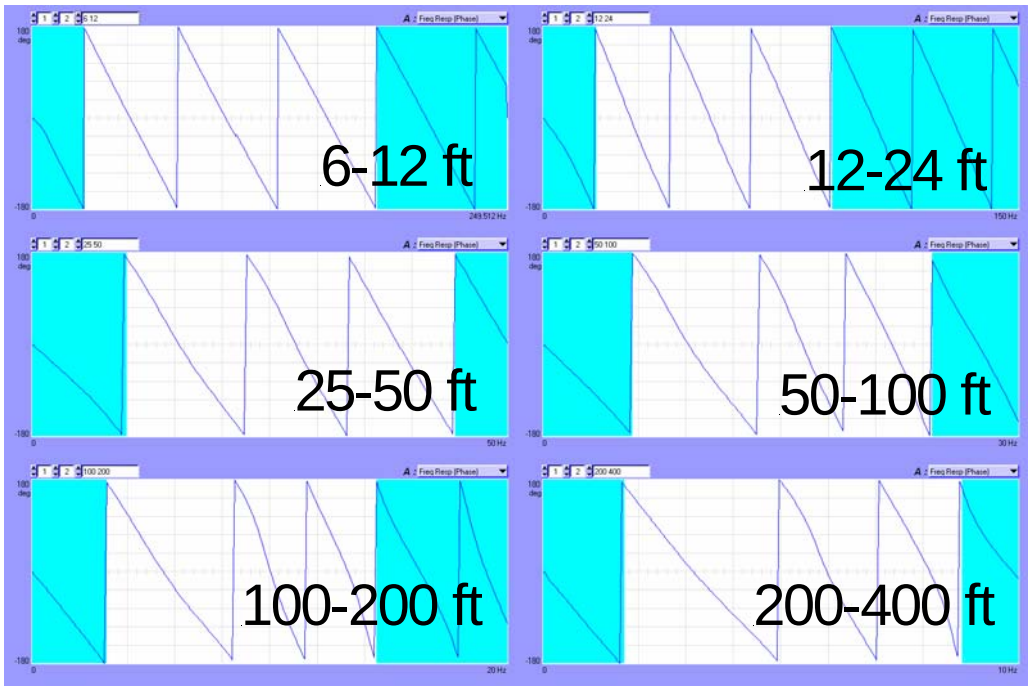

Figure A-5 **Masked phase plots for receiver spacing of 6, 12, 25, 50, 100 and 200 ft for the Baseline Profile 1a.**

Baseline Profile 2b

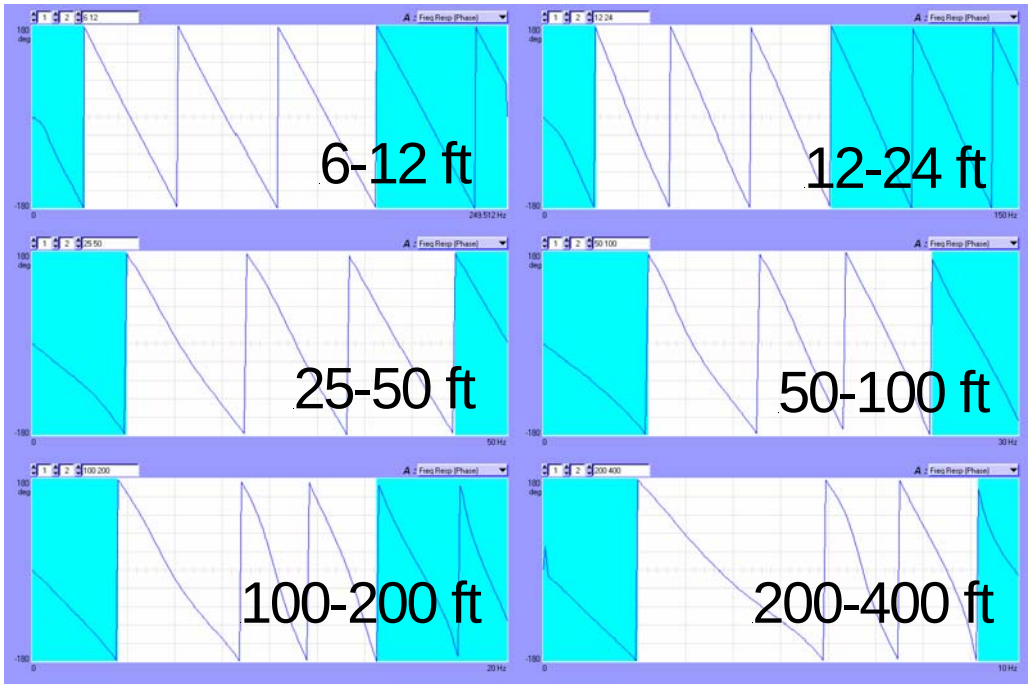

Figure A-6 **Masked phase plots for receiver spacing of 6, 12, 25, 50, 100 and 200 ft for the Baseline Profile 2b.**

Baseline Profile 2c

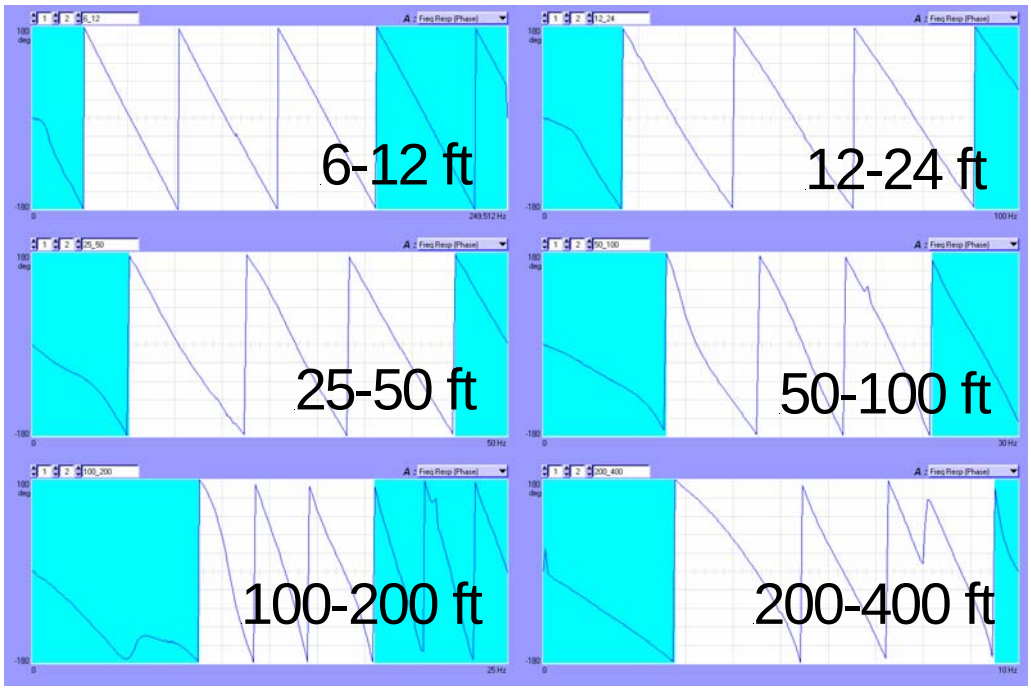

Figure A-7 **Masked phase plots for receiver spacing of 6, 12, 25, 50, 100 and 200 ft for the Baseline Profile 2c.**

Baseline Profile 2d

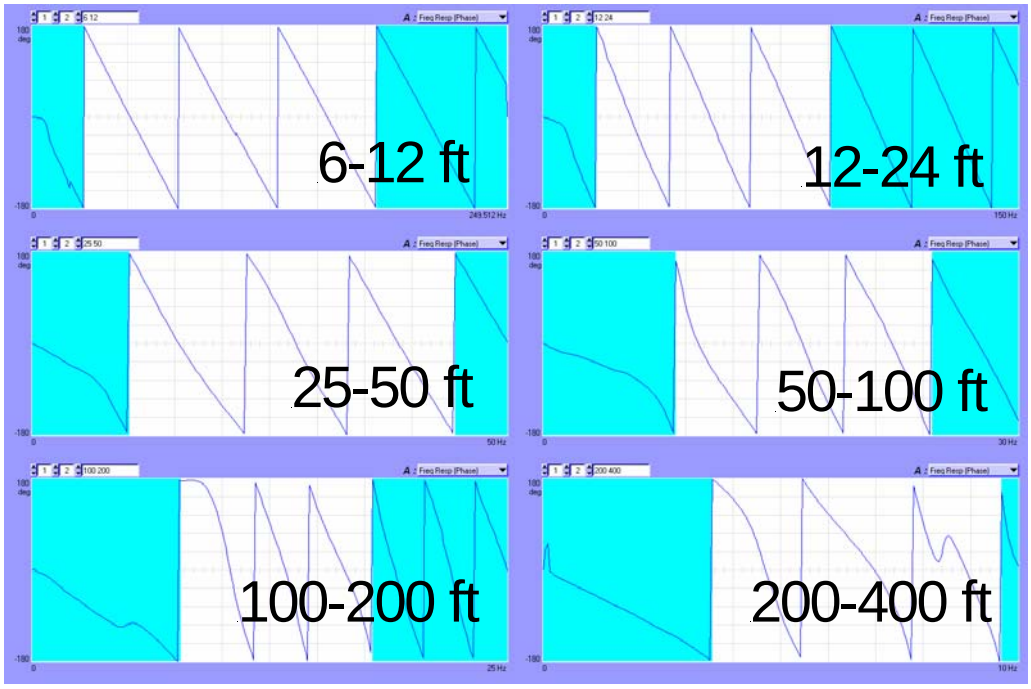

Figure A-8 **Masked phase plots for receiver spacing of 6, 12, 25, 50, 100 and 200 ft for the Baseline Profile 2d.**

Baseline Profile 3a

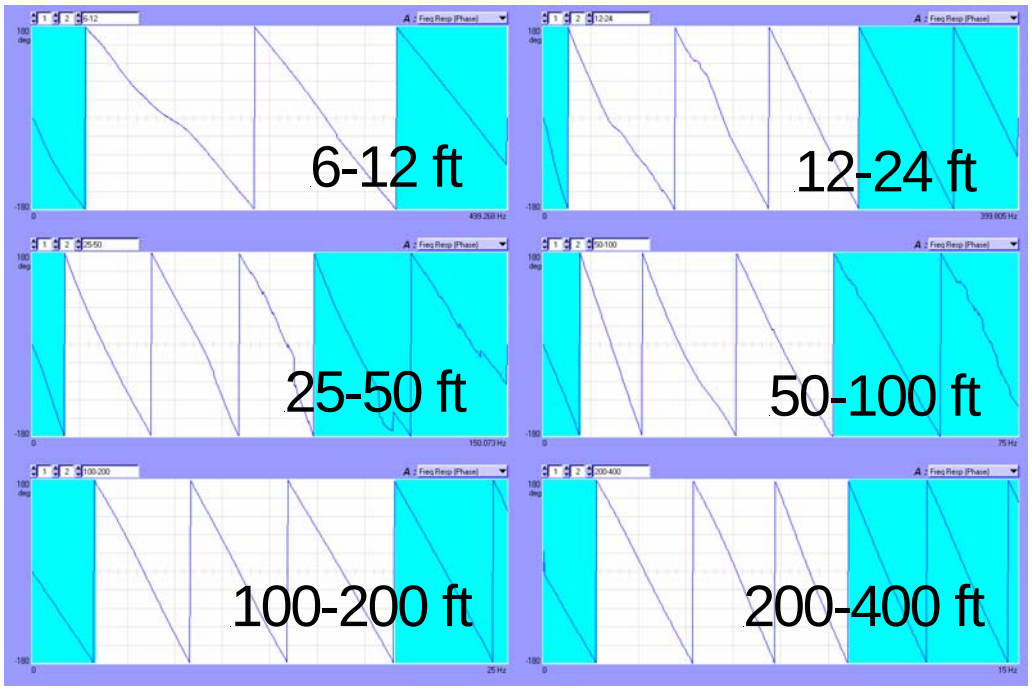

Figure A-9 **Masked phase plots for receiver spacing of 6, 12, 25, 50, 100 and 200 ft for the Baseline Profile 3a.**

Baseline Profile 3b

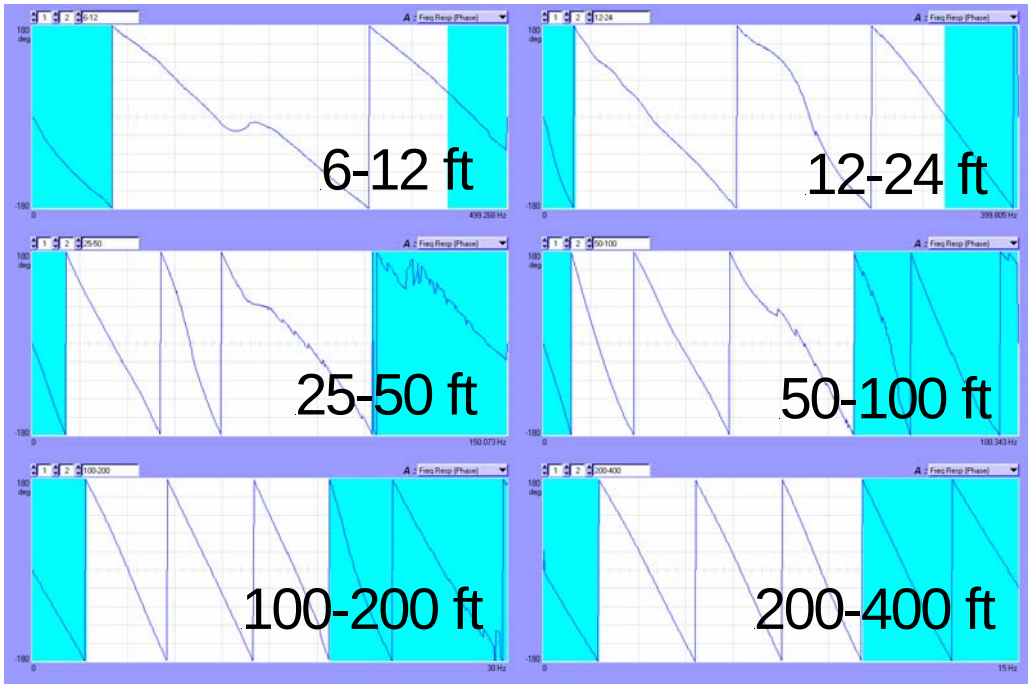

Figure A-10 **Masked phase plots for receiver spacing of 6, 12, 25, 50, 100 and 200 ft for the Baseline Profile 3b.**

Baseline Profile 3c

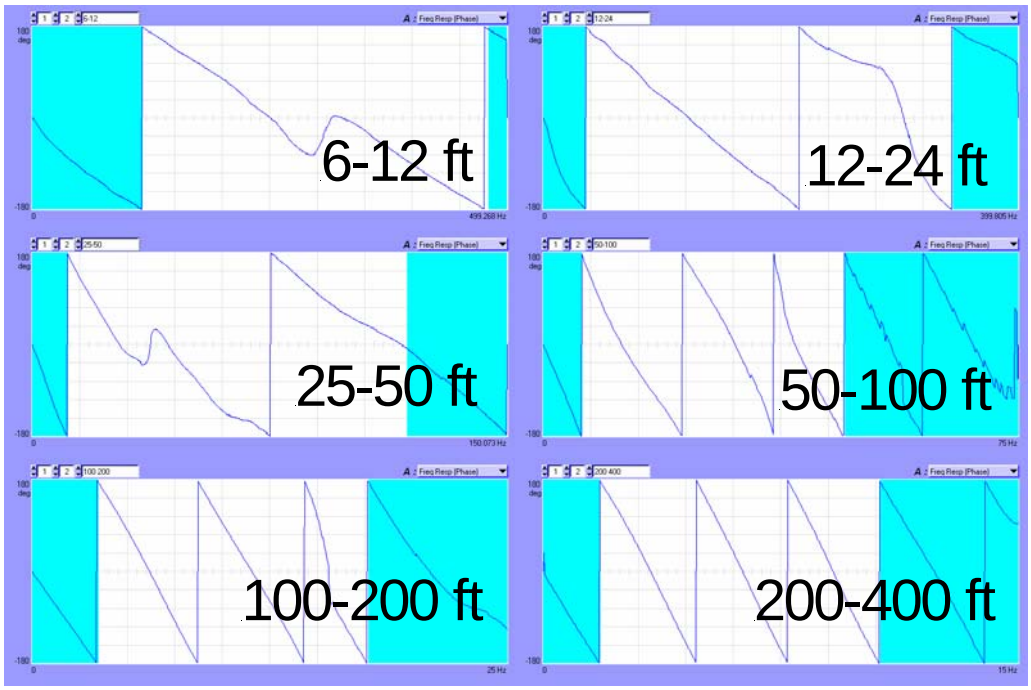

Figure A-11 **Masked phase plots for receiver spacing of 6, 12, 25, 50, 100 and 200 ft for the Baseline Profile 3c.**

Baseline Profile 4a

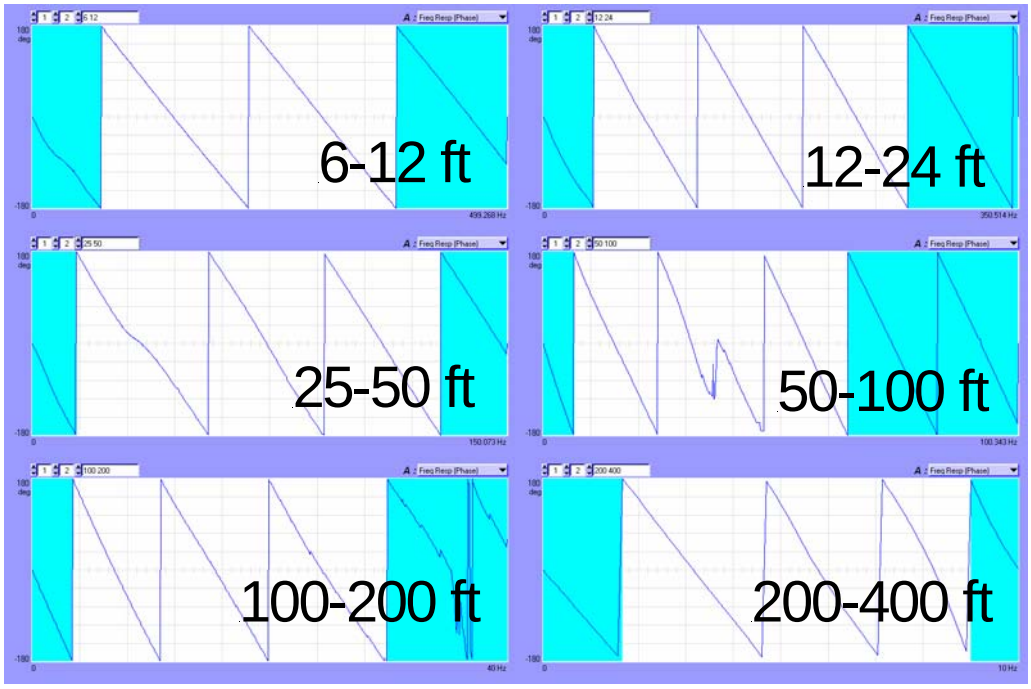

Figure A-12 **Masked phase plots for receiver spacing of 6, 12, 25, 50, 100 and 200 ft for the Baseline Profile 4a.**

Baseline Profile 4b

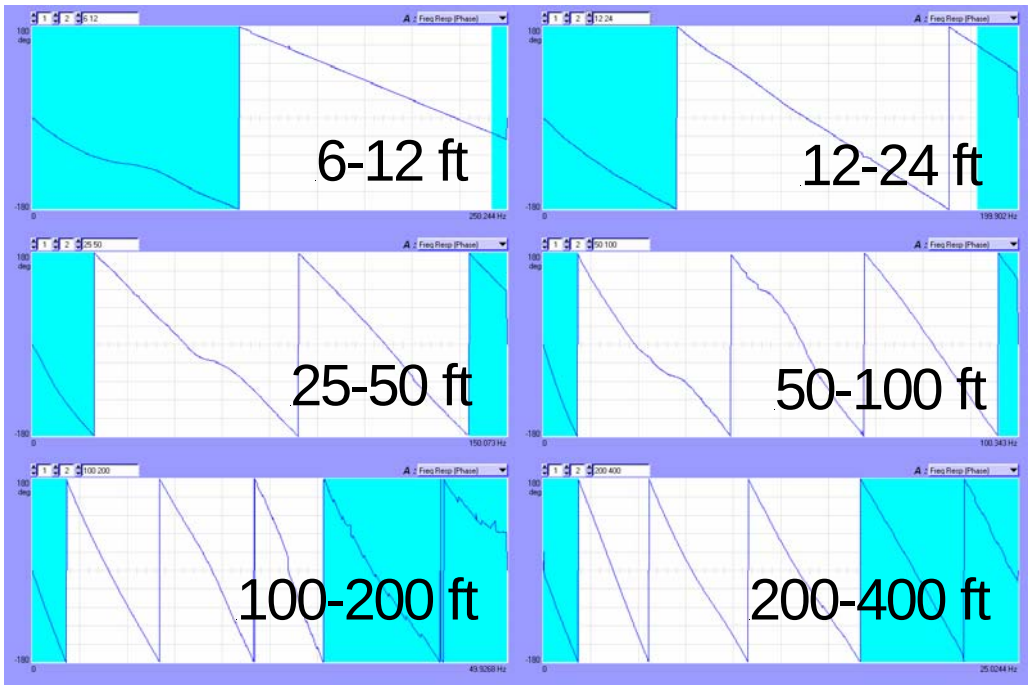

Figure A-13 **Masked phase plots for receiver spacing of 6, 12, 25, 50, 100 and 200 ft for the Baseline Profile 4b.**

Baseline Profile 4c

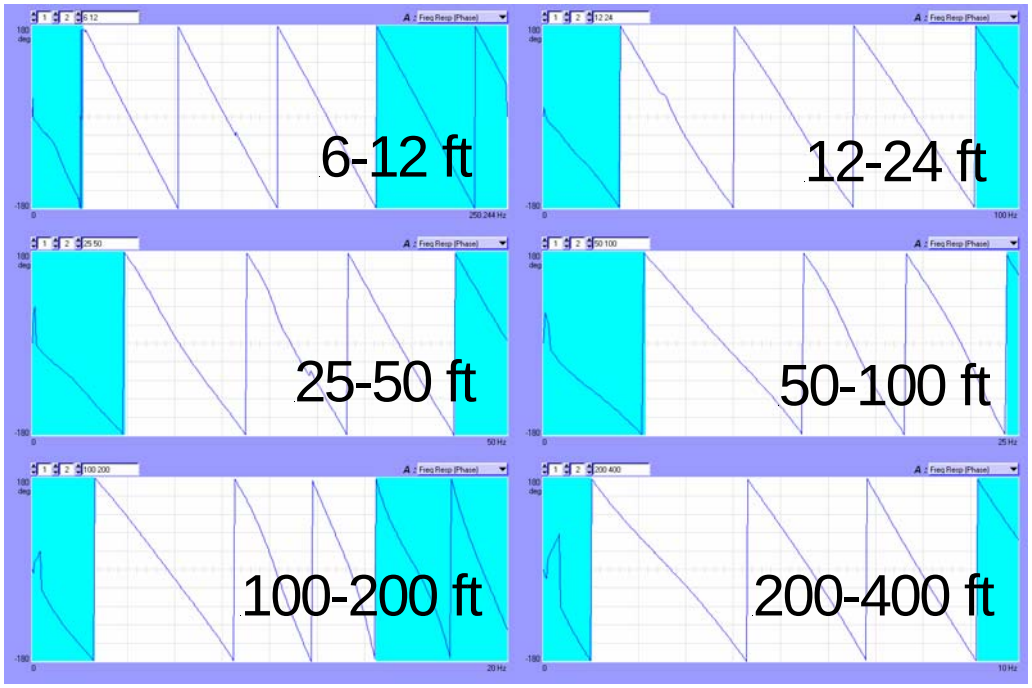

Figure A-14 **Masked phase plots for receiver spacing of 6, 12, 25, 50, 100 and 200 ft for the Baseline Profile 4c.**

Baseline Profile 5a

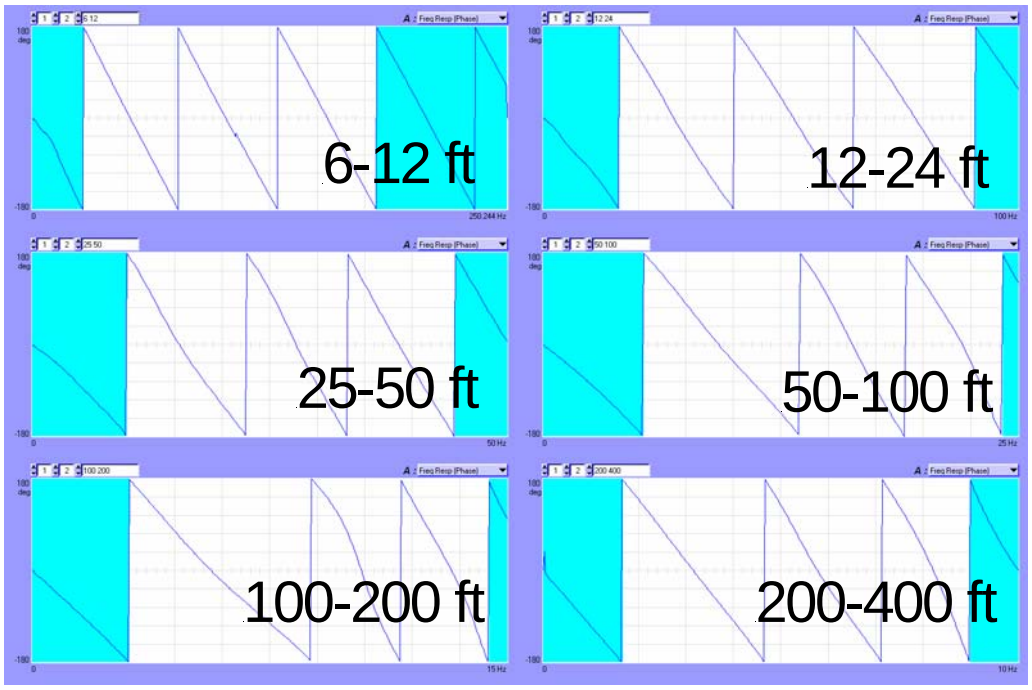

Figure A-15 **Masked phase plots for receiver spacing of 6, 12, 25, 50, 100 and 200 ft for the Baseline Profile 5a.**

Baseline Profile 5b

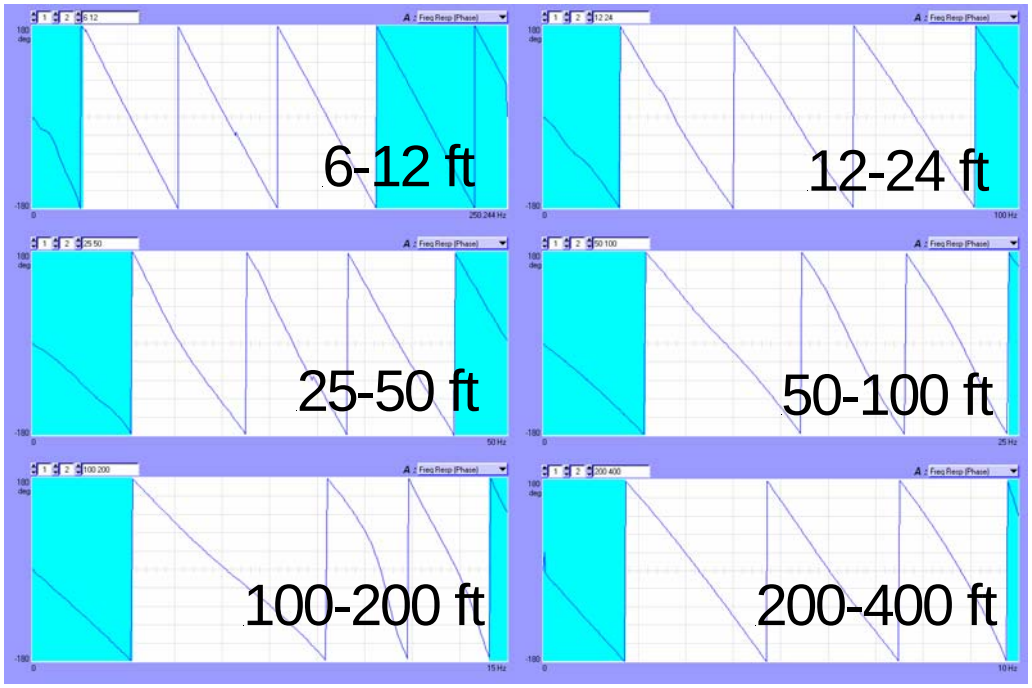

Figure A-16 **Masked phase plots for receiver spacing of 6, 12, 25, 50, 100 and 200 ft for the Baseline Profile 5b.**

Baseline Profile 5c

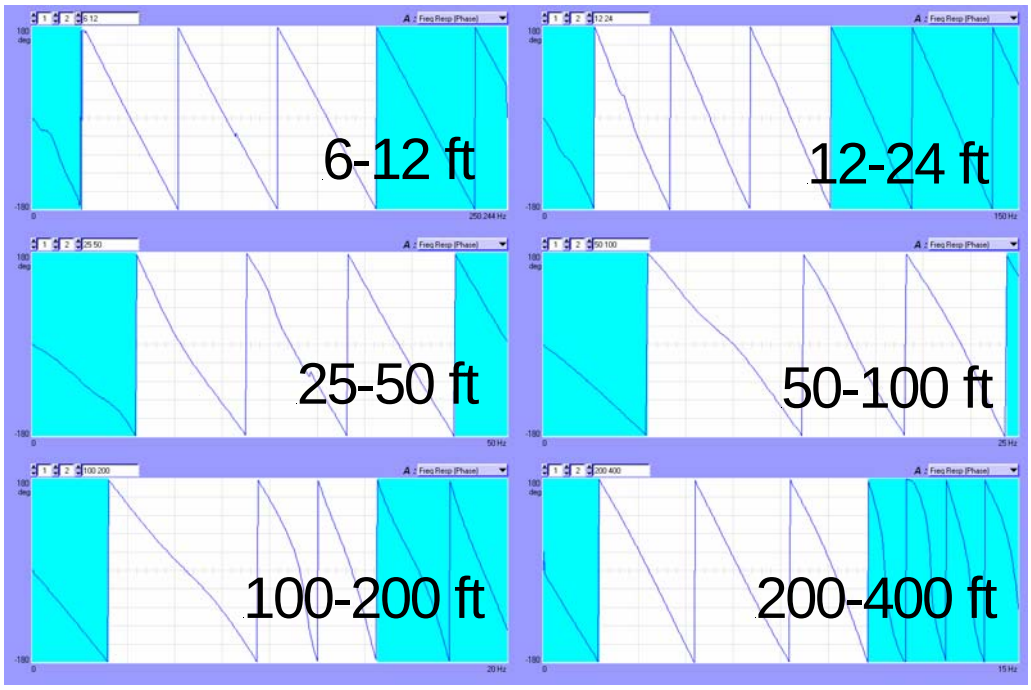

Figure A-17 **Masked phase plots for receiver spacing of 6, 12, 25, 50, 100 and 200 ft for the Baseline Profile 5c.**

Baseline Profile 6a

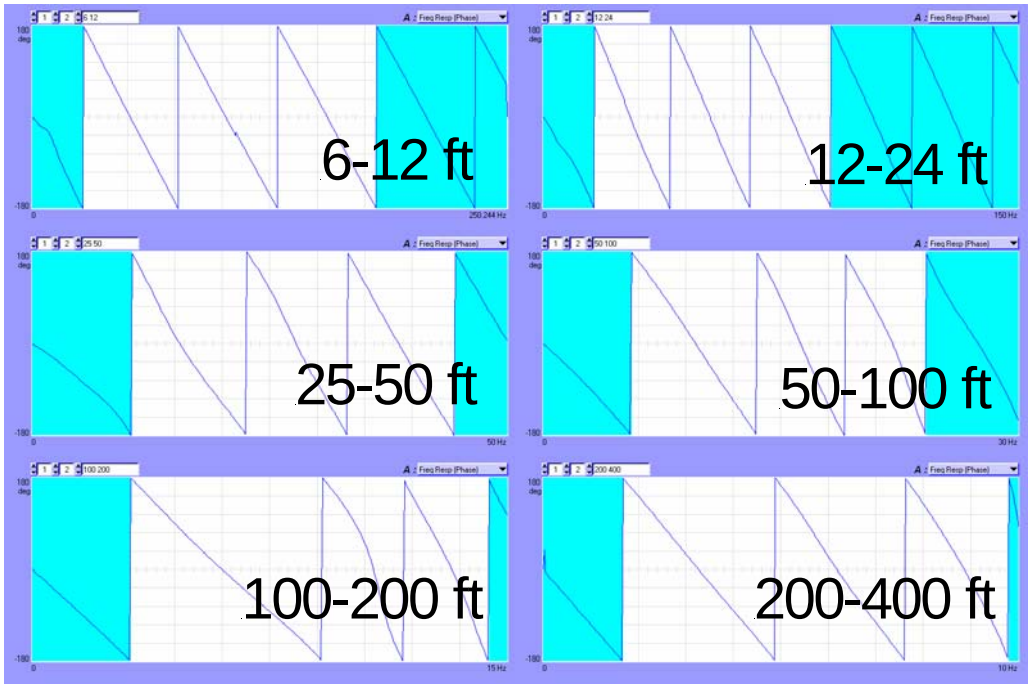

Figure A-18 **Masked phase plots for receiver spacing of 6, 12, 25, 50, 100 and 200 ft for the Baseline Profile 6a.**

Baseline Profile 6b

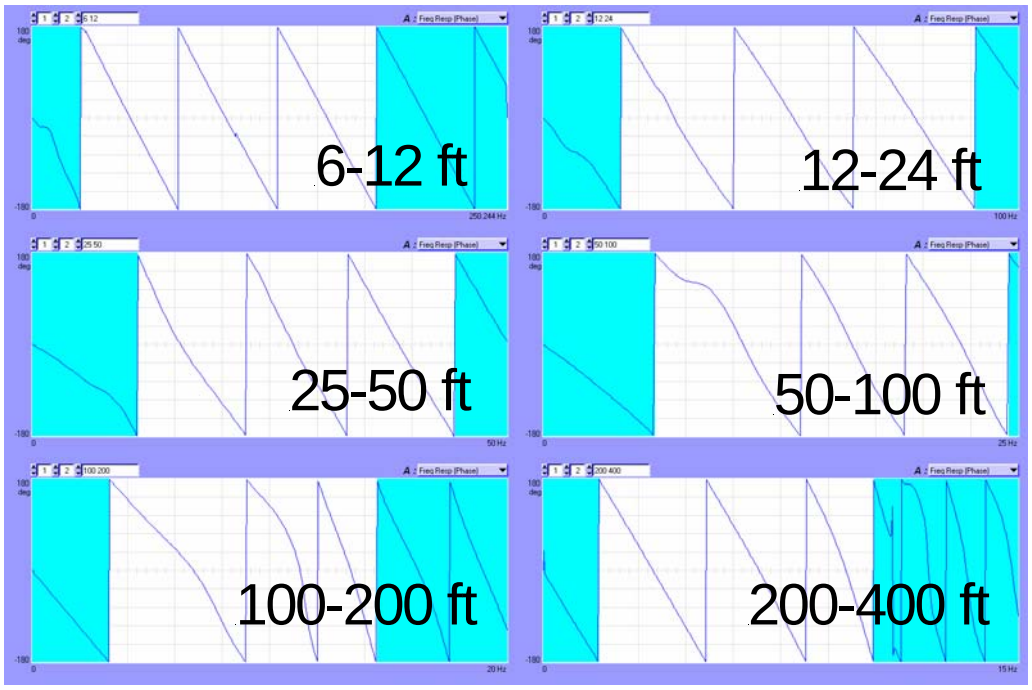

Figure A-19 **Masked phase plots for receiver spacing of 6, 12, 25, 50, 100 and 200 ft for the Baseline Profile 6b.**

Baseline Profile 6c

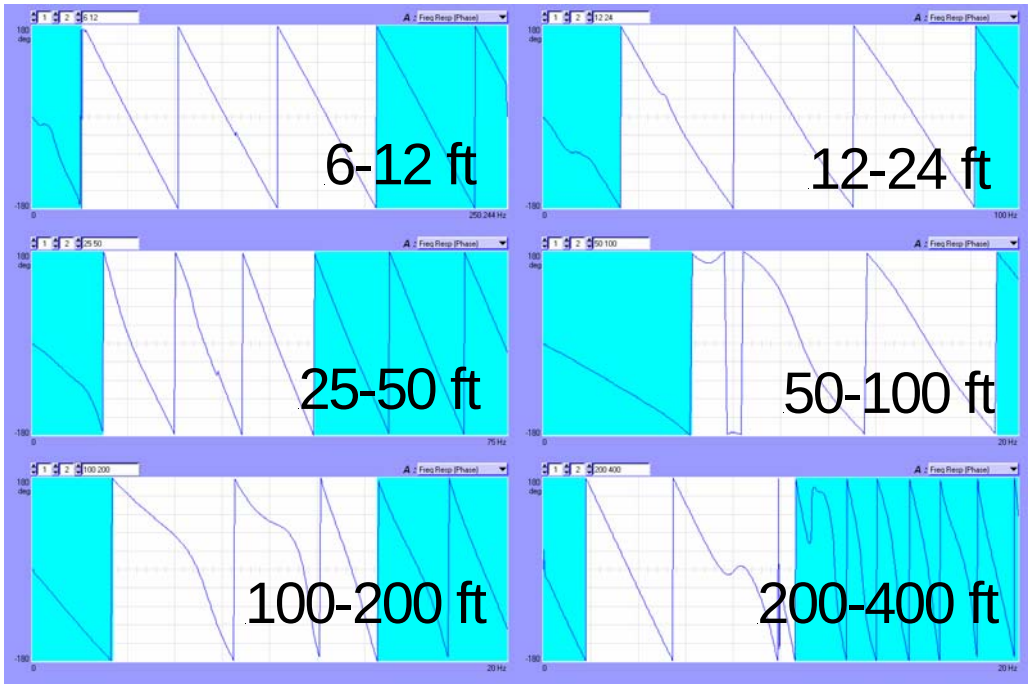

Figure A-20 **Masked phase plots for receiver spacing of 6, 12, 25, 50, 100 and 200 ft for the Baseline Profile 6c.**

Baseline Profile 7a

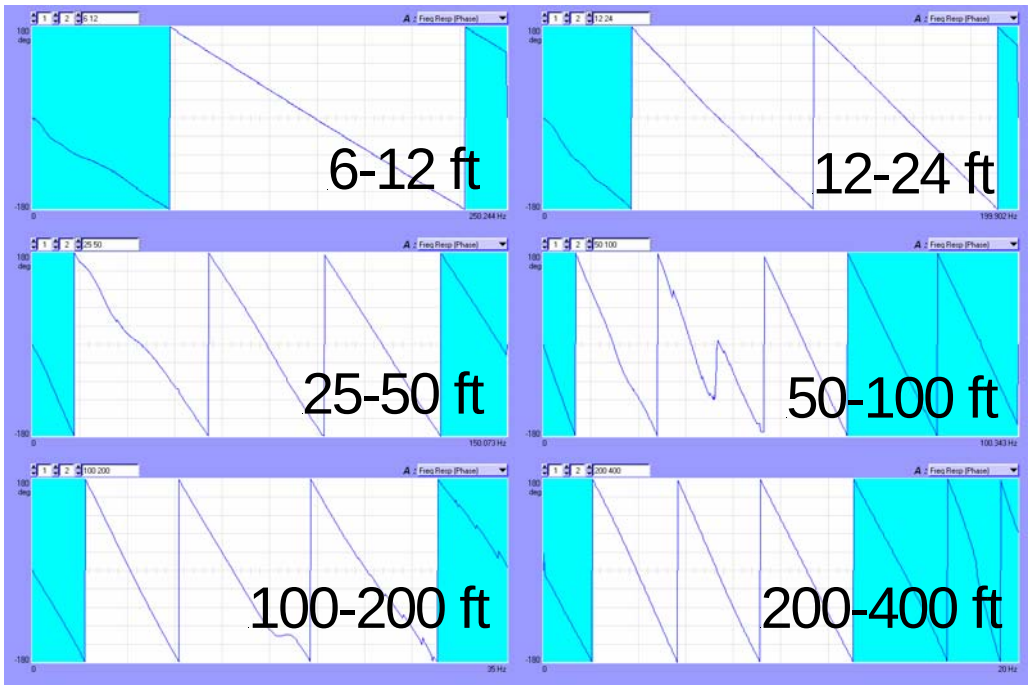

Figure A-21 **Masked phase plots for receiver spacing of 6, 12, 25, 50, 100 and 200 ft for the Baseline Profile 7a.**

Baseline Profile 7b

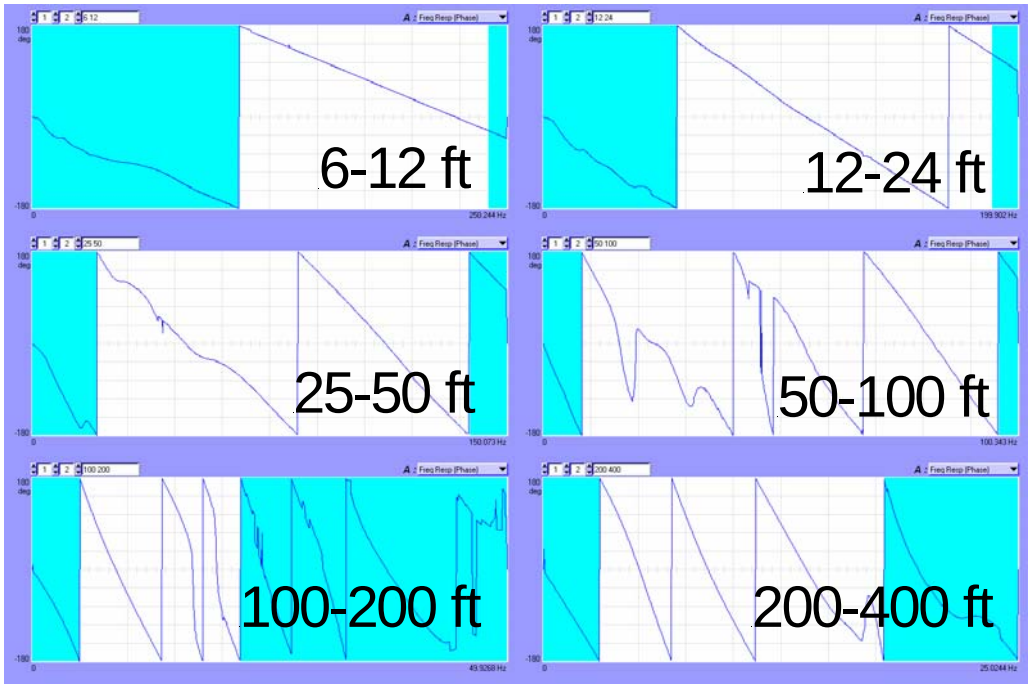

Figure A-22 **Masked phase plots for receiver spacing of 6, 12, 25, 50, 100 and 200 ft for the Baseline Profile 7b.**

Baseline Profile 7c

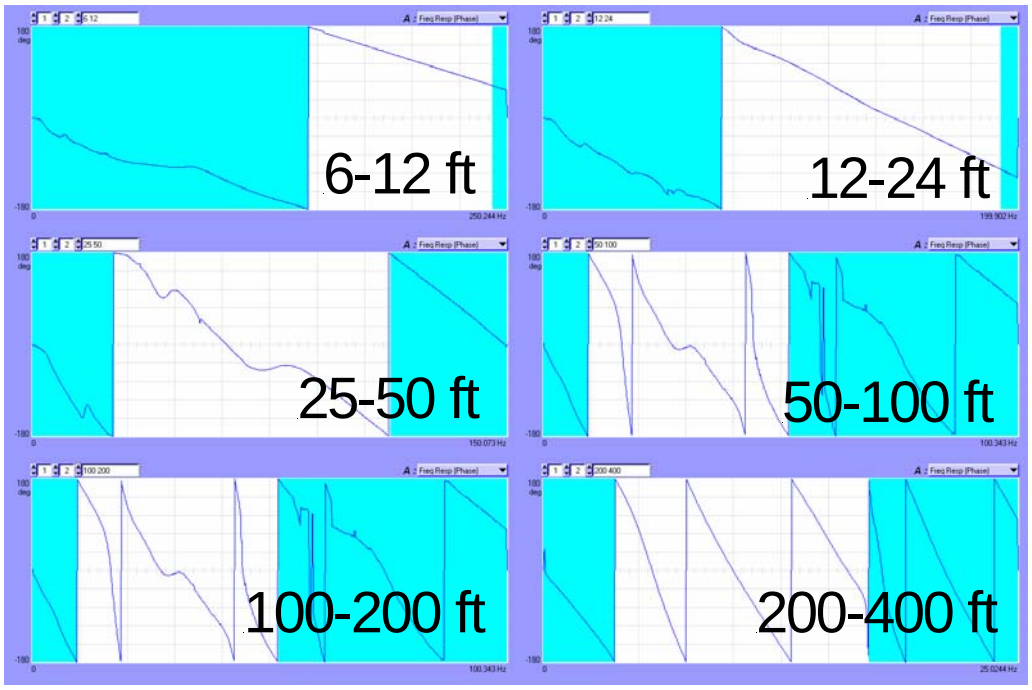

Figure A-23 **Masked phase plots for receiver spacing of 6, 12, 25, 50, 100 and 200 ft for the Baseline Profile 7c.**

References

Achenbach, J.D., (1973). *Wave Propagation in Elastic Solids*, North Holland Publishing Company

Andrus, R.D. and Stokoe, K.H., II, (1999) "SASW Testing to Delineate Potentially Liquefiable Zones and Evaluate Remediation Measures," 7th U.S. – Japan Workshop on Earthquake Resistance Design of Lifeline Facilities and Contermeasures Against Liquefaction, Seattle, WA., August 15-17

ASTM (1991). "Standard Test Methods for Crosshole Seismic Testing." ASTM Designation: D4428/D 4428M-91, July.

Bedford, A., and Drumheller, D.S., (1994). *Introduction to Elastic Wave Propagation*, J. Wiley and Sons Ltd, Chichester, England

Brown, L.T., Boore, D.M. and Stokoe, K.H. II, (2002). Comparison of shear-wave slowness profiles at 10 strong-motion sites from noninvasive SASW measurements and measurments made in boreholes, Bull. Seism. Soc. Am., 92, 3116-3133.

EPRI. (1993). "Seismic hazard methodology for the central and eastern United Sates," Report NP-4726, Electric Power Research Institute, Palo Alto, California.

Foti, S. (2000). *Multistation Methods for Geotechnical Characteristics using Surface Waves*, Ph.D. Dissertation, Politecnico di Torino

Gucunski, N., and Woods, R.D. (1991). "Inversion of Rayleigh wave dispersion curve for SASW test." 5th Int. Conf. on Soil Dynamics and Earthquake Eng., Kalsruhe, pp. 127-138

Gucunski, N., and Woods, R.D. (1992). "Numerical simulation of SASW test." Soil Dynamics and Earthquake Engineering., Kalsruhe, pp. 127-138

Hamming, R.W. (1973). "Numerical Methods for Scientists and Engineers." 2nd Ed., MacGraw-Hill Inc., N.Y.

Hardin, B.O., (1978). "The Nature of Stress-Strain behaviour for soils. State-of-the-art Report," *Proceedings of the Specialty Conference on Earthquake Engineering and Soil Dynamics*, Pasadena, June, ASCE, pp. 3-90

Haskell, N.A., (1953). "The Distribution of Surface Waves on Multilayered Media," *Bulletin of the Seismological Society of America*, Vol. 43, pp. 17-34

Heisey, S., Stokoe, K.H. II, and Meyer, A.H. (1982). “Moduli of pavement systems from spectral analysis of surface waves,” Transportation Research Record 852, pp. 22-31

Hollrah, M. (2005). Development and Implementation of an Underwater System for Interface Wave Measurments, M.S. Thesis, the University of Misssouri at Columbia, 139 pp.

Joh, J.H. (1996). *Advances in Interpretation and Analysis Techniques for Spectral-Analysis-Of-Surface-Waves (SASW) Measurements*, Ph.D. Dissertation, the University of Texas at Austin, 240 pp.

Joh, J.H. (2003). FitSASW, Chung-Ang University, AngSeong, Korea

Kausel, E., and Peek, R., (1982). “Dynamic Loads in the Interior of a Layered Stratum: An Explicit Solution,” *Bulletin of the Seismological Society of America*, Vol. 72 pp. 1459-1481

Kausel, E., and Roesset, J., (1981). “Stiffness Matrices for Layered Soils,” *Bulletin of the Seismological Society of America*, Vol. 70, pp. 1743-1761

Lee, Byung-Sik, (1996). *Analytical Studies of Surface Wave Propagation Along the Seafloor for Application to Spectral-Analysis-of-Surface-Waves (SASW) Testing*, Ph.D. Dissertation, the University of Texas at Austin, 333 pp.

Miller, G.F., and H. Pursey (1955). “On the Partition of Energy Between Elastic Waves in a Semi-Infinite Solid,” *Proceedings Royal Society*, London, A, v.233, pp.55-69

Nazarian, S., Stokoe, K.H. II, and Hudson, W.R. (1983). “Use of spectral analysis of surface waves method for determination of moduli and thicknesses of pavement systems, Transportation Research Record, No. 930, pp. 38-45

Nazarian, S., and Stokoe, K.H. II. (1984). “Nondestructive testing of pavements using surface waves.” Transportation Research Record 993, pp. 67-79

Nazarian, S. and Desai, M.R. (1993). “Automated surface wave method: field testing.” Journal of Geotechnical Engineering Vol. 119

Nigbor, R. L., and T. Imai (1994). “The suspension P-S velocity logging method, in geophysical Characterization of Sites,” *Technical committee for XIII ICSMFE*, A. A. Balkema, Rotterdam, The Netherlands, 57-61

Park, C.B., R.D. Miller, Xia, J. (1999). “Multichannel Analysis of Surface Waves,” *Geophysics*, Vol 64, No. 3, May-June, pp. 800-808

Redpath, B.B., Edwards, R.B., Hale, R.J. and Kintzer, F.Z. (1982). “Development of field techniques to measure damping values for near-surface rocks and soils,” Report URS/John A. Blume and Associates, San Francisco, 120 pp.

Redpath, B.B. and Lee, R.C. (1986). “In situ measurments of shear wave attenuation at a strong-motion recording site,” Report, U.S. Geological Survey Contract 14-08-001-21823, URS/John A. Blume and Associates, San Francisco.

Richart, J.E., Jr., J.R. Hall Jr., and R.O. Woods, (1970). *Vibrations in Soils and Foundations*, Englewood Cliffs, New Jersey Prentice-Hall Inc.

Rix, G.J. (1987). *A source listing of DispGPIB, a program for the data reduction of SASW measurments*, Ph.D. Dissertation, The University of Texas at Austin.

Rix, G.J. and Leipski, A.E. (1991). “Accuracy and resolution of surface wave inversion. Recent advances in instrumentation, data acquisition and testing in soil dynamics.” Geotechnical special publication, No. 29, N.Y., ASCE 1991, pp. 17-23

Robertson, P.K., and Campanella, R.G. (1985). “Liquefaction potential of sands using the CPT. Journal of Geotechnical Engineering, ASCE, Vol. 111, No. 3, pp. 384-403.

Sanchez-Salinero, I. (1987). *Analytical Investigation of Seismic Methods Used for Engineering Applications*, Ph.D. Dissertation, The University of Texas at Austin, 401 pp.

Stokoe, K.H., S.W. Wright, J.A. Bay, and J.M. Roesset, (1994), “Characterization of Geotechnical Sites by SASW Method,” *Geophysical Characteristics of Sites*, ISSMFE Technical Committee #10 for XII ICMFE, A.A. Balkema Publishers, Rotterdam & Brookfield, Netherlands pp.785-816

Stokoe, K.H. II, Joh, S.H., and Woods, R.D. (2004), “The contributions of in situ geophysical measurements to solving geotechnical engineering problems,” Proceedings ISC-2 on Geotechnical and Geophysical Site Characterization, Vianna Da Fonseca and Mayne.

Tarantola, A. (1987). “Inverse Problem Theory: Methods for Data Fitting and Model Parameter Estimation.” New York: Elsevier, 600 pp.

Thompson, W.T., (1950), “Transmission of Elastic Waves through a Stratified Solid Medium,” *Journal of Applied Physics*, Vol. 21, pp. 89-93

Tokimatsu, K., Tamura, S., and Kojima, H. (1992). “Effects of multiple modes on Rayleigh wave dispersion.” Journal of Geotechnical Engineering, ASCE, 118(10), 1529-1543

Wolf, J.P. and Obernhuber, P. (1982). Free-field response from inclined SH-waves and Love-waves, Earthquake Engineering and Structural Dynamics, 10, pp. 823-845.

Wolf, J.P. (1985). Dynamic soil-structure interaction, Prentice-Hall, Inc., Englewood Cliffs, NJ, 466 pp.

Yuan D., and Nazarian S. (1993). “Automated surface wave method: inversion technique.” Journal of Geotechnical Engineering., Vol. 119, No. 7, ASCE, pp. 1112-1126